A cross-scale model for the evolution of influenza within a single season

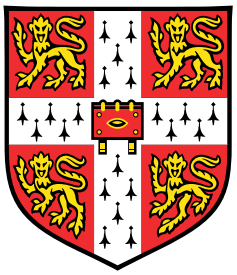

Venetia Aikaterini Karamitsou

Supervisor: Prof. Julia Gog

Department of Applied Mathematics and Theoretical Physics
University of Cambridge

This dissertation is submitted for the degree of
Doctor of Philosophy

Hughes Hall

July 2021

To my dad, for always being my inspiration.

To my mom, for always being my rock.

To Helen, because you are my soulmate.

Declaration

I hereby declare that except where specific reference is made to the work of others, the contents of this dissertation are original and have not been submitted in whole or in part for consideration for any other degree or qualification in this, or any other university. This dissertation is my own work and contains nothing which is the outcome of work done in collaboration with others, except as specified in the text and Acknowledgements. This dissertation contains fewer than 65,000 words including appendices, bibliography, footnotes, tables and equations and has fewer than 150 figures.

Venetia Aikaterini Karamitsou
July 2021

Acknowledgements

I want to thank everyone who made this possible.

Thank you, from the bottom of my heart, to the Disease Dynamics group in Cambridge. Petra Klepac, Stephen Kissler, Sophie Ip, Maria Tang and Jordan Skittrall, I could not have done this without you. Thank you for the brainstorming sessions and your feedback on my presentations. Thank you for the smallest random things that made my day so many times. Thank you for being kind and patient with me when I was going through my admittedly way too many tough phases. And thank you for letting me sleep on the office couch and not even taking a ridiculous picture of me. I cannot imagine ever finding a research group better than you and I am so incredibly lucky that I had the chance to be surrounded by you these years.

Thank you to Prof Simon Tavaré and Dr Orsola Spivack for your guidance and feedback on my first year report. Prof Tavaré I still remember that you told me you worked on a model about basking sharks in Scotland, one day I hope to follow in your steps.

Thank you to the George and Maria Vergottis Fund for financially supporting me through my PhD. Your scholarship made it possible for me to come study in Cambridge. Thank you to my college, Hughes Hall, for their personal, academic, and financial support and especially to Dr Philip Johnston for being one of the kindest people I have ever had the luck and pleasure to meet.

Thank you Prof Juliet Pulliam, and the rest of SACEMA, for your hospitality, amazing discussions and constructive feedback. You made me feel at home when I visited SACEMA and you inspired me to really start dreaming about somehow becoming a "field mathematician". This is still my dream, and I might not know how yet but one day I will dive with sharks for math!

Thank you to the people back in Johns Hopkins University, because without your support and guidance I could have never made it here. Ed Scheinerman and Richard Brown, you

were the most amazing, caring and helpful academic supervisors I could have wished for. Prof Donald Geman and Prof Laurent Younes, thank you for giving me the opportunity to work with you and get to listen to your brilliance. Prof John Wierman, thank you for believing in me and guiding me into the mathematician that I am today. Prof Jack Morava, to say that it was my absolute honor to work with you and get even a small glimpse into how beautifully your mind works would be the understatement of the century. Thank you for being so open and and kind and funny and approachable.

Thank you to my Cambridge friends, y'all know I wouldn't have survived this PhD without you. Phil, Damir, Renaud, Tiago, Barzan, Dilar, Kasia, Vincent, Eun-joo, Eve, Karen, Katie, Jordan, Matt, Will, Beth and Yelena thank you for the laughs, the tears, the serious talks and everything in-between. In different ways, each of you inspired me to be a better person and I am grateful to you for that. Thank you to the Uni Handball team, and especially Alex, for keeping me sane and giving me a way to somehow still have fun even when things got bad.

Thank you to the friends who were in a different country but always felt so close. Eleni, Liza, you two always feel right next to me even when we have an ocean between us. Thomako, Korylle, Limnie, Kantoglako, Tsoumi, Anna thank you for always making me laugh and feel like things will someday somehow get better.

Thank you Dr Filippos Kouniakis for turning me into a functional person all those many many times I was a big old mess. Thank you for calming down all those anxiety voices in my brain and giving me the peace and silence I needed to finish this.

Thank you to my doggos, Melissa and Balou, because you were my little walking borking uppers. You can't read this (but how amazing would it be if you could), but you little sweethearts are my whole world.

And lastly and most importantly, thank you Julia. I was trying to find how to express my gratitude to you not just for the jaw-droppingly brilliant and insightful mathematician that you are or for the incredibly understanding and inspiring supervisor, but most of all for the person that you are. I couldn't come up with something that would do you justice in just one paragraph (or ten). So I guess, thank you for being you.

Abstract

In this thesis we develop a mathematical cross-scale model for the evolution of influenza within a single season. We model evolution as the emergence and spread of a mutant strain in a population that is already invaded by a parent resident strain. This allows us to investigate both the emergence dynamics of a mutant strain as well as the subsequent competition dynamics between the two strains. Our main research goal is to study the effects of a homologous vaccine against the resident strain on the epidemiological and evolutionary dynamics of the disease.

Due to the complexity of cross-scale models, we first develop a simpler population-level SIR-type model for the evolution of influenza. Assuming an outbreak that is initiated by a single resident strain, we study the significance of the mutant's emergence time by introducing it in the population at different times. We then also derive a probability density function for the emergence of the mutant in the population. Finally we incorporate vaccination to our model, and arrive at the conclusion that intermediate levels of vaccine-induced immuno-protection are the most beneficial for the emergence and spread of the mutant strain.

We then start building towards a cross-scale model by developing a dynamical within-host model for the evolution of influenza. Our goal is for emergence to be a stochastic event, so we derive a probability density for the within-host emergence of a mutant strain. We also incorporate vaccination to our model and assess its impact on the viral loads of the two strains.

Having analyzed our within-host model, we then couple it with a between-host SI model. The links between the two scales are the population-level transmission rates, which we assume are linear functions of the within-host viral load. We first investigate how varying the within-host parameters affects the population-level fitness of the two strains, and then we study our model's results under different forms of the within-host emergence density. Finally we add vaccination to our cross-scale model, and arrive at the same conclusion that intermediate values of immuno-protection are the most inducive to the emergence and spread of a mutant strain in the population.

Table of contents

List of figures

List of tables

Chapter 1

Introduction

1.1 Influenza overview

1.1.1 The burden of influenza

Influenza viruses are among the most common causes of human respiratory infections and can cause high morbidity and mortality. Influenza affects 2% to 10% of the global population, resulting in 250,000 to 500,000 deaths annually [92]. The burden of influenza, which according to the CDC takes into account the number of influenza illnesses, medical visits, flu-associated hospitalizations, as well as flu-associated deaths, can be much higher among the children, the elderly, and immuno-compromised individuals [179, 270]. Each year 15–45% of children are infected with influenza, and about 870,000 children aged less than 5 years and 300,000 children aged less than 1 year all over the world require hospitalization [203]. Influenza outbreaks have occurred since at least the Middle Ages [287]. In addition to seasonal influenza outbreaks, pandemic influenza viruses have been emerging occasionally in the last several centuries. Pandemic strains can cause significantly more infections and deaths compared to seasonal ones. The "Spanish flu" pandemic of 1918 is estimated to have caused the death of 50 million people worldwide [158]. Vaccination is considered the most efficient public health intervention to reduce the burden of influenza [261].

1.1.2 Relevant biology

Influenza types, subtypes and strains

Influenza is a respiratory disease caused by certain RNA viruses of the Orthomyxoviridae family. It is divided into four main types, A, B,C and D which are determined by antigenic differences in their nucleoprotein (NP) and matrix protein [217]. Influenza type A is the most interesting from an epidemiological and evolutionary perspective, because it can infect humans and various other mammals as well as avian species and can undergo significant immunological changes. Influenza B is confined primarily to humans and contributes significantly to influenza-related deaths. Humans were considered the only hosts of influenza B until 1999, when data showed that it can also infect seals [38]. Little is known about influenza C compared to the other types, but so far it has been shown to infect humans, dogs and pigs [318]. Influenza D was first isolated from clinically-ill pigs with influenza-like symptoms in the USA in 2011. It was subsequently isolated from cattle, which until then was a species never considered to be susceptible to influenza. While phylogenetic analysis showed that type D shares some significant similarities with type C, influenza D exhibits no cross-reactivity with human type C antisera, does not reassort with influenza C to generate viable progeny and finally exhibits a new mechanism to generate the M1 protein. As a result, influenza D has been classified as a new genus of the Orthomyxoviridae family [146, 283]. In 2016 White *et al*. performed a serological study on human serum samples from 35 cattle-exposed and 11 non-cattle-exposed adults to screen for influenza D antibodies using hemagglutination inhibition (HI) and microneutralization (MN) assays [306]. The HI assay showed a 91% seroprevalence among the cattle-exposed individuals, while the MN assay showed a 97% seroprevalence in the same group. The authors emphasized that while it is still not known whether influenza D causes disease in humans, their findings indicate that it could be an emerging pathogen threat among cattle-workers.

Influenza A viruses have been responsible for the majority of recorded epidemics and pandemics [3]. They are further divided into subtypes based on differences in the surface proteins hemagglutinin (HA) and neuraminidase (NA). The CDC reports that there are currently 18 different types of HA and 11 different types of NA, and that while that leads to 198 potential different influenza A subtypes only 131 have been detected in nature. In a 2011 paper, Deng *et al*. report that real-time Reverse-Transcription PCR (RT-PCR) is the most widely used assay for influenza virus typing and subtyping [72]. A more recent technology for the detection and subtyping of influenza A (though not limited to influenza)

is pyrosequencing, which is a sequencing by synthesis technique that can be used for short sequence and SNP analysis [81, 258]. It has been extensively used in influenza molecular surveillance for SNP detection and for mutation screening [72]. We note that several more influenza detection, typing and subtyping methods exist, including but not limited to double immunodiffusion assays, ELISA and real-time PCR. Influenza types (and subtypes in the case of influenza A) are also subdivided into strains, which are distinguished by variations in their genetic sequence. The WHO Expert Committee on Influenza recommended a two-part nomenclature system for influenza viruses in a 1980 memorandum [2]: a strain designation and a description of the HA and NA antigens. This revised nomenclature followed the WHO's classification systems published in 1953, 1959, 1971 and 1980. The revised strain designation for types A,B and C is required to include the following information (taken directly from [2]):

1. A description of the antigenic type of the virus based on the antigenic specificity of the NP and M proteins (A, B, C or D).
2. The host of origin. This is not necessary for strains isolated from humans, but is mandatory for strains isolated from non-human hosts.
3. Geographical origin.
4. Strain number (or serial number/ laboratory identification number).
5. Year of isolation.

The description of the HA and NA antigens applies only to influenza A viruses, and needs to include the following information:

1. An index describing the antigenic character of the HA subtype, such as H1 and H3.
2. An index describing the antigenic character of the NA subtype, such as N1 and N2.

Therefore, an example of an influenza strain would be "A/Alaska/135/2015(H3N2)" (taken from the Influenza Research Database) where:

1. The type of the strain is A.
2. The host that the sample was isolated from is human, as otherwise the name of the strain would have to include the non-human host.
3. The location where it was isolated is Alaska.
4. The serial number is 135.

5. The sample collection year is 2015.

6. The strain's subtype is H3N2.

In the same WHO 1980 memorandum, it is mentioned that "it is implicit that a given H or N subtype designation will encompass strains exhibiting a considerable degree of antigenic variation within the subtype. The precise antigenic position of an influenza virus within a subtype may be defined by indicating similarities to designated reference strains". A commonly used experimental method to define the antigenic phenotype of an influenza strain is the hemagglutination inhibition (HI) assay, which measures the cross-reactivity of one strain's HA protein against antisera developed using a different (reference) strain [150].

Influenza virus life cycle

Influenza viruses preferentially replicate in the epithelial cell layers of the respiratory tract of their host, but their target cells can also include macrophages and other leukocytes [159]. The infection process within the host begins as follows: the influenza virus enters a host cell using its HA protein to bind to the sialic acid on the surface of the host cell membrane and then releases its RNA, in the form of individual viral ribonucleoprotein (vRNP) complexes, into the cell's nucleoplasm. Inside the host cell nucleus, viral RNA polymerase performs the transcription and replication of the influenza genome. The newly synthesized vRNPs exit the nucleus and travel to the cell membrane for viral assembly. Once there they combine with each other and become encased in protein shells, called capsids, to form new viral particles which are referred to as virions [85]. These virions are then released from the host cell where they may find and infect new susceptible target cells. The number of virions present in a given volume is called the viral load or viral titer, and in the case of influenza is often measured in viral RNA copies per milliliter of nasal swab or aerosol sample.

Immune responses to influenza

The immune system has several mechanisms to combat the spread of an infection. The first line of defense is the rapid innate immune response. Viral endocytosis triggers the activation of pattern recognition receptors within the host cell, which in turn triggers the secretion of type I interferons (IFN). IFN is a type of cytokine with antiviral as well

as immunostimulatory properties and plays an important role in regulating the immune system. Infected cells also secrete other types of cytokines, such as proinflammatory cytokines which enhance the binding of leukocytes to endothelial cells in the interior of blood vessels, thus making their travel to the site of the infection easier. Additionally, infected cells produce chemokines which act as messengers to leukocytes. Epithelial cells as well as leukocytes have also been reported to undergo apoptosis in response to influenza infections [159]. The innate immune response can be triggered within as little as three hours of an influenza infection [220]. There is also the much slower adaptive immune response which is vital for the establishment of protective immunity. The adaptive immune response can be divided into two main mechanisms: humoral and cellular immunity. Humoral immunity involves the actions of antibodies, which are produced by plasma B cells and whose main role is to bind to antigens that are found outside of infected cells. Cellular immunity on the other hand occurs inside infected cells and is mediated by T lymphocytes rather than antibodies. Antigen-presenting cells express a pathogen's antigens and in response helper T cells release cytokines whose function is to help cytotoxic T cells bind to infected cells and kill them. It is important to note that even independently of the innate and adaptive immune responses, the process of viral protein synthesis, packaging and production of progeny virions is very damaging for the target cells. This often leads to virus-induced cytolysis, which stops the new virion synthesis and limits the spread of the infection.

We will now discuss in further detail the interferon response to the influenza virus. This is because in chapter 3 we will study a within-host viral kinetics model which explicitly takes into account the impact of the innate immune response on the viral growth via the action of interferon. The IFNs are a family of antiviral cytokines and are classified into three types based on their amino acid sequence and the type of receptor through which they signal. Type I IFNs were discovered in 1957 [153] and consist of several different molecules. Among them, in the case of humans, are 13 distinct IFN-α genes and one IFN-β gene. These are among the major IFNs secreted following influenza virus infection, both in-vivo and in-vitro [167]. The type III IFN family (IFN-λ) has very similar functions to the antiviral cytokines of the type I IFN family but restricted activity, because its receptors are primarily restricted to epithelial cell surfaces in the respiratory and gastrointestinal tracts while type I IFN receptors are expressed at the surface of all cells [278]. It is important to mention that the type II IFN, which only has a single member called IFN-γ, also has some well-characterized antiviral effects but is secreted by activated T lymphocytes and natural killer (NK) cells rather than in direct response to

viral infection [247].

The induction of IFN becomes stimulated following the recognition of pathogen-associated molecular patterns (PAMPs) of invading viruses, which are absent in uninfected cells. The subsequent binding of IFN into its receptors at cell surfaces leads to the upregulation of several hundreds interferon-stimulated genes (ISGs), whose role is to establish an antiviral state and limit the spread of the virus. Some of these ISGs that have been identified as pivotal during an influenza infection are the following: the Mx family of GTPases which can retain the incoming viral genome in the cytoplasm and prohibit nuclear import [133, 313], viperin which can inhibit viral release from the plasma membrane of infected cells [299] and the IFN-induced transmembrane (IFITM) family members (especially IFITM3) which can inhibit viral entry [45, 97]. For single stranded RNA (ssRNA) viruses like influenza, PAMPs are often certain features of viral RNA which are not normally present in cellular RNAs, such as regions of double-stranded RNA (dsRNA) made during viral replication [167]. As early as 1967 Lampson *et al*. demonstrated that the presence of dsRNA induces IFN production [181]. Research has shown that non-plasmacytoid dendritic cells (DC) produce high levels of IFN-α in response to the presence of dsRNA in the cytoplasm [74, 155]. However, influenza has evolved a mechanism to counteract this aspect of the immune response by means of the non-structural protein 1 (NS1). The primary function of NS1 is to inhibit the host IFN response through a variety of distinct molecular mechanisms [94]. One of these mechanisms is by binding to and sequestering dsRNA, thereby stopping the production of type I IFN by conventional DC [32, 114, 145]. Plasmacytoid dendritic cells (pDC) though, which are a unique subset of DC capable of releasing large amounts of type I interferon following a viral encounter, have been shown to produce high levels of IFN-α even after infection with wild-type influenza [62, 156]. In 2004 Diebold *et al*. tested the hypothesis that pDC possess a way of recognizing influenza that does not depend on dsRNA detection. Their results showed that TLR7 receptors, which are pathogen-recognition receptors (PRRs) that belong to the Toll-like receptor (TLR) family of transmembrane proteins, are capable of recognizing influenza ssRNA and stimulate the production of IFN-α by pDC [73]. The authors underlined that this is a unique property of pDC and that conventional DC cannot produce high levels of IFN in response to TLR signalling. Another type of PRRs that has been implicated in the induction of IFN by influenza viruses are the RIG-I-like receptors (RLRs), which play a key role in the production of IFN by non-pDC [167]. The majority of RLRs though are confined to the cytoplasm, while influenza virus transcription and replication occurs in the nucleus (unlike many other RNA viruses which replicate exclusively in the cytoplasm).

As a result the RIG-I and MDA-5 receptos of the RLR family, which cannot access the nucleus, cannot directly sense the viral replication and activate the IFN response. Moreover incoming as well as progeny vRNAs are encapsidated into vRNPs and can therefore evade PRR recognition as they traverse the cytoplasm, whereas naked vRNAs would have been detected by RIG-I and MDA-5 receptors and activated the IFN response. Furthermore, the NS1 protein has been shown to directly inhibit the activation of the RIG-I receptors [234].

Mutation and antigenic drift, shift and thrift

Research has shown that influenza has a high mutation rate, estimated roughly at 2×10^{-5} substitutions per nucleotide per cellular infection [216, 225, 264]. This has been primarily attributed to the error-prone replication of the virus within the target cells. The influenza viral RNA-polymerase lacks a proofreading function, and often places the wrong nucleotide (or sequence of nucleotides) in the wrong position of the influenza genome. These point mutations are often neutral or deleterious for the virus, but can also be beneficial. A study by Visher *et al*. in 2016 in which the researchers generated mutant variants from a parent influenza strain found that approximately 30% of the mutations were lethal, and among the viable mutants most were weakly deleterious or neutral, some were very deleterious and only very few were weakly beneficial [297]. Lyons & Lauring reported very similar findings in [200]. Beneficial mutations that occur in antigenic sites are particularly important because they can help the virus escape neutralizing antibodies. Other beneficial mutations might lead to drug resistance, faster replication, better binding to target cells or even cross-species transmission [144, 297]. Even small genetic changes can have a strong impact on the virus' phenotype. In [67] Conenello *et al*. compared sequences of human influenza A strains isolated during some major outbreaks, including the 1918 pandemic. Using a mouse model, they identified a single mutation in the PB1-F2 protein to be responsible for the large increases in the viral growth and virulence of these strains.

The gradual accumulation of mutations in the HA and NA proteins (and more generally in the influenza genome) is referred to as antigenic drift, and is partially responsible for the virus' ability to escape the immune response and re-infect hosts. The effects of antigenic drift were observed as early as 1947 [106]. In 1979 Laver *et al*. used antigenic mapping and sequence analysis of the escape mutants which emerged in the presence

of monoclonal antibodies against the HA and NA proteins to identify four antigenic sites (also referred to as epitopes) on the head domain of the HA [184]. In 1990 Wilson and Cox identified a fifth antigenic site on the head of HA [310]. In the same paper they further reviewed the cumulative molecular changes in the HA of various influenza strains from 1968 to 1987 and concluded that the amino acid substitutions which led to the antigenic drift of the virus were largely confined to those five epitopes. In 1992 Webster *et al*. established an antigenic map of the N2 neuraminidase molecule using neuraminidase inhibition (NI) and ELISA tests and identified three and possibly four antigenic sites [301]. As the antigenic sites are what the host immune system uses to recognize and kill influenza viruses, if their phenotype changes due to mutations then the immune cells might fail to recognize them even if the host has been previously infected by a different influenza strain.

Influenza A viruses can undergo antigenic changes via another route, which is referred to as antigenic shift. Antigenic shift occurs when more than one strains coinfect the same host and exchange gene segments in a process called reassortment. The most dramatic antigenic changes have happened when segments from strains circulating in non-human hosts, such as birds and swine, were combined with segments from human strains. Two examples are the 2009 H1N1 pandemic, which originated from swine, and the 1918 Spanish flu pandemic, whose source was a an avian influenza-like lineage [212]. While reassortment had been recognized at least as early as 1982 as a mechanism via which novel influenza genotypes with pandemic potential can emerge [304], the more recent advancements in gene sequencing technology have allowed for very descriptive evolutionary studies using genomic data [151]. Various such studies have shown that mixed infection, a prerequisite for reassortment, is a common occurrence during seasonal influenza [118, 151, 237]. Studies have shown that reassortment occurs frequently between the H1N1 and H3N2 subtypes. Since the reemergence of H1N1 in the human population in 1977, these viruses have co-circulated with viruses of the H3N2 subtype. While it was only in 2001 that influenza A H1N2 viruses emerged via genetic reassortment between viruses of these two subtypes, earlier reassortants between them had briefly circulated from 1978 to 1980 and 1988 to 1989 but did not become established in the human population [123]. Evidence has also shown that reassortment occurs frequently within the H3N2 subtype. In 2006 Schweiger *et al*. used H3N2 viruses isolated in Germany from 1998 to 2005 to show that a surprisingly high 70% of viruses from 1998-1999 were the result of reassortment and had distinct genome compositions [266]. They also found though that the next year was characterized by the prevalence

of a single reassortant strain, which they assumed was because the 1999-2000 H3N2 viruses achieved the best evolutionary fitness. It is important to note that the authors isolated reassortant strains in each of the seasons studied. In 2016 Poon *et al*. performed whole genome deep sequencing on swabs collected from a set of 84 individuals, which consisted of index cases with confirmed influenza along with their household contacts, in Hong Kong [237]. The virus samples were collected during the first wave of the 2009 H1N1 pandemic in Hong Kong, when seasonal H3N2 viruses were also confirmed to be circulating. The author's analysis showed that approximately 66% of the H3N2-infected patients and 40% of the H1N1/2009-infected patients likely harbored mixed lineage infections. Bourret *et al*. in 2013 [42] and Bourret *et al*. in 2017 [43] studied the evolution and adaptation mechanisms of a duck influenza A virus isolate during passage in swine tracheal cells. Their work was motivated by evidence that swine might be an intermediate host for adaptation of avian influenza strains to humans and for enabling reassortment between strains of avian and human origins. The results of their 2013 study showed that while the original isolated virus was a mixture (specifically had two different versions of 6 of the 8 gene segments), the adaptation to swine led to multiple genetic changes and to the fixation of a single version on all gene segments. The authors reported that all the nucleotide differences observed in segment 2 of the adapted virus originated simultaneously during the adaptation and were therefore the result of reassortment. They concluded that the wildtype field isolates of duck influenza were most likely the result of coinfection in the natural reservoir, and are what provided the virus with the genetic diversity to adapt to the new host system. Using the same experimental setup in 2017, Bourret *et al*. studied the functional impact on viral fitness of the genetic changes in the different segments, as well as their interactions. Their analysis showed that rescued virus bearing all 8 segments from the adapted virus showed a clear growth advantage over rescued virus bearing all eight segments from the parental, wildtype virus. The authors were further able to identify using reverse genetic studies exactly which segments from the adapted virus had the most positive main effect on viral growth (segments 2 and 4), and which had only weak or no effects. In 2021 Ganti *et al*. coinfected mallards and guinea pigs with H3N8 and H4N6 subtypes (both typical viruses isolated naturally from mallards) to quantify reassortment and also study the effects of host-species on the within-host genetic diversity attributed to reassortment [112]. The authors isolated virus from several different time points during the mallards' and guinea pigs' infections and then performed genotyping of all eight segments to evaluate whether they were from H3N8 or H4N6 origins. They reported that in all individuals of both species and at all the time points examined, reassortment was detected, though reassortant genotypes were

considerably less common in guinea pigs than in mallards. The authors attributed this to the negative selection of less fit variants and the relatively little opportunity for reassortment since both the avian subtypes used cannot replicate efficiently in mammalian hosts. It is important to underline that reassortment may also be deleterious, in which case the resulting viruses are removed by purifying selection [246].

The high mutation rate of influenza alone should lead to a "diffuse cloud of antigenic types on a variety of genetic backgrounds", as Wikramaratna *et al*. argue in [309]. An examination of influenza's evolution within the last century though shows that the virus is characterized by the replacement of circulating strains with new distinct strains that are able to re-infect hosts immune to earlier subtypes [98, 309]. Research has identified a few different factors that may contribute to this perhaps paradoxical limited antigenic diversity of influenza:

- New mutants are short-lived because of a nonspecific, strain-transcending immune response which decays rapidly with the time since last exposure but prevents reinfection by any new strain [98].
- While the genetic changes of the influenza virus are gradual, the antigenic changes are punctuated due to complex genetic-to-antigenic change maps [169]. As Koelle *et al*. report in [169], the traditional distance metrics which translate the genetic differences between two strains to the degree of cross-immunity between them tend to consider strains whose genetic sequences vary by a larger number of amino acid changes as more antigenically distant. But evidence has shown that even a single amino acid change can be enough to create an immune-escape mutant, while as many as 19 amino acid changes can have a very small impact on the antigenic properties of a new mutant. To account for this Koelle *et al*. focused on the epidemiological and evolutionary dynamics of clusters of influenza strains instead of individual strains, where each cluster consisted of strains that are antigenically equivalent. This prevented reinfection by strains in the same cluster and effectively extended cross-immunity until an antigenically novel strain emerged.
- The antigenic distances between strains coupled with the host's recent immune history only allow for a small number of predominant phenotypes [30]. Bedford *et al*. modelled the genetic and antigenic evolution of influenza in 2012 using a two-dimensional Euclidean space to describe the antigenic phenotype of each strain [30]. The concept of strain space and the idea of representing antigenic

distance as the distance between points in geometric space had already been investigated by Lin *et al*. in 1999 [190] and by Gog and Grenfell in 2002 [121]. Bedford *et al*. used the HI between sampled strains to inform their distance in the antigenic space. Within this framework various genetically distinct strains occupied the same position in the antigenic space. As a result, following infection by a certain strain reinfection was highly unlikely by strains which occupied either the same or some neighboring antigenic space.

- The host immune response against epitopes of low to intermediate variability that are shared between strains, together with antibodies targeting highly variable strain-specific epitopes, generate a network of cross-protection that limits the antigenic diversity of influenza [249, 309, 322]. This model is referred to as "antigenic thrift" in the literature. Recker *et al*. argue in [249] that there is no need for models to "explicitly represent mutation as a process with many degrees of freedom" because that requires making assumptions about the manner and rate at which genetic diversity is generated as well as how it translates to antigenic diversity. The authors instead developed a multi-epitope model which incorporates various alleles encoding the dominant epitope regions and further allows for life-long partial cross-immunity to accumulate as hosts become infected with the different alleles that define a particular antigenic type. The key immunological parameters that the authors investigated were the degree of cross-immunity that results from previous infection by an antigenic type that contains at least one allele in common with the current challenge strain, and the degree of additional cross-immunity arising from accumulated exposure to more than one allele. Their results showed that single-strain epidemics can occur for many different values of these two parameters and further illustrated that explicitly modeling the mutational process is not required in order to generate cyclical epidemics and antigenic type switching.

1.1.3 Vaccination

Vaccination is the primary strategy for the prevention and control of influenza outbreaks. In 1933 Smith, Andrewes and Laidlaw first isolated the influenza A virus from the nasal secretions of infected patients [276]. In 1936 Burnet discovered that the flu virus can be grown in embryonated hen's eggs [101]. These were only two of the many significant developments that led to the first clinical trials of experimental influenza vaccines beginning in 1936 [107]. The first inactivated influenza vaccine only targeted influenza A. Much progress has been made since then and nowadays there are various different types of

influenza vaccines in circulation.

Two different strategies by which influenza vaccines induce an immune response is by introducing either killed or weakened viruses into the vaccinated individual. These result in the inactivated influenza vaccine (IIV) and the live attenuated influenza vaccine (LAIV) respectively. IIVs contain killed viruses, which cannot replicate within vaccinated individuals, and are safe for both healthy and immunodeficient individuals. LAIVs on the other hand contain live virus and are the result of genetic reassortment between some given wild type and some cold-adapted, temperature-sensitive, phenotypically attenuated Master Donor Virus (MDV) strains [157, 257]. LAIVs need to replicate within vaccinated individuals to induce an immune response, and are therefore contraindicated for immunosuppressed individuals. The CDC reports that the immune response to an LAIV is virtually identical to that following natural infection, while an IIV leads to humoral but little to no cellular immunity and also to diminishing antibody titers against the inactivated antigens over time.

While the first influenza vaccine targeted only a single strain of influenza A, nowadays there are vaccines which are designed to immunize against three or four strains of influenza A and B. The valence of an influenza vaccine refers to the number of strains it immunizes against. Until a few years ago the most prevalent influenza vaccine was trivalent and targeted two influenza A strains and one influenza B strain. In 2012 a new vaccine was introduced which targeted four influenza strains [290]. This quadrivalent vaccine protects against two different lineages of influenza B virus (B/Victoria and B/Yamagata), which in recent years have been co-circulating during most seasons and have been shown to be so antigenically different that vaccination of immunologically unprimed children with a strain from one lineage did not induce detectable neutralizing antibodies to viruses from the other [269]. Despite the progress in vaccine production and the growth of influenza vaccination programs since the production of the first influenza vaccine though, the virus' capacity for immune escape makes the continual update of current vaccines necessary. Recent advancements in vaccine technology are attempting to resolve this issue by developing cross-protective and even universal vaccines that can potentially protect against all influenza strains [238]. Such vaccines aim to raise antibodies against viral components of influenza that have been shown to be more conserved compared to the head region of HA and the NA [284], which most current inactivated vaccines target. More specifically, vaccines that target the head region of

HA have been shown to reduce susceptibility to infection but also to be strain-specific and immunodominant, which makes it necessary for them to be updated regularly [221]. Vaccines that target the stalk region of the HA protein have been shown to reduce susceptibility to infection as well as offer cross-protection within and across subtypes in animal models [204]. Vaccines that target influenza's matrix proteins and nucleoprotein have been demonstrated to reduce viral shedding, offer cross-protection and potentially reduce disease severity and infectiousness but have no effect on susceptibility (both in animal models and human challenge studies) [34, 189, 239, 298]. Immunity to these proteins is mediated by T-cells rather than antibodies [147]. Early work by McMichael *et al*. in 1983 suggested that T-cells have a half-life of 3 years [209], while a 2015 study by van de Sandt *et al*. found that T-cell immunity can last as long as 10 years [263]. Finally vaccines that specifically target epitopes of limited variability in the head domain of HA have been shown to be cross-reactive [289]. Mathematical modeling studies by Arinaminpathy *et al*. in 2012 [17] and 2020 [18] , Zhang *et al*. in 2013 [320] and 2014 [321] and Subramanian *et al*. in 2016 [284] have demonstrated the various beneficial effects of cross-protective and universal vaccines in controlling influenza's transmission and evolution.

In 2012 Arinaminpathy *et al*. [17] investigated the results of cross-protective vaccines on the epidemiological and evolutionary dynamics of influenza by incorporatig cross-protective vaccination to the "epochal evolution" model developed by Koelle *et al*. in 2006 [169] and then expanded upon by Koelle *et al*. in 2010 [171]. The epochal evolution model assumes that HA evolves along a neutral antigenic network and that, while most substitution mutations do not result in a significant antigenic change, the accumulation of these genetic mutations can ultimately result in a context-specific mutation that facilitates immune escape. Arinaminpathy *et al*. assumed that cross-protective immunity acquired by vaccination reduces transmission but has no effect on susceptibility. Their results showed that cross-protective vaccination significantly slows down antigenic drift via its transmission-dampening effect, which they attributed to two main reasons. Firstly, by lowering infection prevalence mutants are generated at a reduced rate. Secondly, the lower cumulative incidence implies fewer individuals with HA immunity acquired via infection, thereby eroding the transmission advantage of any antigenically novel strain that might arise. The authors concluded that large scale immunization programs with cross-protective vaccines can be very effective in limiting both seasonal and pandemic sizes and slowing down antigenic drift, but also highlighted the importance of existing

strain-specific vaccines for certain risk groups.

In 2016 Subramanian *et al*. used a two-component model to directly compare the effects of two different vaccination programs, one based on conventional strain-matched vaccines and the other on universal vaccines targeting T-cell antigens, on the epidemiological and evolutionary dynamics of influenza [284]. The first component of their model described the acquisition of immunity via natural infection and vaccination, while the second, interepidemic, component described the loss of immunity through antigenic drift, waning cross-protective immunity and population turnover. Their results showed that large-scale universal vaccination slows down antigenic evolution by dampening seasonal transmission and therefore allowing for little strain-specific immunity to drive selection of new variants. On the contrary, strain-specific vaccines were shown to accelerate antigenic drift. The authors also showed that both strain-specific and universal vaccines can reduce seasonal epidemic sizes, but that universal vaccines were more effective at interrupting transmission. Finally, universal vaccines were shown to reduce the epidemic size in the case of a pandemic, whereas strain-matched vaccines allowed for an increased pandemic size. This is consistent with experimental findings in a ferret challenge study by Bodewes *et al*. in 2011 [37], which showed that vaccination against a seasonal influenza A strain (A/H3N2) reduced the induction of heterosubtypic immunity against the highly pathogenic avian influenza A/H5N1. It is important to underline though that Subramanian *et al*. concluded that universal vaccines should be considered strategically complementary to strain-matched vaccines, rather than their replacement. The sterilizing immunity of strain-specific vaccines is essential for the protection of specific risk groups such as the immunocompromised and the elderly, while the long-lived cross-protective T-cell immunity offered by universal vaccines can significantly reduce transmission and does not contribute to HA selection pressure.

Finally, in a 2020 study Airnaminpathy *et al*. investigated the potential unintended population consequences of universal influenza vaccines [18]. The authors built on previous work by Arinaminpathy *et al*. in which they developed a deterministic, compartmental, age-structured model, which also took into account different levels of prior immunity for each of the age groups, to describe the effects of vaccination on seasonal influenza at a national level in the USA [16]. Arinaminpathy *et al*. incorporated two types of immunity in their 2020 model. Firstly, HA-specific immunity which is acquired either via infection or strain-matched vaccination and reduces susceptibility to infection but is

strain-specific and does not offer any protection against the novel pandemic viruses that the authors investigated. Secondly, cross-protective immunity which can be acquired either via infection or a universal vaccine and offers protection across different subtypes, but does not affect susceptibility to infection. Rather, it is mediated by T-cell immunity and reduces the viral load during infection thereby reducing transmissibility. The authors initially simulated a population that undergoes a universal vaccination program and is then exposed to a seasonal influenza strain, and then tested how such a population would react to a subsequent pandemic strain. Their results showed that at low levels of coverage, universal vaccination may actually increase the pandemic size. They attributed this to the fact that the universal vaccine significantly reduced seasonal incidence (even at low coverage), thereby allowing for a large pool of individuals who have been neither vaccinated nor infected and are consequently very vulnerable to an emerging pandemic strain. At larger coverages though, the authors illustrated that a universal vaccine can reduce both the seasonal epidemic and the pandemic sizes, relative to the absence of vaccination. The authors further studied how a population which has already undergone a seasonal vaccination program, either with a strain-matched or a universal vaccine, as well as a seasonal epidemic, would react to a universal vaccine escape variant. They defined such an escape variant as a virus showing vaccine escape to all the antigenic targets of a universal vaccine but still remaining susceptible to HA-specific immunity. The authors underlined that recent research has demonstrated that single mutations can affect escape both from narrow and broad antibodies against HA [86] and therefore the possibility of such universal vaccine escape variants emerging should not be overlooked. In the case where the vaccination program was simulated using strain-matched vaccines the authors found that the two epidemics, the seasonal one and the subsequent escape variant one, are of comparable size. But in the case where the vaccination program was simulated with a universal vaccine, while the first epidemic size was smaller compared to the case of vaccination with a strain-specific vaccine, the subsequent epidemic brought on by the escape variant was considerably larger. The authors therefore concluded that a vaccination program which combines conventional, strain-matched vaccines with universal vaccines could offer the best protection, especially at large coverages.

It is important to have the appropriate terminology to describe the effects of a vaccine. As Shim and Galvani point out in [271], the terms vaccine efficacy and vaccine effectiveness are sometimes used interchangeably in the modeling literature. For the sake of clarity and consistency, throughout this thesis we will refer to the reduction in susceptibility of vaccinated individuals as the vaccine efficacy. We will use vaccine effectiveness

to refer to the reduction in the transmission rate of an average individual in a population that consists of both vaccinated and fully susceptible individuals compared to the transmission rate of an average individual in a population that consists only of fully susceptible individuals. These definitions are in accordance with [271] and will be useful to our work because they highlight that efficacy refers only to a single-host level while effectiveness also takes into account the indirect protection offered both to vaccinated and unvaccinated individuals as a result of the lower infection prevalence in a population with a vaccination program. A vaccine's effectiveness is often estimated using a case test-negative design, which is defined in the following way [109]. The study subjects are patients who visit medical institutions due to influenza-like illness (ILI) during the influenza season. Those who test positive for influenza are classified as cases and those who test negative as controls. Since the number of individuals who have already received the vaccine is known for each category, the vaccine effectiveness (VE) is then calculated as $VE = (1 - \text{vaccination odds ratio}) \times 100\%$.

Routine annual vaccination against influenza is now a standard measure as part of many countries' public health programs. Despite the success of vaccination in reducing the burden of influenza, vaccines do not affect all individuals equally. The vaccine-induced protection is critically dependent on an individual's immune status and history. For instance, antibodies from a previous exposure can inhibit the effects of the vaccine. This heterogeneity in the strength of the vaccine-induced immunity leads to varied levels of vaccine efficacy among vaccinated individuals, and could even lead to as many as 60-70% of elderly or immuno-compromised individuals having little to no response to the vaccine [3]. Moreover, the vaccine-induced protection may be hindered by the antigenic drift of the virus. In the Northern hemisphere, where the flu season is from November to April, the decision of which strains the next season's vaccine is going to include is made by the WHO by February of the current season. This is necessary in order to give adequate time for the vaccine manufacturing and distribution process, but also means that the virus has enough time to undergo antigenic changes. Anti-influenza drugs, such as oseltamivir, have also been developed but vaccination still remains the main method of controlling influenza.

1.2 Modelling approaches

1.2.1 Between-host models

The study of infectious disease data began with the work of John Graunt in his 1662 book "Natural and Political Observations made upon the Bills of Mortality", as Brauer reports in [48]. The Bills of Mortality were weekly records of numbers and causes of death in London parishes which began in 1592 and were then kept continuously from 1603 on. Infectious disease modelling also has a very long history, starting with the pioneering work of Daniel Bernoulli in 1760 [33]. Bernoulli developed what is regarded as the first epidemic model in order to study the benefits of inoculating against smallpox based on data regarding its incidence and case fatality, as well as the safety of variolation. Many years after that the public health physician Sir Ronald Ross developed what eventually became one of the most influential modeling frameworks in epidemiology. In the second edition of his book *The Prevention of Malaria* published in 1911, Ross introduced a simple compartmental model to study the dynamics of the transmission of malaria between mosquitoes and humans. At the time it was generally believed that malaria could not be eliminated so long as mosquitoes were present in a population. Ross instead showed that reducing the mosquito population below a critical threshold would be sufficient to eliminate malaria, and subsequent field trials supported his results, leading to significant advancements in malaria control. More specifically, as Bacaër reports in his book *A Short History of Mathematical Population Dynamics* [23], one of the mathematical models published by Ross in 1911 consisted of a system of two differential equations, one to describe how the number of humans infected with malaria $I(t)$ varies with time and one to describe how the number of mosquitoes infected with malaria $i(t)$ varies with time t. Ross considered the non-trivial steady state solution to his system of equations and found an expression for a critical threshold $n^\star$ for the mosquito population, above which $I > 0$ and $i > 0$ and therefore the disease becomes endemic. He concluded that if the total number of mosquitoes n is reduced below this critical level $n^\star$ then the only remaining steady state of his system would be the trivial one, namely $I = 0$ and $i = 0$, and therefore malaria would be eradicated. It is of particular importance that Ross's work showed that it is not necessary to exterminate all mosquitoes in a population in order to eliminate malaria.

In a sequence of three papers between 1927 and 1933 [163–165], Kermack and McKendrick extended Ross' work on compartmental disease models by introducing new ideas such as the stochastic aspect of infection and recovery and generalizing already

published ideas such as the effects of an individual's age of infection, which had already been introduced by Ross and Hudson in 1917 [260]. In what is nowadays referred to as the standard Susceptible-Infected-Recovered (SIR) model [90], susceptible individuals S come into contact with infected individuals I and become infected at a constant per-capita rate β. Infected individuals recover after an average of $1/\nu$ days, having gained full immunity. It is assumed that the initial population of N individuals remains fixed and that there are no births or natural deaths. While this model has become known as the Kermack-McKendrick epidemic model, it is actually only a special case of their 1927 model [163]. In the more general model both the infectiousness and the recovery rate depend of the time since infection. We will present the SIR model in more detail in chapter 2, where we will extend it to study the spread and evolution of influenza in a heterogeneous population that consists of fully susceptible as well as vaccinated individuals.

The concept of $\mathscr{R}_0$

An important parameter in disease modeling is the basic reproduction number of a pathogen, which is denoted as $\mathscr{R}_0$ and defined as the expected number of secondary cases per primary case in an otherwise uninfected population. Dietz reports in [79] that the concept of $\mathscr{R}_0$ goes back to demography, where it is called the net reproduction rate, and can be found in publications as early as 1886. Macdonald adapted it and introduced the "basic reproduction rate" to epidemiology in 1952 [202] in the context of malaria. In 1964 Smith used Macdonald's definition of $\mathscr{R}_0$ to calculate the minimum population proportion that needs to be vaccinated to stop the transmission of arboviruses. In 1990 Diekmann, Heesterbeek and Metz developed a mathematically rigorous framework for $\mathscr{R}_0$ and proposed to name it the "basic reproduction number" instead of "rate", as it is dimensionless [76].

As Heesterbeek argues in [149], "the most fundamental step in the development of $\mathscr{R}_0$ in epidemiology was taken in the seminal paper by Kermack and McKendrick in 1927", even though they did not attach a symbol or a name to their threshold concept. Heesterbeek enumerates the assumptions made by Kermack and McKendrick in their 1927 paper [163]:

1. A single infection triggers an autonomous process within the host.

2. The disease has only two possible outcomes: complete immunity or death.
3. Contacts are according to the law of mass-action.
4. All individuals are equally susceptible.
5. The population is closed.
6. The population size is large enough to justify a deterministic description.

Let $S(t)$ be the density of susceptibles in the population at time t. The time that has elapsed since an individual became infected is called the infection age and denoted by τ. Then the above assumptions lead to the following integral equation:

$$\dot{S}(t) = S(t) \int_0^\infty A(\tau)\dot{S}(t-\tau)d\tau \tag{1.1}$$

where $\dot{S}$ represents $\frac{dS}{dt}$ and $A(\tau)$ is defined as the expected infectivity of an individual with infection age τ. To better understand this equation we note that given the closedness of the population the quantity $-\dot{S}(t)$ is precisely $I(t,0)$, which is the density of new infected individuals emerging at time t. This leads to:

$$-\dot{S}(t-\tau) = I(t-\tau,0) = I(t,\tau)$$

where $I(t,\tau)$ describes the incidence of infected individuals at time t who have been infected for a time τ. We can then reformulate equation (1.1) as the following system:

$$\frac{\partial I}{\partial t} + \frac{\partial I}{\partial \tau} = 0 \tag{1.2}$$

$$I(t,0) = S(t) \int_0^\infty A(\tau)I(t-\tau,0)d\tau \tag{1.3}$$

We note that the expression

$$\Lambda(t) \coloneqq \int_0^\infty A(\tau)I(t-\tau,0)d\tau$$

is called the force of infection and describes the per capita probability per unit time to become infected. In order to obtain a formula for $\mathscr{R}_0$, we may consider the steady state at the absence of an infection. Then $S(t)$ in equation (1.1) may be replaced with the constant S_0, which denotes the density of the population at the start of the epidemic where every

individual is assumed to be susceptible. This leads to the following expression for $\mathscr{R}_0$:

$$\mathscr{R}_0 = S_0 \int_0^\infty A(\tau) d\tau \tag{1.4}$$

If we assume as in the SIR model that the per capita transmission rate β and recovery rate ν remain constant both over the real time t and the infection age τ, and that the probability that an infected individual remains infectious at infection age τ follows an exponential distribution, then $A(\tau)$ is given by the expression:

$$A(\tau) = \beta e^{-\nu\tau}$$

Substituting this into equation (1.4) and performing the integration leads to the well known formula for the SIR model

$$\mathscr{R}_0 = \frac{\beta S_0}{\nu}$$

We note that given the simplicity of the SIR model we may also arrive at the same expression for $\mathscr{R}_0$ in a more intuitive way. Since an infection lasts for an average of $1/\nu$ time units and an infected individual transmits the disease at a per-capita rate β, then each infective makes on average βS_0 successful transmissions per unit of time and does this for an average of $1/\nu$ units of time. This again leads to

$$\mathscr{R}_0 = \frac{\beta S_0}{\nu}$$

The $\mathscr{R}_0$ can be used to answer critical questions such as when will a primary case lead to an epidemic. It is straightforward to show that the disease will spread if $R_0 > 1$ and will go extinct otherwise. We will demonstrate this in chapter 2, where we will give a more detailed analysis of the SIR model and its properties.

Evolution at the between-host level

In 1987 Pease argued that a significant obstacle to modeling influenza using simple compartmental models such as the classical SIR is antigenic drift [228]. Influenza outbreaks are often characterized by the co-circulation of interacting strains with different phenotypes, where infection by one strain might lead to various degrees of cross-protection from other strains. It is therefore important to understand the factors that drive strain

turnover and evolution.

In 1981 Levin and Pimentel published a paper in which they investigated the competition between two types of parasites for available hosts [188]. Since then this type of "competition for available hosts" model and its extensions have been used extensively in the influenza modeling literature to describe the effects of the competition between co-circulating strains. As Kucharski *et al*. report in [177], early models assumed that infection from one strain confers total immunity to the other for the duration of the infection. In 1964 Elveback *et al*. studied the competition dynamics between two strains under this assumption of total interference by extending the discrete, single-strain Reed-Frost epidemic model [93]. In 1979 Dietz adapted the 1964 Elveback *et al*. model to continuous time, extended it to include population birth and death rates and then studied the steady states of the resulting system and their stability [78].

Motivated by the cross-protective immune responses induced by natural infection with a given strain of influenza, Castillo-Chavez *et al*. in 1989 [54] and Andreasen *et al*. in 1997 [14] extended the classical SIR model to allow for the co-circulation of cross-reactive strains where infection by one strain leads to partial cross-immunity from the others. In their 1989 paper, Castillo-Chavez *et al*. studied a two-strain discrete-time model that included partial cross-immunity, age structure and age-specific mortality. The authors found that the model exhibited very complicated dynamics, such as damped oscillations, sustained periodic behavior and chaotic behavior. Motivated by the difficulty in analyzing such a model, the authors also extended the Dietz-Elveback continuous time model for homogeneous populations to include different degrees of cross-immunity.

In 1994 Gupta *et al*. and Gupta and Day investigated the impact of the antigenic diversity of malaria on the parasite's transmission dynamics [126, 129]. The authors report that the average age of humans at their first infection with malaria is typically less than 1 year in most endemic areas, and that this has been interpreted as evidence of the parasite's high transmissibility. A different interpretation though, which can also explain why there can be a high risk of infection and prevalence even when the parasite transmissibility is low, is that a long period is required to develop immunity due to the antigenic diversity of the parasite. In this framework, immunity is acquired only after exposure to many different circulating strains. Gupta *et al*. developed an age-structured model which consisted of a system of partial differential equations and incorporated overlapping

categories of immune and exposed hosts and applied it to epidemiological data of five antigenically distinct strains, collected in a highly malarious area of Papua New Guinea. Their results showed that infection by a given malaria strain induces some degree of strain-specific, infection-blocking immunity and that reinfection is often a consequence of exposure to different, independently transmitted strains (though this does not preclude the possibility of reinfection with the same strain). In 1998 Gupta *et al*. demonstrated that the co-circulation of several antigenically diverse pathogens can result in very complex dynamics [127]. The authors showed that a sufficiently small level of cross-immunity led to all strains coexisting in the host population with stable abundance. A sufficiently high level of cross-immunity on the other hand led to stable discrete strain structure, which was characterized by a set of strains which share no alleles (and are assumed to not interfere with each other's transmission or within-host fitness) dominating the population. Finally, at intermediate levels of cross-protection the authors found no stable strain structure. Instead, the relative proportions of the different strains exhibited cyclical or chaotic dynamics. In 1999 Lin *et al*. used a simpler "linear three-strain model", in which one of the strains confers partial cross-protection to the other two while these two induce no reciprocal cross-reaction, to show that herd immunity alone can lead to sustained oscillations in the case of influenza A [190].

A major drawback of various multi-strain models is that their analysis can become very complicated as the number of strains increases. In 2002 Gog and Grenfell developed a model that was capable of capturing the dynamics of a large number of antigenic strains under the assumptions of reduced transmissibility and polarized immunity, which states that partial cross-immunity acts to render only some of the hosts totally immune [121]. The authors initially used a linear strain space to describe the mutation and cross-immunity interactions between strains, but also studied the effects of a two-dimensional strain space. Their results showed that, given a short-infection/long host-lifetime time scale, strains occur in clusters but are transient due to strain-specific immunity accumulating and mutation giving rise to increasingly distant strains.

Many early multi-strain models assumed that strain turnover is mediated by the loss of immunity due to the birth and death of hosts. The *Pease* Susceptible-Infective-Recovered-Susceptible (SIRS) model published by Pease in 1987 [228] assumed instead that strain turnover is governed mainly by the frequent introduction of novel genetic variants in the population to which hosts only have partial immunity. This shift in perspective has proven

to be very influential in the field of evolutionary epidemiology. As Andreasen and Gog report in their review of Pease's 1987 paper [13], the *Pease* model was actually the "first epidemic model that could account for how the association between influenza and its human host evolved over long periods" and "hinged on the view that the epidemiological, immunological and evolutionary dynamics cannot really be separated". We note though that Pease assumed that only one strain may circulate in the population at any given time. Motivated by Pease's evolutionary model and by experimental data which showed that the probability of recovered individuals being reinfected by new circulating strains increases linearly with the time since last infection, Casagrandi *et al*. developed the Susceptible-Infective- Recovered- Cross-immune (SIRC) model in 2006 [53]. The new compartment C describes individuals who have already been infected by a given strain and are therefore partially protected from antigenically similar strains. Given a dominant circulating strain, individuals in R are those who recovered from the dominant strain and are currently completely immune to it. After some period of time though, those individuals move to the C class because they now only have partial immunity to the new dominant strain that has emerged since they were last infected. The resulting framework of a moving frame in immune space is exactly the same as in Pease's approach. In 2004 Grenfel *et al*. created the term "phylodynamics" to describe the melding of epidemiology, immunodynamics and evolutionary biology [125].

1.2.2 Within-host models

In recent years the advancements made in quantitative virology have helped the development of mathematical models which can describe the dynamics of influenza within a particular host or cell culture. This within-host modeling of influenza viruses has such a relatively short history that in fact, according to Baccam *et al*. in [24], prior to 2006 there appear to have only been three papers written in English on the dynamics of influenza within a single host. The first of these was in 1976, and introduced a compartmental model of influenza A dynamics in experimentally infected mice [182]. While the model captured well the trajectory of the viral load during the course of the infection, its compartments did not correspond to the host immune response and therefore could not explain how immunological factors affect viral dynamics. The second paper was published in 1994 and introduced a model that was a system of ten ordinary differential equations (ODEs), each describing the dynamics of cells that are involved in the immune response [36]. The drawback was the number of parameters, which was more than sixty due to

the author's attempt to capture the complexity of the human immune system. The third paper was published in 2005 and introduced a cellular automaton model that described the effects of spatial heterogeneities in the spread of influenza A within a single infected host [27].

A significant amount of experimental and mathematical research has been done on the within-host dynamics of influenza since the work by Baccam *et al*. in 2006. Here we will briefly review the general form of one of the simplest and most influential models of within-host influenza kinetics published by Baccam *et al*. in 2006 [24]. We will refer to this model as the TIV model throughout this thesis. In this section we will only describe the model and mention some of its properties. In chapter 3 we will go into more detail regarding the TIV model, since we will use it as the foundation of a within-host model we will develop to study the dynamics and evolution of influenza within-host. The TIV model consists of a series of ODEs that describe how the populations of target cells, infected cells and virions change throughout an individual's infection. Target cells T become infected by virions V at some rate β and enter the infected compartment I. Infected cells I release new progeny virions at some rate p and die at some rate δ, which means that their lifespan is exponentially distributed with a mean of $1/\delta$ days. It is assumed that infected cells start releasing new virions as soon as they become infected. Finally free virions that are circulating within the host are cleared by the immune system at some rate c. The immune response is incorporated implicitly in the TIV model via the death rate of infected cells δ and the clearance rate of free virions c, and is assumed to be constant throughout the infection.

The TIV model could be considered the within-host conceptual analogue of the classical SIR model from population disease modeling. The target cells can be mapped to the susceptible hosts at the between-host level and the infected cells to the infected hosts. Moreover in the TIV model infection always leads to cell death, which is mathematically equivalent to infection leading either to host death or to recovery with no chance of reinfection in the context of the SIR model. Finally the infection of target cells by virions in the TIV model and the inability of infected cells to directly infect other cells can be mapped to the infection pathway of a vector-borne disease in the between-host context. Both models have been very influential in the influenza modeling literature, partially because they can be used to extract a great deal of information about the research topics

at hand while maintaining their simplicity.

Similarly to population disease modeling, an important parameter in within-host disease modeling is the basic reproduction number $\mathscr{R}_0$, which in this context is defined as the average number of secondary infections that would be caused by the introduction of a single infected cell into a population of fully susceptible cells [195]. We note that this definition is equivalent to the population-level $\mathscr{R}_0$ which we defined earlier in section 1.2.1. The TIV model's simplicity means that the $\mathscr{R}_0$ can be obtained by multiplying the number of free virions that an infected cell produces over its lifespan by the number of cells that a free virion infects over its lifespan. Therefore in the TIV model we have:

$$\mathscr{R}_0 = \frac{p\beta T_0}{c\delta}$$

where T_0 denotes the initial target cell population.

The TIV model has proven to be a very powerful tool in analyzing within-host influenza dynamics [65]. This is partially because the simplicity of the model agrees with the simplicity of viral titer curves, which have been shown experimentally to grow exponentially until they reach a peak and then decay exponentially [28]. More complex models have been developed, and we will briefly discuss some of them here.

In 2006 Baccam *et al*. added a delay in the virion production by infected cells [24]. This latency phase, which is often denoted E in the literature, occurs between the infection of a target cell by a virion and the production of new virions by the newly infected cell. We will refer to the TIV model with delay as the TEIV model throughout this thesis. Hancioglu *et al*. in [136] and Lee *et al*. in [185] attempted to incorporate the complexity of the immune response into the TIV model and considered, among others, the actions of cytotoxic T-cells, antibodies and antibody-producing plasma cells. While their models are more biologically accurate than the much simpler TIV model, their results are limited by overparametrization. This is an inherent issue with within-host models of this form, since obtaining the appropriate experimental data to inform the model parameters is very difficult given the many different and interacting layers of the immune response. Therefore many researchers have opted for a better balance in this trade-off between capturing biological complexity and inferring parameters from data. In 2010 Saenz *et al*. extended the TEIV model by explicitly incorporating the innate immune response via the action of

type I interferon (IFN) [262] and tested it using a dataset of viral load and infected cell levels in horses. Their results showed that the inclusion of IFN alone was enough to describe the disease dynamics, whereas a model without it could not fit the data adequately.

A different class of TIV-based models are those which consider cell tropism, defined as the degree to which different types of host cells support viral replication. In 2010 Dobrovolny *et al*. extended the TEIV model to include two different target cell populations, a default and a secondary [83]. The authors' motivation was to capture the preferential binding of different influenza strains to cells depending on the presence of certain receptors on their surface. They also used their model to implicitly capture the immune response by having the secondary target cell population represent cells that are protected from infection at various degrees. In 2012 Reperant *et al*. investigated the effects of spatial structure and cell tropism by developing a TIV-based model with two different target cell populations (which also included the actions of interferon, cytotoxic T cells and antibodies) and applying it to three different respiratory compartments [253]. Each compartment was characterized by its unique set of initial conditions, which included the initial target cell population and the virus clearance rate and pathogenicity. The authors allowed virions and interferon to flow between compartments. Their work described how influenza spreads in a spatially-structured respiratory tract and shed light into the different ways that disease progression may occur.

Evolution at the within-host level

Theoretical and experimental research has shown that within-host evolution can have strong effects not only on the disease expression within the infected individual but also on the epidemiology of pathogens [5]. A common strategy to study evolution in vitro, which we also use in this thesis, is to model a within-host infection with two or more competing strains [5, 229, 235, 252]. The strains are often assumed to be phenotypically distinct, and can differ in traits such as their replication rate or virulence. Depending on the research question at hand, the strains might be introduced into the host at the same or different times during the infection or the infection might start with only a resident or wild type strain present and a mutant strain might emerge stochastically later in the infection. This strategy is easy to implement with TIV-like models because it simply requires the model to be broken down into sub-compartments which correspond to the different viral strains.

1.2.3 Cross-scale models

So far we have briefly presented some published models which have been vital for the understanding of disease dynamics either at the between- or the within-host scale. A generic way to define and differentiate these two scales is that between-host models describe the dynamics of a disease by keeping track of the number of susceptible and infected individuals in a population, while within-host models describe how a disease spreads within one infected individual, usually by following the number of target cells, infected cells and virions inside the host (at minimum). But researchers have made the observation that the transmission of a virus is largely affected by the disease expression within infected individuals, which is in turn determined by the within-host viral dynamics. This has led to the development of models which link the between- and within-host scales. We will refer to these as cross-scale models throughout this thesis, but we note that they are often called nested models in the literature [68, 119, 210].

For the purposes of this thesis, we will focus on cross-scale models which explicitly link within- and between-host dynamics. As a result we require cross-scale models to include an explicit dynamical model at the within-host scale, so the equations which describe the between-host dynamics need to keep track of the age of infection. This is because between-host parameters such as the transmission rate, the virulence and the recovery rate need to rely explicitly on within-host quantities such as the viral load and the number of healthy target cells, which change throughout an individual's infection. We note that various models have been published which consist of a population-level model that only implicitly depends on within-host processes. While such models are not the primary focus of this thesis, they have yielded insightful results and we will give a short overview of some of them.

We will briefly discuss some of the earliest cross-scale models which do not explicitly link the within- and between-host scales. In 1994 Nowak and May published a model for the evolution of parasitic virulence which included superinfection [219]. They extended an SI-type model to include superinfection by adding multiple infectious compartments that corresponded to a variety of parasites, each with a different virulence value. Nowak and May assumed that in the case of a superinfection a more virulent strain always takes over a host infected by a less virulent strain. Therefore while they did not explicitly consider the within-host competition dynamics between parasites of different virulences that infect the same host, their definition of superinfection still inherently relied on within-host

processes and had an effect on between-host transmission. It is interesting to point out that even with this arguably simple definition for superinfection, Nowak and May's model still exhibited some very complicated dynamics. In 1995 May and Nowak published a model for the evolution of parasitic virulence that included coinfection [206]. The authors again extended an SI-type model to include multiple infectious compartments which corresponded to different parasites invading a population. They assumed that individual hosts can be coinfected by a number of different parasites with different virulence values and that there is no competition among the different parasites within the same host. In their model the infectivity of each parasite was completely unaffected by the presence of other parasites in the same host. As May and Nowak pointed out in their 1995 paper, their superinfection [219] and coinfection [206] models "represent the two opposite extremes in situations where hosts experience multiple infection with many different strains of a parasite". It is not surprising then that they yield very different results when it comes to the number and virulence range of persisting parasites.

We will now briefly present some published work in cross-scale modeling and discuss its findings. Our goal here is to highlight some interesting results which suggest that cross-scale models can be crucial for the understanding of influenza's dynamics, but also to point out some of the challenges inherent to cross-scale modeling.

In 2009 Chen *et al*. published a paper in which they investigated the effects of within-host viral kinetics and exhaled droplet size on the indoor transmission of influenza [63]. The authors utilized a within-host TIV-type model to obtain the viral load throughout an individual's infection with influenza A. They then defined a droplet generating function for the amount of a host's exhaled virus-carrying bioaerosol droplets per time, which depended on the within-host viral load as well as the size and number of exhaled particles either via coughing or sneezing. The amount of a host's exhaled droplets per time was then used to obtain a between-host transmission rate that depended on the age of the infection. Therefore the authors' droplet generating function was key to their model's results, as it provided the link between the within-host viral load and the population-level transmission rate. The authors used experimental data to fit this function, and found that a linear dependence on the viral load gave satisfactory results. As they pointed out though, their results are difficult to validate due to the scarcity of experimental data on the amount of exhaled virus-carrying droplets in indoor environments. A similar breath plume model published by Halloran *et al*. in 2012 also found that a linear relation

between the viral load and the concentration of exhaled pathogens per unit volume of air could capture well a different empirical dataset [134]. It is interesting to note though that in a 2020 study Leung *et al*. reported that the majority of influenza patients they tested did not shed any PCR-detectable virus in respiratory droplets or aerosols during a 30-minute breath exhale collection [187]. The few patients that shed virus only did so in very low amounts and some of them did not cough at all during the procedure. As the authors highlight, such a finding could indicate that transmission via the inhalation of viral particles requires prolonged closed contact. It also implies that further experimental testing is needed to quantify the effects of coughing and sneezing. An earlier study published by Yan *et al*. in 2018 found no detectable viral RNA in respiratory droplets in the majority of influenza patients tested, but detected influenza RNA in fine aerosols in the majority of patients [317]. We note that both sets of researchers used the same human source bioaerosol sampler (named Gesundheit-II) for their 30 minute breath exhale collections and both used reverse transcription PCR to quantify the viral RNA in the breath samples. The discrepancy in their findings further highlights the need for additional experimental testing on the amount of viral load in exhaled breath, coughs and sneezes. Accurate estimates of this could offer very valuable insight into the link between viral shedding and infectiousness, and would therefore have a significant impact on cross-scale models such as the ones we discussed by Chen *et al*. [63] and Halloran *et al*. [134].

In 2013 Handel *et al*. used a cross-scale model to study the effects of temperature on the between-host fitness of various strains of influenza A [137]. To describe between-host transmission they used a system of coupled differential equations which kept track of the age of infection and which could also take into account both direct and environmental transmission routes. The authors used a TIV model to inform the between-host transmission rate as a function of the age of infection. More specifically they considered three different scenarios: the transmission rate being a linear function of the within-host viral load, the transmission rate being proportional to the logarithm of the viral load and the transmission rate being proportional to the viral load multiplied by total amount of shedding (the latter was described as a sigmoid function of the viral load). The authors cited previously published experimental work to justify all three scenarios. Based on these they developed different expressions for the population-level $\mathscr{R}_0$ of the virus and used them as a measure of the virus' between-host fitness. Their analysis showed evidence for a trade-off between virus persistence at low vs high temperatures. Depending on the main route of transmission (direct or environmental) and the presumed link between the transmission rate and the viral load, the authors showed that strains which had high

persistence at high temperatures and therefore reached high viral loads within-host were in some cases less fit at the population-level than strains which had a smaller persistence at high temperatures, and thus were not able to replicate as effectively within-host. This work illustrates a significant advantage of cross-scale models, namely that they offer a way to directly compare the effects of factors from different scales on the question at hand. It further highlights the cross-scale models' usefulness when investigating competing selection pressures from different scales, since in this case single-scale models might even fail to give accurate qualitative predictions. Handel *et al*. emphasized the need for further experimental data in the discussion section of their paper. We note that this is a common issue with cross-scale models, as they require appropriate data from both the between- and within-host scales. The results of Handel *et al*. are sensitive to the presumed relationship between the transmission rate and the viral load, but the scarcity of experimental data makes all three of their choices reasonable. Therefore, it would be very difficult to use their results in order to make accurate quantitative predictions. This is not a criticism of the authors' work though, as their analysis was not aimed at making quantitative predictions. We simply highlight the difficulty in obtaining experimental datasets that can accurately inform cross-scale models.

1.3 Thesis Motivation

There are two key papers which motivated this thesis, and the aim of both was to discuss some interesting open problems in disease modeling. The first was published by Gog *et al*. in 2015 and reviewed some of the main challenges in modelling pathogen dynamics both within-host and across-scales [122]. The second was published by Wikramaratna *et al*. also in 2015 and focused on the main challenges in modeling interacting strain dynamics [308].

Some of the key questions that have been inspired by these papers and that this thesis aims to answer are:

- How does vaccination with a strain-specific vaccine affect the spread and evolution of influenza within-host, between-host and across scales? This is the main question that drives our work.

- Is the explicit linking of the scales necessary to describe the effects of the competing factors from different scales which determine how vaccination affects the epidemiological and evolutionary dynamics of influenza? Can we capture the same dynamics using a simpler single-scale model?
- How can we simulate efficiently a computationally intensive cross-scale model?
- Given the scarcity of empirical data, how can we model the within-host emergence of a mutant influenza strain? Is it enough to use a TIV model with two-strain structure? If not then what are the minimum extensions necessary (innate immunity, adaptive immunity, spatial structure)?

1.4 Thesis Summary

One of our main goals in this thesis is to develop a cross-scale vaccination model for the epidemiological and evolutionary dynamics of influenza within a single season. We will model the evolution of influenza as the emergence and subsequent growth of a mutant strain, either at the within- or the between-host scale. We are particularly interested in comparing the results of our cross-scale vaccination model to those of a between-host vaccination model that describes the population-level emergence dynamics of a mutant strain and the subsequent competition dynamics with its parent resident strain.

In Chapter 2 we will develop a two-strain SIR model that includes vaccination and describes the emergence dynamics of a mutant strain in the population as well as the competition dynamics with its parent resident strain. We will initially treat the appearance time of the mutant strain as a fixed parameter of our model and study its effect on the spread and final size of the mutant. Afterwards we will develop an expression for the probability of a mutant strain emergence at any given time throughout the epidemic. Finally we will vary the efficacy of the vaccine against each strain as well as the vaccination coverage to identify which conditions are the most beneficial for the emergence and successful spread of a mutant strain in the population.

In Chapter 3 we will develop a two-strain within-host model to describe the emergence dynamics of a mutant strain and its subsequent competition dynamics with the parent resident strain. We will begin by extending the TIV model published by Baccam *et al.* in 2006 [24] to include two strains and investigate how the within-host time of appearance

of the mutant strain affects its survival and growth. Our analysis of the two-strain TIV model will motivate us to adapt a slightly more complicated model published by Saenz *et al*. in 2010 [262] because it incorporates explicitly the action of the innate immune response. We will extend the *Saenz* model to include two strains and examine how the additional components of our extended *Saenz* model change the emergence dynamics of the mutant strain. We will then develop an expression for the within-host emergence density of the mutant strain and finally we will add vaccination to our two-strain *Saenz* model and show how it affects the emergence and subsequent competition dynamics between the two strains.

In Chapter 4 we will develop a cross-scale model to describe the epidemiological and evolutionary dynamics of influenza within a single season, which does not yet incorporate the effects of vaccination. The model that we will use as the foundation of our own cross-scale model was published by Coombs *et al*. in 2007 [68]. Our cross-scale model will link explicitly the between- and within-host scales via the between-host transmission rates, which we will assume are linear functions of the within-host viral load. The between-host tier of our cross-scale model will be a simple SI model while the within-host tier will be our extended *Saenz* model. Our analysis will initially focus on how the within-host parameters affect the population-level fitness of the two strains. We will then examine closely how the within-host emergence time and the age of infection affect the between-host transmission rates, as this is what differentiates our cross-scale model from standard population-level models that only consider constant transmission rates. Finally we will study our model's results using three different functional forms for the within-host emergence density of the mutant strain.

In Chapter 5 we will incorporate vaccination to our cross-scale model. We will capture the effects of vaccination simply as an increase in one of the within-host strain-specific parameters, specifically the viral clearance rates for the resident and the mutant strains. Then by varying the within-host clearance rates as well as the vaccination coverage, the fitness of the mutant strain, the within-host mutation rate and the assumed form of the within-host emergence density we will study the resulting impact on the final sizes of the two strains in the population and identify which conditions promote the within-host emergence and growth and subsequent population-level spread of a mutant strain.

Chapter 2

A between-host model for the evolution of influenza

2.1 Introduction

In this chapter we will present a population-level model for the epidemiological and evolutionary dynamics of influenza. We will develop a model which describes the emergence dynamics of a mutant strain in a population during a single influenza season, and the subsequent competition dynamics with its parent resident strain. We will further examine how vaccination affects the emergence potential and growth of the mutant strain and arrive at the perhaps counter-intuitive conclusion that intermediate values of immunoprotection are the most beneficial for the emergence and spread of the mutant.

2.2 Background

We will first present the well-established SIR model, which we will use as the foundation of our own model in section 2.3. We discussed the SIR model in chapter 1, but in section 2.2.1 we will explore it in further detail and analyze some of its key results. Then in section 2.2.2 we will discuss a published extension of the SIR model that includes vaccination.

2.2.1 The classical SIR model

The classical SIR model is defined by the following differential equations:

$$\frac{dS}{dt} = -\beta SI \tag{2.1}$$

$$\frac{dI}{dt} = \beta SI - \nu I \tag{2.2}$$

$$\frac{dR}{dt} = \nu I \tag{2.3}$$

with the initial conditions

$S(0) = S^0 \in \mathbb{R}_+$, $I(0) = I^0 \in \mathbb{R}_+$ and $R(0) = R^0 \in \mathbb{R}_+$

Here $S(t)$ denotes the fraction of susceptible individuals in the population at time t, $I(t)$ the fraction of infected individuals and $R(t)$ the fraction of recovered individuals. The total size of the population is $N = 1$ and remains constant throughout the duration of the epidemic. The parameter $\beta > 0$ is the transmission rate of the disease, and is often regarded as the product of the contact rate and the probability of infection given a contact with an infectious individual. The parameter ν is the recovery rate of infected individuals, from which it follows that $1/\nu$ is the average length of the infectious period. We note that there is an equivalent formulation of the SIR model where $N > 1$, $S(t)$, $I(t)$ and $R(t)$ represent numbers of individuals and the units of the transmission rate β and the recovery rate ν are per-capita. However in this chapter we will use the $N = 1$ formulation.

The classical SIR model is based on a number of underlying assumptions:

- The only way that an individual can leave the susceptible compartment is to become infected, and the only way that an individual can leave the infected compartment is to recover. Therefore the total population $S(t) + I(t) + R(t) = N = 1$ is fixed.
- Those who recover from the disease gain full immunity.
- The transmission rate is constant among all individuals of the population because all members of the population mix homogeneously with one another, and each member has exactly the same probability of becoming infected given a contact with an infected individual.

- The infectious period is exponentially distributed with a recovery rate that is constant among all infected individuals. Therefore variables such as age, sex, social structure and age of infection do not have any effect on the dynamics of the disease. It is interesting to note that Kermack and McKendrick's general epidemic model in [163] allows for a dependence on the age of infection, which in turn allows for recovery rates that are not exponentially distributed.

We will now present some established results of the SIR model. This is because we will derive some similar results for our extended SIR model in section 2.4. As we mentioned in chapter 1, one of the most important epidemiological parameters in infectious disease modeling is the basic reproduction number $\mathscr{R}_0$. In the classical SIR model, the formula for $\mathscr{R}_0$ is

$$\mathscr{R}_0 = \frac{\beta}{\nu}$$

where β is the rate at which new cases are produced by an infectious individual in a fully susceptible population ($N = S(0) = 1$) and $1/\nu$ is the average infectious period.

In order for an epidemic to occur the number of infected individuals needs to increase at the onset. This is equivalent to requiring $dI/dt > 0$ at the initial stages after $I(0)$ infectives have been introduced into the population. Then by equation (2.2)

$$\beta SI > \nu I$$
$$\frac{\beta S}{\nu} > 1$$

and since at the outset of the epidemic it is valid to approximate $S(0) = 1$, then the disease can invade if and only if

$$\mathscr{R}_0 > 1$$

2.2.2 Adding vaccination to the classical SIR model

We will now discuss an extension of the SIR model that includes vaccination. Vaccination can be incorporated into the classical SIR model via the simple addition of a new compartment, usually named V, designated to keep track of the fraction of vaccinated individuals

in the population. Some of the earliest SVIR models appear in [3, 19, 176, 194, 271], though the history of incorporating vaccination in epidemiological models is considerably longer [9, 80]. An example of an SVIR model for an acute infection in a closed, homogeneous population (adapted from [3]) takes the following form

$$\frac{dS}{dt} = -\beta SI \tag{2.4}$$

$$\frac{dV}{dt} = -(1-\sigma)\beta VI \tag{2.5}$$

$$\frac{dI}{dt} = \beta SI + (1-\sigma)\beta VI - \nu I \tag{2.6}$$

$$\frac{dR}{dt} = \nu I. \tag{2.7}$$

with the initial conditions

$S(0) = S^0 \in \mathbb{R}_+$, $V(0) = V^0 \in \mathbb{R}_+$, $I(0) = I^0 \in \mathbb{R}_+$ and $R(0) = R^0 \in \mathbb{R}_+$

The SVIR model presented in equations (2.4)-(2.7) is a simplification of the original SVIR model by Alexander *et al.* in [3]. This is because we chose to present the portion of the *Alexander* SVIR model that will be relevant to our own SVIR-type model, which will be presented in the next section. We note though that the *Alexander* SVIR model from [3] further incorporates the recruitment of new individuals to the population via birth and immigration, as well as the reduction of individuals due to natural death and emigration. Here we omitted the relevant terms because in our own SVIR-type model we will assume that the population remains closed during the epidemic. Moreover, the *Alexander* SVIR model considers the effects of waning immunity. Here we omitted those terms too because our model will not consider waning immunity. Finally the *Alexander* SVIR model assumes that susceptible individuals become vaccinated at some constant rate throughout the epidemic. This is an assumption that we will investigate later in section 2.7.4.

In the SVIR model from equations (2.4)-(2.7), the parameter $\sigma \in [0,1]$ is the reduction in susceptibility of a vaccinated individual. When $\sigma = 0$ the vaccine has no effect against the disease, while $\sigma = 1$ implies that the vaccine provides full immunity to every individual who receives it. Given the definition of σ, this model assumes that vaccination

reduces the susceptibility of vaccinated individuals to infection. Other alternatives include assuming that the vaccine reduces infectiousness (or equivalently transmissibility) or that it reduces both susceptibility and infectiousness. We chose to first present a reduced-susceptibility version of the SVIR model because it provides the simplest way to incorporate the effects of vaccination to the SIR model. In section 2.7.5 though we will also discuss the slightly more complicated reduced-transmissibility version of the SVIR model. We investigate both versions because in chapter 5 we will develop a cross-scale vaccination model which will use the reduced-transmissibility vaccination assumption by construction, and we want to facilitate a direct comparison between the results of the population-level model of this chapter and the cross-scale model of chapter 5.

The SVIR model presented in this section is based on all the assumptions of the classical SIR model. It further assumes the following:

- Once the outbreak starts no further vaccination takes place.
- Vaccination reduces susceptibility to infection.

2.3 A two-strain SVIR model

We will now present a two-strain SVIR model we developed to study the evolution of influenza, which is modelled here as the successful emergence and growth of a mutant strain in a population within a single influenza season. Our two-strain SVIR model has the following form:

$$\frac{dS}{dt} = -\beta_1 S I_1 - \beta_2 S I_2 \tag{2.8}$$

$$\frac{dV}{dt} = -(1-\sigma_1)\beta_1 V I_1 - (1-\sigma_2)\beta_2 V I_2 \tag{2.9}$$

$$\frac{dI_1}{dt} = \beta_1 S I_1 + (1-\sigma_1)\beta_1 V I_1 - \nu_1 I_1 \tag{2.10}$$

$$\frac{dI_2}{dt} = \beta_2 S I_2 + (1-\sigma_2)\beta_2 V I_2 - \nu_2 I_2 \tag{2.11}$$

$$\frac{dR_1}{dt} = \nu_1 I_1 \tag{2.12}$$

$$\frac{dR_2}{dt} = \nu_2 I_2 \tag{2.13}$$

with initial conditions

$S(0) = S^0 \in \mathbb{R}_+,\ V(0) = V^0 \in \mathbb{R}_+,\ I_i(0) = I_i^0 \in \mathbb{R}_+$ and $R_i(0) = R_i^0 \in \mathbb{R}_+$

for $i = 1,2$ and more specifically

$V(0) = c \in [0,1],\ I_i(0) = I_i^0 \in [0,1],\ R_i(0) = 0$ and $S(0) = 1 - c - I_1^0 - I_2^0$,

where c is the vaccination coverage, namely the proportion of the population that receives the vaccine.

Here $S(t)$ and $V(t)$ are the fractions of unvaccinated and vaccinated individuals in the population who are susceptible to either strain at time t, respectively. $I_i(t)$ is the fraction of individuals infected with the ith strain at time t and $R_i(t)$ the fraction recovered from the ith strain, for $i = 1,2$. The parameters β_i and ν_i are the transmission and recovery rates associated with the ith strain respectively. The parameter $\sigma_i \in [0,1]$ is the vaccine efficacy, namely the proportion by which the vaccine reduces the susceptibility of an individual to the ith strain.

The two-strain SVIR model is based on all the aforementioned assumptions of the classical SIR and SVIR models from sections 2.2.1 and 2.2.2 respectively. It further assumes the following:

- Infection by one strain leads to total immunity not only to the infecting strain, but also to the second one. This form of immunity is referred to as full cross-immunity.
- A host can be infected by one strain at most. Coinfection is not possible.

We note that the two assumptions of the *Alexander* SVIR model from section 2.2.2, namely that once the outbreak starts no further vaccination takes place and that vaccination reduces susceptibility to infection, will both be changed and investigated later in the chapter. More specifically in section 2.7.4 we will assume that vaccination takes place at some constant rate during the epidemic, and in section 2.7.5 we will assume that the

vaccine reduces infectiousness instead of susceptibility.

For the sake of convenience we will break down the epidemic into two sub-epidemics in the analysis of our model. More specifically, we will refer to the increase of individuals infected by the resident strain as the sub-epidemic driven by the resident strain and equivalently the increase of individuals infected by the mutant as the sub-epidemic driven by the mutant. This division is supported in our model by our assumptions of full cross-immunity and no coinfection.

2.4 Basic properties

2.4.1 The basic, control and effective reproduction numbers

In the absence of vaccination, the ith strain's basic reproduction number in our two-strain SVIR model is simply the average number of secondary cases of strain i produced by a single individual infected with the ith strain during their infective period in a fully susceptible population. Therefore

$$\mathscr{R}_{0,i} = \frac{\beta_i}{\nu_i}, \text{ for } i = 1,2 \tag{2.14}$$

But to account for the partial immunity of vaccinated individuals, it is useful to consider the control reproduction number $\mathscr{R}_c$ as well. Here,

$$\mathscr{R}_{c,i} = \frac{\beta_i}{\nu_i} \times S(0) + \frac{\beta_i}{\nu_i} \times (1-\sigma_i)V(0) = \mathscr{R}_{0,i} \times \Big[S(0) + (1-\sigma_i)V(0)\Big] \tag{2.15}$$

Setting the vaccine coverage as $V(0) = c$ and assuming that $S(0) + V(0) = N = 1$ then leads to

$$\mathscr{R}_{c,i} = \mathscr{R}_{0,i} \times \Big[(1-c) + (1-\sigma_i)c\Big] = \mathscr{R}_{0,i} \times (1 - c\sigma_i) \tag{2.16}$$

Equation (2.16) can then be used to derive the threshold vaccine coverage required to prevent an outbreak by the ith strain, which translates to finding the vaccine coverage c that would entail $\mathscr{R}_{c,i} = 1$. So using equations (2.14) and (2.16) the calculation reduces to

$$c_i^\star = \frac{1 - \frac{\nu_i}{\beta_i}}{\sigma_i} = \frac{1 - \frac{1}{\mathscr{R}_{0,i}}}{\sigma_i} \tag{2.17}$$

Equation (2.17) gives us a formula for the minimum vaccine coverage $c_i^\star$ for which the ith strain cannot cause an outbreak, but it could be the case that $c_i^\star > 1$. More specifically, we may derive from equation (2.17) that

$$c_i^\star > 1 \iff \frac{1}{\mathscr{R}_{0,i}} + \sigma_i < 1$$

Therefore, unless the vaccine has perfect efficacy against the ith strain (which occurs when $\sigma_i = 1$), there can be cases where no amount of vaccination can prevent an epidemic. The relationship between $c^\star$, $\mathscr{R}_0$ and σ is illustrated in figure 2.1 for a single strain epidemic.

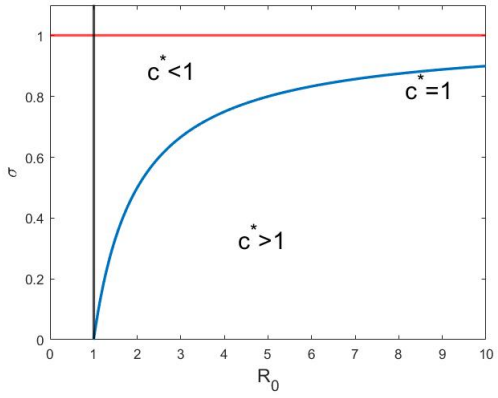

Fig. 2.1 The minimum vaccination coverage $c^\star$ for a single strain epidemic as a function of the basic reproduction number $\mathscr{R}_0$ and the vaccine efficacy σ.

Both calculations for $\mathscr{R}_0$ and $\mathscr{R}_c$ assume that everyone in the population is susceptible, with the only exception being those who have immunity through vaccination. But if the two strains are introduced at different times, then the full cross-immunity assumption implies that everyone who has been infected by the earlier strain will have full immunity against the later one. Therefore a more suitable measure for the transmission potential of each strain in this case is the effective reproduction number $R_{eff}(t)$, which can account for the depletion of susceptibles due to infection by one strain. In a fully susceptible population it is defined as

$$\mathscr{R}_{eff,i}(t) = \frac{\beta_i}{\nu_i} \times S(t) \ = \mathscr{R}_{0,i} \times S(t) \tag{2.18}$$

where $S(t)$ is the fraction of susceptible individuals at time t. Finally, the control effective reproduction number $\mathscr{R}^c_{eff}(t)$ further accounts for the imperfect immunity of vaccinated individuals and is defined as

$$\mathscr{R}^c_{eff,i}(t) = \mathscr{R}_{0,i} \times \left[S(t) + (1-\sigma_i)V(t)\right] \tag{2.19}$$

As was the case with the classical SIR model in the previous section, we are again interested in finding a threshold which determines whether the outbreak will occur. Since we are now considering two strains though, and because we will be especially interested in studying the conditions under which a mutant strain can appear in the population and grow, we will develop two thresholds: one to describe whether the sub-epidemic driven by the resident strain will occur and an equivalent one for the mutant strain. In order for the resident strain to successfully cause a sub-epidemic it requires $dI_1/dt > 0$. Using equation (2.10) of our two-strain SVIR model, this translates to:

$$\beta_1 S I_1 + (1-\sigma_1)\beta_1 V I_1 - \nu_1 I_1 > 0 \iff$$

$$\frac{\beta_1}{\nu_1} S + \frac{\beta_1}{\nu_1}(1-\sigma_1)V > 1$$

Evaluating the second expression at time $t = 0$ and subbing in for $\mathscr{R}_{c,1}$ leads to the conclusion that the resident strain can invade the population if

$$\mathscr{R}_{c,1} > 1$$

A similar calculation leads to the conclusion that the mutant strain can cause a sub-epidemic if

$$\mathscr{R}_{c,2} > 1$$

but that is under the assumption that the mutant strain is present in the population at time $t = 0$. In our implementation of the two-strain SVIR model though we will assume that initially only the resident strain is present and that the mutant may appear in the

population as a result of random mutations occurring within hosts infected with the resident. Therefore a more appropriate threshold to determine whether the mutant will generate a sub-epidemic if it appears in the population at some time $t = \tau$ is:

$$\mathscr{R}^{c}_{eff,i}(\tau) > 1 \tag{2.20}$$

2.5 The probability of a mutant strain emergence

In order to motivate our expression for the probability of a mutant strain emergence, we will first discuss some of our relevant modeling choices. We assume that initially there is only a resident strain causing an epidemic. At any time during the outbreak, we assume that a new strain may appear in the population as a result of random mutations within an infected host. The mutant strain might disappear before it has a chance to grow or it could spread in the population, which would then lead to two strains, the resident and the mutant, co-circulating. We assume that individuals can only be vaccinated at the beginning of the outbreak and primarily against the resident strain. We refer to such a vaccine which contains the same strain as the one causing the epidemic as a homologous vaccine. The efficacy of the vaccine against the mutant strain will be varied for our purposes. In section 5.8 of this chapter we will discuss in more detail how a homologous vaccine could offer some partial immunity to a newly emerged mutant strain if the mutant is antigenically similar enough to the resident strain, and equivalently how it might offer little to no protection if the resident and mutant strains are antigenically distinct.

Given a mutation rate ε per infection from the resident to the mutant strain, and given that at time τ there are $I_1(\tau)$ individuals infected with the resident strain (strain 1), then the rate of appearance of the mutant strain in the population at time τ is $\varepsilon I_1(\tau)$. We can use the probability of extinction of a branching process to account for the case that the mutant appears in the population but fails to cause a sub-epidemic. Assuming that a mutant strain appears in a fully susceptible population it will survive with probability $\left(1 - 1/\mathscr{R}_{0,2}\right)$, as it is established by Allen *et al.* in [6], where $\mathscr{R}_{0,2}$ is the mutant's basic reproduction number. This probability has been used extensively in epidemic models and originates from a paper published by Whittle in 1955 [307], in which he showed that for a single-strain epidemic in a stochastic Markov chain SIR model if $\mathscr{R}_0 > 1$ then a major outbreak will occur with probability $\left[1 - \left(1/\mathscr{R}_0\right)^{i^0}\right]$, where i^0 is the number of the initial infectious individuals. In the same paper Whittle demonstrated that this threshold is the

same for the deterministic SIR model. A potential drawback with using the survival probability $\left(1-1/\mathscr{R}_{0,2}\right)$ to test for a mutant strain emergence in the scope of our model is that this expression assumes that the $\mathscr{R}_0$ of the mutant strain remains constant throughout the outbreak and therefore fails to account for the depletion of susceptible hosts due to infection by the resident strain. Since we assume full cross-immunity, using $\mathscr{R}_{0,2}$ would overestimate the mutant's probability of survival. Furthermore we will examine cases where the vaccine against the resident strain has some effect on the mutant strain as well, so instead of R_0 we use the control effective reproduction number $\mathscr{R}^c_{eff,2}(\tau)$. Therefore, the rate of emergence of the mutant strain at time τ can be estimated by

$$\lambda(\tau) = \varepsilon I_1(\tau) \times \left(1 - \frac{1}{\mathscr{R}^c_{eff,2}(\tau)}\right) \tag{2.21}$$

with emergence here referring specifically to the appearance and subsequent survival of the mutant strain and $\mathscr{R}^c_{eff,2}(\tau) \geq 1 \ \forall \tau$. In the case that $\mathscr{R}^c_{eff,2}(t) < 1$ then we simply define $\lambda(t) = 0$. In the analysis of our model we will be studying not only whether the mutant strain is able to emerge at some given time τ, but also what its final size will be at the end of the epidemic. Using a survival analysis framework and treating $\lambda(\tau)$ as the hazard function, we may then express the probability density function for the emergence of a mutant strain at time τ as

$$f(\tau) = \lambda(\tau) \times e^{-\int_0^\tau \lambda(t)dt} \tag{2.22}$$

where the second term is the probability that the mutant has not emerged before time τ and corresponds to the survival function $S(\tau)$ used in survival analysis. This term is necessary since emergence at time τ inherently assumes that no successful appearance and survival has occurred before time τ. We emphasize that f is an improper probability density since emergence may not occur at all during the outbreak. This means that f may fail to integrate to 1. So given an epidemic duration of D days, we set $p_D = 1 - \int_0^D f(\tau)d\tau$ as the probability that no emergence occurs during the outbreak.

Given a probability density function f for the emergence of a mutant strain in a population, we may express the ith strain's expected final size $\mathbb{E}(FS_i)$ as:

$$\mathbb{E}(FS_i) = \int_0^\infty (FS_i|\tau) f(\tau) d\tau \tag{2.23}$$

where $FS_i|\tau$ is the final size of the ith strain given that the mutant strain appears at time τ. We note that for a given τ and considering that infection can only lead to recovery in our model, the final size of each strain can be calculated as $R_i(D)$, namely the proportion of individuals throughout the epidemic who became infected with the ith strain and recovered. Furthermore, we emphasize that by assuming the appearance of the mutant strain at some time τ during the outbreak we may be forcing the mutant to appear at a time when it cannot grow. We do not consider such a case to be a mutant strain emergence, merely an appearance. We will explore the effects of τ in detail in section 2.7.1.

2.6 Methods

The primary goal of our two-strain SVIR model is to explore the infection dynamics when a mutant strain emerges during an influenza outbreak in a population that consists of both vaccinated and fully susceptible individuals. To that end, we assume that the epidemic is initiated by a single strain which we refer to as the resident strain or strain 1. Some proportion of the population is assumed to be vaccinated against the resident strain by the start of the outbreak. We assume that the vaccine is homologous to the resident strain and reduces susceptibility to infection. We further assume that once the outbreak begins no more individuals become vaccinated. When an individual becomes infected with the resident strain there is a chance that mutations will occur inside them which will lead to a mutant strain (strain 2) emerging in the population at some time τ during the epidemic. Then from time τ onward there are two strains, the resident and the mutant, circulating in the population and competing for hosts either until the end of the outbreak or until one of them disappears. The efficacy of the vaccine against the mutant strain varies between simulations, ranging from no effect to total immunity.

The two-strain SVIR model has the following initial conditions:

- $\tau \in [0, D]$, where D is the duration of the epidemic in days. The case that $\tau = D$ is used to signify that no emergence has taken place during the epidemic. We will discuss our specific choice for D in the next paragraph.

- $V(0) = c = 0.63$ is the proportion of vaccinated individuals in the population.
- $I_1(0) = 4.8 \times 10^{-5}$ is the initial infective seed. It was chosen simply to ensure that the epidemic would start and finish within D days.
- $S(0) = 1 - c - I_1(0) \approx 0.37$ is the proportion of individuals in the population who are fully susceptible to the virus at the beginning of the outbreak.
- $I_2(\tau) = I_1(0)$ and $I_2(t) = 0 \quad \forall t < \tau$. We model the emergence of the mutant in the population as the introduction of some proportion of hosts infected by the mutant strain at time τ, and set this proportion equal to the initial infective seed of the resident strain.

The parameter values are presented in table 2.1 below and will be referred to throughout this chapter as the reference values. The mutation rate per infection was chosen as the value of ε which results in a mutant cumulative emergence probability of 0.9 throughout the outbreak. The reason for such a high emergence probability is that we are interested in exploring the competition dynamics when a resident and a newly emerged mutant co-circulate in a population, so we wanted to facilitate the appearance and growth of a mutant strain. This is further elaborated in section 2.7.2, where we also show that our results would have been qualitatively similar had a smaller ε been used.

We note that Public Health England (PHE) reports the following seasonal influenza vaccine coverages for the winter 2019-2020 season: 60.4% in primary school children [242], 74.3% in frontline healthcare workers [244], 72.4% in GP registered patients aged over 65 years old, 44.9% in patients aged six months to under 65 years in one or more clinical risk groups and 43.8% in patients aged two and three years old (includes both "healthy" and at risk) [243]. PHE reports that the overall vaccine uptake for the ages of six months up to 65 years based on GP registered patient data was 13.9% in the winter 2019-2020 season [243]. This is significantly lower than our choice of $c = 0.63$, but that does not pose an issue with our model for two main reasons. Firstly, we are interested in studying the competition dynamics between the two strains when the coverage is high because that highlights the impact of vaccination. Secondly, we will later vary the vaccination coverage from 0 to 1 so some of our main results will not depend on our initial choice of the vaccination coverage. The vaccine efficacy σ_1 against the resident strain was taken from the Influenza Annual Report: Winter 2018 to 2019 published by Public Health England in 2019 [241]. We note that there is a discrepancy between our

mathematical definition of vaccine efficacy and the way in which Public Health England estimates the vaccine effectiveness, and we will address this issue in the Discussion section (section 5.8) of this chapter.

The transmission rates β_i were chosen so that $\mathscr{R}_{0,1} = 2$ and $\mathscr{R}_{0,2} = 1.5$, given an average infectious period $1/\nu_i$ of 5 days for $i = 1, 2$. The basic reproduction numbers $R_{0,1}$ and $R_{0,2}$ of the resident and mutant strains respectively were chosen simply to satisfy reported values for the R_0 of influenza. Specifically Cauchemez *et al.* report in [55] R_0 values which range from 1.4 to 2.2. The choice to make the mutant strain less fit than the resident was made so as to underline the effects of the fitness advantage that the mutant gains from a vaccine which targets only the fitter resident strain. This is further elaborated in section 2.7.3.

The duration of the outbreak was set at 150 days, which we chose with the usual peak influenza season in the UK (December through February) in mind, together with the month leading to it and the month after it ends. The average infection length was chosen as 5 days to be consistent with the infection duration from our within-host model for the evolution of influenza which will be presented in the next chapter (chapter 3). This is because ultimately we want to compare the results of our population-level two-strain SVIR model from this chapter with the results of our cross-scale model which explicitly takes into account processes that occur at the within host level and will be presented later in chapter 4.

Parameter	Description	Value	Units	Source
β_1	transmission rate of resident strain	$2/5$	days^{-1}	
β_2	transmission rate of mutant strain	$3/10$	days^{-1}	
$1/\nu_i$	average length of infection with ith strain	5	days	
$\mathscr{R}_{0,1}$	resident basic reproduction number	2		[55]
$\mathscr{R}_{0,2}$	mutant basic reproduction number	1.5		[55]
σ_1	proportion by which vaccine reduces susceptibility to resident strain	0.44		[241]
σ_2	proportion by which vaccine reduces susceptibility to mutant strain	varies		
c	fraction vaccinated	0.63		[240]
τ	time of emergence of mutant strain	varies	days	
ε	mutation rate per infection	9.1		
D	outbreak duration	150	days	

Table 2.1 Parameters of the two-strain SVIR model

The model is implemented in Matlab by first running the original, single-strain SVIR model from section 2.2.2 from time $t = 0$ until $t = \tau$. This is because until time τ we have $I_2(t) = 0$. Then from time $t = \tau$ until $t = D$ we run our two-strain SVIR model. This is conceptually equivalent to running the two-strain SVIR model from time $t = 0$ until time $t = D$ and switching the value of $I_2(\tau)$ from 0 to some positive number.

2.7 Results

2.7.1 The effects of the time of emergence

One of our key questions of interest is how the time of emergence of the mutant strain affects the competition dynamics between the two strains. Intuitively, it's logical to expect that the longer it takes for the mutant to emerge, the smaller its final size will be.

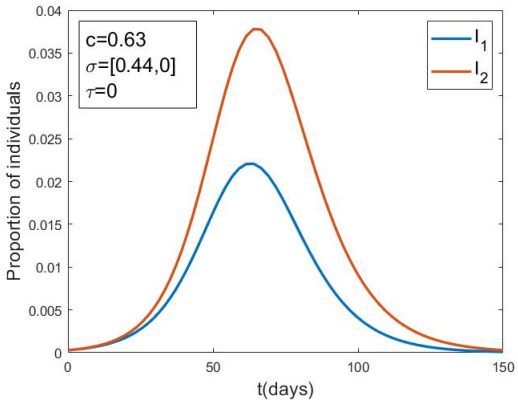

(a) Infectious groups dynamics when $\tau = 0$. This is the case that the outbreak is initiated by both the resident and mutant strains. This plot underlines the impact of vaccination, which results in the weaker mutant strain having higher prevalence than the resident.

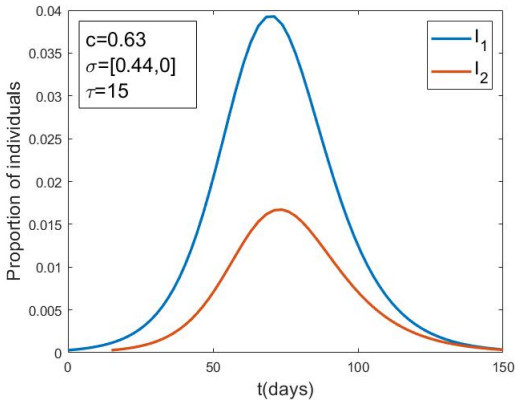

(b) Infectious groups dynamics when $\tau = 15$. Contrasting this to plot (a) highlights the importance of the time of emergence. The value of τ is the only difference in the parameters of plots (a) and (b), and we note that a later τ greatly reduces the prevalence of the mutant strain even though the mutant is unaffected by the vaccine ($\sigma_2 = 0$).

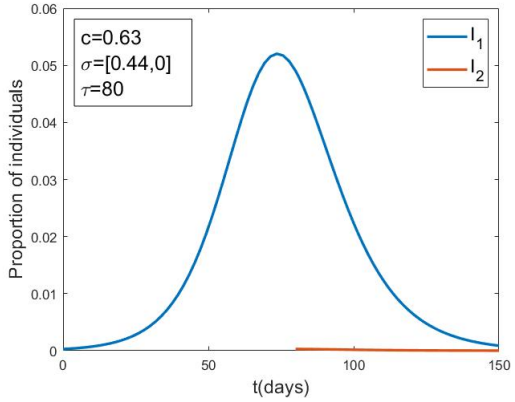

(c) Infectious groups dynamics when $\tau = 80$. This is a case where the mutant strain appears but is unable to grow (so we do not consider this case to be an emergence). This plot illustrates the results of forcing the appearance of the mutant strain at a time when it cannot survive.

Fig. 2.2 The effects of the time of emergence τ of the mutant strain on the dynamics of the infectious groups $I_1(t)$ and $I_2(t)$. The three plots in this figure are the results of three simulations of our two-strain SVIR model, where the only difference between the simulations is the value of τ. The rest of the parameters were kept at their reference values from table 2.1. We note that we present the vaccine efficacy against the two strains as $\sigma = [\sigma_1, \sigma_2]$, and here the vaccine has no effect against the mutant strain ($\sigma_2 = 0$).

Figure 2.2 shows the dynamics of the infectious compartments I_1 and I_2 in three scenarios: when the two strains are introduced in the population at the same time [plot (a)], when the mutant emerges relatively early in the epidemic and has a chance to spread [plot (b)], and when the mutant appears so late that it fails to grow [plot (c)]. All other parameters of the model remain constant at their reference values from table 2.1 and we further assume that the vaccine has no effect on the mutant strain, signified here by the fact that $\sigma_2 = 0$. It is interesting to note that because of that assumption, the vaccine offers a large enough fitness advantage to the weaker mutant strain that its prevalence surpasses that of the fitter resident strain when the outbreak is initiated by both the resident and mutant strains, as plot (a) illustrates. Figure 2.2 provides some initial evidence that a later τ has detrimental effects on the prevalence of the mutant strain, but only considers three values for τ. Therefore we will now explore the relationship between τ and the final sizes of the two strains in more detail.

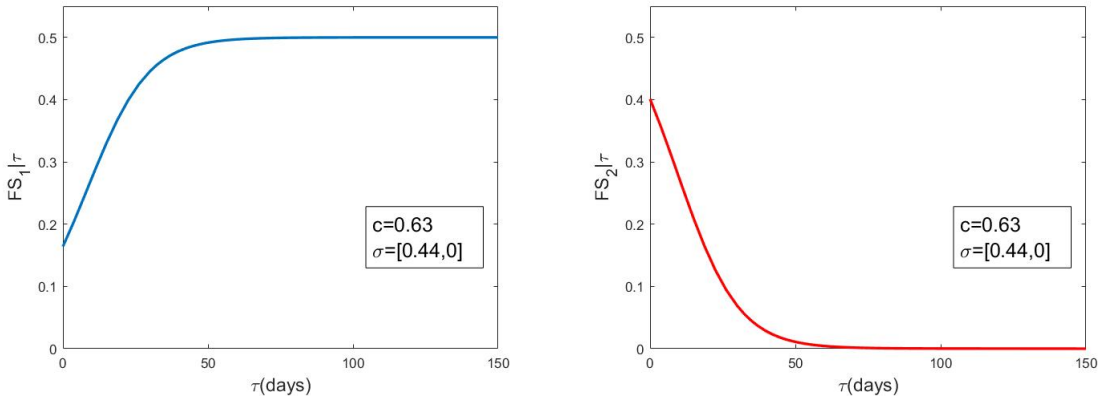

(a) The final size of the resident strain is computationally a non-decreasing function of τ.

(b) The final size of the mutant strain is computationally a non-increasing function of τ.

Fig. 2.3 The final sizes of the resident and mutant strains as a function of the time of emergence τ. Since in this case the vaccine has no effect on the mutant, the decrease in the mutant's final size as τ increases can be explained by the depletion of potential hosts available to the mutant due to infection with the resident strain.

Figure 2.3 illustrates the effects of the time of emergence τ on the final sizes of the two strains. A later τ means that the resident strain has had more time to circulate and infect hosts. Under our assumption of full cross-immunity, these infections with the resident strain lead to the mutant having a smaller number of individuals susceptible to it. As a result the mutant's final size is computationally a non-increasing function of τ, as plot (b) illustrates. Since the two strains are in direct competition for available hosts, the detrimental effect of a later τ on the mutant strain translates to a beneficial effect on the resident strain, as it allows it more time to spread without any competition from the

mutant. This is numerically why the final size of the resident strain is a non-decreasing function of τ, as plot (a) shows.

So far, figure 2.2(c) with the forced introduction of the mutant strain on day 80 of the epidemic showed that there exist values of τ for which the mutant strain may appear but fail to grow. Moreover figure 2.3 showed that the final sizes of the resident and the mutant plateau after some value of τ, which could imply that emergence is no longer possible past that value. To explore this we can calculate exactly what the cutoff time for the mutant's emergence is using its effective control reproduction number $\mathscr{R}^c_{eff,2}$, since as soon as that drops below 1 the mutant's probability of survival becomes zero and therefore emergence is no longer possible in our model.

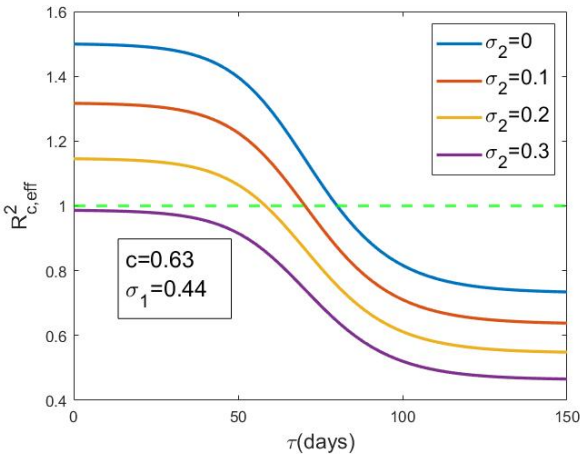

Fig. 2.4 The effective control reproduction number $\mathscr{R}^c_{eff,2}(t)$ of the mutant strain for different values of the vaccine efficacy σ_2 against the mutant strain.

Figure 2.4 illustrates what the window of emergence is for different values of the vaccine efficacy σ_2 against the mutant strain. It is not surprising that as the vaccine-induced protection against the mutant strain increases, the mutant's $\mathscr{R}^c_{eff,2}(\tau)$ decreases faster, leading to shorter emergence intervals. We note that even for a relatively small value of σ_2 (here 0.3) emergence becomes impossible for the mutant.

2.7.2 The probability of emergence

The results we have presented so far are from simulations in which we fixed some value for τ at the beginning of the simulation. This resulted in cases as the one exhibited in figure 2.2(c), where the mutant strain appeared very late during the outbreak and failed to grow. We then used the mutant's effective control reproduction number $\mathscr{R}^c_{eff,2}(t)$ to calculate the value of τ after which no emergence can occur. But while $\mathscr{R}^c_{eff,2}(t)$ can determine the mutant's window of potential emergence, it does not provide much insight into how the mutant's chances of emergence change within that window. To explore this we examine the mutant's probability of emergence using the probability density function for emergence that we derived in section 2.5. We repeat the pdf for emergence $f(\tau)$ and the rate of emergence $\lambda(\tau)$ here for convenience:

$$\lambda(\tau) = \varepsilon I_1(\tau) \times \left(1 - \frac{1}{\mathscr{R}^c_{eff,2}(\tau)}\right)$$

$$f(\tau) = \lambda(\tau) \times e^{-\int_0^\tau \lambda(t)dt}$$

We note that $f(\tau) = 0 \iff \mathscr{R}^c_{eff,2}(\tau) = 1$, as our expressions assume that $\varepsilon > 0$ and $\mathscr{R}^c_{eff,2}(\tau) \geq 1$.

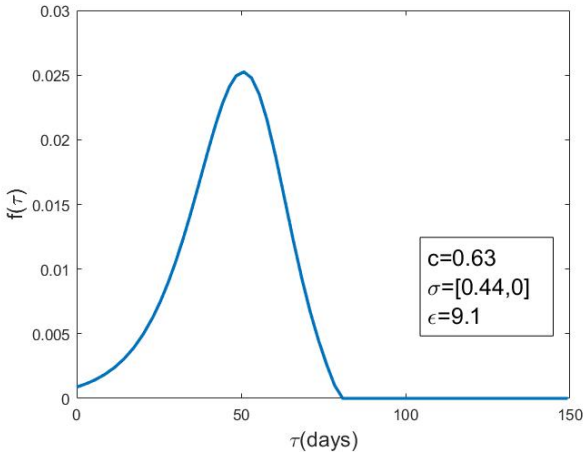

Fig. 2.5 The probability density function for the emergence of the mutant strain during the outbreak. Here we assume again that the vaccine has no effect on the mutant strain, namely $\sigma_2 = 0$. Since f is an improper density, the overall probability of emergence during the outbreak can be calculated as $\int_0^D f(\tau)d\tau$. This was calculated numerically in Matlab using the *trapz* function to be 0.9.

Figure 2.5 shows how the probability density function f for the emergence of a mutant strain changes throughout the epidemic. In the early stages of the outbreak the probability of emergence is low due to the small fraction of infected individuals. As that starts to increase the mutant's chance to emerge increases as well, until it reaches a maximum. After that maximum is attained the probability of emergence starts decreasing again because of the depletion of susceptible individuals available to the mutant due to infection with the resident strain.

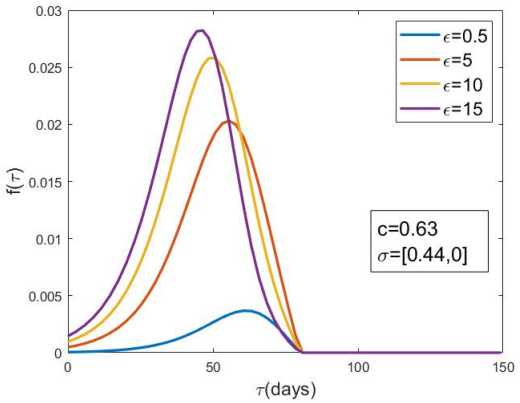

(a) $f(\tau)$ for different ε. We note that all the curves drop to zero at $\tau = 80.9$ days.

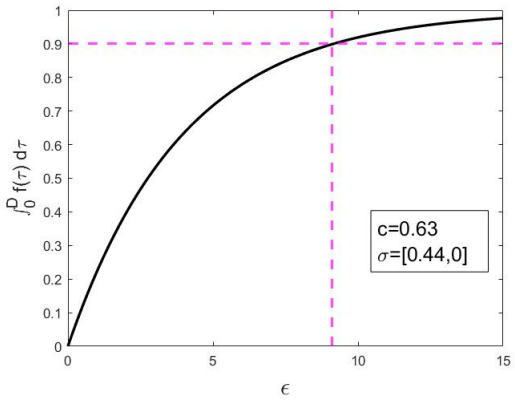

(b) The cumulative probability of emergence $\int_0^D f(\tau)d\tau$ is a non-decreasing function of the mutation rate per infection ε. The dashed line is at our reference value $\varepsilon = 9.1$, which leads to a cumulative emergence probability of 0.9.

Fig. 2.6 The effects of the mutation rate ε on the mutant's probability of emergence.

Figure 2.6 describes the effects of the mutation rate per infection ε on the mutant's probability of emergence. It is not surprising that as ε increases, the cumulative probability $\int_0^D f(\tau)d\tau$ that the mutant will emerge during the outbreak increases as well, as plot (b) illustrates. Given our expressions for the emergence density f and the rate of emergence λ, we may conclude that given any $\varepsilon > 0$ the determining factor of the length of the potential emergence interval is the control effective reproduction number $\mathscr{R}^c_{eff,2}$ of the mutant, which does not depend on ε. This is because, as we mentioned in the beginning of this section, $f(\tau) = 0 \iff \mathscr{R}^c_{eff,2}(\tau) = 1$ assuming $\varepsilon > 0$ and $\mathscr{R}^c_{eff,2}(\tau) \geq 1$. This is illustrated in plot (a) where the different curves, each of which corresponds to a different mutation rate ε, all become zero at the same τ. Plot (a) further shows that among the four values of ε we considered, the larger values increase the maximum of the emergence density $f(\tau)$ and also make emergence more likely earlier in the epidemic. This can be explained by the fact that given some proportion of infected individuals at time τ, a higher ε implies a larger appearance rate $\varepsilon I_1(\tau)$ and a lower probability $e^{-\int_0^\tau \lambda(t)dt}$ that emergence has not occurred before τ. It is important to note that the $f(\tau)$ curve does not

change qualitatively in any fundamental way for the different values of ε considered here.

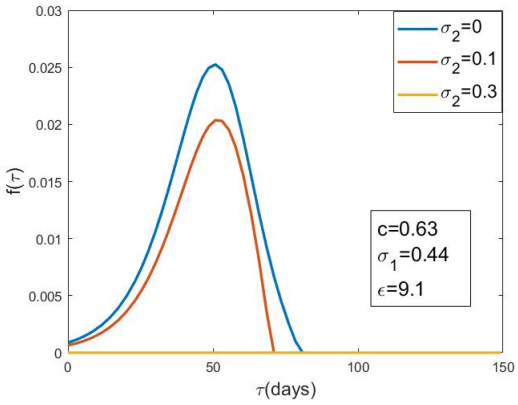

(a) $f(\tau)$ for different σ_2

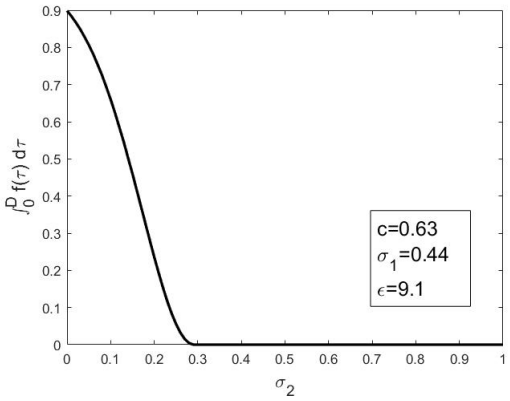

(b) The cumulative probability of emergence $\int_0^D f(\tau)d\tau$ is a non-increasing function of the vaccine efficacy σ_2 against the mutant strain. We note that even given a very high mutation rate of $\varepsilon = 9.1$ relatively small values of σ_2 are enough to ensure that no emergence occurs during the outbreak.

Fig. 2.7 The effects of the vaccine efficacy σ_2 against the mutant strain on the mutant's probability of emergence.

So far our results assume that the vaccine has no effect on the mutant strain. Figure 2.7 describes the effects of the vaccine efficacy σ_2 against the mutant strain on the mutant's probability of emergence. Given some fixed vaccination coverage c and efficacy against the resident strain σ_1, plot (b) shows that increasing σ_2 can reduce the cumulative probability of emergence down to zero even for relatively small values of σ_2 and even under the assumption of a very high mutation rate. We note that increasing σ_2 decreases the mutant's effective control reproduction number $\mathscr{R}^c_{eff,2}(\tau)$ for any given τ $\big($by definition of $\mathscr{R}^c_{eff,2}(\tau)\big)$. This has a twofold impact on the mutant strain, as illustrated for some specific values of σ_2 in plot (a). Firstly it shortens the potential emergence interval since the length of the interval is determined by the first τ at which $\mathscr{R}^c_{eff,2}(\tau)$ is smaller than 1. Secondly it decreases the mutant's probability of survival given appearance at some time τ, which is $\big(1 - 1/\mathscr{R}^c_{eff,2}(\tau)\big)$. Since this is one of the terms which make up the emergence density $f(\tau)$, decreasing it will in turn decrease the density at τ as plot (a) exhibits.

2.7.3 The effects of vaccination

Considering that vaccination is the primary control strategy against influenza epidemics, it is crucial to understand its effects not only on disease incidence, but also on the evolutionary dynamics of influenza. Since we model the evolution of influenza as the

potential emergence and spread of a mutant strain, it is important to explore how the vaccine efficacy and coverage affect the probability of emergence of a mutant strain and its expected final size.

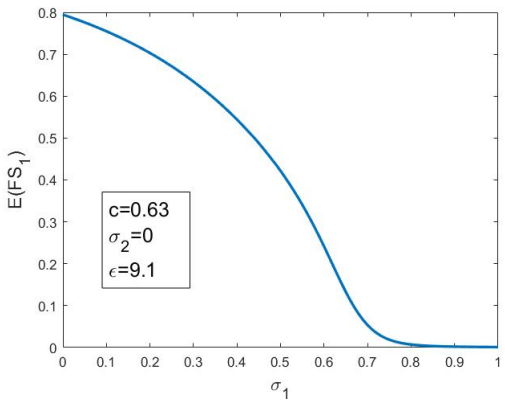

(a) The expected final size of the resident strain is a non-increasing function of the vaccine efficacy σ_1 against the resident. We note that $\mathbb{E}(FS_1) > 0 \; \forall \sigma_1$. Even when $\sigma_1 = 1$ and the vaccine offers perfect immunity against the resident strain there will still be some small proportion that contracts the resident strain because only 63% of the population is assumed to be vaccinated.

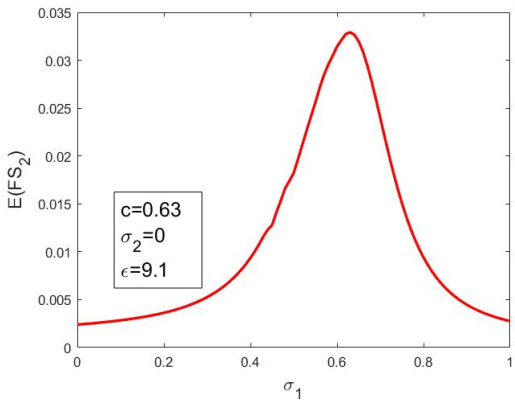

(b) The expected final size of the mutant strain is larger for intermediate values of the vaccine efficacy σ_1 against the resident strain.

Fig. 2.8 The effects of the vaccine efficacy σ_1 against the resident strain on the expected final sizes of the resident and mutant strains.

Figure 2.8 describes the effects of the vaccine efficacy σ_1 against the resident strain on the expected final sizes of the two strains. The left plot shows that the expected final size of the resident strain decreases as σ_1 increases. There are two factors which can account for this, one direct and one indirect. Firstly it is logical that as the vaccine efficacy against the resident strain increases its prevalence will decrease because it will have fewer individuals available to it for infection. Moreover, given some emergence time τ for the mutant strain, a higher σ_1 offers a fitness advantage to the mutant by lowering the susceptibility of individuals to the resident strain and therefore hindering its transmission. Because of our assumption of full cross-immunity, this leads to a smaller final size for the resident strain and in turn to a smaller $\mathbb{E}(FS_1)$. Plot (b) describes the relationship between the expected final size of the mutant strain and the vaccine efficacy σ_1 against the resident strain. The increasing portion of the plot can be attributed to the fitness advantage that the mutant strain gains as the vaccine becomes more efficient in reducing the susceptibility of individuals to the resident strain. This decreases the resident's transmission, leaving more potential hosts available to the mutant. The decreasing portion on the other hand can be explained by the significant reduction in the number of individuals infected with the resident strain as σ_1 becomes

large, which decreases the mutant's appearance rate $\varepsilon I_1(\tau)$ for any given τ and in turn decreases its probability of emergence. Therefore there appear to be two conflicting factors which determine the expected final size of the mutant for different values of σ_1.

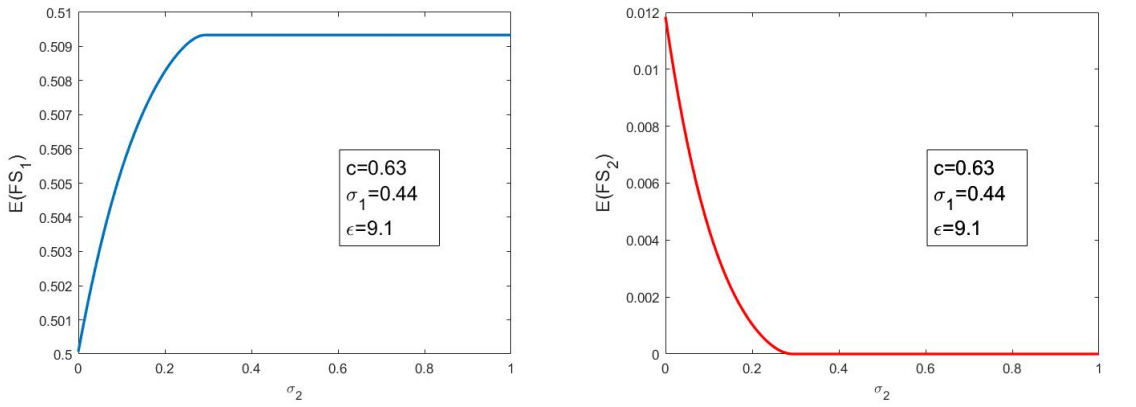

(a) The expected final size of the resident strain is a non-decreasing function of σ_2 due to the detrimental effects of a larger σ_2 on the potential emergence and spread of the mutant strain. We note though that the change in $\mathbb{E}(FS_1)$ as σ_2 increases is very small.

(b) The expected final size of the mutant strain is a non-increasing function of the vaccine efficacy σ_2 against the mutant. We note that plots (a) and (b) have different y-axes scales (this was done only for the sake of presentation).

Fig. 2.9 The effects of the vaccine efficacy σ_2 against the mutant strain on the expected final sizes of the resident and mutant strains.

Figure 2.9 describes the effects of the vaccine efficacy σ_2 against the mutant strain on the expected final sizes of the two strains. The left plot shows that the expected final size of the resident strain increases as σ_2 increases. Given the direct competition between the two strains, this can be attributed to the detrimental effect of a higher σ_2 on both the probability of emergence and the final size of the mutant strain given appearance at some time τ. We note though that varying σ_2 has a very small effect on on $\mathbb{E}(FS_1)$, which can be attributed to the fact that the resident strain is assumed to be fitter than the mutant and also to initiate the outbreak. The right plot shows that the expected final size of the mutant strain decreases as σ_2 increases. Given a mutant emergence at some time τ, a higher value for σ_2 reduces the infection risk of vaccinated individuals from the mutant strain thereby decreasing its final size. Moreover we have already illustrated that as σ_2 increases both the cumulative probability of emergence of the mutant and the emergence density for any given τ decrease $\big($figure 2.7$\big)$. Since the final size given some τ and the emergence density f are the two quantities which determine the mutant's expected final size, it is logical then that $\mathbb{E}(FS_2)$ is a non-increasing function of σ_2.

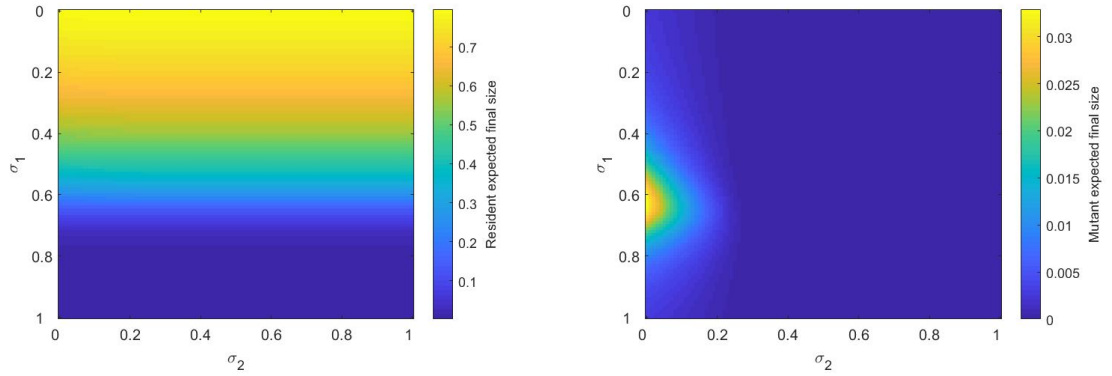

(a) The expected final size of the resident strain as a function of the vaccine efficacy against each strain. All parameters except σ_1 and σ_2 remain at their reference values.

(b) The expected final size of the mutant strain as a function of the vaccine efficacy against each strain. All parameters except σ_1 and σ_2 remain at their reference values. We note that plots (a) and (b) have different scales.

Fig. 2.10 The effects of the vaccine efficacy on the expected final sizes of the resident and mutant strains.

Figure 2.10 describes the effects of the vaccine efficacy σ_1 against the resident and σ_2 against the mutant strain on the expected final sizes of the two strains. The left plot shows how the expected final size of the resident strain changes with σ_1 and σ_2. We see that for a given σ_1 variations in σ_2 appear to have little to no effect on $\mathbb{E}(FS_1)$. This is not surprising if we consider that the emergence density is small for any given τ, as figure 2.5 from section 2.7.2 showed, and that the mutant strain is assumed to be weaker than the resident. The right plot shows how the expected final size of the mutant strain changes with σ_1 and σ_2. We see that for small values of σ_2 varying σ_1 results in the same behavior as the one illustrated in plot (b), namely that intermediate values of σ_1 are the most beneficial to the mutant strain. For larger values of σ_2 though the vaccine's improved efficacy becomes the main determinant of $\mathbb{E}(FS_2)$, while variations in σ_1 have almost no effect on it anymore.

So far we examined how the expected final sizes of the two strains will change as we vary the vaccine efficacy σ_1 and σ_2 against the resident and mutant strains respectively, while keeping the vaccination coverage c constant. We will now investigate the effects of changing the vaccination coverage on the expected final size of each strain.

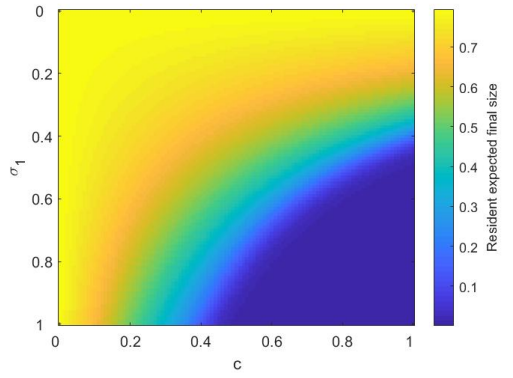

(a) The expected final size $\mathbb{E}(FS_1)$ of the resident strain decreases as the vaccine efficacy σ_1 and vaccination coverage c increase.

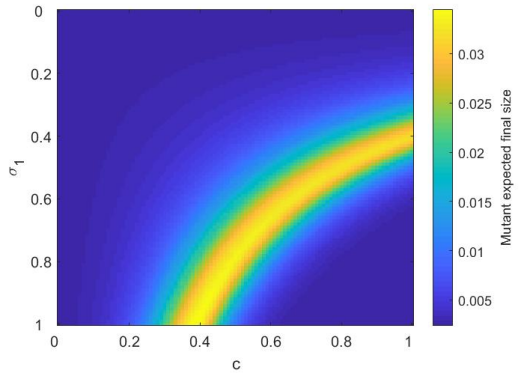

(b) The expected final size $\mathbb{E}(FS_2)$ of the mutant strain reaches large values in three cases: for intermediate values of both c and σ_1, for large values of σ_1 and intermediate values of c and for large values of c and intermediate values of σ_1.

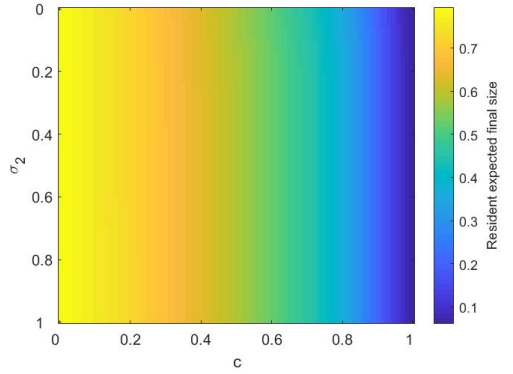

(c) The expected final size $\mathbb{E}(FS_1)$ of the resident decreases as the vaccination coverage c increases, and is almost unaffected by variations in σ_2.

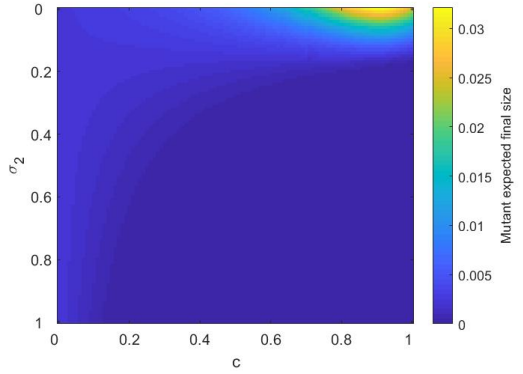

(d) Given an intermediate or larger value for σ_2, the expected final size $\mathbb{E}(FS_2)$ of the mutant strain is close to zero even for small values of c.

Fig. 2.11 The effects of the vaccine coverage c and the vaccine efficacy σ_i against the ith strain on the expected final sizes of the two strains. Whenever a parameter wasn't explicitly varied it was kept constant at its reference value. The plots in the left column describe how changes in c, σ_1 and σ_2 affect the expected final size of the resident strain while the plots in the right column how they affect the expected final size of the mutant strain.

Figure 2.11 describes how the expected final size of the two strains changes as we vary the vaccine coverage c and the vaccine efficacy against the ith strain σ_i.

- Plot (a) shows that the expected final size of the resident strain decreases as the number of individuals who receive the vaccine increases and as the efficacy σ_1 increases.

- Plot (b) shows that intermediate values of vaccination coverage and vaccine efficacy against the resident strain are among the most beneficial for the emergence and spread of the mutant strain. Moreover we see that given an intermediate value of c, large values of σ_1 also lead to increases in the expected prevalence of the mutant. The same holds for intermediate values of σ_1 and large values of c. All these three cases can be explained by the same reasoning: conditions which offer

a fitness advantage to the mutant (such as an intermediate c and very large σ_1, or an intermediate c and σ_1) lead to higher expected final sizes for the mutant because they hinder the spread of the resident strain. But if the detrimental effect on the resident strain becomes too large (as is the case with a very large c and σ_1), this will in turn decrease the mutant's expected final size because it will reduce its chances of emerging in the population.

- Plot (c) illustrates that changes in the vaccine efficacy σ_2 against the mutant strain have almost no effect on the expected final size of the resident strain even when c, and therefore the vaccine effectiveness, is large (given that σ_1 remains at its reference value of 0.44). This is in accordance with the results of figure 2.10(c), which showed that increasing σ_2 from 0 to 1 led to less that a 1% increase in $\mathbb{E}(FS_1)$ for a vaccination coverage of 0.63.
- Plot (d) shows that the expected final size of the mutant strain attains its largest values when σ_2 is very small or zero, and the vaccination coverage c is large. This is unsurprising, since it describes a case where the majority of the population is vaccinated against the resident strain with a vaccine that has little to no effect on the mutant strain. This offers a significant fitness advantage to the mutant, leading to a larger expected prevalence. On the other hand given a larger value of σ_2 we see again that even very small values of c are enough to ensure a very small expected final size for the mutant strain. It is important to note that even when everyone in the population is vaccinated ($c = 1$), the outbreak still occurs and therefore the mutant strain has a chance to emerge. This is because the vaccine offers only partial protection from the infection, and specifically here the efficacy σ_1 is 0.44.

2.7.4 An alternative vaccination model : continuous vaccination

One of the assumptions of our two-strain SVIR model is that individuals cannot be vaccinated once the epidemic starts. In this section we will change this and instead assume that while some fraction of the population received the vaccine prior to the outbreak, susceptible individuals become vaccinated at a constant rate a throughout the duration of the epidemic. The only difference then in the formulation of our model is that the S-equation now includes a $-aS$ term and the V-equation a $+aS$ term. The vaccination rate a was calculated as the rate which results in an infection prevalence of 25% in an outbreak with only the resident strain present and with 63% of the population having

already received the vaccine by the start of the outbreak. This is half the prevalence of a single-strain epidemic under our previous vaccination program. Our particular choice for a is not significant though, our only consideration was to not choose a value that would completely impede the growth of the two strains. Our goal is to simply investigate whether adding a constant vaccination rate throughout the epidemic will qualitatively alter our model's results in some fundamental way. All other parameters of the model are kept constant at their reference values from table 2.1. We note that the vaccination coverage c remains at its reference value of 0.63 but now refers to the initial vaccination coverage, as more individuals receive the vaccine throughout the epidemic.

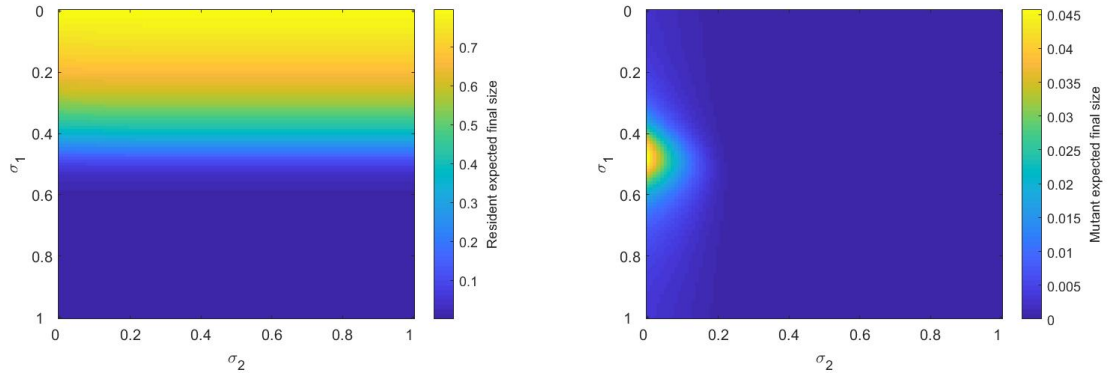

(a) The expected final size of the resident strain as a function of the vaccine efficacy against each strain.

(b) The expected final size of the mutant strain as a function of the vaccine efficacy against each strain. We note that the scale is different between this plot and plot (a).

Fig. 2.12 The effects of the vaccine efficacies σ_1 and σ_2 on the expected final sizes of the resident and mutant strains under the assumption of a constant vaccination rate $a = 0.02$. All other parameters except σ_1 and σ_2 remain at their reference values. Both plots are qualitatively very similar to their corresponding plots from figure 2.10, where no vaccination occurs after the onset of the epidemic.

Figure 2.12 shows that our continuous vaccination model results are qualitatively similar to our previous model where we assumed that vaccination occurs prior to the onset of the outbreak. Therefore our model results are not very sensitive to using a vaccination program which includes a constant vaccination rate throughout the epidemic as opposed to using our original assumption that no further vaccination occurs once the outbreak begins. Very importantly, we can still conclude using plot (b) that intermediate values of the vaccine efficacy σ_1 against the resident strain lead to the highest expected prevalences for the mutant strain.

2.7.5 Sensitivity to the form of vaccine immunity

The formulation of our two-strain SVIR model in equations (2.8)-(2.13) of section 2.3 depends on the assumption that the vaccine reduces the susceptibility of individuals to infection. In this section we will change this and instead assume that the vaccine reduces the transmissibility of the virus from infected individuals to new cases. We will first motivate the form of our reduced transmissibility model, and then we will present it and analyze some of its key results.

We now define $\sigma_i \in [0,1]$ as the proportion by which the vaccine reduces the transmissibility of the ith strain from infected individuals who have received the vaccine to new cases. Assuming again that vaccination only occurs prior to the onset of the epidemic, this reduced transmissibility framework necessitates the division of infected individuals into four categories:

- I_1^S: individuals who used to be fully susceptible and became infected with the resident strain
- I_2^S: individuals who used to be fully susceptible and became infected with the mutant strain
- I_1^V: individuals who were vaccinated and became infected with the resident strain
- I_2^V: individuals who were vaccinated and became infected with the mutant strain

The key difference between these four categories as far as vaccination is concerned is that the I_1^S and I_2^S classes will transmit the virus at some β_1 and β_2 rates respectively, while the I_1^V and I_2^V classes will transmit it at some reduced $(1-\sigma_1)\beta_1$ and $(1-\sigma_2)\beta_2$ rates. Our two-strain SVIR model with reduced transmissibility then becomes:

$$\frac{dS}{dt} = -\beta_1 S I_1^S - (1-\sigma_1)\beta_1 S I_1^V - \beta_2 S I_2^S - (1-\sigma_2)\beta_2 S I_2^V \tag{2.24}$$

$$\frac{dV}{dt} = -\beta_1 V I_1^S - (1-\sigma_1)\beta_1 V I_1^V - \beta_2 V I_2^S - (1-\sigma_2)\beta_2 V I_2^V \tag{2.25}$$

$$\frac{dI_1^S}{dt} = \beta_1 S I_1^S + (1-\sigma_1)\beta_1 S I_1^V - \nu_1 I_1^S \tag{2.26}$$

$$\frac{dI_1^V}{dt} = \beta_1 V I_1^S + (1-\sigma_1)\beta_1 V I_1^V - \nu_1 I_1^V \tag{2.27}$$

$$\frac{dI_2^S}{dt} = \beta_2 S I_2^S + (1-\sigma_2)\beta_2 S I_2^V - \nu_2 I_2^S \tag{2.28}$$

$$\frac{dI_2^V}{dt} = \beta_2 V I_2^S + (1-\sigma_2)\beta_2 V I_2^V - \nu_2 I_2^V \tag{2.29}$$

$$\frac{dR_1}{dt} = \nu_1 I_1^S + \nu_1 I_1^V \tag{2.30}$$

$$\frac{dR_2}{dt} = \nu_2 I_2^S + \nu_2 I_2^V \tag{2.31}$$

with initial conditions

$S(0) = S^0 \in \mathbb{R}_+,\ V(0) = V^0 \in \mathbb{R}_+,\ I_i^S(0) = I_i^{0,S} \in \mathbb{R}_+,\ I_i^V(0) = I_i^{0,V} \in \mathbb{R}_+$ and $R_i(0) = R_i^0 \in \mathbb{R}_+$

for $i = 1,2$ and more specifically

$V(0) = c \in [0,1],\ I_i^S(0) = I_i^{0,S} \in [0,1],\ I_i^V(0) = I_i^{0,V} \in [0,1],\ R_i(0) = 0$ and $S(0) = 1 - c - I_1^{0,S} - I_1^{0,V} - I_2^{0,S} - I_2^{0,V}$,

where c is the vaccination coverage, namely the proportion of the population that receives the vaccine.

Here $S(t)$ and $V(t)$ are the fractions of unvaccinated and vaccinated individuals in the population who are susceptible to either strain at time t, respectively. $I_i^S(t)$ is the fraction of individuals infected with the ith strain at time t who used to be fully susceptible and $I_i^V(t)$ is the fraction of individuals infected with the ith strain at time t who were vaccinated. $R_i(t)$ is the fraction recovered from the ith strain, for $i = 1,2$, and includes both individuals who used to be fully susceptible and individuals who received the vaccine. The parameters β_i and ν_i are the transmission and recovery rates associated with the ith strain respectively. The parameter $\sigma_i \in [0,1]$ is the vaccine efficacy, defined here as the proportion by which the vaccine reduces the transmissibility of the ith strain from an infected individual to new cases.

Our two-strain SVIR model with reduced transmissibility is based on the same assumptions as our two-strain SVIR model with reduced susceptibility from section 2.3, with the

only exception being that the vaccine now reduces infectiousness instead of susceptibility.

The methods, implementation, initial conditions and parameter values of the two-strain SVIR model with reduced transmissibility remain exactly the same as those of our two-strain SVIR model with reduced susceptibility from section 2.3. We only note that here:

- $I_1^S(0) = 4.8 \times 10^{-5}$. This is the same initial infective seed as the one we used in section 2.3.
- $I_1^V(0) = 0$. So we assume that the outbreak begins via the infection of individuals who have not received the vaccine.

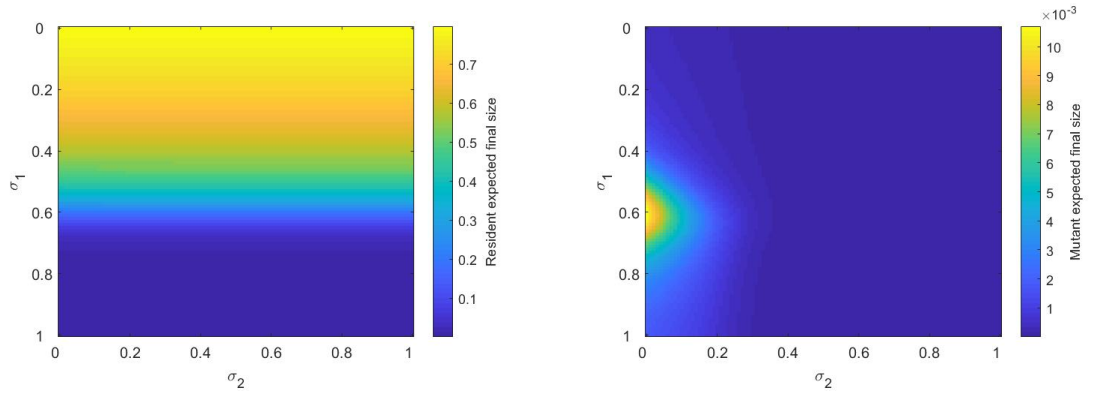

(a) The expected final size of the resident strain as a function of the vaccine efficacy against each strain.

(b) The expected final size of the mutant strain as a function of the vaccine efficacy against each strain. We note that the scale is different between this plot and plot (a).

Fig. 2.13 The effects of the vaccine efficacy on the expected final sizes of the resident and mutant strains under the assumption of reduced transmissibility. All parameters except σ_1 and σ_2 remain at their reference values. We emphasize that the two plots have different scales. Both plots are qualitatively very similar to their corresponding plots from figure 2.10, where no we assumed that the vaccine reduces susceptibility.

Figure 2.13 illustrates the effects of varying the vaccine efficacy σ_1 against the resident strain and σ_2 against the mutant on the expected final sizes of the two strains. Plot (a) shows that varying σ_2 has a very limited effect on the expected final size of the resident strain, while on the other hand varying σ_1 has a strong one. We see that reducing the transmissibility of the resident virus by approximately 60% or more in vaccinated individuals leads to an expected final size of almost zero for the resident strain. This happens for every value of σ_2, which further highlights the small impact of the vaccine efficacy against the mutant strain on the spread of the resident. We emphasize though that our results are merely qualitative and we are not arguing that such a vaccine efficacy

will guarantee the same results in a real epidemic. Plot (b) shows that intermediate values of the vaccine efficacy σ_1 against the resident strain are the most beneficial for the potential emergence and spread of a mutant strain in our model. This result is the same qualitatively as the one given by our two-strain SVIR model with reduced susceptibility from section 2.3, and can be explained by the same reasoning. As the vaccine efficacy σ_1 against the resident strain initially increases, it offers a fitness advantage to an emerging mutant strain by limiting the transmission potential of its competitor resident strain. But when σ_1 becomes so large that the resident strain cannot spread effectively, then the emergence potential of the mutant strain decreases. This in turn decreases its expected final size, accounting for the decreasing portion of plot (b) along the σ_1 axis.

This section with the reduced transmissibility and the previous one with the constant vaccination rate challenge two important assumptions of our original two-strain SVIR model with reduced susceptibility from section 2.3. We have shown though that our results remain the same qualitatively under these different assumptions, and most significantly that under all three frameworks intermediate values of immunoprotection are the most inducive to the emergence and spread of a mutant strain.

2.8 Discussion

This chapter examines the emergence and subsequent competition dynamics of a mutant influenza strain drifted from a parent resident strain in a population during a single influenza epidemic. Of key interest is the impact of a partially effective vaccine on the epidemiological and evolutionary viral dynamics.

Our most significant and perhaps counter-intuitive result is that antigenic drift, which is modelled here as the emergence and spread of a mutant strain, appears most likely to occur at intermediate values of immunoprotection. We use the expected final size of the mutant strain as an indicator of antigenic drift by assuming that a larger expected final size increases the chances of the mutant strain reaching fixation. Based on the results from section 2.7.3, intermediate values for the vaccine coverage and efficacy against the resident strain maximize the mutant's expected final size. This adds a new layer of consideration to influenza vaccination strategies. Traditionally influenza vaccination programs aim to control the seasonal outbreaks via vaccination against the

strains expected to circulate in the current season. But the results of our model imply that vaccination programs should also consider how likely the current vaccine is to aid the potential emergence of mutant strains. Such a situation could become very dangerous especially if the mutant strain is antigenically different enough from its parent resident strain to be resistant to the effects of a homologous vaccine. In such a case the newly emerged mutant would be spreading in a population consisting of hosts who have little natural or artificial immunity to it. Our results emphasize that to prevent such a scenario it is important for the current vaccine to either be a broad cross-protective vaccine or to induce a high immune pressure against the resident strain but that it is also critical that a large proportion of the population is vaccinated. As figure 2.11 shows, the case where the vaccine efficacy against the resident strain is high but only an intermediate portion of the population receives the vaccine is actually very inducive to the emergence and successful spread of a mutant strain.

It is important to emphasize that our prediction that intermediate levels of vaccination coverage and efficacy against a resident strain would be the most beneficial for the potential establishment of a mutant strain is not entirely novel. Grenfell *et al*. argue in [125] that the highest rate of viral adaptation to host immunity occurs at intermediate levels of the strength of the immune response. They attribute this to two conflicting factors. The first is the within-host selection strength, which increases with the strength of the immune response and therefore leads to a higher adaptation rate. The second is the viral abundance, which decreases as the level of immunity increases and therefore leads to a lower adaptation rate. Translating this to our own framework, the equivalent argument would be that on one hand a larger vaccine efficacy against the resident strain leads to a higher expected prevalence for the mutant, but if on the other hand the prevalence of the resident becomes too low then emergence becomes less likely. Therefore our results extend the argument by Grenfell *et al*. to the population-level emergence and spread of mutant strains.

We will now discuss the assumptions and limitations of our model. One of the key assumptions of our model is that of full cross-immunity, namely that infection with one strain offers full immunity both to the infecting and to the other strain. If the newly emerged mutant strain is antigenically similar to its parent resident strain then there is strong evidence to support our full cross-immunity assumption. Infection with a given influenza strain results in the generation of long-lived antibodies which are specific to the

hemagglutinin (HA) and neuraminidase (NA) surface proteins of the infecting strain [222]. The implication of this aspect of the adaptive immune response is that a subsequent challenge with an antigenically similar strain might not lead to an infection. Even if it does, the reinfection is often mild because the host should be able to immediately procure high levels of strain-specific antibodies [295]. A historical example that illustrates the effects of strain-specific antibodies is when H1N1 re-emerged to cause an epidemic in 1977 after being absent from the human population since 1957, and infected mostly individuals younger than 20 years. The 1957 and 1977 strains were collected and found to be antigenically and genetically very similar, which implies that the older individuals retained their immunity from the first 1957 outbreak [90]. We may conclude then that this long-lived strain-specific immunity that follows a natural infection by a given influenza strain makes the full cross-immunity assumption appropriate for our model if the mutant strain is antigenically similar to the resident.

A scenario of interest arises though when the mutant strain is antigenically distant from the resident, since that is precisely when the mutant is most dangerous. Even in this case there is some evidence to support our full cross-immunity assumption. Immunological [21, 135, 183] and epidemiological [98] studies have shown that infection by a given influenza strain results in a temporary antigen-nonspecific immunity which can last up to a few months. This can partially explain why people who become infected once during a single influenza season have a significantly lower risk of reinfection even by an antigenically different second strain, as Zarnitsyna *et al*. report in [319]. It is important to note that we are only considering mutant strains which arise from the process of antigenic drift. Pandemic strains, which evidence suggests are primarily the result of genetic reassortment, exhibit different dynamics [166]. Therefore we may conclude that even if the co-circulating resident and mutant strains are antigenically different the assumption of full cross-immunity is still applicable in our single-season influenza model.

Considering that a key question we attempt to answer with this model is how vaccination affects the evolution and spread of influenza, it is important to address all our assumptions regarding vaccination and evaluate their impact on the validity and robustness of our results. We assume that no vaccination occurs after the onset of the epidemic, which in our model is in November (a month before the start of peak influenza season in the northern hemisphere). The CDC reports that for the 2014-2015 up to the 2016-2017 influenza seasons in the US only an approximate further 10% of individuals at most were

vaccinated after November of the current season [56–58]. Therefore our assumption of a zero vaccination rate once the epidemic starts is not unrealistic (at least in the case of the US). But we also considered a different vaccination program in which individuals continue receiving the vaccine at some constant rate throughout the duration of the epidemic. Figure 2.12 from section 2.7.4 shows that our results would not differ qualitatively under this new vaccination strategy. Most importantly, our prediction that intermediate levels of the vaccine efficacy against the resident strain are the most beneficial for the potential emergence and spread of a mutant strain would still be valid.

Given any vaccination strategy we need to define how the vaccine affects the virus. This is a complicated question for a variety of reasons, perhaps most importantly due to the difficulties in translating experimental results to mathematical quantities. We defined vaccine efficacy in our model as the proportion by which the vaccine reduces susceptibility to infection, and used the value for the adjusted vaccine effectiveness reported by Public Health England during the winter 2018-2019 influenza season to inform our model parameter. The vaccine effectiveness was estimated using a case test-negative design, which Foppa *et al*. showed to be valid and unbiased under fairly general assumptions [103]. But this way to estimate the vaccine effectiveness does not translate exactly to our definition of vaccine efficacy because it inherently incorporates the effects of the indirect protection offered to unvaccinated individuals from the reduced infection prevalence in a population which includes vaccinated individuals. This implies that our reference value for the vaccine efficacy might overestimate the level of protection that the vaccine offers. This is not a significant problem in our model though, since our key results come from varying the vaccine efficacy against each influenza strain and examining the corresponding effect on each strain's expected prevalence.

While research suggests that influenza is a rapidly mutating virus [216, 297], most of our results still use an unrealistically high mutation rate. This was deliberately chosen so in order to facilitate the emergence and spread of the mutant strain as we are interested in its competition dynamics with its parent resident strain. Our results remain the same qualitatively when much smaller mutation rates were used, as figure 2.6 illustrated. We emphasize though that all our results in this chapter are qualitative, as we are not aiming to make accurate quantitative predictions regarding the evolutionary dynamics of influenza but simply to gain a better insight into how vaccination affects them.

We assume that only a single mutant strain may emerge during the outbreak. From a population genetics perspective, it would have been important for the model to account for the continuous accumulation of point mutations in the hemagglutinin (HA) protein. Even immune-escape mutants can accumulate too many deleterious mutations after they emerge in a population and end up disappearing too quickly to establish a viral lineage [172]. This is a level of complexity that our model does not explicitly consider, although the survival term in our expression for the probability of emergence from section 2.5 can partially account for all the mutants that appear but suffer rapid loss without propagating in the population. Furthermore there is no evidence for the explosive antigenic diversity of circulating strains that influenza's high mutation rate alone would suggest [236]. This can be partially explained by the competition between antigenically closely related seasonal strains to spread in a population that often mostly consists of partially immune hosts. We can imagine that if instead each mutation led to immune escape strains, then these mutants would take over separate niches and we would observe greater antigenic diversification [288]. As this is not the case and influenza exhibits constrained diversity, it should be a justifiable simplification to only allow for a single mutant strain to emerge during an epidemic. We note though that our model can be extended to include multiple strains simply by adding more infectious compartments, and also a linear or non-linear antigenic strain space such as the ones used by Gog and Grenfell in [121].

While our two-strain SVIR model can capture the conflicting factors that appear to determine the evolutionary dynamics of influenza in a population that utilizes a vaccination program, we can make a number of changes to facilitate further exploration. These include:

- Allowing for partial cross-immunity or waning strain-transcending immunity following natural infection with a given strain. We expect this to have a significant impact on our model's results, as it will allow for mixed infections or reinfections following recovery. Currently the only case where an individual might have two strains circulating within them in our model is if they were initially infected with the resident strain but then had the mutant emerge within them, though this process is only implicitly incorporated to our model via our expression for the population-level probability of emergence. Partial cross-immunity would increase the mutant's control effective reproduction number $\mathscr{R}^{c}_{eff,2}$ by introducing a new group of individuals that the mutant could infect following its appearance in the population, thereby improving its chances of emergence. It would also widen the mutant's emergence

window, since as we demonstrated in section 2.7.2 $\mathscr{R}^c_{eff,2}$ is the main determinant of the length of the mutant's emergence interval.

- Adding heterogeneity to the population in the form of age structure. We do not expect this to alter our model's results in a fundamental way, as it does not affect the assumption of total cross-immunity or the key emergence potential of the mutant strain. Incorporating age structure though would allow us to investigate research questions such as: how should vaccination of certain age groups be prioritized in order to minimize the spread of the infection and how does that in turn affect the emergence dynamics of the mutant strain?

- Incorporating multiple strains via the addition of more infectious compartments. As we have already discussed in chapter 1, increasing the number of strains can lead to several analytical and computational challenges. We could start with only adding a third strain though, which could be either a second resident strain or a second possible mutant strain. The former could be thought of as modeling a population where seasonal strains of both the H1N1 and the H3N2 subtypes are co-circulating, but only one of those strains can give rise to a mutant strain. Such a model naturally lends itself to the addition of a fourth strain, so that both resident strains are allowed to mutate. Under our original assumption of total cross-immunity, we expect such a framework to have a negative impact on the emergence and spread of mutant strains, as they would have to compete with two strains already circulating in the population. Under a partial cross-immunity assumption though we expect the resulting model to exhibit significantly more complicated dynamics, especially if we assume cross-reactivity between all strains. If instead we consider a model where two different mutant strains could emerge, we may either assume that they are both the immediate result of mutations occurring in the resident strain or that only the first mutant is a direct result of mutations in the resident strain and then the second mutant can only arise from the first, making the successful emergence of the first mutant strain a prerequisite for the emergence of the second one. Under our simplifying assumption of total cross-immunity we do not expect our model's results to change in a fundamental way. It would be interesting though to investigate questions such as under what conditions/ parameter values a strain-matched vaccine against the resident would provide enough pressure that a weaker first mutant could emerge in the population and survive long enough to then give rise to a fitter mutant.

2.9 Summary

In this chapter we presented a population-level model for the epidemiological and evolutionary dynamics of influenza during a single influenza season. We used it to study the emergence potential of a mutant strain and the subsequent competition dynamics with its parent resident strain. We focused on the question of how vaccination affects the antigenic drift dynamics of influenza, which we modelled here as the potential emergence and expected growth of a mutant strain. Our results showed that intermediate levels of immunoprotection are most likely to facilitate the antigenic drift of influenza, and that it is critical for vaccination programs to aim for a vaccine which exerts high immune pressure onto the expected current-season strain but also to aim for a large vaccination coverage. Our model took explicitly into account only processes occurring at the between-host level, so in chapter 4 we will compare its results to those of a cross-scale model whose population dynamics are explicitly informed by processes occurring at the within-host level.

Chapter 3

A within-host model for the evolution of influenza

3.1 Introduction

Our goal in this chapter is to develop a within-host influenza model to describe the emergence dynamics of a mutant strain during an infection with a resident strain as well as the consequent competition dynamics between the two strains. We will begin by extending one of the simplest and most versatile within-host disease models, the TIV model published by Baccam *et al*. in [24], to include two strains. Then we will adapt a slightly more complicated model developed by Saenz *et al*. in [262] and modify it to include two strains. Our analysis of the extended *Saenz* model will initially focus on the effects of the mutant's emergence time on the disease dynamics. Then, in order to investigate the possible times during an infection at which a mutant strain can appear and survive, we will develop an expression for the emergence density of the mutant. Finally we will add vaccination to our extended *Saenz* model.

3.2 Background

3.2.1 The TIV model

In 2006, Baccam *et al*. published a simple but very influential model of within-host influenza A kinetics [24]. We refer to it as the TIV model throughout this thesis. It consists

of the three following ODEs:

$$\frac{dT}{da} = -\beta TV \tag{3.1}$$

$$\frac{dI}{da} = \beta TV - \delta I \tag{3.2}$$

$$\frac{dV}{da} = pI - cV \tag{3.3}$$

Here $T(a)$ denotes the number of uninfected target cells at time a, $I(a)$ the number of infected cells at time a and $V(a)$ the infectious viral titer at time a, where a denotes the age of infection. The parameter β is the infectivity rate. Infected cells I produce new virions at a rate p per cell, and die at a rate δ per cell where $1/\delta$ is the average life-span of an infected cell. Free virions that are circulating within the host are cleared by the immune system at a rate of c per day.

The TIV model is based on a number of underlying assumptions:

- Infected cells immediately start shedding virus.
- The binding of free virions with target cells causes only a negligible decrease in the viral load, which is why there is no $-\beta TV$ term in (3.3).Since an infected cell that has reached the virion-producing stage can release $10,000 - 20,000$ progeny virions per day [211], it is justifiable to ignore the loss of a single virion that is needed to infect a target cell.
- Infection ends due to the depletion of target cells.
- The innate immune response is included implicitly in the model via the clearance rate c and the death rate of infected cells δ.

The TIV model has been used extensively in the literature and was often the foundation on which other within-host disease models were built. It has appeared in the influenza literature [29, 131], dengue literature [31, 66] and also in the chronic disease literature [230, 231].

3.2.2 The Saenz model

While the TIV model is a simple but powerful model, it comes with some potential drawbacks. The most relevant one to the scope of this thesis is the indirect way in which the model captures the immune response, namely via the parameters for the clearance rate of free virions c and the death rate δ of infected cells. This has a negative impact on exploring the potential emergence of a mutant strain within-host. We will explore this in detail in section 3.4. To account for this, we will explore a more complicated but better applicable to the goals of this thesis within-host influenza model published by Saenz *et al*. in 2010 [262] which explicitly considers some aspects of the innate immune response. For simplicity, we refer to this model as "the *Saenz* model" throughout this thesis.

A key assumption of the TIV model is that as soon as a target cell becomes infected it starts releasing progeny virions. Experiments have shown though that the influenza virus requires some time to replicate within an infected cell [159]. In the *Saenz* model the authors assume that when a target cell becomes infected it first enters an eclipse phase, before it starts releasing progeny virus. We underline that Baccam *et al*. also studied the effects of adding an eclipse phase to the TIV model in [24]. This eclipse phase is important within the scope of this thesis firstly because it slows down viral kinetics and secondly because the cells which are in it are natural candidates for a potential mutation. This will be further elaborated in section 3.4.

The Saenz model has the following formulation:

$$\frac{dT}{da} = -\beta VT - \phi FT \tag{3.4}$$
$$\frac{dE_\alpha}{da} = \beta TV - k_\alpha E_\alpha \tag{3.5}$$
$$\frac{dW}{da} = \phi FT - m\beta VW - a_w W \tag{3.6}$$
$$\frac{dE_\gamma}{da} = m\beta VW - k_\gamma E_\gamma \tag{3.7}$$
$$\frac{dR}{da} = a_w W \tag{3.8}$$
$$\frac{dI}{da} = k_\alpha E_\alpha + k_\gamma E_\gamma - \delta I \tag{3.9}$$
$$\frac{dV}{da} = pI - cV \tag{3.10}$$

$$\frac{dF}{da} = nqE_\gamma + qI - dF \tag{3.11}$$

(3.12)

In this model:

- $T(a)$ is the number of susceptible target cells at time a. T_0 is the epithelial cell population size of the equine respiratory tract (the data used in the Saenz *et al*. paper came from experiments in horses).
- $V(a)$ is the viral load at time a, and is expressed as the number of RNA copies per milliliter of nasal secretion.
- $E_\alpha(a)$ is the number of previously fully susceptible target cells at time a that have been infected but are not yet releasing progeny virions. This compartment is called E_1 in the Saenz *et al*. paper [262]. We change the notation here only for the sake of clarity because we will later introduce a second strain to the model.
- k_α is such that $1/k_\alpha$ is the average duration of the eclipse phase of E_α cells.
- F is the IFN that infected cells are secreting.
- β is the rate at which free virions infect available target cells.
- ϕ is a measure of the efficiency of IFN to induce an antiviral state in target cells, and is expressed in IFN fold change daily. Moreover, ϕT is the rate at which susceptible cells become protected due to the action of IFN.
- $W(a)$ is the number of prerefractory cells at time a, which are target cells which have been primed by IFN but are not yet fully protected.
- a_w is such that $1/a_w$ is the average time that it takes for a prerefractory cell in W to become fully protected. This was denoted as a in [262], but we changed it here because we use a to denote the age of infection.
- m is the IFN-reduced infectivity, so that $0 < m \leq 1$, where values close to 0 mean that IFN greatly reduces infectivity and if $m = 1$ then IFN has no effect on infectivity. Prerefractory cells W become infected at a rate $m\beta V$.
- $E_\gamma(a)$ is the number of cells at time a that used to be prerefractory but have been infected and have the virus replicating within them. Just like E_α cells, they are not yet releasing any progeny virions. Similarly to E_α, this compartment is called E_2 in

the Saenz *et al*. paper but we changed it here for the sake of notational clarity in the extended two-strain *Saenz* model, which we will present in section 3.4.

- k_γ is such that $1/k_\gamma$ is the average duration of the eclipse phase of E_γ cells.
- $R(a)$ is the number of refractory cells at time a , which are fully immune to the virus.
- $I(a)$ is the number of infected cells at time a that are producing progeny virions.
- δ is the death rate of infected cells.
- p is the production rate of progeny virions by infected cells.
- c is the clearance rate of free virions.
- q is the rate per day at which infected cells I produce IFN.
- n is the IFN-reduced production.
- d is the rate per day of IFN clearance.

All these compartments are illustrated in Figure 3.1, which is taken directly from the original Saenz *et al*. paper [262].

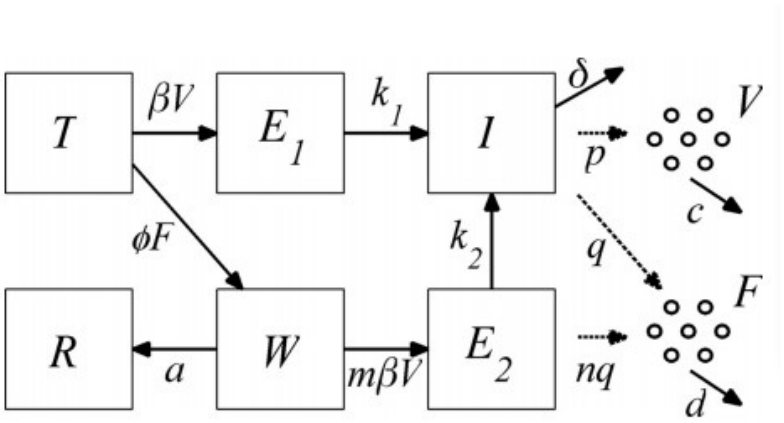

Fig. 3.1 Diagram of the infection dynamics in the *Saenz* model. This figure is taken directly from [262].

The *Saenz* model is based on the following assumptions:

- The binding of free virions with target cells causes only a negligible decrease in the viral load, which is why there is no $-\beta VT$ term in equation (3.10).

- Once a cell becomes fully immune to infection and enters the R compartment, it cannot leave.
- Infection leads to death for cells in the I compartment, either due to the detrimental effects of the virus inside them or due to the action of the immune system.

The Saenz model takes into account some key immunological factors that could potentially affect the evolution of influenza, and given that it consists of a system of ODEs it is also computationally efficient. This is why we use it here as the basis of our own within-host model, which we will present in section 3.4 and then build upon in sections 3.5 and 3.6.

3.3 The TIV model with deterministic emergence

3.3.1 Model presentation

Since our goal in this chapter is to develop a within-host model for the evolution as well as the dynamics of influenza, a useful starting point is to extend the Baccam *et al*. TIV model from [24] to include two strains and study the resulting emergence dynamics. This is the formulation of our two-strain TIV model:

$$\frac{dT}{da} = -\beta_1 T V_1 - \beta_2 T V_2 \tag{3.13}$$
$$\frac{dI_1}{da} = \beta_1 T V_1 - \delta_1 I_1 \tag{3.14}$$
$$\frac{dI_2}{da} = \beta_2 T V_2 - \delta_2 I_2 \tag{3.15}$$
$$\frac{dV_1}{da} = p_1 I_1 - c_1 V_1 \tag{3.16}$$
$$\frac{dV_2}{da} = p_2 I_2 - c_2 V_2 \tag{3.17}$$

Everything is defined in the exact same way as in the original TIV model. Namely, $T(a)$ is the number of target cells at time a, $V_i(a)$ is the viral load of the ith strain at time a, $I_i(a)$ is the number of cells at time a that are infected by the ith strain, β_i is the infectivity rate of the ith strain, c_i is the clearance rate of the ith strain and p_i is the rate of production of

new virions of the ith strain by a cell in the I_i compartment.

This model is based on all the same assumptions as the TIV model, and furthermore supposes that:

- Target cells can only be infected once and only with a single strain. No coinfection can occur at the cellular level.
- There is no competition between strains except for available target cells.

3.3.2 Methods

The aim of the two-strain TIV model is to explore the infection dynamics when a mutant strain appears within a host sometime during the course of an influenza infection with a resident strain. Therefore the host is initially infected only with the resident strain (strain 1 in the notation of our model). Infection begins via the introduction of some virions of the resident strain inside the host. This is in accordance with data that influenza uses virions to spread among individuals [152]. These virions start entering the host's target cells and replicating inside them. While the replication happens instantaneously in this model, it plays a vital role in the model dynamics. This is because viral replication is an error-prone process [264], so we assume that at some time α a mutation occurs which leads to a cell that was originally infected with the resident strain to produce mutant virions instead. Therefore mutation is modelled here as the introduction of some mutant viral load inside the host at some time α during the infection. After time α both strains are circulating inside the host and compete against each other for available target cells either until the end of the infection or until one of them disappears.

Here the time of appearance of the mutant strain α does not depend on the age of the infection, the amount of target cells still present or the viral load of the resident strain. This assumption is oversimplifying and will be changed in section 3.5, where the emergence of the mutant will happen stochastically and α will be a function of the host's current state. But throughout this section α is treated as a fixed parameter of the model, which means that we are forcing the appearance of a mutant strain. But as we will demonstrate in section 3.3.3, under certain conditions the mutant viral load only decreases after its forced appearance. We will not consider this case to be a mutant strain emergence, merely an appearance. Therefore in this section emergence is defined

as the appearance of the mutant strain at some time α, after which the mutant viral load increases (even if that increase is very small and the mutant viral load disappears quickly after its introduction at α).

Our extended two-strain TIV model has the following initial conditions:

- $\alpha \in [0, D]$, where D is the duration of the infection. The case that $\alpha = 0$ is a coinfection with two strains instead of a within-host mutant emergence, but we include it here for the sake of mathematical convenience.
- $T(0) = 3.5 \times 10^{11}$. This is the estimate for the number of epithelial cells in the equine respiratory tract, as given in Saenz *et al*. [262].
- $V_1(0) = 0.16$. This value comes from [262] as well, but was halved to account for the appearance of a second strain.
- $I_1(0) = 0$.
- $V_2(0) = 0$. This is because there are no cells infected with the resident strain at time 0, so no mutation could have taken place.
- $I_2(0) = 0$.
- $V_2(\alpha)$=0.16. This is the same as the initial viral load of the resident strain, and also includes the case of a coinfection.
- $I_2(\alpha) = 0$.

The parameter values are shown in table 3.1, and they all come from the Saenz *et al*. paper [262]. We will refer to the parameter values in table 3.1 as the "reference values".

Parameter	Description	Value	Units	Source
β_i	Infectivity rate of ith strain	1.4×10^{-4}	(RNA copies)$^{-1}$ ml NS day^{-1}	[262]
p_i	Virus production rate for ith strain	1.4×10^{-5}	RNA copies (ml NS)$^{-1}$ day^{-1} cell^{-1}	[262]
c_i	Free virus clearance rate for ith strain	5.2	Rate of virus clearance day^{-1}	[262]
$1/\delta_1$	Average lifespan of cells infected with resident strain	$1/2$	Days	[262]
$1/\delta_2$	Average lifespan of cells infected with mutant strain	Varies	Days	

Table 3.1 Parameters of the two-strain TIV model

We note that the virus shedding data were obtained as daily measures of RNA copies per milliliter of nasal secretion (NS), as it is reported by Saenz *et al.* in [262].

We will consider three cases for the relative fitness of the mutant compared to that of the parent resident strain: a neutral mutant which despite its mutation is functionally identical to the resident strain (this is the case for many influenza mutations, as stated in [297]), a weaker mutant which leads to infected cells dying twice as quickly and a fitter mutant which doubles the lifespan of infected cells. In the notation of the model, $\delta_2 = 2\delta_1$ for the weaker mutant and $\delta_2 = (1/2)\delta_1$ for the fitter mutant. The biological motivation here is that the fitter mutant could have a beneficial mutation which interferes with immune signalling pathways, thus slowing down the immune response. The results of the two-strain TIV model using this definition for the fitness of the mutant will be presented in section 3.3.3.

But we underline that this is not the only way in which we can defined the relative fitness of the mutant in this model. The ith strain has four parameters associated with it, namely the death rate of infected cells δ_i, the viral clearance rate c_i, the transmission rate β_i and and the virion production rate p_i. Therefore we could also define a beneficial mutation as one that leads to a higher rate of production of mutant virions p_2 or to a lower clearance rate c_2. The effects of these different definitions on some key infection-related quantities

will also be presented in section 3.3.3.

The model is implemented in Matlab by first running the original TIV model from section 3.2.2 from time $t = 0$ until time $t = \alpha$. That is because until time α both V_2 and I_2 remain at zero. Then from time $t = \alpha$ until time $t = D$ we run the full two-strain TIV model. Conceptually this is equivalent to running the two-strain TIV model from $t = 0$ until $t = D$ and switching the value of $V_2(\alpha)$ from 0 to 0.16. Various plots in this chapter will be in log-scale (this will be explicitly stated). Since all plots were generated in Matlab, we note that Matlab's *log* function refers to the natural logarithm.

3.3.3 Results

Results using the reference values

We will begin our analysis of the two-strain TIV model by first assuming that the parameters are fixed at their reference values from table 3.1. We also assume that the relative fitness of the mutant strain depends only on the choice of the death rate of cells infected with the mutant, namely δ_2.

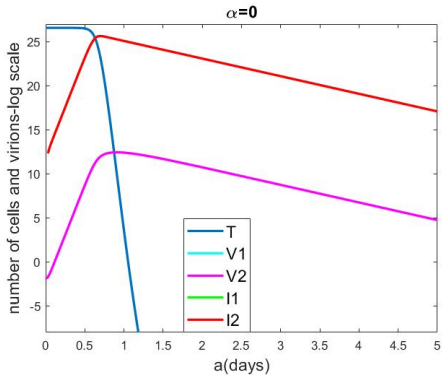

(a) The curves for V_1 and V_2 as well as the curves for I_1 and I_2 fully overlap because this plot represents a coinfection with two functionally identical strains.

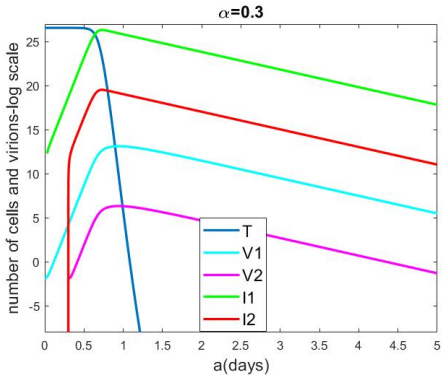

(b) Here the mutant is neutral and therefore functionally identical to the resident strain, but it emerges at time $\alpha = 0.3$. This is why the I_2 and V_2 curves remain below the I_1 and V_1 curves respectively. When plotting the log curves of I_1 and I_2 we begin at some time $t > 0$ and $t > \alpha$ respectively to avoid plotting y-values at or around $-\infty$.

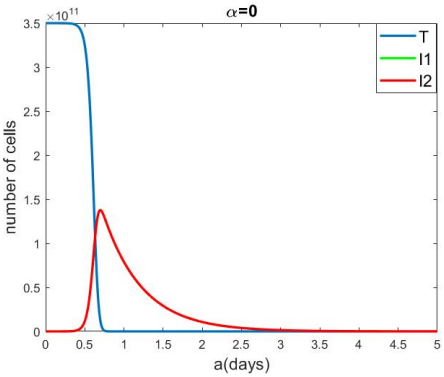

(c) I_1 and I_2 curves fully overlap due to coinfection with identical strains.

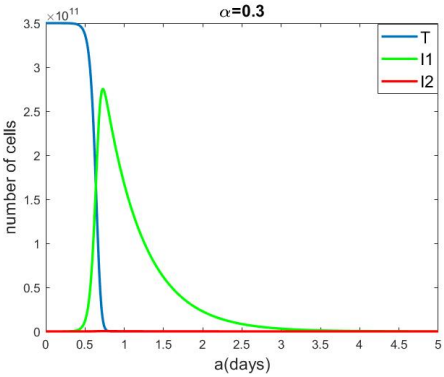

(d) The disadvantage of the neutral mutant strain which appears here at $\alpha = 0.3$ means that throughout the duration of the infection the number of cells it infects is much smaller than the number of cells that the functionally identical resident cell infects.

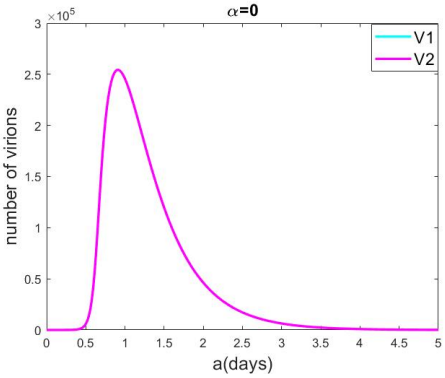

(e) V_1 and V_2 curves fully overlap due to coinfection with identical strains.

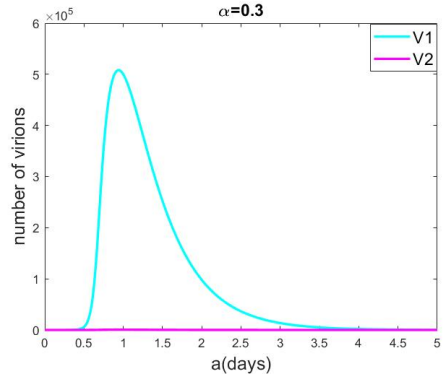

(f) The later appearance of the mutant strain compared to the case of coinfection in plot (e) has a very strong impact on its viral load.

Fig. 3.2 Infection dynamics for a neutral mutation and two different values for the time of emergence α. Here $\delta_2 = \delta_1 = 2$. The plots in the left column are the result of simulating the model with $\alpha = 0$. The plots in the right column are the result of simulating the model with $\alpha = 0.3$. The two plots in each row describe the same compartments, but for a different α. A pairwise comparison in each row shows that the later α leads to lower mutant viral load as well as a smaller number of cells infected by the mutant throughout the duration of the infection.

Figure 3.2 illustrates the dynamics of the target cells, infected cells and viral loads of the two strains in the case of a neutral mutation and for two different values of the mutant appearance time α: the plots in the left column represent the case of a coinfection with a resident and a neutral mutant strain and therefore assume that $\alpha = 0$, while the plots in the right column assume that $\alpha = 0.3$ days. Given that this difference in α is the only difference between these two columns, a comparison between them can provide some initial insight into the effects of the emergence time α on certain key infection dynamics. More specifically, a comparison between plots (a) and (b) shows that the later α led to a smaller viral load for the mutant throughout the duration of the infection, as opposed to its viral load in the case of a coinfection. This is also true for the number of target cells infected by the mutant strain throughout the infection. Since we used only two different values for the emergence time α here, we will now investigate this negative effect of a later α on the mutant's viral load in more detail.

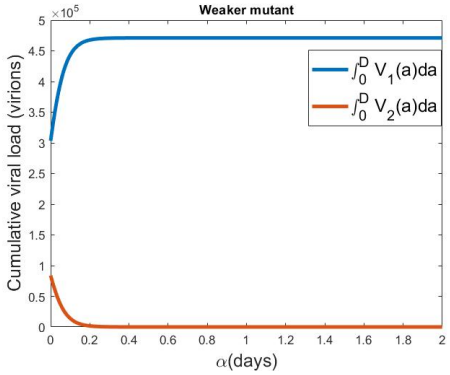

(a) Deleterious mutation : in the case of $\alpha = 0$, which is when $\int_0^D V_2$ achieves its maximum, the weaker mutant has a significantly smaller cumulative viral load compared to the fitter resident strain

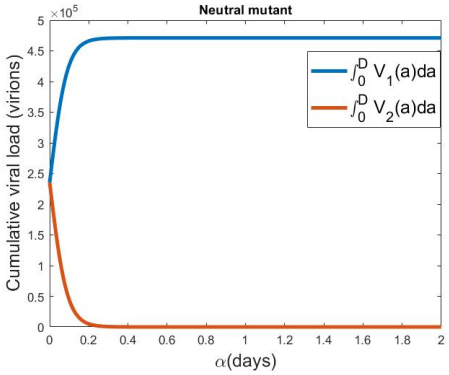

(b) Neutral mutation : the y-intercept of both curves is the same because the case $\alpha = 0$ represents a coinfection with two functionally identical strains, both of which have the same initial viral load.

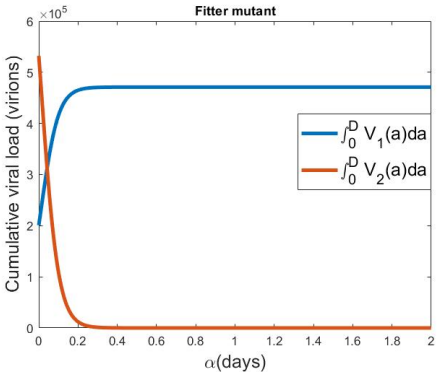

(c) Beneficial mutation : the fitter mutant attains its maximum cumulative viral load at $\alpha = 0$, and it is larger than the corresponding cumulative viral load of the weaker resident strain.

Fig. 3.3 The cumulative viral load of each strain as a function of the time of emergence α.

To further explore the importance of the time of emergence, we can examine how the cumulative viral load of each strain changes with the emergence time α. The cumulative viral load of the ith strain is defined here as the area under the viral load curve of the ith strain, namely $\int_0^D V_i(a)da$, where D is the duration of the infection in days. Our results in figure 3.3 show that for all three types of mutants the cumulative viral load is computationally a non-increasing function of the emergence time. We observe that in all three plots there is an initial rapid decrease in the cumulative viral load of the mutant, which illustrates the strong effect of α on the spread of the mutant. We note though that after some α the cumulative viral loads of both strains appear to be settling to some constant value, which suggests that the effect of the emergence time diminishes. This may be because in these cases the mutant appears so late in the infection that there are very few or no target cells available to it for infection and therefore it cannot grow its viral load. To formally assess this though, we will need to investigate the mutant's window of emergence.

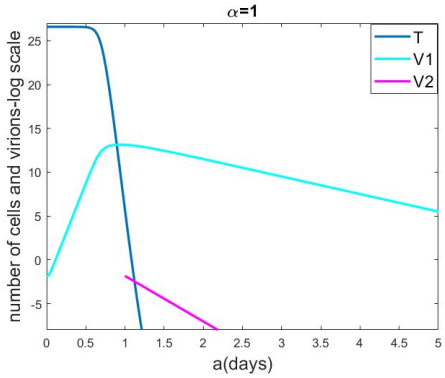

Fig. 3.4 Example where a fitter mutant appears but fails to establish, as its viral load only decreases after its forced introduction at $\alpha = 1$.

Figure 3.4 illustrates the case where a mutant strain appears outside of its emergence window and therefore fails to grow. We obtained this plot by forcing the appearance of the mutant at $\alpha = 1$ day. We emphasize that in our framework this represents a mere appearance of the mutant strain, but not an emergence.

While figure 3.4 illustrates the viral dynamics when a mutant strain appears too late in the infection, it does not provide any insight into the width of the mutant's emergence

window except that it is shorter than $\alpha = 1$ day. To investigate this, we can first look into how many target cells a single cell infected by the mutant can expect to infect before it dies. If we consider the case of coinfection, namely that $\alpha = 0$, then this is precisely the basic reproduction number of the mutant strain R_0^m. A cell infected with the mutant strain remains infectious for an average of $1/\delta_2$ days before it dies. It releases p_2 virions per day on average, each of which survives for an average of $1/c_2$ days and can infect any of the T_0 target cells available to it with a success rate β_2. Therefore the R_0 of the mutant strain has the following form:

$$R_0^m = \frac{1}{\delta_2} \times \frac{p_2 T_0}{c_2} \times \beta_2 \tag{3.18}$$

This formula is known and was reported as such by Baccam *et al.* in their original paper that first described the TIV model [24]. If the mutant strain appears during the infection at some time other than $\alpha = 0$ though then R_0^m might not be a good indicator of the mutant's chances of survival. That is because R_0^m assumes that the mutant has the whole epithelial cell population of the respiratory tract (T_0) available to it for infection. But that is not the case here, as until time $a = \alpha$ the resident strain has been depleting the target cells. Therefore a more useful measure of the mutant's window of emergence in this case is the effective reproduction number R_{eff}^m, which takes into consideration the infection of target cells by the resident strain and has the following formula:

$$R_{eff}^m(a) = \Big[\frac{1}{\delta_2} \times \frac{p_2 T_0}{c_2} \times \beta_2\Big] \times \frac{T(a)}{T_0} \tag{3.19}$$

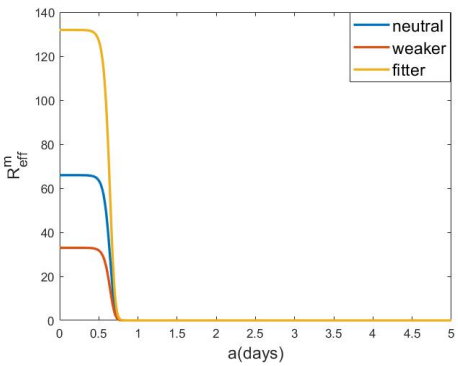

(a) $R^m_{eff}(a)$ of all mutants. The large R^m_0 values of all mutants are not surprising considering that at time $a = 0$ there are 3.5×10^{11} target cells available for them to infect.

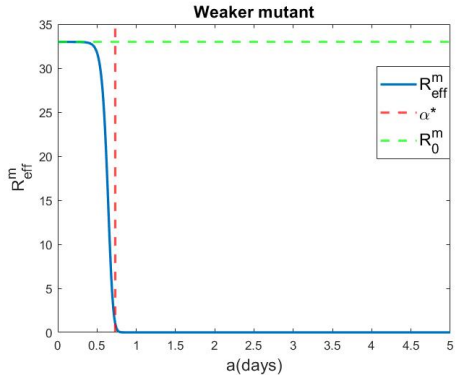

(b) $R^m_{eff}(a)$ of weaker mutant. Here the emergence cutoff time is $\alpha^* = 0.73$ days.

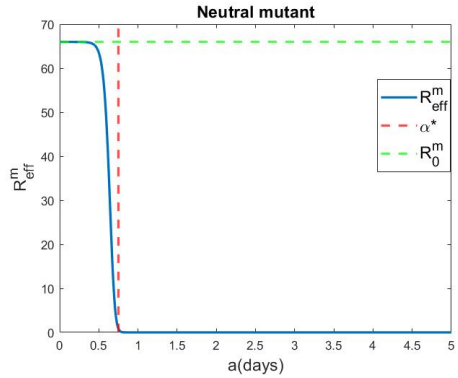

(c) $R^m_{eff}(a)$ of neutral mutant. Here $\alpha^* = 0.74$ days.

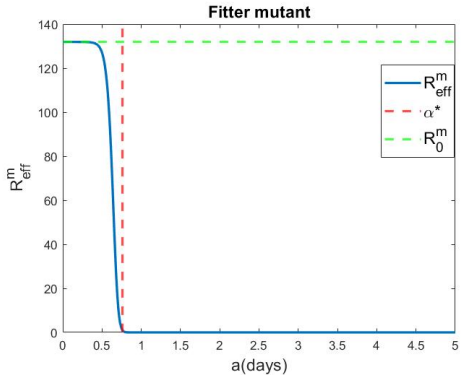

(d) $R^m_{eff}(a)$ of fitter mutant. Here $\alpha^* = 0.76$ days.

Fig. 3.5 The effective reproduction number R^m_{eff} for all types of mutant strains. The values α^* were calculated as the first values of time for which $R^m_{eff} < 1$.

Figure 3.5 shows how R^m_{eff} changes during the infection for all three types of mutants. There are two important observations here:

- R^m_0, which is just $R^m_{eff}(0)$, can take some high values but this is not surprising given the abundance of available target cells.
- $R^m_{eff}(a)$ decreases very quickly.

The rapid decrease of R^m_{eff} is due to the reduction in the number of target cells available to the mutant due to infection by the resident strain. This is why the R^m_{eff} curves follow a very similar trajectory to that of the target cells, as a comparison between figure 3.5 and figure 3.2 illustrates. The consequence is that the mutant may only emerge during the first day of infection in our two-strain TIV model.

Parameter Sensitivity

We will now investigate the effects of some of the model parameters on the within-host dynamics, both for the original TIV model and for the extended, two-strain TIV model. First we will vary some parameters of the original TIV model from section 3.2.1, and show how these changes affect the viral load during the course of the infection (figure 3.6). Then we will vary some parameters of the two-strain TIV model and illustrate how they affect some key infection-related quantities (figure 3.7).

For the original, one-strain TIV model we vary the following parameters from 50% up to 150% of their reference values:

- $c = 5.2$: the rate of clearance of free virions
- $\beta = 1.4 \times 10^{-4}$: the infectivity rate
- $\delta = 2$: the death rate of infected cells
- $p = 1.4 \times 10^{-5}$: the production rate of new virions by infected cells
- $V_0 = 0.32$: the initial viral load

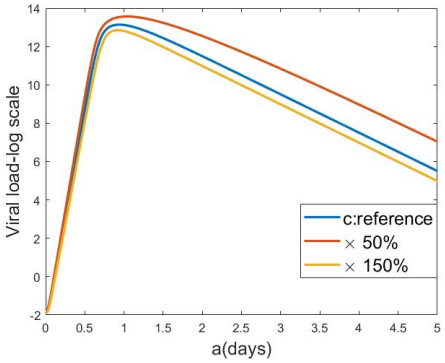

(a) A lower clearance rate c leads to a higher viral load throughout the infection.

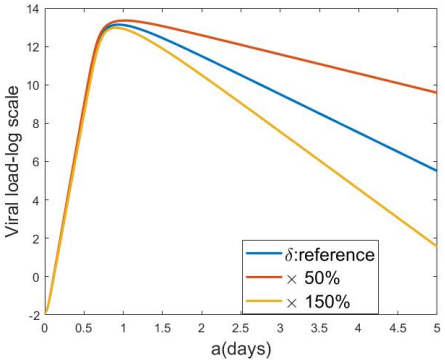

(b) The effect of lowering the death rate of infected cells δ is similar to that of lowering c, but more pronounced.

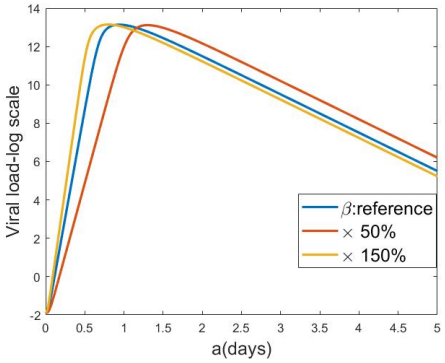

(c) Increasing the infectivity rate β speeds up viral kinetics and leads to an earlier peak for the viral load.

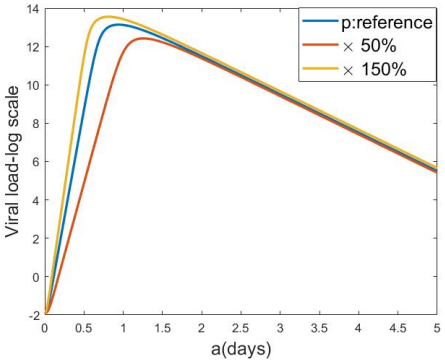

(d) Increasing the rate of virion production p also speeds up viral kinetics, but unlike increasing β it also leads to a larger maximal viral load.

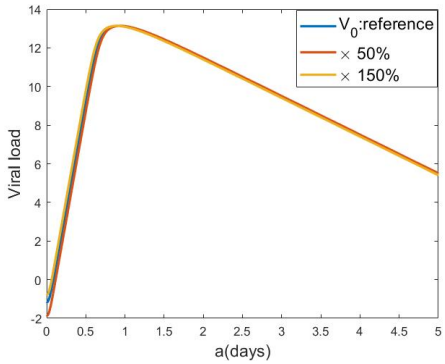

(e) Varying the initial viral load V_0 does not appear to have a strong effect on the viral load curve.

Fig. 3.6 Parameter sensitivity of the one-strain TIV model. When varying one parameter the rest remain constant at their reference values.

The following observations can be made from figure 3.6:

- Decreasing the rate of clearance of free virions c and the death rate of infected cells δ leads to a higher viral load throughout the infection. It also leads to an increase in the peak viral load.

- Increasing the infectivity rate β and the virion production rate p speeds up the viral kinetics.
- Changing V_0 does not have a strong effect on the dynamics.

All these observations are unsurprising, but they will provide a useful visual aid in interpreting the effects of the parameters of the slightly more complicated two-strain TIV model.

As we discussed in section 3.3.2, there are more ways to define the relative fitness of the mutant other than varying the death rate δ_2 of cells infected with it. To study how a different definition for the relative fitness of the mutant would affect the results of our two-strain TIV model, we will now vary the strain-specific clearance rate of free virions c_i, infectivity rate β_i and the virion production rate p_i and explore their effects on some key infection-related quantities. Specifically, we will study their impact on the cumulative viral loads of the two strains, the maximal viral loads and the times at which those maxima were attained.

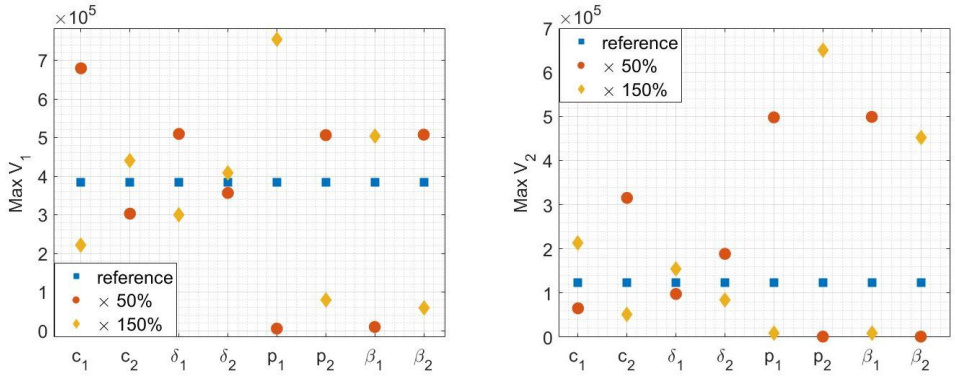

(a) The virion production rate p_i has the strongest impact on the maximal viral load of the ith strain.

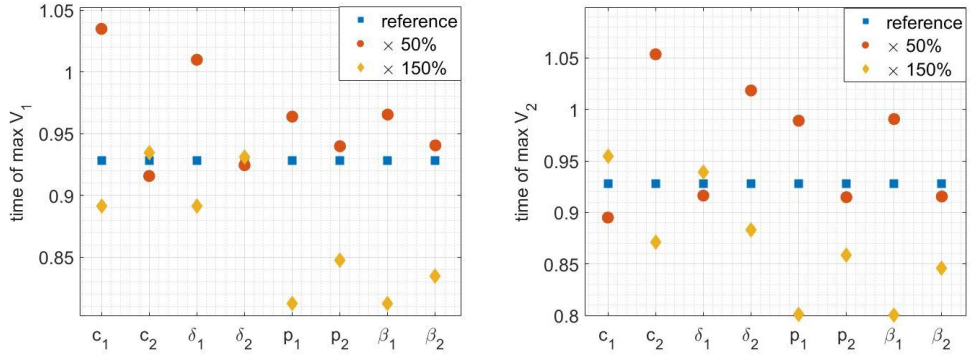

(b) The virion production rate p_i and the infectivity rate β_i have the strongest effect on the time of the peak viral load of the ith strain.

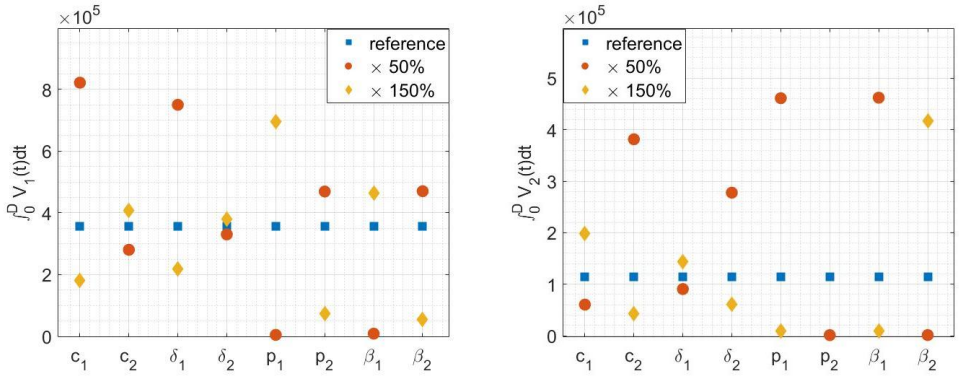

(c) Decreasing the clearance rate c_1 has the largest positive effect on the cumulative viral load of the resident strain. On the other hand decreasing p_1 and β_1 has the largest positive effect on the cumulative mutant viral load, as that provides it with a significant fitness advantage over the resident strain.

Fig. 3.7 Parameter sensitivity of the two-strain TIV model. Here the mutation is neutral ($\delta_2 = \delta_1$) and $\alpha = 0.05$ days. When varying one parameter the rest remain constant at their reference values from Table 3.1.

We can make the following observations based on figure 3.7:

- The results when varying c_i and when varying δ_i are very similar, as their groupings in all the graphs of figure 3.7 indicate. Though still comparable, changing c_i appears to have a stronger effect on the peak viral load than changing δ_i for both strains.

- Increasing p_i and β_i speeds up the time at which the ith strain achieves its maximal load. This is not surprising, since a larger p_i leads to the viral kinetics happening more quickly since more virions are produced by each cell infected with the ith strain. Therefore the time of the peak viral load of the ith strain comes earlier in the infection. Increasing β_i increases the success rate of virions infecting target cells, thereby also speeding up viral kinetics.

As was the case with the parameter sensitivity analysis of the original TIV model, these observations are unsurprising. But they indicate that our choice for the relative fitness of the mutant does not affect the model dynamics in a fundamental way.

3.3.4 Theoretical work

Given the simplicity of the two-strain TIV model, we will follow the work of Hadjichrysanthou *et al*. in [131] to obtain analytical formulas for the cumulative viral load of each strain and for the number of target cells remaining at the end of infection, which in the notation of the model are $\int_0^\infty V_i(a)da$ and $T(\infty)$.

From equation (3.13) it follows that

$$\int_0^\infty \frac{\dot{T}}{T}da = -\beta_1 \int_0^\infty V_1 da - \beta_2 \int_0^\infty V_2 da \tag{3.20}$$

To simplify the notation, let $A_{V_i} = -\beta_i \int_0^\infty V_i da$ for $i = 1,2$

Rewriting (3.20) using the new notation, we obtain

$$\beta_1 A_{V_1} + \beta_2 A_{V_2} = -\ln T(\infty) + \ln T(0) \tag{3.21}$$

Integrating equation (3.16) leads to

$$V_1(\infty) - V_1(0) = p_1 \Big[\int_0^\infty I_1 da \Big] - c_1 A_{V_1} \tag{3.22}$$

Therefore

$$\int_0^\infty I_1 da = (1/p_1)[V_1(\infty) - V_1(0) + c_1 A_{V_1}] \tag{3.23}$$

Similarly

$$\int_0^\infty I_2 da = ({}^1/_{p_2})[V_2(\infty) - V_2(0) + c_1 A_{V_2}] \tag{3.24}$$

Now, by adding equations (3.13)-(3.15) we obtain

$$\frac{dT}{da} + \frac{dI_1}{da} + \frac{dI_2}{da} = -\delta_1 I_1 - \delta_2 I_2 \tag{3.25}$$

Integrating this we obtain

$$T(\infty) - T(0) + I_1(\infty) - I_1(0) + I_2(\infty) - I_2(0) = -\delta_1 \int_0^\infty I_1 da - \delta_2 \int_0^\infty I_2 da \tag{3.26}$$

Viral shedding at the beginning and at the end of an influenza infection is very small, as various experiments have shown [24, 262]. So we can make the biologically justifiable assumptions that $V_i(\infty) = V_i(0)$ for $i = 1, 2$. We will also assume that $I_i(\infty) = 0$. Under these assumptions, substituting equations (3.23) and (3.24) into (3.26) leads to the following formula:

$$-\frac{\delta_1 c_1}{p_1} A_{V_1} - \frac{\delta_2 c_2}{p_2} A_{V_2} = T(\infty) - T(0) - I_1(0) - I_2(0) \tag{3.27}$$

Considering that $T(0)$, $I_1(0)$ and $I_2(0)$ are all initial values of the two-strain TIV model and therefore known, if we had an expression for $T(\infty)$ then we could solve for the cumulative viral loads A_{V_1} and A_{V_2} using equations (3.21) and (3.27). Regrettably I have not been able to find such an expression from the model equations.

3.3.5 Conclusion

The analysis of our two-strain TIV model with the deterministic emergence of a mutant strain highlights the biological intuition that the relative fitness of a mutant strain compared to that of the parent resident strain and the time of appearance of a mutant strain are critical in determining the mutant's survival and spread. The model suffers though from the same limitations as the original TIV model, namely the very rapid near-depletion of target cells due to infection and the merely implicit inclusion of the immune response. We expect both of these factors to potentially have a strong impact on emergence dynamics and on the width of the possible emergence window.

3.4 The Saenz model with deterministic emergence

3.4.1 Model presentation

The results of the two-strain TIV model show that the time of appearance of the mutant strain is critical in determining its viability and spread. In the context of the TIV model this is only because of the depletion of available target cells due to infection by the already circulating resident strain. Since the goal of this chapter is to build a model that can capture both the viral and the evolutionary dynamics of influenza within a host, it is important to investigate if there are other factors that affect the window of emergence of the mutant strain. A logical next step then would be to explore the effects of the innate immune response on the emergence dynamics. The biological intuition is to explore how an infection with a resident strain and its effects on the host immune system impact the potential emergence of a mutant strain. To this end we extend the *Saenz* model from [262], which we have already presented in section 3.2.2, to include two strains. This is the formulation of our two-strain *Saenz* model:

$$\frac{dT}{da} = -\beta_1 V_1 T - \beta_2 V_2 T - \phi F T \tag{3.28}$$

$$\frac{dE_{\alpha,1}}{da} = \beta_1 V_1 T - k_\alpha E_{\alpha,1} \tag{3.29}$$

$$\frac{dE_{\alpha,2}}{da} = \beta_2 V_2 T - k_\alpha E_{\alpha,2} \tag{3.30}$$

$$\frac{dW}{dt} = \phi F T - m(\beta_1 V_1 + \beta_2 V_2) W - a_w W \tag{3.31}$$

$$\frac{dE_{\gamma,1}}{da} = m\beta_1 V_1 W - k_\gamma E_{\gamma,1} \tag{3.32}$$

$$\frac{dE_{\gamma,2}}{da} = m\beta_2 V_2 W - k_\gamma E_{\gamma,2} \tag{3.33}$$

$$\frac{dR}{da} = a_w W \tag{3.34}$$

$$\frac{dI_1}{da} = k_\alpha E_{\alpha,1} + k_\gamma E_{\gamma,1} - \delta_1 I_1 \tag{3.35}$$

$$\frac{dI_2}{da} = k_\alpha E_{\alpha,2} + k_\gamma E_{\gamma,2} - \delta_2 I_2 \tag{3.36}$$

$$\frac{dV_1}{da} = p_1 I_1 - c_1 V_1 \tag{3.37}$$

$$\frac{dV_2}{da} = p_2 I_2 - c_2 V_2 \tag{3.38}$$

$$\frac{dF}{da} = q_1 E_{\gamma,1} + q_2 E_{\gamma,2} + q_1 I_1 + q_2 I_2 - dF \tag{3.39}$$

The definitions of the compartments and the parameters remain as in the original *Saenz* model, adjusted only to include a second strain. Here strain 1 refers to the resident strain and strain 2 to the mutant. Susceptible target cells (T) become infected by virions of the resident strain (V_1) at an infectivity rate of β_1 and by virions of the mutant strain (V_2) at an infectivity rate of β_2. They can also become prerefractory to infection due to the action of type I interferon (F) at a rate ϕ. While in this prerefractory state (W), cells can still be infected by virions of either strain but at a reduced rate $m\beta_i$. They finally become refractory and completely immune to infection (R) after they have stayed in this prerefractory state for an average $1/a_w$ days. Susceptible target cells (T) that have been infected by either viral strain but have not yet started releasing progeny virions move to an eclipse phase ($E_{\alpha,i}$) and stay there for an average of $1/k_\alpha$ days until the virus has finished replicating inside them. Similarly prerefractory cells (W) that have been infected by the ith strain first move to an eclipse phase ($E_{\gamma,i}$) and stay there for an average of $1/k_\gamma$ days. Cells infected by the ith strain that have reached the virion producing stage (I_i) die from the infection or as a result of the immune response at a rate δ_i. They produce progeny virions at a rate p_i and secrete interferon at a rate q_i. Cells that have been infected after they were primed by interferon but have not reached the virion-producing stage yet ($E_{\gamma,1}$ and $E_{\gamma,2}$) also secrete interferon at a rate of q_i, depending on which strain they were infected by. Circulating interferon decays at a rate d, while free virions of the ith strain are cleared by the immune system at a rate c_i.

The two-strain deterministic *Saenz* model is based on all the assumptions of the original Saenz model (section 3.2.2), as well as on the following extension-specific assumptions:

- Cells can only be infected once and only by a single strain.
- There is no competition between strains except for available target cells.

3.4.2 R_0 calculation

The basic reproduction number of the resident strain R_0^r, and of the mutant strain R_0^m, can be derived intuitively from the equations of the two-strain Saenz model. A cell infected with the resident strain at time $a = 0$ remains infectious for an average of $1/\delta_1$ days, and then dies. It produces an average p_1 virions per day, each of which survives for $1/c_1$ days

on average and can infect any of the T_0 available target cells. It is important to note here that at $a = 0$ all epithelial cells are target cells. Therefore they are all fully susceptible to infection at a rate β_1 given contact with a virion of the resident strain. This results in the following formula for the basic reproduction number of the resident strain:

$$R_0^r = \frac{1}{\delta_1} \times \frac{p_1 T_0}{c_1} \times \beta_1 \tag{3.40}$$

Similarly the basic reproduction number of the mutant strain is:

$$R_0^m = \frac{1}{\delta_2} \times \frac{p_2 T_0}{c_2} \times \beta_2 \tag{3.41}$$

We can corroborate these formulas using the next generation matrix approach to computing R_0 [89]. The infectious subsystem of the two-strain Saenz model associated with the resident strain consists of the V_1, I_1, $E_{\alpha,1}$, W, $E_{\gamma,1}$ and F compartments. Let $x = (x_1, x_2, x_3, x_4, x_5, x_6)^t$, where $x_k \geq 0$, be the number of cells or virions in each compartment of the infectious subsystem. We define x so that its elements correspond to the order in which the compartments were mentioned, for example x_1 corresponds to V_1, x_2 to I_1 etc. The disease free equilibrium of the full two-strain Saenz model is $(T_0, 0, 0, ..., 0)$, so all the compartments except the target cells are at zero. So let $x^* = (0,0,0,0,0,0)^t$ correspond to the infectious subsystem at the disease free equilibrium. Define $\mathscr{F}_j(x)$, where $j \in \{1,2,3,4,5,6\}$, to be the rate of appearance of new infections in the jth compartment of the infectious subsystem. Moreover let $\mathscr{V}_j^+(x)$ be the rate of transfer of cells into the jth compartment of the infectious subsystem by all other means except a new infection. Equivalently let $\mathscr{V}_j^-(x)$ be the transfer rate of cells out of the jth compartment. Finally let $\mathscr{V}_j(x) = \mathscr{V}_j^- - \mathscr{V}_j^+$. Then using the equations of the two-strain Saenz model, we obtain the following:

$$\mathscr{F}(x) = \begin{pmatrix} 0 \\ 0 \\ \beta_1 V_1 T \\ 0 \\ m\beta_1 V_1 W \\ 0 \end{pmatrix}$$

$$\mathscr{V}^+(x) = \begin{pmatrix} p_1 I_1 \\ k_\alpha E_{\alpha,1} + k_\gamma E_{\gamma,1} \\ 0 \\ \phi F T \\ 0 \\ q_1 E_{\gamma,1} + q_1 I_1 \end{pmatrix}$$

$$\mathscr{V}^-(x) = \begin{pmatrix} c_1 V_1 \\ \delta_1 I_1 \\ k_\alpha E_{\alpha,1} \\ m\beta_1 V_1 W + aW \\ k_\gamma E_{\gamma,1} \\ dF \end{pmatrix}$$

Then the Jacobian of $\mathscr{F}(x)$ at the disease-free equilibrium x^* is a 6×6 matrix of all zeros, with the exception of a single non-zero entry $\beta_1 T_0$ in position $(3,1)$. Define $F = \frac{\partial \mathscr{F}}{\partial x}\Big|_{x^*}$ (so that F is the Jacobian of $\mathscr{F}$ at the disease-free equilibrium). The Jacobian for $\mathscr{V}(x)$ at x^* is:

$$V = \frac{\partial \mathscr{V}}{\partial x}\Big|_{x^*} = \begin{pmatrix} c_1 & -p_1 & 0 & 0 & 0 & 0 \\ 0 & \delta_1 & -k_\alpha & 0 & -k_\gamma & 0 \\ 0 & 0 & k_\alpha & 0 & 0 & 0 \\ 0 & 0 & 0 & a & 0 & -\phi T_0 \\ 0 & 0 & 0 & 0 & k_\alpha & 0 \\ 0 & -q_1 & 0 & 0 & -q_1 & d \end{pmatrix}$$

Then the next generation matrix is defined as FV^{-1}, and R_0 as its spectral radius [89]. Doing these calculations leads to

$$R_0^r = \frac{1}{\delta_1} \times \frac{p_1 T_0}{c_1} \times \beta_1$$

which is the same expression as that given by the intuitive approach. The equivalent calculations with the infectious subsystem associated with the mutant strain corroborate the formula for R_0^m shown in equation (3.41).

3.4.3 Methods

Our approach remains the same as in our two-strain TIV model from section 3.3. We suppose that infection begins only with the resident strain present, and at some time α during the infection we force the appearance of a mutant strain.

The time of appearance of the mutant strain α again does not depend on the age of the infection, the amount of target and prerefractory cells present, the viral load of the resident strain or the interferon concentration. Similarly to the extended TIV model, α is treated again as a fixed parameter. Therefore we define emergence again again as the appearance of the mutant strain at some time α, after which the mutant viral load increases.

The model has the following initial conditions:

- $\alpha \in [0, D]$, where D is the duration of the infection. The case $\alpha = 0$ represents a coinfection with two strains and not a mutant strain emergence. It is included here for the sake of convenience.
- $T(0) = 3.5 \times 10^{11}$. This is the estimate for the epithelial cell population of the equine respiratory tract, as given in Saenz *et al.* [262].
- $V_1(0) = 0.16$. This comes from [262] as well. The authors used an initial viral load of 0.32, but here it is halved to account for the appearance of a second strain.
- $I_1(0) = 0$.
- $V_2(0) = 0$. Since there are no cells infected with the resident strain at time $t = 0$ there can also be no mutant virions present.
- $I_2(0) = 0$.
- $V_2(\alpha) = 0.16$. This is the same as the initial viral load of the resident strain.
- $I_2(\alpha) = 0$.
- $F(0) = 0$. This is because there are no infectious cells at time $t = 0$.
- $E_{\alpha,1}(0) = W(0) = E_{\gamma,1}(0) = R(0) = 0$.
- $E_{\alpha,2}(0) = E_{\gamma,2}(0) = E_{\alpha,2}(\alpha) = E_{\gamma,2}(\alpha) = 0$.

The parameter values of the model are presented in table 3.2, and almost all come from the Saenz *et al.* paper [262]. The only deviation is the value for m, which is the IFN-reduced infectivity. The authors use $m = 1$ in [262], but then the susceptibility of pre-refractory cells to infection is the same as that of the target cells. In order to incorporate the reduced infectivity of cells primed by interferon in our extended, two-strain *Saenz* model, we used $m = 0.9$ in our simulations. We will explore other possible values for m in section 3.4.4. We will refer to the parameter values in table 3.2 as the "reference values".

Parameter	Description	Value	Units	Source
β_i	Infectivity rate of ith strain	1.4×10^{-4}	(RNA copies)$^{-1}$ ml NS day^{-1}	[262]
p_i	Virus production rate for ith strain	1.4×10^{-5}	RNA copies (ml NS)$^{-1}$ day^{-1} cell^{-1}	[262]
q_i	IFN production by cells in I_i	5×10^{-10}	IFN fold change day^{-1} cell^{-1}	[262]
c_i	Free virus clearance rate for ith strain	5.2	Rate of virus clearance day^{-1}	[262]
$1/k_i$	Average duration of eclipse phases	$1/2$	Days	[262]
$1/a_w$	Average duration of prerefractory phase	$1/4$	Days	[262]
$1/\delta_1$	Average lifespan of cells infected with resident strain	$1/2$	Days	[262]
$1/\delta_2$	Average lifespan of cells infected with mutant strain	Varies	Days	
d	IFN clearance	6.8	Rate of IFN clearance day^{-1}	[262]
ϕ	IFN efficiency	56	(IFN fold change)$^{-1}$ day^{-1}	[262]
m	IFN-reduced infectivity	0.9		
α	Time of emergence of mutant strain	Varies	Days	

Table 3.2 Parameters of two-strain *Saenz* model

Initially we will assume that the relative fitness of the mutant strain depends only on the choice of death rate of cells infected with the mutant. So for a neutral mutation we assume $\delta_2 = \delta_1$, for a beneficial mutation $\delta_2 = (1/2) \times \delta_1$ and for a deleterious mutation $\delta_2 = 2\delta_1$.

The model is implemented in Matlab by first running the original, one-strain Saenz model from section 3.2.2 from time $a = 0$ until time $a = \alpha$. That is because V_2 remains at zero until time α, which in turn means that all the quantities associated with the mutant strain are zero. Then at time $a = \alpha$ we run the two-strain Saenz model. Conceptually this is the same as running the extended, two-strain Saenz model from $a = 0$ until $a = D$ and switching the value of $V_2(\alpha)$ from 0 to 0.16.

3.4.4 Results

Results using the reference values

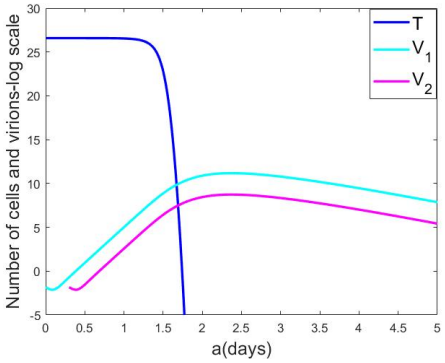

(a) The viral load initially decreases due to the inclusion of the first eclipse phase. We note that the y-axis is in natural-log scale and that $T_0 = 3.5 \times 10^{11}$, so $ln(T_0) = 26.6$

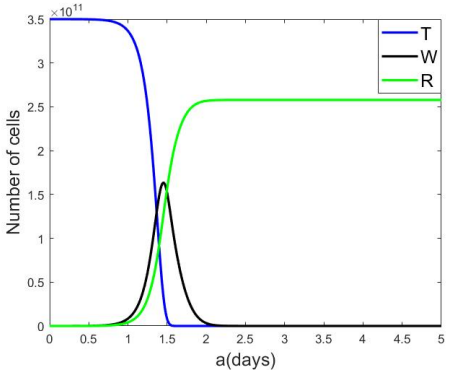

(b) The target cells are depleted, but not only due to infection. A portion of them becomes refractory due to the action of IFN.

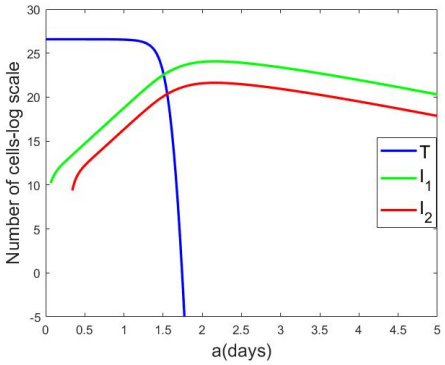

(c) The log-trajectories of I_1 and I_2 begin at some time $t > 0$ and $t > \alpha$ respectively. This is done only for illustration purposes, as otherwise their y-intercept would be at $-\infty$.

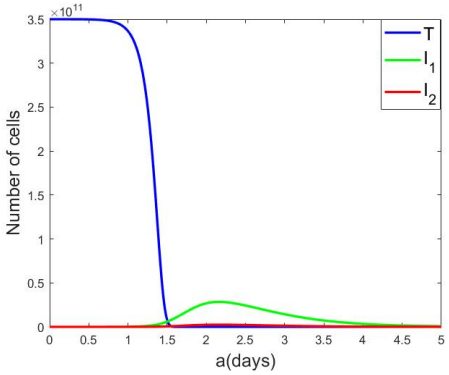

(d) This is the same as plot (c) but is not in log-scale.

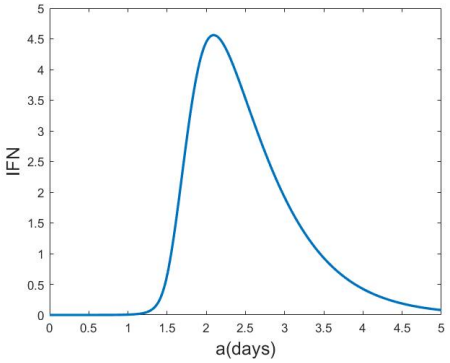

(e) IFN is secreted by cells in the I_i and $E_{\gamma,i}$ compartments.

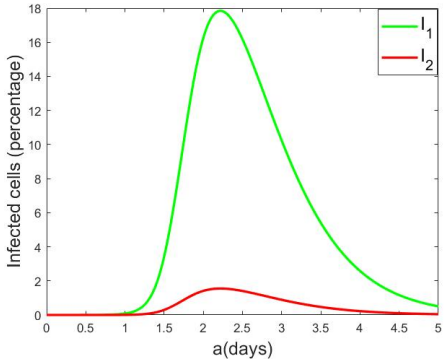

(f) The percentages of cells infected with the resident and mutant strains, each normalized by its corresponding average lifespan.

Fig. 3.8 Within-host dynamics for a neutral mutation ($\delta_2 = \delta_1$) and $\alpha = 0.3$. All the plots in this figure were generated in a single simulation of the two-strain Saenz model.

Figure 3.8 illustrates some key disease dynamics for the specific case that a neutral mutant emerges at time $\alpha = 0.3$ days. The initial decrease in the viral load that is evident in plot (a) is due to the effects of the eclipse phase. More specifically, as soon as the virus is introduced inside the host the virions start entering the host's target cells. But that triggers the immune response which starts clearing the free virions (this is captured by the parameter c_i in the model). Moreover the virus requires some time to replicate within a target cell before new virions can be synthesized and released, specifically an average of $1/k_\alpha = 1/k_\gamma = 1/2$ days. Therefore this initial decrease in the viral load can be attributed to the delay in the production of progeny virions by infected cells, and to the action of the immune system which is destroying any circulating virions. As we have already discussed, a potentially problematic aspect of the TIV model with regard to modeling emergence dynamics is its very rapid near-depletion of target cells. The two-strain *Saenz* model rectifies this by incorporating a strong innate immune response via the anti-viral action of type I interferons, and by including two eclipse phases which slow down viral kinetics. The result, as shown in plot (b), is that target cells decrease more slowly compared to the TIV model.

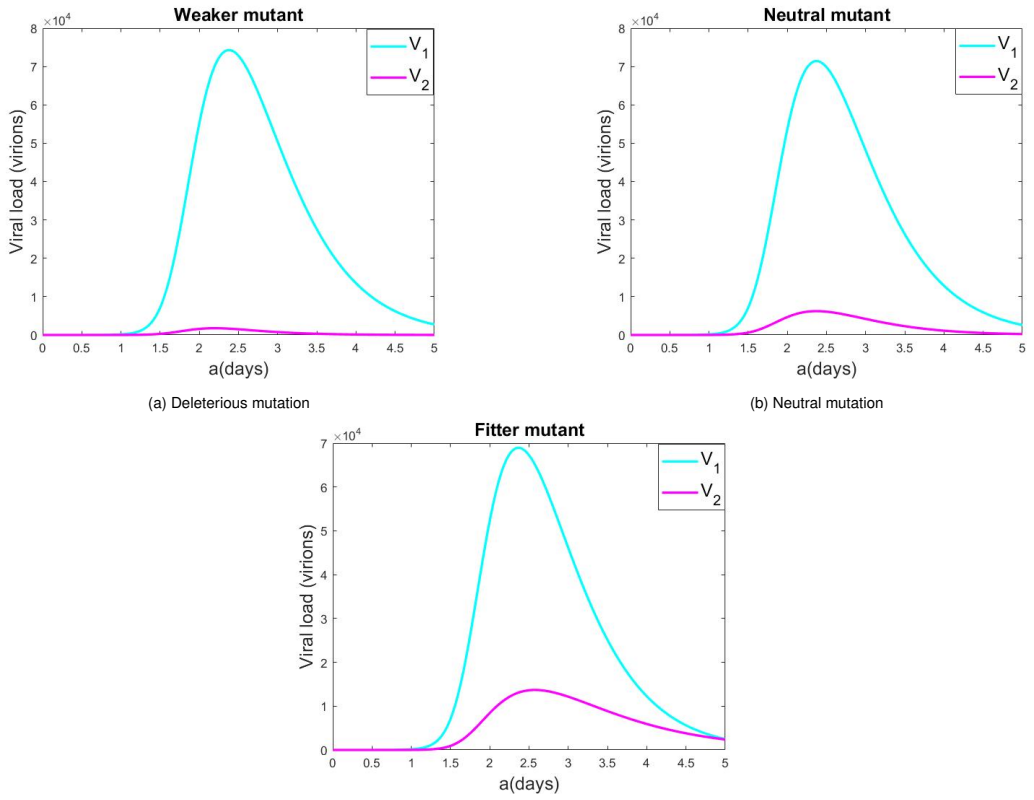

(a) Deleterious mutation

(b) Neutral mutation

(c) Beneficial mutation

Fig. 3.9 The viral loads of both strains during the course of the infection for all three types of mutation. In all cases the viral load peaks close to $a = 2.5$ days and then decreases rapidly due to the depletion of the available target cells. Here $\alpha = 0.3$.

Figure 3.9 illustrates how the viral loads of both strains change during the course of the infection for all three types of mutants. We observe that our two-strain *Saenz* model appears to capture well the documented peak viral load at around 2 days post-infection [24, 51, 262]. All three plots show a rapid decline in the viral load following its peak. This can be explained by the loss of available target cells due to infection and the effects of interferon, and also by the death of virion-producing infected cells (captured here by the parameter δ_i for the ith strain).

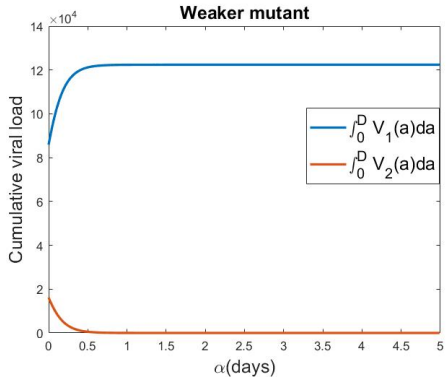

(a) Deleterious mutation : in the case of $\alpha = 0$, which is when $\int_0^D V_2$ achieves its maximum, the weaker mutant has a significantly smaller cumulative viral load compared to the fitter resident strain.

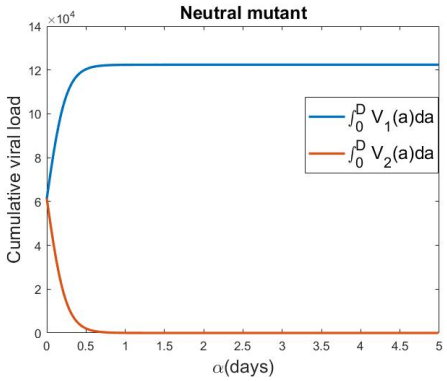

(b) Neutral mutation : the y-intercept of both curves is the same because the case $\alpha = 0$ represents a coinfection with two functionally identical strains, both of which have the same initial viral load.

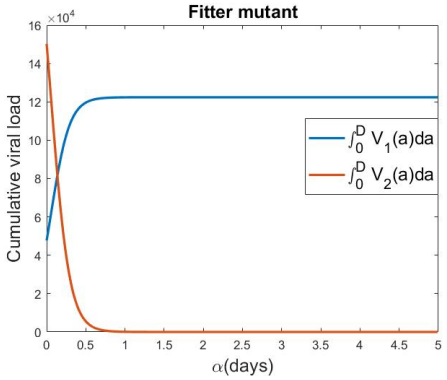

(c) Beneficial mutation : the fitter mutant attains its maximum cumulative viral load at $\alpha = 0$, and it is larger than the corresponding cumulative viral load of the weaker resident strain.

Fig. 3.10 The cumulative viral load for each strain as a function of the time of emergence α. For all three mutational fitness profiles the mutant cumulative viral load is a non-increasing function of α.

Figure 3.10 illustrates the importance of the time of appearance α for the survival and successful spread of the mutant strain. For all three types of mutation the mutant's cumulative viral load is unsurprisingly a non-increasing function of α. More specifically, for all three cases there is an initial rapid decrease in the mutant cumulative viral load, followed by its near-settling to some constant value close to zero. This indicates that after some certain α the effect of the time of appearance on the cumulative viral load diminishes. It is interesting then to explore if this is because emergence is no longer possible for the mutant, and what exactly is the associated cut-off value for α. In order to obtain such exact values for the value α^* after which the mutant strain can no longer emerge we can follow the same approach as in section 3.3.3 and use the mutant's effective reproduction number R^m_{eff}, which takes the following form:

$$R^m_{eff}(a) = R^m_0 \times \frac{T(a) + mW(a)}{T_0}, \tag{3.42}$$

where $mW(a)$ are the prerefractory cells at time a that can be infected and R_0^m is known since it was already calculated in section 3.4.2.

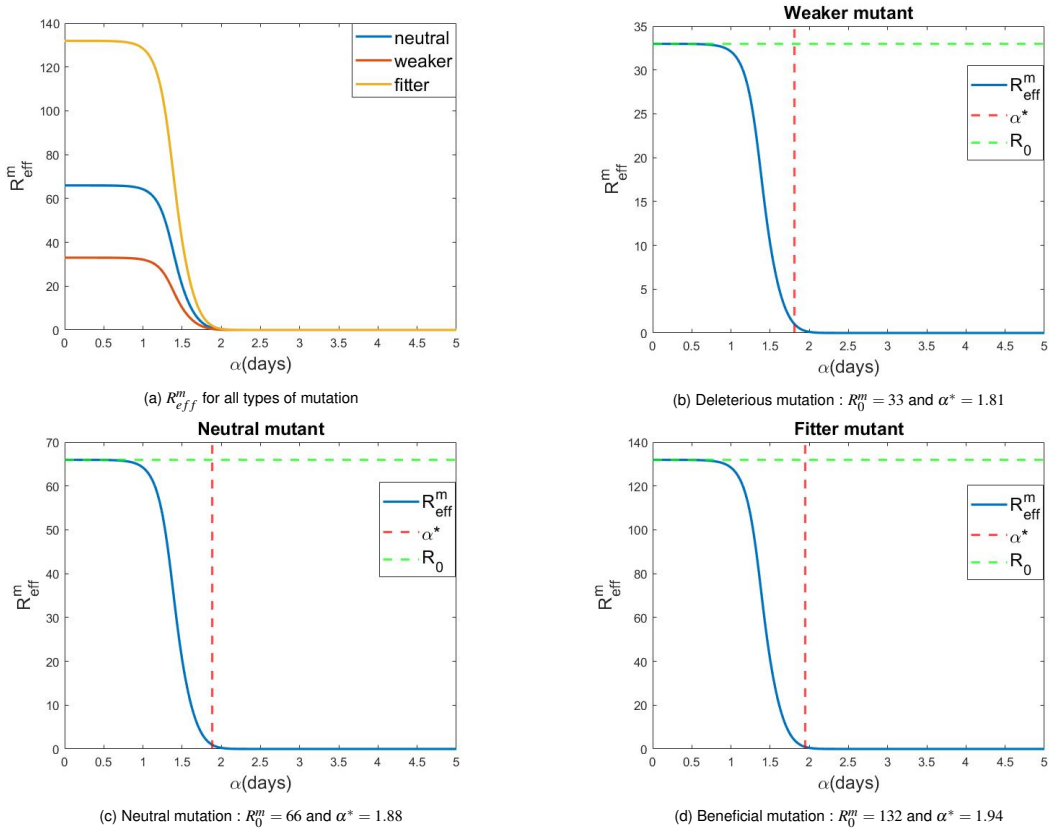

(a) R^m_{eff} for all types of mutation

(b) Deleterious mutation : $R_0^m = 33$ and $\alpha^* = 1.81$

(c) Neutral mutation : $R_0^m = 66$ and $\alpha^* = 1.88$

(d) Beneficial mutation : $R_0^m = 132$ and $\alpha^* = 1.94$

Fig. 3.11 R^m_{eff} for neutral, deleterious and beneficial mutations. The value α^* is defined as the first value of α for which R^m_{eff} falls below 1. Despite the considerable differences in the R_0^m of the three types of mutation, their associated values of α^* are very similar.

Figure 3.11 shows how R^m_{eff} changes during the course of the infection for all three types of mutation. While R^m_{eff} can initially take some very high values, it decreases very quickly. This is unsurprising given its dependence on the amount of target cells available, which also explains why the R^m_{eff} trajectories resemble the trajectory of the target cells. This dependence on the number of target cells available may also explain why, despite the significant differences in the basic reproduction numbers of the three mutant types, their associated α^* values are still very similar. In all three cases, the mutant strain can only emerge during the first two days of infection.

The two-strain TIV model from section 3.3 has a stricter window for emergence, as a comparison between figures 3.5 (from section 3.3.3) and 3.11 shows. More specifically,

the cut-off values α^* are earlier for the two-strain TIV model for all three types of mutation. This can be attributed to the very rapid depletion of target cells due to infection in the TIV model. In the two-strain Saenz model on the other hand, target cells are still being depleted due to infection but many of them also become prerefractory. This means that they can still be infected by the already circulating resident strain, but at a reduced rate. Moreover, in the Saenz model infected cells do not immediately start shedding virus. This leads to a slower decrease in the number of cells available to the mutant strain compared to the TIV model, and allows it to successfully appear and spread at later times during the infection.

Parameter sensitivity analysis

So far we have only used the death rate of infected cells to define the relative fitness of the mutant strain in our extended *Saenz* model. We will now investigate how the within-host dynamics are affected if we use a different definition for the fitness of the mutant. Moreover the majority of the reference values of our model's parameters were taken from the Saenz *et al*. paper [262], with the exception of the value for the IFN-reduced infectivity m. We will now also vary some of the extended *Saenz* model's parameters and study their effects on certain key infection-related quantities. The parameters explored are the following:

- p_i : the production rate of virions of the ith strain.
- β_i : the infectivity rate of the ith strain.
- ϕ : IFN efficiency. The rate at which target cells become primed by IFN and move to the prerefractory class is ϕF.
- q_i : the rate of production of IFN. The cells which secrete IFN are in the I_i and $E_{2,i}$ compartments.
- c_i : the rate of clearance of free virions of the it strain.
- δ_i : the death rate of cells infected with the ith strain.
- m : IFN-reduced infectivity. Cells in the prerefractory state W have been primed by interferon and are infected at a reduced rate $m\beta_i W$.
- k_α : $1/k_\alpha$ is the average duration of the eclipse phase E_α.
- k_γ : $1/k_\gamma$ is the average duration of the eclipse phase E_γ.

The parameters are varied by 50% up to 150% of their reference values. When one parameter is varied all others remain constant at their reference values.

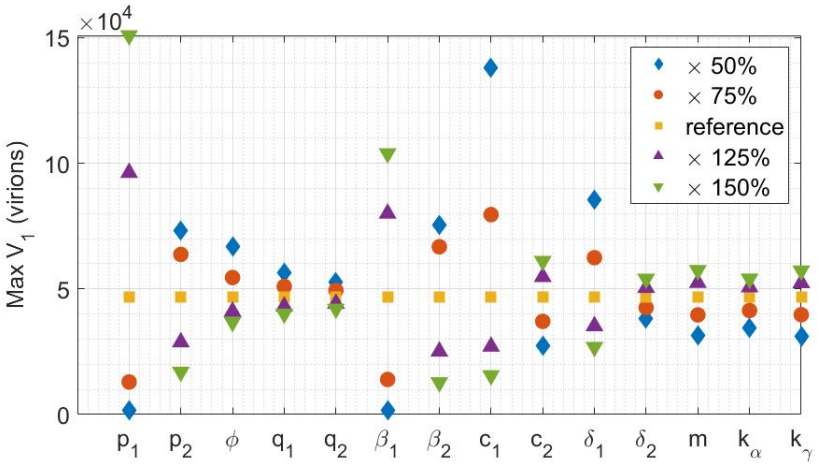

(a) p_1 and c_1 have the strongest effect on the maximum of V_1

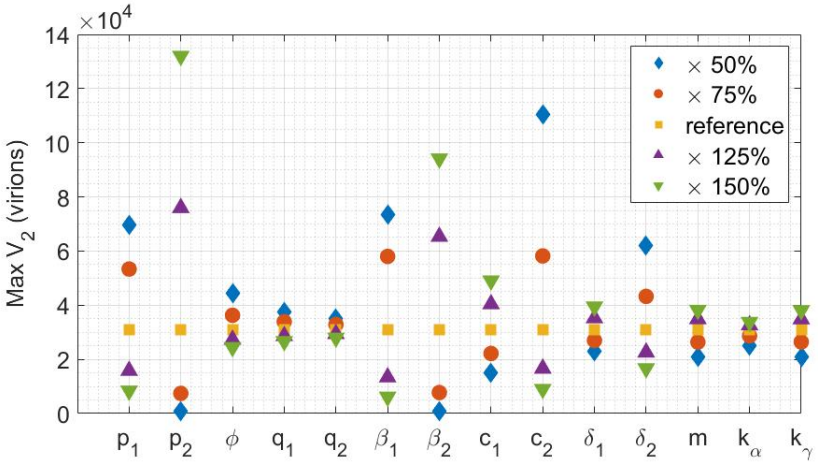

(b) p_2 and c_2 have the strongest effect on the maximum of V_2

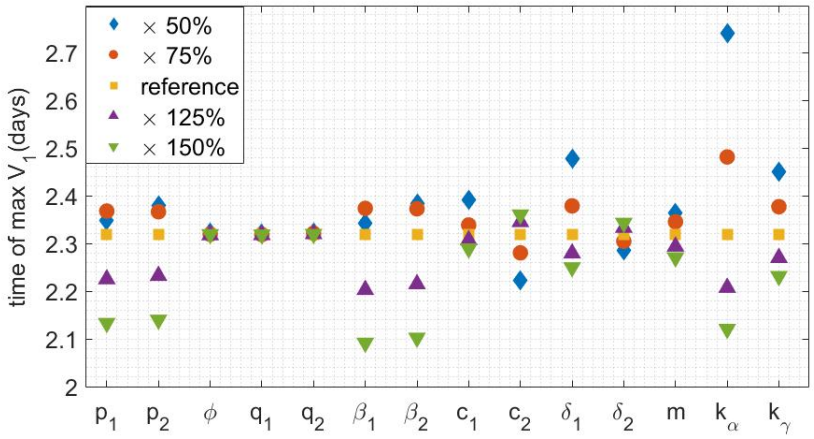

(c) Increasing p_i, β_i and k_α speeds up viral kinetics the most and results in an earlier resident peak viral load.

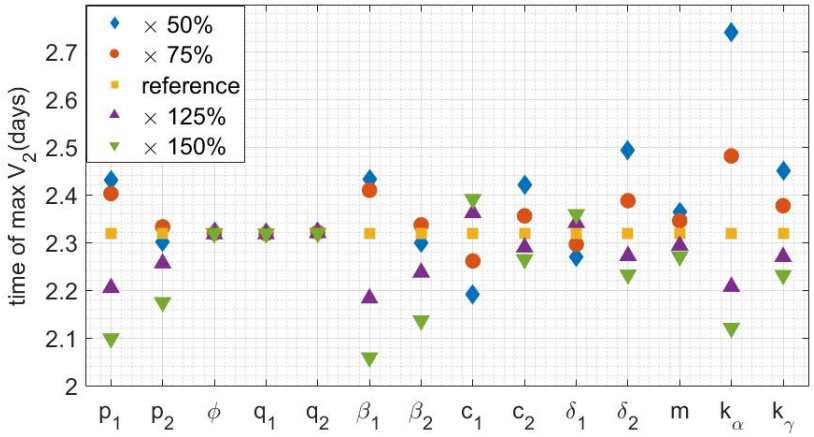

(d) Increasing p_i, β_i and k_α speeds up viral kinetics the most and results in an earlier mutant peak viral load.

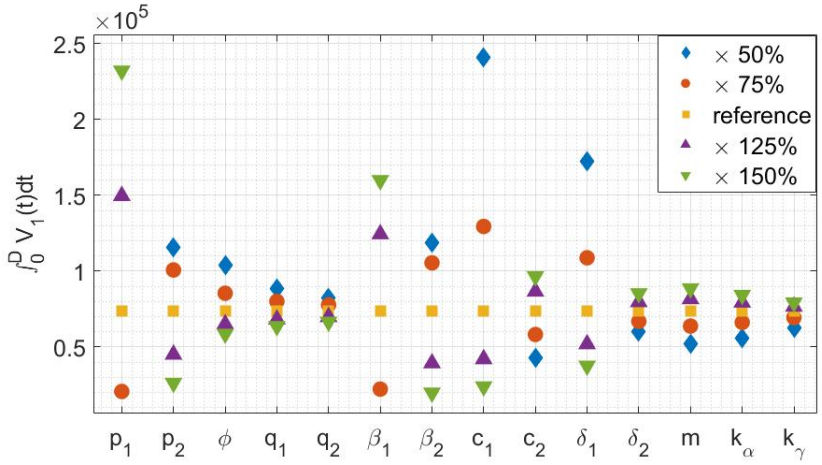

(e) Decreasing c_1 and δ_1 and increasing p_1 has the strongest effect on $\int_0^D V_1$.

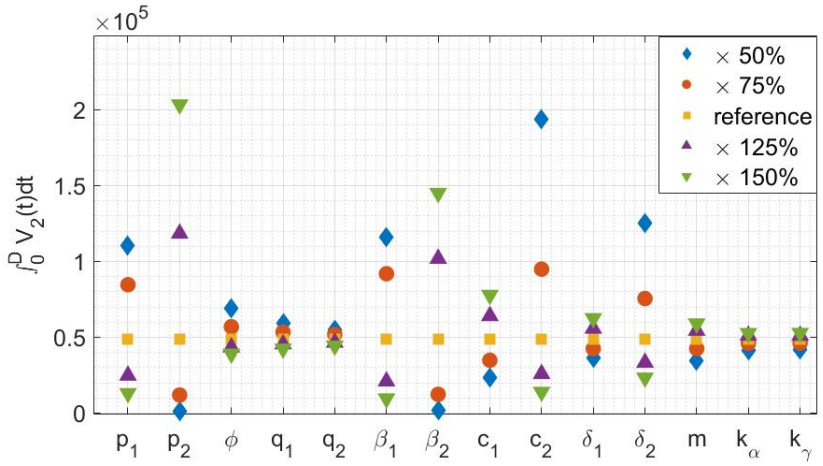

(f) Increasing p_2 has the strongest effect on $\int_0^D V_2$, followed very closely by decreasing c_2 and then by decreasing δ_2, p_1 and β_1.

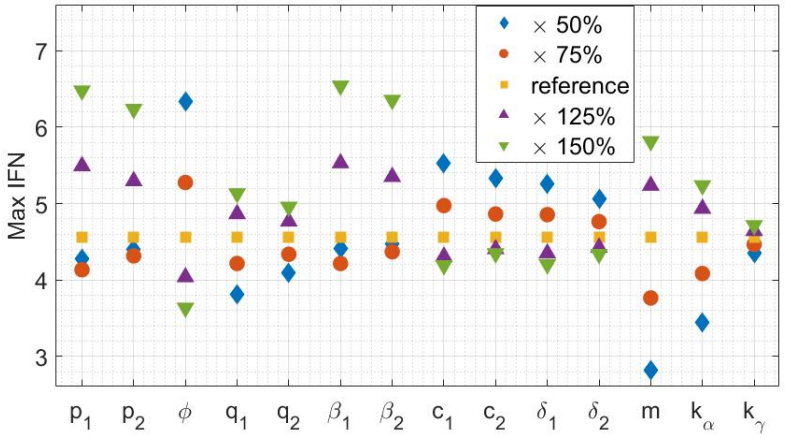

(g) Increasing m and decreasing ϕ, p_i and β_i have the strongest positive effect on the maximum IFN concentration.

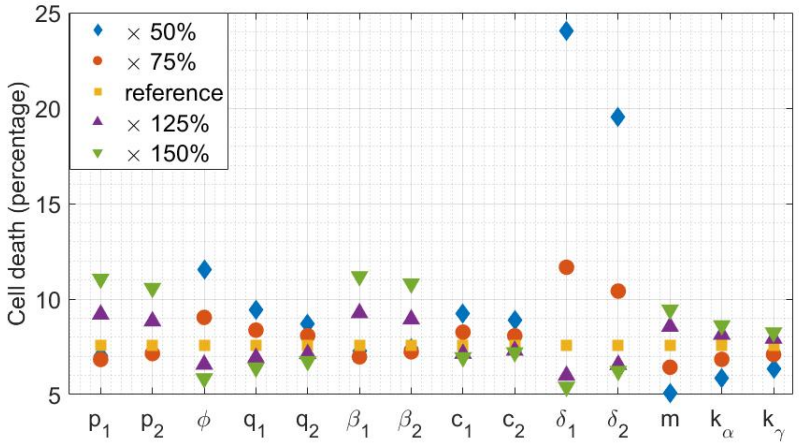

(h) The cell death percentage is defined here as the sum of the integrals of the I_1 and I_2 percentages during the infection, each normalized by the corresponding average lifespan of an infected cell. Decreasing δ_1 has the strongest effect on cell death.

Fig. 3.12 Parameter sensitivity analysis for the two-strain Saenz model. Each plot explores the effects of the parameters on one specific infection-related quantity. Here the mutation is neutral and $\alpha = 0.05$ days.

The following observations can be made from figure 3.12:

- The rate of production of virions of the resident strain p_1 has an intermediate to strong effect on all quantities studied. Increasing p_1 greatly increases the maximum and cumulative viral loads of the resident strain, and therefore increases the total amount of cells infected as well. Increasing p_1 speeds up viral kinetics and leads to an earlier time of peak viral load both for the resident and the mutant strain. Since the two strains are in competition against each other for available target and prerefractory cells, a higher p_1 leads to lower maximum and cumulative viral loads for the mutant. The equivalent effects are also observed for p_2, though slightly less pronounced. This is because the mutant strain appears here at $\alpha = 0.05$, which is very early but still means that the resident strain has a small advantage over the mutant.

- Varying the infectivity rate of the resident strain β_1 yields very similar results to varying p_1. The same holds for β_2 and p_2. This similarity is not surprising since p_i and β_i have a strong impact on the speed of viral kinetics.

- Decreasing the rate of clearance of free virions of the resident strain c_1 has a strong positive effect on the maximum and cumulative viral loads of the resident strain. This is not surprising, since a lower c_1 implies a less efficient immune system response with regard to killing off circulating virions. Due to competition between the strains decreasing c_1 has a deleterious effect on the mutant strain, such as reducing the mutant maximum and cumulative viral loads. The rate of clearance of virions of the mutant strain c_2 has the analogous effects.

- The death rate of cells infected with the resident strain δ_1 has very similar effects to that of c_1, namely decreasing it greatly increases the maximum and cumulative viral loads of the resident strain. But unlike c_1, δ_1 naturally has a significant impact on the cell death percentage too. Again due to the competition between the resident and mutant strains, decreasing δ_1 has detrimental effects on the mutant strain. The equivalent effects are observed for δ_2.

- The average duration of the first eclipse phase $1/k_\alpha$ has a strong effect on the time of the peak viral load both for the resident and the mutant strains. This is because a larger k_α means that fully susceptible target cells move more quickly into the virion producing stage, thus speeding up viral kinetics. The parameter k_α also has an intermediate effect on the maximum IFN concentration. Cells in the first eclipse phase do not secrete IFN. It is only infected cells (I_i) and cells in the second eclipse

phase ($E_{\gamma,i}$) which secrete IFN, but a smaller k_α means that cells stay in the first eclipse phase longer.

- The parameter q_i affects only the peak IFN concentration and the cell death. Since q_i is the rate of production of IFN by cells in the I_i and $E_{\gamma,i}$ compartments it is unsurprising that it has an effect on the maximum IFN concentration. Moreover, since higher amounts of IFN mean that more target cells become prerefractory and then completely immune to infection, it is not surprising that increasing q_i decreases the cell death throughout the infection.

- The IFN efficiency ϕ has a significant effect on the maximum IFN concentration. This is expected as increasing it leads to target cells becoming prerefractory at a faster rate, which in turn decreases the amount of IFN-secreting infected cells throughout the infection.

- The IFN-reduced infectivity of prerefractory cells m has unsurprisingly a significant effect on the peak IFN, as well as a weak effect on cell death.

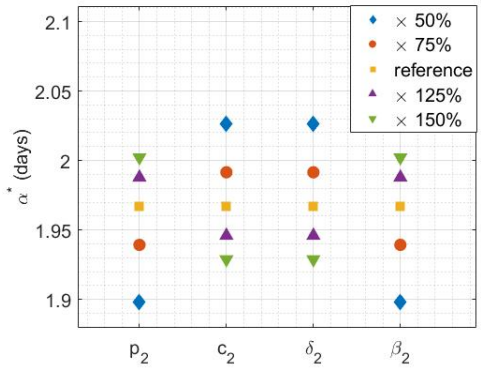

Fig. 3.13 The effects of varying some key mutant-specific parameters on the cut-off time for emergence α^*. The parameters explored here are the ones which appear in the R_0^m formula. None of them appear to have a significant effect on α^*, as its values only range inside $[1.85, 2.03]$

Our default definition for the relative fitness of the mutant assumes that mutation affects only the death rate δ_2 of cells infected by the mutant strain. The biological intuition here is that a fitter mutant could have a beneficial mutation that interferes with immune signalling pathways, thus slowing down the immune response. Some other strain specific parameters which could have been used to define the mutant's relative fitness are p_i, c_i and β_i. We could think of a beneficial mutation as one that increases the accuracy and reliability of the viral RNA replication, leading to more viable virions being synthesized

and therefore to a larger p_2. Or as one that improves the virions' efficiency in binding with target cells and therefore leads to a higher β_2. Or finally as one that improves the virions' evasion of the host immune response and in turn leads to a lower c_2. We can use figures 3.12 and 3.13 to conclude that the within-host dynamics of the two-strain Saenz model would be similar had any of these possible definitions been used instead of the default, which depends only on δ_2. Firstly, we have already been demonstrated using figure 3.12 that the effects of δ_2 and c_2 are very similar. If the relative fitness depended instead on the production rate of virions p_2 or the infectivity rate of the mutant strain β_2, the main difference would be that the viral loads would peak slightly earlier during the infection. That peak would still occur sometime between the second and third days of infection though (figures 3.12c and 3.12d), thus not affecting the within-host dynamics in a substantial manner. Therefore we may conclude that the results of our extended *Saenz* are not highly sensitive to the definition of the relative fitness of the mutant strain.

3.4.5 Conclusion

Our two-strain *Saenz* model with deterministic emergence appears to be a good basis for a within-host model that describes the dynamics and evolution of influenza. Some of its most significant advantages for the scope of this thesis are its computational efficiency and its inclusion of the innate immune response and of the two eclipse phases. The analysis of our extended *Saenz* provided some valuable insight into the importance of the time of emergence for the spread of the mutant strain. So far though we have forced the appearance of a mutant strain by choosing a specific value for α and using it as one of the model's fixed parameters. But as we demonstrated in section 3.4.4, if α comes very late in the infection then the mutant will fail to grow. Therefore a next step in understanding the emergence dynamics of a mutant strain would be to consider in more depth the factors which affect its viability at different appearance times and incorporate them into our extended *Saenz* model.

3.5 The Saenz model with stochastic emergence

3.5.1 The probability of emergence

When considering an infection with only the resident strain, at time α there are $E_\alpha(\alpha) + E_\gamma(\alpha)$ cells which have been infected by the resident strain but have not yet started

releasing progeny virions. Since we are assuming that influenza mutations are the results of mistakes occurring during the error-prone viral replication phase, an eclipse cell infected originally by a virion of the resident strain could produce virions of the mutant strain instead. The mutation rate $\hat{\varepsilon}$ of influenza, expressed as substitutions per nucleotide per cell infection (s/n/c), has been estimated in various published studies [264, 297]. But not all nucleotide mutations result in antigenic changes. We restrict our calculations only to the nucleotides which code for the hemmagglutinin (HA) and neuraminidase (NA) proteins. This is because various analyses have shown that mutations in these two influenza surface proteins are the main drivers of antigenic drift [200, 207, 291]. Most substitution mutations do not result in functional or antigenic changes in the influenza proteins [312]. Therefore we will further assume that only 10% of the HA-coding and NA-coding nucleotides can potentially generate an antigenic change and that only 0.05% of the substitution mutations in these nucleotides will successfully result in an antigenic change. This probability that a substitution mutation in the HA- and NA-coding nucleotides will result in an antigenic change is chosen by us and is semi-arbitrary. We will address this at length in the Discussion section of this chapter.

Continuing towards our expression for the probability of emergence, it is important to also account for the fact that substitution errors often result in lethal mutations [200], while we are only interested in viable ones. Moreover experimental studies have shown that different types of mutation occur at different frequencies [297]. Using a deleterious mutation as an example, we can express the rate of appearance of a weaker,viable mutant as:

$$app(\alpha) = (\varepsilon\rho_w) \times \big(k_\alpha E_\alpha(\alpha) + k_\gamma E_\gamma(\alpha)\big) \tag{3.43}$$

where the multiplication by k_α and k_γ is because at time α only a portion of cells in the two eclipse phases will to move to the I_2 class and start releasing progeny virions. Here ε is the mutation rate when restricting only to the HA- and NA-coding nucleotides that could lead to antigenic mutations and ρ_w is the probability that mutation leads to a viable, weaker mutant.

As we have previously demonstrated in section 3.4.4, not all viable mutants can grow following their appearance. To account for this, an approach used in models of mutant strain emergence at a population level is to calculate the mutant's probability of survival using results from branching processes [307], while also accounting for the loss of

available hosts due to infection by the resident strain [143]:

$$P(\text{survival } | \text{appearance at } \alpha) = 1 - \frac{1}{R^m_{eff}(\alpha)}$$

where $R^m_{eff}(\alpha)$ is the effective reproduction number of the mutant strain. This term however does not take immunological feedbacks, such as the size of the resident strain and its impact on the mutant viral load, into account. If a mutant strain survives but remains at a very small viral load throughout the infection or only infects very few target cells then its impact on the infection dynamics could be negligible compared to that of the resident strain. Therefore we will only consider that a mutant strain successfully emerges within a host if it reaches a certain threshold in its total number of virions. That threshold will be explored in section 3.5.2. Using again a deleterious mutation as an example, our expression for the probability of survival and adequate growth of a weaker mutant strain is then:

$$P_w(\text{survival \& growth } | \text{appearance at } \alpha) = \left(1 - \frac{1}{\mathscr{R}^{m,w}_{eff}(\alpha)}\right) \times \mathbb{1}^w_{(c_2 \int_\alpha^D (V_2(a)da) \geq s^*)} \tag{3.44}$$

where $\mathbb{1}$ is the indicator function and s^* is the aforementioned size threshold. It is important to note that $\int_\alpha^D V_2(a)da$ depends on the time of appearance α but also on the fitness of the strain.

Using equations (3.43) and (3.44), we can express the rates of appearance, survival and adequate growth of a weaker, neutral and fitter mutant respectively as:

$$\lambda_w(\alpha) = (\varepsilon\rho_w) \times \left(k_\alpha E_\alpha(\alpha) + k_\gamma E_\gamma(\alpha)\right) \times \left(1 - \frac{1}{R^{m,w}_{eff}(a)}\right) \times \mathbb{1}^w_{(c_2 \int_\alpha^D (V_2(a)da) \geq s^*)}$$

$$\lambda_n(\alpha) = (\varepsilon\rho_n) \times \left(k_\alpha E_\alpha(\alpha) + k_\gamma E_\gamma(\alpha)\right) \times \left(1 - \frac{1}{R^{m,n}_{eff}(a)}\right) \times \mathbb{1}^n_{(c_2 \int_\alpha^D (V_2(a)da) \geq s^*)}$$

$$\lambda_f(\alpha) = (\varepsilon\rho_f) \times \left(k_\alpha E_\alpha(\alpha) + k_\gamma E_\gamma(\alpha)\right) \times \left(1 - \frac{1}{R^{m,f}_{eff}(a)}\right) \times \mathbb{1}^f_{(c_2 \int_\alpha^D (V_2(a)da) \geq s^*)}$$

Emergence at some time α inherently assumes that before α either no mutant appeared or some mutant appeared but failed to establish. Using results from survival analysis and treating $\lambda(\alpha)$ as a hazard function, we can express the probability that no mutant strain has emerged up to time α as $e^{-\int_0^\alpha \lambda_n(a)da}$, using the case of a neutral mutation

as an example. Therefore using the rate of emergence at α and the probability that no emergence has occurred before α, we may express the probability density function f for the emergence of a mutant strain at time α as:

$$f_w(\alpha) = \lambda_w(\alpha) \times e^{-\int_0^\alpha \lambda_w(a)da}$$
$$f_n(\alpha) = \lambda_n(\alpha) \times e^{-\int_0^\alpha \lambda_n(a)da}$$
$$f_f(\alpha) = \lambda_f(\alpha) \times e^{-\int_0^\alpha \lambda_f(a)da}$$

This formulation depends on the following underlying assumptions:

- An infected cell can only produce virions of a single strain.
- The duration of the infection at the cellular level is exponentially distributed and contacts follow a Poisson process. This is necessary for the probability of survival being $\left(1 - 1/R_{eff}^m\right)$ [75].

The parameter values are in table 3.3. The values of ρ_w, ρ_n and ρ_f all come from [297], where Visher *et al*. generated 128 viruses from an influenza A strain (A/WSN/33/H1N1), each with a single nucleotide mutation, and then performed a competitive fitness assay to measure their fitness against that of the parent strain. The percentage of lethal mutations was found to be 30%. It is important to note that the authors grouped weakly deleterious and neutral mutations together in their analysis, because the fitness values they derived for their weakly deleterious mutants were not statistically different from the fitness value of the parent strain. Since in this chapter we are not differentiating between weakly and strongly deleterious mutations, we use the results of the authors' "weakly deleterious and neutral mutations" group to inform only the parameters of our neutral mutant. A similar analysis by Lyons & Lauring in [200] resulted in very similar probabilities for lethal, deleterious, neutral and beneficial mutations.

Parameter	Description	Value	Units	Source
Nuc	Number of nucelotides in influenza genome	13588	n	[44]
Nuc_{HA}	Number of nucelotides coding for HA	1778	n	[44]
Nuc_{NA}	Number of nucelotides coding for NA	1413	n	[44]
$\hat{\varepsilon}$	Mutation rate (all nucleotides)	2.3×10^{-5}	s/n/c	[264]
ε	Mutation rate (given 10% of HA and NA coding nucleotides)	$2.7 \times 10^{-10} = (2.3 \times 10^{-5}) \times \left((1778+1413)/13588\right) \times 0.1 \times 0.0005$	s/n/c	
ρ_w	Probability that mutation leads to a viable and weaker mutant	$0.7 \times \left(\frac{35}{90}\right)$		[297]
ρ_n	Probability that mutation leads to a viable and neutral mutant	$0.7 \times \left(\frac{47}{90}\right)$		[297]
ρ_n	Probability that mutation leads to a viable and beneficial mutant	$0.7 \times \left(\frac{7}{90}\right)$		[297]

Table 3.3 Parameters for the extended *Saenz* model with stochastic emergence

In this section the three types of mutation are defined again by the choice of the death rate δ_2 of cells infected by the mutant strain. As a result, the effective reproduction numbers R^m_{eff} for all three mutants are known from section 3.4.4.

3.5.2 Results

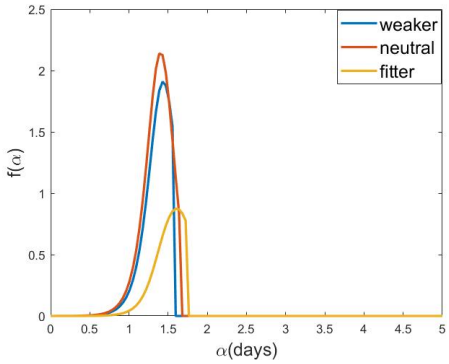

(a) The emergence density of a mutant strain for all types of mutation. Using Matlab's *trapz* function we calculated the cumulative within-host probability as 0.71 for a weaker strain, 0.91 for a neutral and 0.37 for a fitter.

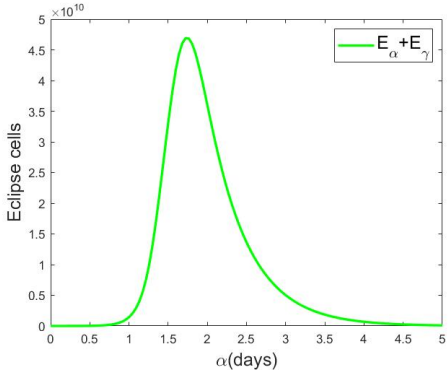

(b) The trajectory of cells in the two eclipse phases E_α and E_γ together.

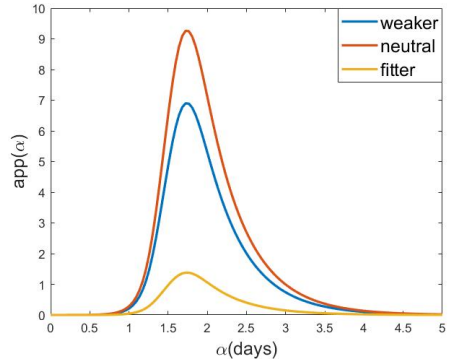

(c) The rate of appearance for each type of mutant strain. The plot indicates that mutants can appear on most days of the infection. Given the definition of $app(\alpha)$ it is not surprising that its curve resembles that of the eclipse cells in plot (b).

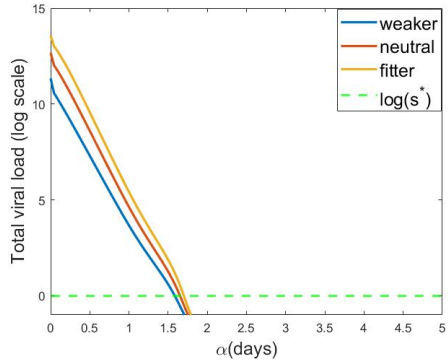

(d) The total viral load for each type of mutation given a forced appearance at α. The cut-off value s^* is the minimum growth condition from equation (3.44), which a mutant needs to meet in order to emerge successfully. Here $s^* = 1$.

Fig. 3.14 Stochastic emergence of all three types of mutants in the two-strain Saenz model. Here $s^* = 1$.

Figure 3.14 shows how the emergence density of a mutant strain changes during the course of the infection for each type of mutation [plot (a)]. Initially there are very few eclipse cells [plot (b)], resulting in small chances of emergence. As the number of the eclipse cells increases so does the density of emergence, until it reaches a maximum and then drops to and remains at zero. This is because of the survival probability term in our expression for the emergence density, which requires that the mutant's effective reproduction number R^m_{eff} is larger than 1 at the time of emergence. Moreover the cut-off for emergence can also be attributed to our sufficient growth condition $\int_\alpha^D (V_2(a)/da) \geq s^*$ that any mutant which appears at some time α must meet in order to emerge successfully [plot (d)]. These two conditions force the possible emergence window to be early in the infection, specifically within the first two days for all mutants when $s^* = 1$, as is the case in figure 3.14. It should be noted however that mutants can keep appearing through most

of the infection, as plot (c) illustrates. The within-host emergence probability in the cases of a neutral and a weaker strain is very high (0.91 and 0.71 respectively), while for a fitter mutant it is significantly smaller (specifically 0.37). This is due to the findings of Visher *et al*. in [297], according to which very few mutations lead to a viable, fitter mutant. It can still be argued though that the cumulative emergence probabilities are very high in our model for all three types of mutation. We will investigate the reasons behind this in the next section (section 3.5.3) and also address them at length in the Discussion section of this chapter (section 3.7).

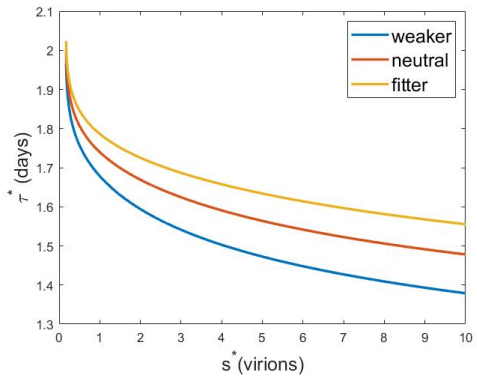

Fig. 3.15 The cutoff value α^* after which no successful emergence can occur as a function of s^*. This was calculated as the first value of the appearance time $\alpha \in [0, D]$ for which the total mutant viral load $c_2 \int_{\alpha}^{D} V_2(a)da$ drops below the given s^*. For a mutant to reach a higher total viral load it needs to emerge earlier in the infection, which is why α^* is a non-increasing function of s^*.

Figure 3.15 shows the sensitivity of the stochastic emergence model to the choice of the sufficient growth cutoff value s^*. By definition as s^* increases our condition for the minimum total mutant viral load given emergence at some time α becomes stricter. As a result the latest time α^* after which no mutant could reach the minimum size s^* comes earlier in the infection. This is why α^* is a non-increasing function of s^*. Since a very small value for the growth cutoff would allow for a wider window of emergence, it is useful to calculate what is the smallest value that s^* could take. For analytical purposes we suppose $D = \infty$ throughout this calculation. If we introduce some mutant viral load $V_2(0)$ at time $\alpha = 0$ and only allow it to decrease until it reaches zero, then its virion production rate p_2 must be zero. Then from the dV_2/da equation of the extended Saenz model (equation 3.38 in section 3.4) it follows that:

$$V_2(a) = V_2(0) \times e^{-c_2 a}$$

Then the sufficient growth condition $c_2 \int_{\alpha}^{\infty} V_2(a)da \geq s^*$ becomes:

$$V_2(0) \int_0^{\infty} \left(e^{-c_2 a} da\right) \geq \frac{s^*}{c_2} \Rightarrow$$
$$-\frac{V_2(0)}{c_2} e^{-c_2 a}\Big|_{a=0}^{a=\infty} \geq \frac{s^*}{c_2} \Rightarrow$$
$$V_2(0) \geq s^*$$

Therefore mathematically the minimum value that s^* could take is the mutant initial viral load $V_2(0)$, but that corresponds to a mutant strain which dies off very quickly. So to ensure sufficient growth we will require that at least $s^* \geq 2V_2(0)$.

3.5.3 The mutant's window of emergence

As we discussed in the previous section, our within-host emergence density results in a very narrow emergence window for the mutant strain for all three types of mutation. In this section we will try to identify the factors that lead to such a small potential emergence interval. For the sake of simplicity we will only consider the case of a neutral mutant strain.

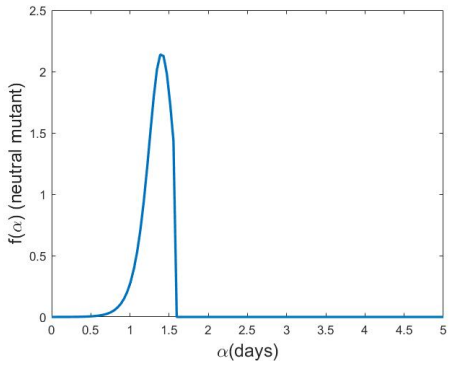

(a) The emergence density for a neutral mutant. Here $f(\alpha) = 0\ \forall \alpha \geq 1.68$ because any $\alpha > 1.68$ does not satisfy our final size requirement $s^\star = 1$ (though it does satisfy $\mathscr{R}^m_{eff}(\alpha) > 1$ until $\alpha = 1.88$). We note that f reaches its peak at $\alpha_{peak} = 1.39$ days.

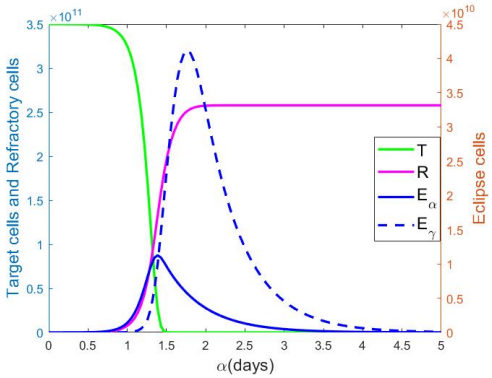

(b) The population of E_α cells peaks earlier than that of the E_γ cells. We note that there are 2 y-axes in this plot and they have different scales.

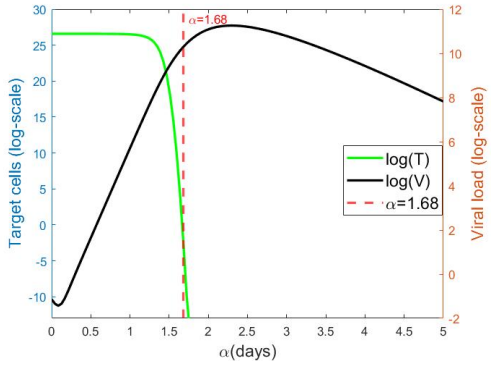

(c) The number of target cells remains relatively constant until the viral load approaches a value close to its peak, and then it decreases very rapidly. We note that there are 2 y-axes in this plot and they have different scales.

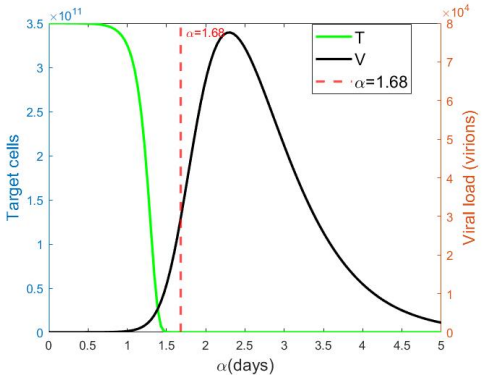

(d) The same plot as (c) but not in log-scale. We note that there are 2 y-axes in this plot and they have different scales.

Fig. 3.16 The window of emergence of a neutral mutant strain in our within-host model when the parameters are fixed at their reference values from Tables 3.3 and $s^\star = 1$. All plots are the result of a single simulation of our within-host model.

Figure 3.16 shows how the emergence density of a neutral mutant strain changes throughout the infection [plot (a)], along with some relevant within-host quantities. Plot (b) shows how the number of target cells, refractory cells and eclipse cells changes throughout the infection. We focus on the eclipse cells E_α and E_γ because they are the candidates for mutation. We see that E_α cells are more prominent compared to E_γ cells earlier in the infection. This is not surprising, since E_γ cells are cells which started as target cells, then moved into the prerefractory W compartment via the action of interferon and then became infected at a reduced rate $m\beta$. E_α cells on the other hand are simply target cells which have been infected but have not reached the virion-producing stage yet. Since the E_α cells increase and reach their peak numbers earlier than the E_γ cells, we may conclude that their contribution to the potential emergence of the mutant is higher than that of the E_γ cells. We note that the numbers of refractory cells begin to take off

in the middle of the second day of infection, and can account for some of the decrease in T. Plot (c) shows how the numbers of target cells and virions change in log-scale throughout an infection with the resident strain. We observe that the population of target cells remains relatively constant in the initial stages of the infection until the viral load approaches its peak, and then it depletes very rapidly. Since the number of target cells T makes up part of our expression for the effective reproduction number $\mathscr{R}_{eff}^{m,w}$ of the mutant, this drastic decrease in T also leads to a rapid decrease in $\mathscr{R}_{eff}^{m,w}$. As a result, if the mutant had appeared under these circumstances it would not be able to spread efficiently due to the lack of target cells available to it. The minimum final size condition in our expression for the emergence density accounts for such mutants and ensures that they cannot emerge. This explains why the window of emergence cannot extend past $\alpha^\star = 1.68$, which is the first α that fails our $s^\star = 1$ condition. We underline that plot (c) also illustrates the log-linear phase of rapid virus growth followed by the log-linear phase of slower virus decay. Plot (d) depicts the same quantities as plot (c), namely the number of target cells and virions, but not in log-scale. We include it in this figure because it highlights the small interval from the time that the viral load starts to grow until the time that emergence is no longer possible in our model. It further highlights the two phases of exponential growth and decay of the virus. Using these four plots, the shape of the emergence density can be explained as following:

- E_α cells start to increase towards the end of the first day of infection. E_γ cells and virions start to increase later in the infection. Therefore for $\alpha < 1$, E_α cells appear to contribute the most to the potential emergence of the mutant. Since their population is still very small though, the probability of emergence is also very small during the first day of infection.

- From the beginning of the second day of infection and until time $\alpha_{peak} = 1.39$ (which corresponds to the maximum of f) the population of E_α cells grows considerably, while the population of E_γ cells starts to grow but is still rather small. The viral load has also increased considerably from its initial size, which is not surprising given the rapid viral expansion displayed in plot (c). Moreover, by the time $\alpha = \alpha_{peak}$ the number of target cells has already started to decrease but is still very large. This abundance of eclipse cells, virions and target cells can account for the increase in f during the second day of infection until it reaches its peak at $\alpha_{peak} = 1.39$ days.

- Between $\alpha = 1.39$ and $\alpha = 1.68$, which corresponds to the cut-off value for emergence in our model given $s^\star = 1$, the number of virions and eclipse cells keeps increasing. On the other hand though the population of target cells has decreased

rapidly to approximately 1% of its original size. This can explain the quick decrease of the emergence density following its peak.

We may conclude that the main determinant of the width of the emergence window is the decrease in the number of target cells. A rapid depletion in the population of target cells entails a narrow emergence window.

3.5.4 Rederiving the probability of survival

In order to further explore the emergence potential of a mutant strain we limit our attention only to the early stages of the mutant's appearance at some time α and investigate its probability of survival in a stochastic setting. We follow a method presented by Pearson *et al*. in [227] to obtain a formula for the probability of extinction by transforming our two-strain Saenz model into its equivalent multi-type branching process. The key difference between our work and the results published in [227] is that the authors considered a coinfection with two strains instead of a mutant strain appearance and focused on the populations of target cells, infected cells and virions. We on the other hand also include eclipse cells and consider the potential effect of the host immune response via the inclusion of prerefractory cells. This accounts for the fact that the later a mutant strain appears the fewer cells are available to it either due to infection by the resident strain or due to the action of type I interferon.

Since we are only interested in the very early stages of a mutant strain appearance at some time α, we assume as in [227] that there are no variations in the number of target and prerefractory cells, namely $T(\alpha) = T$ and $W(\alpha) = W$ are constants. For the sake of clarity we combine the two eclipse phases $E_{\alpha,2}$ and $E_{\gamma,2}$ into a single eclipse phase E_2 with duration $1/k$, where the subscript 2 is because we are interested specifically in the mutant strain (strain 2). This last simplification does not alter the model in any fundamental way since we have been assuming so far that the duration of the two eclipse phases $E_{\alpha,2}$ and $E_{\gamma,2}$ are actually equal. The relevant equations adapted from the two-strain Saenz model are:

$$\frac{dV_2}{dt} = p_2 I_2 - c_2 V_2$$
$$\frac{dE_2}{dt} = \beta_2 V_2 T + m\beta_2 V_2 W - kE_2$$

$$\frac{dI_2}{dt} = kE_2 - \delta_2 I_2$$

Then our system can be fully described by a state vector $\vec{m} = (n_{V_2}, n_{E_2}, n_{I_2})$, where n_{V_2} is the number of virions, n_{E_2} the number of eclipse cells and n_{I_2} the number of infectious cells.

Event	Description	Rate	Transition vector
$V_2 \to E_2$	Virion infects cell	$r_1 = (\beta_2 T + m\beta_2 W)V_2$	$(0,1,0)$
$E_2 \to I_2$	Eclipse cell becomes infectious	$r_2 = kE_2$	$(0,-1,+1)$
$I_2 \to V_2$	Infectious cell releases virion	$r_3 = p_2 I_2$	$(+1,0,0)$
$V_2 \to \emptyset$	Virion dies	$r_4 = c_2 V_2$	$(-1,0,0)$
$I_2 \to \emptyset$	Infectious cell dies	$r_5 = \delta_2 I_2$	$(0,0,-1)$

Table 3.4 Two-strain Saenz model: the discrete time multi-type branching process

Using table 3.4 we can express the probability that the ith event will be the next one to occur as:

$$P_i(\vec{m}) = \frac{r_i(\vec{m})}{Z(\vec{m})}$$

where $Z(\vec{m}) = \sum_{i=1}^{5} r_i(\vec{m})$. Since we can obtain the probability of survival from the probability of extinction, we define extinction as the state $\vec{0} = (0,0,0)$ and, using the same notation as Pearson *et al.* in [227], we express the probability of extinction as:

$$\mathscr{E}(\vec{m}) = \sum_i P_i(\vec{m})\mathscr{E}(\vec{m} + d\vec{m}_i) \tag{3.45}$$

where $d\vec{m}_i$ refers to the ith transition vector from table 3.4. The reasoning behind this expression is as follows: if the system starts at some state $\vec{m}$ then it will transition to some state $\vec{m} + d\vec{m}_i$ with probability $P_i(\vec{m})$. Then the probability of extinction from state $\vec{m}$ is the sum of the extinction probabilities of all states which differ from it by a single transition, weighted by the probability of these transitions. Then substituting in the expressions for $P_i(\vec{m})$ and $\mathscr{E}(\vec{m} + d\vec{m}_i)$ we obtain:

$$\begin{aligned}\mathscr{E}(\vec{m}) =& \frac{(\beta_2 T + m\beta_2 W)V_2}{Z}\mathscr{P}_{V_2}^{n_{V_2}}\mathscr{P}_{E_2}^{n_{E_2}+1}\mathscr{P}_{I_2}^{n_{I_2}} \\ &+ \frac{kE_2}{Z}\mathscr{P}_{V_2}^{n_{V_2}}\mathscr{P}_{E_2}^{n_{E_2}-1}\mathscr{P}_{I_2}^{n_{I_2}+1} \\ &+ \frac{p_2 I_2}{Z}\mathscr{P}_{V_2}^{n_{V_2}+1}\mathscr{P}_{E_2}^{n_{E_2}}\mathscr{P}_{I_2}^{n_{I_2}} \\ &+ \frac{c_2 V_2}{Z}\mathscr{P}_{V_2}^{n_{V_2}-1}\mathscr{P}_{E_2}^{n_{E_2}}\mathscr{P}_{I_2}^{n_{I_2}} \\ &+ \frac{\delta_2 I_2}{Z}\mathscr{P}_{V_2}^{n_{V_2}}\mathscr{P}_{E_2}^{n_{E_2}}\mathscr{P}_{I_2}^{n_{I_2}-1}\end{aligned} \tag{3.46}$$

where $\mathscr{P}_{V_2}$, $\mathscr{P}_{E_2}$ and $\mathscr{P}_{I_2}$ are the probabilities of extinction when starting from a state where only a single virion, a single eclipse cell or a single infected cell is present respectively. We now assume as in [227] that the processes of virion, eclipse cell and infectious cell extinction are independent. Then we may express

$$\mathscr{E}(\vec{m}) = \mathscr{P}_{V_2}^{n_{V_2}}\mathscr{P}_{E_2}^{n_{E_2}}\mathscr{P}_{I_2}^{n_{I_2}} \tag{3.47}$$

Substituting equation 3.47 into 3.46, we then solve for $\mathscr{P}_{V_2}$ by setting $E_2 = 0$ and $I_2 = 0$, for $\mathscr{P}_{E_2}$ by setting $V_2 = 0$ and $I_2 = 0$ and finally for $\mathscr{P}_{I_2}$ by setting $V_2 = 0$ and $E_2 = 0$. Firstly by setting $E_2 = 0$ and $I_2 = 0$ we obtain

$$\mathscr{P}_{V_2}^{n_{V_2}} = \frac{(\beta_2 T + m\beta_2 W)}{Z}\mathscr{P}_{V_2}^{n_{V_2}}\mathscr{P}_{E_2} + \frac{c_2}{Z}\mathscr{P}_{V_2}^{n_{V_2}-1}$$

Dividing by $\mathscr{P}_{V_2}^{n_{V_2}-1}$ and substituting for $Z(n_{V_2},0,0)$ we obtain

$$\mathscr{P}_{V_2} = \frac{(\beta_2 T + m\beta_2 W)}{\beta_2 T + m\beta_2 W + c_2}\mathscr{P}_{V_2}\mathscr{P}_{E_2} + \frac{c_2}{\beta_2 T + m\beta_2 W + c_2} \tag{3.48}$$

Similarly assuming $V_2 = 0$ and $E_2 = 0$, dividing the resulting expression by $\mathscr{P}_{I_2}^{n_{I_2}-1}$ and substituting for $Z(0,0,n_{I_2})$ we obtain

$$\mathscr{P}_{I_2} = \frac{p_2}{p_2 + \delta_2}\mathscr{P}_{V_2}\mathscr{P}_{I_2} + \frac{\delta_2}{p_2 + \delta_2} \tag{3.49}$$

Finally by setting $V_2 = 0$ and $I_2 = 0$ and following the exact same method we conclude that

$$\mathscr{P}_{E_2} = \mathscr{P}_{I_2} \tag{3.50}$$

Solving equations 3.48-3.50 we obtain

$$\mathscr{P}_{V_2} = \min\left(\frac{(p_2+\delta_2)c_2}{(\beta_2 T + m\beta_2 W + c_2)p_2}, 1\right) \tag{3.51}$$

$$\mathscr{P}_{I_2} = \min\left(\frac{(\beta_2 T + m\beta_2 W + c_2)\delta_2}{(\beta_2 T + m\beta_2 W)(p_2+\delta_2)}, 1\right) \tag{3.52}$$

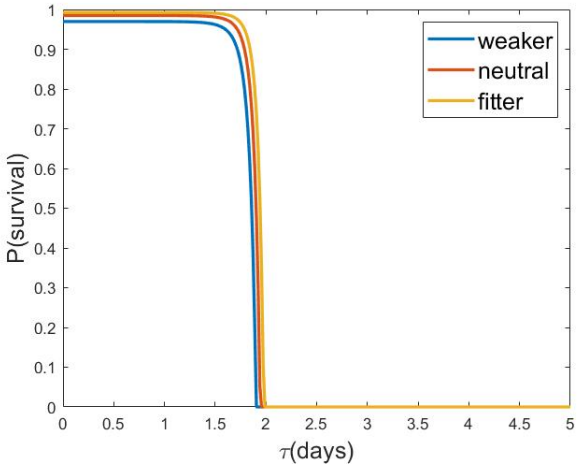

Fig. 3.17 The probability of survival of a mutant strain given appearance at some time α. P(survival) is calculated here as $1 - \mathscr{P}_{V_2}(\alpha)$ using equation 3.51. The curve resembles the trajectory of the target cells during the infection.

Since we are modeling the appearance of a mutant as the introduction of some initial mutant viral load, we can use equation 3.51 to calculate the probability of the mutant's survival given appearance at some time α. The result is presented in figure 3.17. The probability of survival follows a trajectory very similar to that of the target cells. Initially it is very high and then declines very rapidly until it reaches zero.

3.5.5 Conclusion

In this section we developed a probability density function for the emergence of a mutant strain within a host that is initially infected by a resident strain. Our emergence density takes into consideration the mutant's effective reproduction number and also includes a minimum final size requirement for the mutant viral load so as to avoid situations in which the mutant arises within-host but fails to replicate effectively. Our emergence density depends on influenza's mutation rate, which we restricted for our purposes to the substitution mutations in the NA- and HA-coding nucleotides that specifically result in an antigenic change. Plotting the emergence density using the reference values for our two-strain *Saenz* model parameters showed that the cumulative emergence probability throughout the host's infection is high. It also showed that the window of emergence is very narrow, which our analysis suggests can be attributed mainly to the rapid depletion of target cells in our model.

3.6 The Saenz model with vaccination

3.6.1 Adding vaccination

There are various different ways to incorporate vaccination in a within-host influenza model. We will first list four adaptive immune responses to a natural influenza infection or influenza vaccination and for each one we will suggest a simple way that we could include it in our model.

- Antibodies targeted against the HA protein block the ability of the receptor binding site of HA to interact with the host cell surface, thereby preventing attachment and entry. A simple way to incorporate this in our within-host model could be via a decrease in the transmission rate β_i, as β_i captures the successful binding of virions to target cells.
- Antibodies generated against the NA protein limit the release of virus from infected cells [180]. This could be added to our model as a decrease in the virion production rate p_i.
- Antibodies targeting the highly conserved external domain of the M2 protein interfere with virus assembly [180]. We could also add this to our model as a decrease

in the virion production rate p_i, as an inefficient virus assembly would lead to fewer fully functional infectious progeny virions being produced.

- Cytotoxic T-cells enhance viral clearance, which does not confer protection but is important for illness recovery [69]. We can capture this in our model as an increase in the viral clearance rate c_i.

We will capture the effects of vaccination simply via an increase in the clearance rates c_1 and c_2 of the resident and mutant strains respectively. We emphasize that increasing c_i is not the only way in which we could incorporate this aspect of the cellular immune response (or vaccination in general) to our within-host model. We could also explicitly add new compartments for antibodies or T-cells, but our aim is to capture the within-host effects of vaccination in a very simple way. This is because later in chapter 5 we will combine our within-host vaccination model with a between-host model to investigate the epidemiological and evolutionary dynamics of influenza across both scales. Since such cross-scale models can easily become very complicated and computationally intensive, we believe that incorporating vaccination simply as an increase in one of the strain-specific within-host model parameters provides a good starting point. Furthermore we argue that our decision to incorporate the effects of vaccination by varying specifically the viral clearance rates c_i as opposed to varying the transmission rates β_i, the viral production rates p_i or the death rate of infected cells δ_i should not have a significant impact on our model's results. This is because in section 3.4.4 we performed a parameter sensitivity analysis of our extended *Saenz* model and found that varying each one the strain-specific parameters β_i, c_i, δ_i and p_i had similar effects on our model's results.

We will assume that the vaccine is homologous to the resident strain and examine its impact on some key strain-specific dynamics in three different cases: the case that the vaccine offers no cross-protection from the mutant strain, the case that the vaccine offers partial cross-protection from the mutant strain and finally the case that the vaccine offers full cross-protection from the mutant strain. The case of full cross-protection does not entail that the vaccine offers full immunity to the mutant strain, only that the effect of the vaccine is exactly the same on both strains.

We further assume that the host is already vaccinated before the infection begins. Given our definition of vaccination this means that we implement our extended *Saenz* model

exactly as it appears in section 3.4, but with a different value for the clearance rates c_1 and c_2. We vary c_1 and c_2 to explore how vaccine efficacy, defined here as the vaccine-induced increase in the clearance rate c_1, affects the dynamics of the two strains.

3.6.2 Results

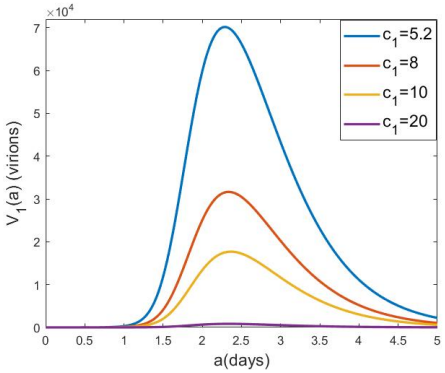

(a) The viral load of the resident strain becomes smaller throughout the infection as c_1 increases, based on the four values of c_1 tested here.

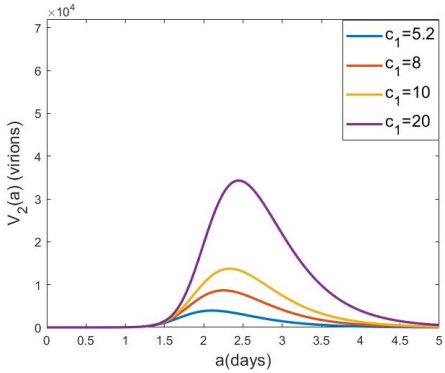

(b) The viral load of the mutant strain becomes larger throughout the infection as c_1 increases, based on the four values of c_1 tested here.

Fig. 3.18 The viral loads of the resident and mutant strains for certain values of the clearance rate c_1. Here we assume that the vaccine has no effect on the mutant strain. The mutant strain is weaker ($\delta_2 = 2\delta_1$) and $\alpha = 0.1$ days.

Figure 3.18 shows the effects of four different values of the clearance rate c_1 on the viral loads of the resident and mutant strains throughout the infection. Since we assume that vaccination acts merely by increasing c_1, we may think of increasing c_1 as the vaccine having an increasingly stronger effect on the resident strain and becoming more efficient in clearing it. For the purposes of this figure we assume that vaccination has no effect on the mutant strain. Plot (a) shows that higher values of c_1 correspond to lower viral loads for the resident strain throughout the infection, while plot (b) shows that the reverse holds true for the mutant. This is not surprising given our assumption that the vaccine acts only on the resident but has no impact on the mutant. As the vaccine becomes more efficient in clearing the resident the mutant strain gains an increasingly larger competitive advantage, allowing it to grow more effectively and reach higher concentrations.

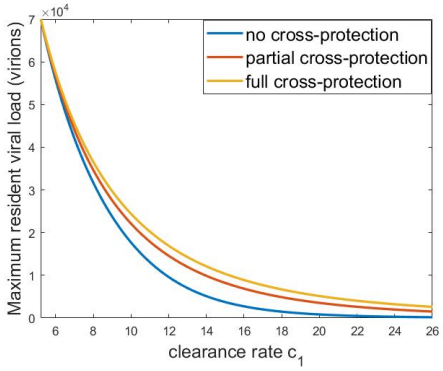

(a) The maximum of V_1 is computationally a non-increasing function of c_1. When the vaccine has no effect on the mutant strain then the mutant gains an advantage in the competition for target cells. This is why the blue curve remains below the curves corresponding to partial and full cross-protection.

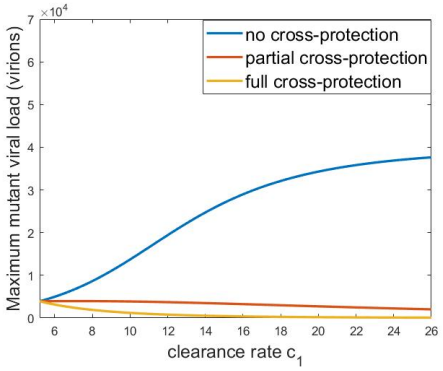

(b) In the case of no cross-protection the maximum of V2 is computationally a non-decreasing function of c_1. This is because as c_1 increases the host immune system becomes more efficient in clearing the resident strain, offering an advantage to the otherwise weaker mutant strain.

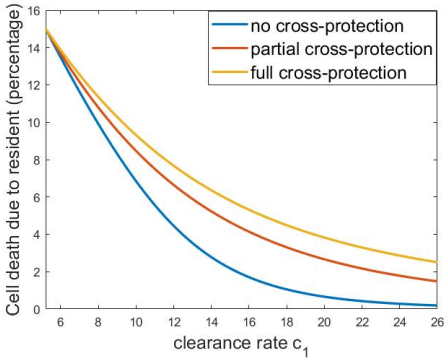

(c) The percentage of cells infected by the resident strain is computationally a non-increasing function of c_1.

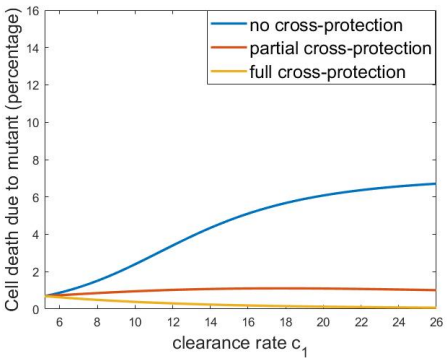

(d) In the case of no cross-protection, the percentage of cells infected by the mutant is computationally a non-decreasing function of c_1.

Fig. 3.19 The effects of a vaccine homologous to the resident strain. The left column illustrates the vaccine's effects on the resident strain and the right column on the mutant. No cross-protection means that the vaccine has no effect on the clearance rate c_2 of the mutant, full cross-protection that it has the same effect on c_2 as it does on c_1 and partial cross-protection that it increases c_2 by half the amount that it increases c_1. Here the mutant strain is weaker ($\delta_2 = 2\delta_1$) and $\alpha = 0.1$ days.

Figure 3.19 illustrates the effects of a vaccine that is homologous to the resident strain on the maximum viral load of the two strains and on the cell death attributed to each strain. We focus on varying only the clearance rate c_1 against the resident strain because we assume that the infection is initiated only by the resident strain and that the mutant strain is the result of random errors that occur during the replication of the resident within eclipse cells. We investigated the effects of vaccination under three different assumptions regarding the efficacy of the vaccine on the emerging mutant strain: full cross-protection which means that the vaccine has the exact same effect on the clearance rate c_2 as it does on c_1, no cross-protection in which case the vaccine has no effect on c_2 and finally partial cross-protection for which we assume that the increase in c_2 due to vaccination is half that of c_1. We make the following observations:

- The maximum viral load of the resident strain is computationally a non-increasing function of the clearance rate c_1. This is illustrated in plot (a) and is not surprising since increasing c_1 has an adverse effect on the growth of the resident.
- The impact of vaccination on the growth of the resident strain is most detrimental when the vaccine has no effect on the mutant strain. This is shown in plot (a) where the blue curve that corresponds to the no cross-protection assumption remains below the partial and full cross-protection curves for all values of c_1 that we tested. This can be attributed to the fitness advantage that the mutant strain gains by a vaccine that is clearing out its competitor resident strain while having no effect on the mutant.
- When the vaccine does not have an effect on the mutant strain, the maximum viral load of the mutant is computationally a non-decreasing function of the clearance rate c_1 as plot (b) indicates. This may again be attributed to the fitness advantage that the mutant gains from a vaccine that is increasingly efficient in clearing the resident strain while at the same time having no effect on the spread of the mutant.
- Our conclusions regarding the effects of the vaccine on the maximum viral load of the two strains still apply when we investigate the cell death attributed to each strain, as plots (c) and (d) illustrate.

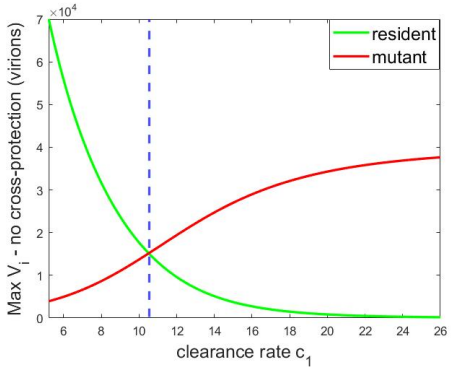

(a) After $c_1 = 10.5$, indicated here by the vertical blue line, the maximum viral load of the weaker mutant remains above that of the resident.

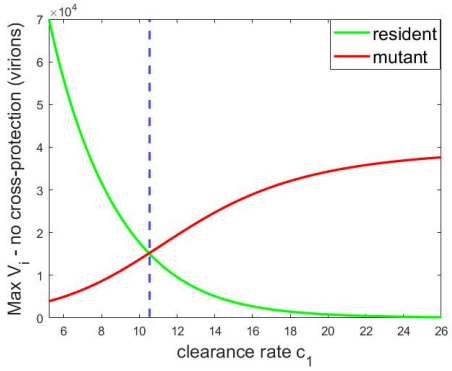

(b) After $c_1 = 12.8$, indicated here by the vertical blue line, the cell death attributed to the weaker mutant remains above that of the resident.

Fig. 3.20 The total cell death percentage and the maximum viral loads of the two strains as the vaccine efficiency against the resident increases. Here the vaccine has no effect on the mutant strain. The mutant strain is weaker ($\delta_2 = 2\delta_1$) and $\alpha = 0.1$ days.

Figure 3.20 shows the effects of vaccination on the maximum viral load of the two strains and the cell death attributed to each strain specifically under the assumption that the vaccine offers no protection from the weaker mutant strain. While we have already

explained the trajectories of both max viral load curves in plot(a) during our analysis of figure 3.19, we chose to present them in the same plot to highlight the beneficial impact on the weaker mutant strain of a vaccine that becomes increasingly efficient in restricting the growth of the resident while having no effect on the mutant. We note that such a vaccine provides such a fitness advantage to the otherwise weaker mutant strain that after a value of $c_1 = 10.5$ the maximum viral load of the mutant remains consistently higher than that of the resident. The equivalent holds for the death of cells infected by either the resident or the mutant strains as plot (b) illustrates.

3.7 Discussion

The main goal of this chapter was to build a within-host influenza model to explore some key factors that affect the potential emergence of a mutant strain within a host and the subsequent competition with its parent resident strain. We began by investigating the emergence dynamics of a mutant strain using as a foundation a very simple within-host model, the TIV model which Baccam *et al*. published in 2006 [24]. Our first step was extending the TIV model to include two strains and then using it to explore the within-host dynamics while forcing the appearance of a mutant strain at some time during the infection with a parent resident strain. Our analysis focused on the effects of the time of appearance and of the relative fitness of the mutant compared to that of the parent resident strain. We showed that, as expected, the later a mutant strain appears during the infection the smaller its viral load and its impact on the infection dynamics. As we illustrated, even a fitter mutant can fail to grow after its forced introduction if it appears too late during the infection. Naturally a quantity of interest was the latest time at which a mutant of some given relative fitness can appear and successfully grow. To study this window of possible emergence we calculated the effective reproduction number of the mutant strain as a function of the age of the infection and discovered that in our two-strain TIV model no mutant can emerge after at most 0.76 days. We attributed this to the very rapid depletion of target cells due to infection by the already circulating resident strain. In order to mitigate this we proceeded to explore the *Saenz* model published by Saenz *et al*. in 2010 [262], which explicitly incorporates the innate immune response via the action of type I interferon and also includes an eclipse phase and can therefore slow down viral kinetics. We extended the *Saenz* model to include two-strains, and then performed the same analysis on the extended *Saenz* model as we did with the extended *TIV* model. Our results showed that including the effects of interferon and the eclipse phase extended

the window of emergence as expected. Using the extended *Saenz* model we also derived an expression for the within-host emergence density of a mutant strain and demonstrated that it is significantly affected by the still rather quick depletion of target cells. Finally we investigated the effects of vaccination on our within-host model and showed that even a weaker mutant strain might dominate the infection if the vaccine-induced pressure against the fitter resident strain is large enough.

The use of experimental research findings for data fitting and estimating model parameters has been a very insightful technique for the within-host modelling of influenza. It is important to emphasize though that obtaining an accurate model where all parameters are identifiable is a significant challenge. In target cell limited models such as the TIV, the TEIV and the *Saenz* models, some of the parameters that often appear and need to be estimated are the infectivity rate β, the virus production rate p, the free-virus clearance rate c, the infected cell death rate δ, the initial viral inoculum V_0 and the initial target cell population T_0. As Smith and Perelson report in [274], the most commonly used methods to estimate these parameters are nonlinear least squares or the maximum likelihood analog. But since not all parameters are identifiable, it has been necessary for modellers to fix some parameters or restrict the ratios of parameters to ensure that they will result in biologically relevant values. A common assumption is that $\frac{\beta T_0}{c} \leq 1$, so that on average each virion infects at most one cell. Moreover, since the basic reproduction number $\mathscr{R}_0$ is given by the product of $\frac{\beta T_0}{c}$ and $\frac{p}{\delta}$ (section 3.4.2), and because reported values of the within-host $\mathscr{R}_0$ for influenza are significantly larger than one [24], another restriction is that $\frac{p}{\delta} >> 1$. We note that T_0 and the eclipse phase duration k are most often fixed, while p, β and V_0 are estimated [24, 29, 140, 141, 262, 274]. Another significant difficulty in estimating the parameters is the wide variety of experimental systems used in various studies. Differences in the type of host (human, ferret, pony, mouse), the virus strains used and the cell types used in in vitro experiments (MDCK cells, A549 cells) make it difficult to generalize parameter estimates to all influenza infections. As Handel *et al*. argue in [141] it is especially hard to estimate β and p since different studies express the virus load in different units. While most parameters of our two-strain *Saenz* model and its various expansions are taken directly from the paper published by Saenz *et al*. in 2010 [262], we still performed a parameter sensitivity analysis in section 3.4.4 to investigate how different parameters values would have impacted the results of our model.

While forcing the appearance of the mutant strain at some specific time during the infection yielded some insightful results, in section 3.5.1 we further developed an expression for the within-host emergence density of a mutant strain. In developing this expression we made some assumptions regarding the amount of HA- and NA-coding nucleotides that can potentially generate an antigenic change (and set it to 10%) and the percentage of substitution mutations in these nucleotides which will successfully result in antigenic change (and set it to 0.02%). While research has shown that not all substitution mutations result in antigenic changes [168, 312], we emphasize that the specific values we chose were semi-arbitrary and were chosen so that the resulting within-host cumulative emergence probability is high enough to facilitate the emergence of the mutant but not so high that every single infection will result in the mutant emerging. More specifically, our choices resulted in a within-host cumulative emergence probability of 0.78 for a weaker mutant, 0.92 for a neutral and 0.36 for a fitter mutant. Therefore there is a high chance that the mutant strain will emerge during a host's infection, but this is not problematic for two main reasons. Firstly we are interested in investigating the competition dynamics between a newly emerged mutant and its parent resident, so facilitating the emergence of the mutant is helpful in this regard. Secondly we do not aim to make quantitative predictions regarding the emergence potential of a mutant strain during a single-strain infection with a resident strain. We are interested in identifying patterns in the emergence and subsequent competition dynamics between the two strains from a qualitative perspective. Larger values for the percentage of substitution mutations that will result in antigenic change (which we set at a very low 0.02%) would lead to the mutant strain emerging in every infected individual, which would be problematic when we couple our within-host model with a population-level model in chapters 4 and 5 because it would give the mutant a significant advantage over the resident under our total cross-immunity assumption. We emphasize though that some of our cross-scale model's main results will come from varying model parameters such as the within-host mutation rate ε.

Our final step in the analysis of our within-host model was to include vaccination into our two-strain *Saenz* model, as one of our key research goals is to describe how vaccination affects the epidemiological and evolutionary dynamics of influenza. We incorporated vaccination to our model simply as an increase in the viral clearance rates c_i. We chose to only capture the effects of vaccination implicitly instead of explicitly adding compartments to our model to describe the action of vaccine-generated antibodies because later in chapter 5 we will combine our within-host vaccination model with a between-host model for the spread of influenza. Such cross-scale models can easily become complicated

and computationally intensive, and as a result we wanted to incorporate the effects of vaccination in the simplest way, by varying the values of one of our within-host model parameters (specifically c_i).

Throughout this chapter we explored the effects of the relative fitness of the mutant strain compared to that of the parent resident strain both on the infection and emergence dynamics. Our definition of relative fitness depended on choosing one of the strain-dependent parameters of the model and assigning to it some value different than its reference value. When the new value would have a positive effect on the mutant's growth we referred to the new strain as a fitter strain, always in comparison to the resident. Similarly if it would have a negative effect then we called the new strain a weaker mutant and if it would have no effect at all then we referred to the resulting new strain as a neutral mutant. In section 3.5 we used the findings of an experiment by Visher *et al*. [297] to inform our probability density function for the emergence of a mutant strain of some specified relative fitness. But Visher *et al*. use a different definition of relative fitness compared to ours. They generated mutant variants from an influenza parent strain, each of which differed from the parent by a single nucleotide substitution, and then had each variant directly compete against the parent strain *in vitro*. They then measured the change in relative frequencies between the parent strain and the variant, used that value as the difference in growth rate and defined relative fitness as the exponent of that value. Therefore there is no direct correspondence between their definition and ours. Moreover there is no experimental guidance that we could find on how exactly a relative fitness such as the one used by Visher *et al*. would inform the parameters which we use to define a mutant strain, such as the mutant virion production rate or the death rate of cells infected by the mutant. The parameter sensitivity analysis that we performed in sections 3.3.3 and 3.4.4 can partially mitigate this uncertainty, since it illustrated that the results of our model are not highly sensitive to changes in the different strain-specific parameters and therefore to the exact definition of relative fitness.

In both our two-strain TIV and *Saenz* models we assume that no coinfection can occur at the cellular level. While this simplifies the model dynamics substantially, it also raises some concerns. Experimental data indicates that cellular coinfection is common in influenza. Fukuyama *et al*. in [110] generated four distinct, color-coded influenza viruses and injected mice with a mixture of them. Their experiments showed that approximately 20% of the bronchial epithelial cells were infected with more than one color-coded virus

at the second day postinfection. Allowing mutant virions to enter cells that are already infected by the resident strain would increase the number of cells available to them, potentially leading to a wider window of emergence for a mutant strain. We expect though that cellular coinfection might not have a very significant effect on the models presented in this chapter, as they both assume that the virus spreads evenly among all available cells [111]. The same reasoning applies to our assumption that infected cells release virions of only a single strain. Throughout this thesis the only mechanism studied for the evolution of influenza is antigenic drift. If we wanted to extend our model to include a different mechanism such as reassortment, then incorporating cellular coinfection might have a strong impact on the model dynamics. The first within-host ODE model of multiple infection at the cellular level was developed by Dixit and Perelson in 2004 [82]. The authors investigated how often drug-resistant recombinant genotypes emerge during HIV infection but assumed that cellular coinfection does not affect the phenotype of infected cells. Koelle *et al*. developed a model of cellular coinfection in 2019 which explicitly took into account the effects of a cell's multiplicity of infection (MOI) [170]. Koelle *et al*. based the structure of their model on epidemiological "macroparasite" models, first described by Roberts, Smith and Grenfell in 1995, whereas the TIV and *Saenz* models mirror instead the structure of epidemiological "microparasite" models. The authors initially kept track of the total number of target cells (which included both uninfected and variably infected cells as they can be targets of further infection), free virus and internalized virus across all target cells. They assumed that the viral production and the cell mortality rates both scale linearly with cellular MOI and that the distribution of cellular MOIs is given by a negative binomial. With these simplifying assumptions they were then able to extend their model to include the action of interferon and to keep track of the reassortants present in the within-host viral population under the assumption that all viruses coming out of a coinfected cell are reassortants. While their model provides significant insights into the effects of cellular coinfection, it is structurally very different to our within-host models presented in this chapter. In 2015 Phan and Wodarz reviewed the challenges of modeling cellular coinfection and reassortment using ODE models, which generally divide the population of infected cells into subpopulations infected with one, two, three etc viruses [233]. The authors referred to this as the "multiple infection cascade" and demonstrated that truncating the cascade to simplify the model can lead to pathological outcomes. More specifically, they showed that for identical model parameters (and therefore competitively neutral strains) shorter infection cascades can lead to competitive exclusion while longer cascades will lead to coexistence. The authors also investigated whether multiple infection can promote the coexistence of two virus strains with different fitness

and concluded that in general, related strains of the same virus are unlikely to coexist in the context of multiple infection. Their analysis highlights the analytical and computational challenges of incorporating multiple infection to an ODE model efficiently, even when the model does not explicitly take into the account eclipse cells or the host immune response. We also note that influenza (along many other viruses) has been shown to also spread via direct cell-to-cell transmission [64, 256]. This is another way that multiple infection may be generated, but modelling it requires very different approaches to what we have described so far in this chapter [173].

The original *Saenz* model in [262] as well as the extension we developed in this chapter are target-cell limited models, which entails that infection ends due to the lack of available target cells. This is also true for the TIV model, but a key difference is that in the TIV model target cells are depleted only because they are lost to infection, while in the Saenz model target cells are depleted either because they become infected or because they become refractory to infection due to the action of type I interferon. In sections 3.4 and 3.5 we showed that the rapid decline of available target cells has a strong impact on emergence, by forcing the mutant's window of emergence to be very narrow and early in the infection. We argued that this rapid decline is a structural issue of our extended *Saenz* model and can be primarily attributed to the free mixing of virions and target cells. Therefore we believe that a spatial within-host model such as the one developed by Reperant *et al*. in [253], where the respiratory system was broken down into three distinct compartments and infection began in one compartment and could then slowly move to the other two, might result in the slower decline of target cells and therefore in a wider emergence window. We note though that while emergence needs to occur early in our model, we showed that the rate of appearance of a mutant strain remains high throughout most of the infection. This is in accordance with experiments which have shown that novel variants can appear and reach a detectable size even five days post-infection [208].

3.8 Summary

In this chapter we developed a within-host model to study the emergence dynamics of a mutant strain during an infection with a parent resident strain. We began by extending the simple TIV model published by Baccam *et al*. in 2006 [24] to include two strains and studied the effects of the mutant's emergence time on the disease dynamics. Our analysis

showed that the very rapid decline of target cells in the two-strain TIV model only allows for a very narrow emergence window early in the infection. In an attempt to mitigate this and slow down the viral kinetics, we then adapted a within-host model that also includes an eclipse phase as well as an innate immune response. Our extended *Saenz* model, based on a model published by Saenz *et al*. in 2010 [262], slowed down the disease dynamics considerably compared to the two-strain TIV model but also resulted in a narrow emergence window early in the infection. In order to investigate how the chances of a mutant strain appearing and growing within that emergence window change, we then developed a probability density function for the emergence of the mutant. Finally we added vaccination to our extended *Saenz* model and showed that even a weaker mutant strain might dominate the infection if the vaccine-induced pressure against the fitter resident strain is high.

Chapter 4

A cross-scale model for the evolution of influenza

Author Contributions

The work presented in this chapter is my own under the guidance of my supervisor Julia Gog, unless it is explicitly stated otherwise. Figure 4.1 in section 4.5.1 describes the grid implementation of our cross-scale model which was suggested by Robin Thompson from the University of Oxford during a two-day discussion between him, myself and my supervisor Julia Gog. Moreover equation (4.30) in section 4.5.1 was developed by both myself and my supervisor, but with significant input from my supervisor.

4.1 Introduction

In this chapter we will develop a cross-scale model to describe the epidemiological and evolutionary dynamics of influenza within a single season. Our model will take explicitly into account dynamical processes that occur at the within-host level. Specifically we will assume that the between-host transmission rates are linear functions of the within-host viral load. The structure of this chapter is as follows: first in section 4.2 we will present a cross-scale model developed by Coombs *et al*. in 2007 [68], which we will use as the foundation of our own cross-scale model. In section 4.3 we will present our cross-scale model by first separating it into its two tiers, the between- and within-host,

and then discussing how to link them. Then in sections 4.4 and 4.5 we will derive some basic properties of our model and describe how to implement it in a computationally efficient manner. Finally in section 4.6 we will present our cross-scale model's results and investigate their sensitivity to the assumed form of the within-host emergence density.

4.2 Background

We will base our model for the cross-scale evolution of influenza on a model published by Coombs *et al*. in 2007 [68], where they examined the within- and between-host selection pressures on the evolution of chronic pathogens with a specific emphasis on HIV. In their publication they studied the competition dynamics between two strains using an SI model that allows the internal state of infected hosts to vary with the age of the infection. We refer to the resulting model as the *original Coombs model* throughout this thesis. The *original Coombs model* is given by the following integro-differential equation system:

$$\frac{dS}{dt} = b - \delta S - \int_0^\infty \int_0^1 \int_0^1 \beta(a, x_0', x_0) I(t, a, x_0) dx_0 dx_0' da \tag{4.1}$$

$$\frac{\partial I(t,a,x_0)}{\partial t} + \frac{\partial I(t,a,x_0)}{\partial a} = -[\delta + \alpha(a, x_0)] I(t, a, x_0) \tag{4.2}$$

$$I(t, 0, x_0') = S \int_0^\infty \int_0^1 \beta(a, x_0', x_0) I(t, a, x_0) dx_0 da \tag{4.3}$$

with the following notation:

- $S(t)$ represents the number of susceptible hosts in the population at time t. Individuals in the class S can be infected by either strain and coinfection is possible.
- The variable $x_0 \in [0,1]$ denotes the fraction of viruses of strain 1 in an initial inoculum that consists of a mix of strains 1 and 2.
- $I(t,a,x_0)$ denotes the density of infected individuals that were infected with an inoculum given by x_0 at time $t-a$.

- The parameter b is the rate at which new individuals are added the population via birth or immigration.
- The parameter δ is the natural death rate.
- The parameter $\beta(a, x_0', x_0)$ is the transmission rate from individuals who were infected with a strain mix x_0 a time units ago to new infections with initial inoculum x_0'.
- The parameter $\alpha(a, x_0)$ is the death rate due to infection, and depends both on the age of infection a and the initial strain mix x_0.

Equation (4.1) describes how the number of susceptible individuals in the population varies over time. It needs to account for new infections generated by infected individuals of all possible infection ages $a \in [0, \infty)$ who were initially infected with all possible strain mixes $x_0 \in [0,1]$ and who are now infecting new cases with all possible mixes $x_0' \in [0,1]$. This explains the presence of the triple integral in the S-equation of the Coombs model. We note that this formulation pre-supposes that susceptible individuals are shared among all strains. Equation (4.2) describes how the density of infected individuals changes both with time and with the age of infection a. This takes into account both individuals who are infected but die due to natural causes via the parameter δ and individuals who are infected and die due to the infection via the parameter $\alpha(a, x_0)$. Finally equation (4.3) describes the rate at which new infections are generated at time t with an initial inoculum defined by x_0'. Equation (4.3) needs to take into account new infections generated by infected individuals of all possible infections ages a who were initially infected with all possible initial strain mixes x_0, which explains the presence of the double integral in the equation.

We note that the authors in [68] simplified their original model by considering a term for the survivorship probability of an infected individual. More specifically, given an individual who was infected by some strain mix x_0 a time units ago, then the probability that they have survived up to the current time is:

$$\sigma(a, x_0) = exp\left(-\delta a - \int_0^a \alpha(z, x_0) dz \right)$$

where $\alpha(a,x_0)$ is the death rate due to infection. This allowed the authors to express the density $I(t,a,x_0)$ of infected individuals who were infected with strain mix x_0 at time $t-a$ as

$$I(t,a,x_0) = I(t-a,0,x_0)\sigma(a,x_0)$$

Using this new expression for $I(t,a,x_0)$ the authors then reformulated their original model into the following equivalent set of an integro-differential equation and a renewal condition:

$$\frac{dS}{dt} = b - \delta S - \int_0^\infty \int_0^1 \int_0^1 \beta(a,x_0',x_0) I(t-a,0,x_0) \times \sigma(a,x_0) dx_0 dx_0' da \tag{4.4}$$

$$I(t,0,x_0') = S \int_0^\infty \int_0^1 \beta(a,x_0',x_0) I(t-a,0,x_0) \times \sigma(a,x_0) dx_0 da \tag{4.5}$$

We will refer to equations (4.4)-(4.5) simply as the *Coombs model* throughout this thesis. This is because we will use this simplified version as the basis of our own cross-scale model, instead of the slightly more complicated *original Coombs model* that includes partial differential equations.

In the *Coombs model* the transmission rate β and the infection-related death rate α depend on the age of infection a, and are therefore the link between the within-host and population dynamics of the infection. The authors used a TIV within host model to inform the parameters β and α in the following way:

- $\beta(a,x_0',x_0) = b_1[V_1(a,x_0',x_0) + V_2(a,x_0',x_0)]$, where b_1 is a scaling factor. Therefore the transmission rate depends linearly on the viral load of the host.
- $\alpha(a,x_0') = a_1\delta[T_0 - T(a,x_0',x_0)]$, where a_1 is a scaling factor. Therefore the infection-related death rate at some age of infection a is defined by the number of epithelial target cells lost to infection up to time a.

The *Coombs model* is based on the following underlying assumptions:

- The transmission rate $\beta(a,x_0',x_0)$ depends linearly on the viral load of the host at some age of infection a.

- The inocula that initiate new infections are fixed in size and their composition depends only on the strain mix of the infected host at the time at which the inocula were produced.
- The infection-related mortality rate $\alpha(a, x_0')$ at some age of infection a depends linearly on the cumulative loss of epithelial target cells up to time a.

4.3 Model presentation

Having presented the *Coombs model*, we will now use it as the foundation of our own cross-scale model, which we will use to study the emergence dynamics of a mutant influenza strain in a fully susceptible population. Similarly to the *Coombs model*, our cross-scale model is defined by a different set of dynamical equations for the between- and the within-host tiers. We will first present the equations that describe the spread of the infection between hosts. As the two scales are linked explicitly in our model, these between-host equations will depend on processes that occur within infected individuals, so we will then present our within host model of viral kinetics. Having presented our two-tiered model and defined the link between its two scales, we will then discuss its various assumptions.

4.3.1 The between-host tier

Using as a foundation the reformulated *Coombs model* [equations (4.4)-(4.5)] from section 4.2, our cross-scale SI model has the following formulation:

$$\frac{dS}{dt} = -S \int_0^\infty \sum_{i=1}^{N} \sum_{j=1}^{N} \beta_{ij}(a) I_i(t-a,0) da \tag{4.6}$$

$$kI_j(t,0) = S \int_0^\infty \sum_{i=1}^{N} \beta_{ij}(a) I_i(t-a,0) da \tag{4.7}$$

with the following notation:

- $S(t)$ denotes the number of susceptible individuals at time t of the epidemic.

- $I_i(t-a,0)$ represents the density (in a) of individuals who became infected with strain i at time $t-a$.
- The constant k is such that $da = kdt$. This accounts for the fact that $I_i(t,a)$ is a density in a whereas the right hand side of equation (4.7) is a number.
- The parameter $\beta_{ij}(a)$ is the transmission rate from individuals who were infected with the ith strain a time units ago to new infections with strain j.
- N denotes the number of strains.

Equation (4.6) is an integro-differential equation that describes how the number of susceptible individuals in the population varies over time. It needs to account for the new infections generated by individuals of all possible infection ages $a \in [0,\infty)$ who initially were infected with the ith strain and are now infecting new cases with the jth strain, where i and j vary over all possible N strains. Equation (4.7) is a renewal condition which describes how new infected cases of the jth strain are generated. It takes into account the contact of susceptible individuals with infected hosts of all possible infection ages who were initially infected with any of the possible N strains, but are now transmitting specifically the jth strain. It is important to emphasize that while these two equations describe the population disease dynamics, they depend on the viral dynamics within infected hosts via the transmission rate $\beta_{ij}(a)$.

We highlight the similarities and differences between our cross-scale SI model defined by equations (4.6) and (4.7) and the *Coombs model* given by equations (4.4) and (4.5) that we presented in the previous section:

- Our model consists of an integro-differential equation and a renewal condition, because we used the *Coombs model* as its foundation.
- There is no birth and natural death rate in our model, unlike the Coombs model. This is a justifiable simplification given that we are studying the dynamics of an acute infection over a relatively short period (here 150 days), whereas Coombs *et al*. were interested in the dynamics of chronic infections such as HIV.
- We are assuming that a new infection can be initiated by exactly one strain, while Coombs *et al*. assume that new infections are initiated by inocula that consist of a

fraction x_0 of viruses of strain 1 and $1-x_0$ of strain 2, where $x_0 \in [0,1]$.

Since in this chapter we will only consider a parent resident strain and a mutant strain, we present the equations of our cross-scale SI model for only two strains, a resident (strain 1) and a mutant (strain 2), and under the assumption that backwards mutation is not possible (namely that $\beta_{21}(a) = 0 \; \forall a$):

$$\frac{dS}{dt} = -S \int_0^\infty \left[\beta_{11}(a) I_1(t-a,0) + \beta_{12}(a) I_1(t-a,0) + \beta_{22}(a) I_2(t-a,0)\right] da \tag{4.8}$$

$$kI_1(t,0) = S \int_0^\infty \beta_{11}(a) I_1(t-a,0) da \tag{4.9}$$

$$kI_2(t,0) = S \int_0^\infty \left[\beta_{12}(a) I_1(t-a,0) + \beta_{22}(a) I_2(t-a,0)\right] da \tag{4.10}$$

4.3.2 The within-host tier

In the presentation of our cross-scale SI model we underlined the dependence of the population-level transmission rates $\beta_{ij}(a)$ on the within-host viral kinetics but we did not specify how these between-host transmission rates will vary with the host's internal state. To this end we now present a within-host model for the dynamics of influenza which we will use to inform our cross-scale SI model. The within-host model we use in this chapter is our extended *Saenz* model, which was presented in chapter 3 (specifically 3.4). For two strains, a resident and a mutant, it has the following formulation:

$$\frac{dT}{da} = -\beta_1^{wh} V_1 T - \beta_2^{wh} V_2 T - \phi F T \tag{4.11}$$

$$\frac{dE_{\alpha,1}}{da} = \beta_1^{wh} V_1 T - k_\alpha E_{\alpha,1} \tag{4.12}$$

$$\frac{dE_{\alpha,2}}{da} = \beta_2^{wh} V_2 T - k_\alpha E_{\alpha,2} \tag{4.13}$$

$$\frac{dW}{da} = \phi F T - m(\beta_1^{wh} V_1 + \beta_2^{wh} V_2) W - a_w W \tag{4.14}$$

$$\frac{dE_{\gamma,1}}{da} = m\beta_1^{wh} V_1 W - k_\gamma E_{\gamma,1} \tag{4.15}$$

$$\frac{dE_{\gamma,2}}{da} = m\beta_2^{wh} V_2 W - k_\gamma E_{\gamma,2} \tag{4.16}$$

$$\frac{dR}{da} = a_w W \tag{4.17}$$

$$\frac{dI_1}{da} = k_\alpha E_{\alpha,1} + k_\gamma E_{\gamma,1} - \delta_1 I_1 \tag{4.18}$$

$$\frac{dI_2}{da} = k_\alpha E_{\alpha,2} + k_\gamma E_{\gamma,2} - \delta_2 I_2 \tag{4.19}$$

$$\frac{dV_1}{da} = p_1 I_1 - c_1 V_1 \tag{4.20}$$

$$\frac{dV_2}{da} = p_2 I_2 - c_2 V_2 \tag{4.21}$$

$$\frac{dF}{da} = q_1 E_{\gamma,1} + q_2 E_{\gamma,2} + q_1 I_1 + q_2 I_2 - dF \tag{4.22}$$

Here strain 1 refers to the resident strain and strain 2 to the mutant. Susceptible target cells (T) become infected by virions of the resident strain (V_1) at an infectivity rate of β_1^{wh} and by virions of the mutant strain (V_2) at an infectivity rate of β_2^{wh}. They can also become prerefractory to infection due to the action of type I interferon (F) at a rate ϕ. While in this prerefractory state (W), cells can still be infected by virions of either strain but at a

reduced rate $m\beta_i^{wh}$. They finally become refractory and completely immune to infection (R) after they have stayed in this prerefractory state for an average $1/a$ days. Susceptible target cells (T) that have been infected by either viral strain but have not yet started releasing progeny virions move to an eclipse phase ($E_{\alpha,i}$) and stay there for an average of $1/k_\alpha$ days until the virus has finished replicating inside them. Similarly prerefractory cells (W) that have been infected by the ith strain first move to an eclipse phase ($E_{\gamma,i}$) and stay there for an average of $1/k_\gamma$ days. Cells infected by the ith strain that have reached the virion producing stage (I_i) die from the infection or as a result of the immune response at a rate δ_i. They produce progeny virions at a rate p_i and secrete interferon at a rate q_i. Cells that have been infected after they were primed by interferon but have not reached the virion-producing stage yet ($E_{\gamma,1}$ and $E_{\gamma,2}$) also secrete interferon at a rate of q_i, depending on which strain they were infected by. Circulating interferon decays at a rate d, while free virions of the ith strain are cleared by the immune system at a rate c_i.

In chapter 3 we also derived an expression for the within-host basic reproduction numbers of the resident and the mutant strains, which we repeat here:

$$\mathscr{R}_0^{r,wh} = \frac{1}{\delta_1} \times \frac{p_1 T_0}{c_1} \times \beta_1^{wh} \tag{4.23}$$

$$\mathscr{R}_0^{m,wh} = \frac{1}{\delta_2} \times \frac{p_2 T_0}{c_2} \times \beta_2^{wh} \tag{4.24}$$

4.3.3 Model assumptions

Our cross-scale model is based on all the assumptions of our extended *Saenz* model from 3.4, as well as on the following assumptions:

- Infection leads to recovery. This is why there is no disease-related mortality rate in our model, as opposed to the Coombs model. This is not a surprising differentiation between our model and the *Coombs model*, since we are considering the dynamics of seasonal influenza while Coombs *et al.* applied their model to HIV.
- The transmission rate depends linearly on the viral load of the host. More specifically we assume as Coombs *et al.* in [68] that:

$$\beta_{ij}(a) = bV_j(a) \tag{4.25}$$

where b is a scaling constant, and $i, j \in 1,2$. This is a very important assumption in our model because the population-level transmission rates are the links between the two scales of our model. We emphasize that the linear dependence we assume here is one of various different ways that we could relate the within-host viral load to the between-host transmission rates. We will discuss these at length in the Discussion section of this chapter (section 4.7).

- Each individual can be infected by exactly one strain. No co-infection can occur. The only case where more than one strains may co-circulate within a single host is if the host was initially infected with the resident strain and then had the mutant strain emerge within them.

For the sake of clarity, we repeat here the assumptions of our extended Saenz model. These are the same as they appear in 3.4:

- The binding of free virions with target cells causes only a negligible decrease in the viral load, which is why there is no $-\beta_i V_i T$ term in equations (4.20) and (4.21).
- Once a cell becomes fully immune to infection and enters the R compartment, it remains immune.
- Infection leads to death for cells in the I_i compartments.
- Cells can only be infected once and by only one strain.
- The competition between strains is mediated purely through the availability of target cells.

4.4 Basic properties

The population-level basic reproduction number $\mathscr{R}_0^{r,p}$ of the resident strain in our cross-scale model can be expressed as:

$$\mathscr{R}_0^{r,p} = \int_0^{D^{wh}} \beta_{11}(a)da \tag{4.26}$$

where $\beta_{11}(a)$ is the rate at which individuals who were initially infected with the resident strain a time units ago and never had the mutant strain emerge within them infect new

individuals. Here D^{wh} denotes the duration of the infection within a host. Similarly, we may express the population-level basic reproduction number of the mutant strain as:

$$\mathscr{R}_0^{m,p} = \int_0^{D^{wh}} \beta_{22}(a)da \tag{4.27}$$

Both these expressions are dependent on infected individuals being infectious for a fixed amount of D^{wh} days. In other words the recovery rate of infected individuals is a Dirac delta function concentrated at D^{wh}. We note though that an equivalent formulation would be to simply define that $\beta_{ij}(a) = 0 \; \forall a > D^{wh}$.

4.5 Methods

As we are interested in the emergence dynamics of a mutant strain in a population, we assume that initially there is only a resident strain causing an epidemic. When an individual becomes infected with the resident strain we keep track of the age of their infection because variations in their within-host viral load will affect their population-level transmission rate. Similarly to the implementation of our extended *Saenz*, we assume that when an individual is infected with the resident strain there is a chance that errors will occur during the within-host viral replication process which will lead to the emergence of a mutant strain within that host. At the between-host level the consequence of this within-host emergence is that the host may transmit either the resident or the newly emerged mutant whenever they infect a new host, with a probability that depends on each strain's viral load at the time of transmission. This in turn can lead to two strains, a mutant and its parent resident, circulating in the population and competing for hosts either until the end of the epidemic or until one of them disappears.

We assume as Coombs *et al.* in [68] that the transmission rate $\beta_{ij}(a)$ is a linear function of the host's viral load. As a result, $\beta_{ij}(a)$ depends implicitly on the time of emergence α of the mutant strain within the host. This is because as we have demonstrated in 3.4.4, the emergence time α has a strong effect on the viral loads of both strains. To emphasize this dependence on α, we will use the notation $\beta_{ij}(a, \alpha)$ to refer to the transmission rate from someone who was infected with the ith strain a time units ago and had the mutant

strain emerge within them at time α to new cases of strain j. More specifically:

$$\beta_{ij}(a,\alpha) = bV_j(a,\alpha)$$

where b is a scaling constant. We note that in the case of an infection initiated by the mutant strain there is no dependence on α because we do not allow for backwards mutation (from mutant to resident) in our model. We define $\alpha = \emptyset$ as the case that no emergence occurs during a host's infection with the resident strain. If we consider such an infection with only the resident strain present, then using equation (4.26) for $\mathscr{R}_0^{r,p}$ we may calculate b as:

$$b = \frac{\mathscr{R}_0^{r,p}}{\int_0^{D^{wh}} V_1(a,\emptyset)da} \tag{4.28}$$

Our model has the following initial conditions:

- $N = 1$ is the size of our population and we assume it remains fixed throughout the outbreak.
- $I_1(0) = 10^{-5}$ individuals.
- $I_2(0) = 0$. This is because we assume that the outbreak is initiated only by resident strain.
- $D^p = 150$ days. This is the duration of the outbreak, and we set it as 150 days to cover the main winter season of influenza in the Northern hemisphere, namely December-February, together with a month leading up to it and a month right after it.
- $D^{wh} = 5$ days. This is the duration of the infection within a host.
- $\mathscr{R}_0^{r,p} = 2$. This was chosen simply to satisfy reported values of the population-level $\mathscr{R}_0$ of influenza. More specifically Cauchemez *et al.* report in [55] that $\mathscr{R}_0$ ranges from 1.4 to 2.2.

Within-host model				
Parameter	**Description**	**Value**	**Units**	**Source**
β_i^{wh}	Infectivity rate of ith strain	1.4×10^{-4}	(RNA copies)$^{-1}$ ml NS day^{-1}	[262]
p_i	Virus production rate for ith strain	1.4×10^{-5}	RNA copies (ml NS)$^{-1}$ day^{-1} cell^{-1}	[262]
q_i	IFN production by cells in I_i	5×10^{-10}	IFN fold change day^{-1} cell^{-1}	[262]
c_i	Free virus clearance rate for ith strain	5.2	Rate of virus clearance day^{-1}	[262]
$1/k_i$	Average duration of eclipse phases	$1/2$	Days	[262]
$1/a_w$	Average duration of prerefractory phase	$1/4$	Days	[262]
$1/\delta_1$	Average lifespan of cells infected with resident strain	$1/2$	Days	[262]
$1/\delta_2$	Average lifespan of cells infected with mutant strain	Varies	Days	
d	IFN clearance	6.8	Rate of IFN clearance day^{-1}	[262]
ϕ	IFN efficiency	56	(IFN fold change)$^{-1}$ day^{-1}	[262]
m	IFN-reduced infectivity	0.9		
α	Time of emergence of mutant strain	Varies	Days	
D^{wh}	Infection duration	5	Days	

Table 4.1 Parameters of the within-host tier of the cross-scale model.

Between-host model				
Parameter	**Description**	**Value**	**Units**	**Source**
D^p	outbreak duration	150	days	
$\mathscr{R}_0^{r,p}$	resident basic reproduction number	2		[55]
b	virus transmission scaling factor	1.63×10^{-11}		chosen to satisfy $\mathscr{R}_0^{r,p} = 2$

Table 4.2 Parameters of the between-host tier of the cross-scale model.

4.5.1 Implementation

We will now describe the implementation of our cross-scale SI model. Unlike the implementation of our models in chapters 2 and 3, here we will go into detail because as Gog *et al*. discuss in [122], one of the significant challenges that cross-scale models present is to implement them with computational efficiency. Towards this end we will pre-calculate the between-host transmission rates and the within-host emergence density so that in our implementation we can use them as parameters of our cross-scale model instead of having to compute them in every simulation of our model.

First we discretize the age of infection a. We assume that $a \in [0, da, 2da, ..., D^{wh}]$ such that $da = 0.5$ days. Moreover we assume that the within-host emergence time $\alpha \in [da, 2da, ..., D^{wh}]$ and use $\alpha = \emptyset$ to denote that no emergence occurs. We note that $\alpha = 0$ is not possible, since the resident strain needs to start replicating within a host before emergence can occur. We also note that da does not need to be constant and a and α do not need to have the same discretization, both choices were made for the sake of simplicity. Since a and α are discrete variables, we define $\hat{a}$ and $\hat{\alpha}$ as their continuous analogues. We underline though that in our Matlab implementation $\hat{a}$ and $\hat{\alpha}$ are not truly continuous. In the discretized version of our cross-scale SI model we will use emergence at some time $\alpha = \alpha^\star$ to denote that in the continuous analogue the mutant strain emerged sometime between $\alpha^\star - da$ and $\alpha^\star$. Therefore we need to modify both our between-host transmission rates $\beta_{ij}(a, \alpha)$ and the within-host emergence density $f(\alpha)$, which so far have been defined with a and α being continuous variables.

Starting with the probability density function $f(\hat{a})$, we obtain the following probability of emergence using our discretized within-host emergence time α:

$$P(\alpha) = \int_{\alpha-da}^{\alpha} f(\hat{\alpha}) d\hat{\alpha} \tag{4.29}$$

We assume that $P(\emptyset)$ denotes the probability that no emergence occurs within the host.

For the discrete version of the transmission rates we need to consider that if the mutant emerges at some time $\alpha = \alpha^{\star}$, which in the continuous analogue means that $\hat{\alpha} \in (\alpha^{\star} - d\alpha, \alpha^{\star}]$, then it might be the case that emergence is significantly more likely for certain values of $\hat{\alpha}$ inside that window depending on the form of the emergence density function $f(\hat{\alpha})$. To account for this we use the following expression for the discretized transmission rates:

$$\beta_{ij}(a, \alpha) = \frac{1}{\int_{\alpha-da}^{\alpha} f(\hat{\alpha}) d\hat{\alpha}} \times \int_{\alpha-da}^{\alpha} \left(f(\hat{\alpha}) \int_{a-da}^{a} \beta_{ij}(\hat{a}|\hat{\alpha}) d\hat{a} \right) d\hat{\alpha} \tag{4.30}$$

where the first term is a normalizing constant.

From equations (4.29) and (4.30) we see that in order to pre-calculate $P(\alpha)$ and $\beta_{ij}(a, \alpha)$ we require $f(\hat{\alpha})$ and $\beta_{ij}(\hat{a}|\hat{\alpha})$ for every value of $\hat{a}$ and $\hat{\alpha}$. We note that given our assumption that the population-level transmission rates are linear functions of the within-host viral load, in order to calculate $\beta_{ij}(\hat{a}|\hat{\alpha})$ we simply need to know $V_i(\hat{a}|\hat{\alpha})$. We can obtain these by simulating our within-host model using the time of emergence $\hat{\alpha}$ as a parameter. We underline again that while we defined $\hat{a}$ and $\hat{\alpha}$ as the continuous analogues of a and α, they are not truly continuous in our Matlab implementation.

We will now describe how to implement efficiently the between-host tier of our cross-scale model using what we will refer to as the grid implementation. First we discretize real time, so that if $\hat{t}$ refers to the continuous time between the start of the outbreak and its end after $D^p = 150$ days, then t is its discrete analogue. Therefore we have $t \in [0, dt, 2dt, ..., D^p]$ where we set $dt = 1$ day. We note that the difference dt between any two consecutive time points can vary, we chose it as constant in our simulations only for the sake of simplicity. This leads to a discrete time SI model for the between-host tier of

our cross-scale model. This additional discretization of the real time t combined with our previous discretization of the age of infection a allow us to simulate our cross-scale SI model efficiently in the following way. Let $I_1^t(a,\alpha)$ denote the number of individuals at time t who were originally infected with the resident strain a time units ago and had the mutant strain emerge within them at time α (including $\alpha = \emptyset$ for the case that no emergence has occured yet). Similarly for $I_2^t(a)$, where the absence of α is because we do not allow for backwards mutation in our model. Keeping track of these for every t, we may use our pre-calculated values of $\beta_{ij}(a,\alpha)$ to numerically solve the discrete SI equations of the between-host tier. We note that an individual who has both the resident and the mutant strain within them can transmit either strain with a probability that depends on the strains' within-host viral load, which we have pre-calculated for every a and α in our discretization. Furthermore keeping track of $I_1^t(a,\emptyset)$ for all possible values of a allows us to perform at each time point a binomial random test for the within-host emergence of the mutant strain where for any given a the number of trials is $I_1^t(a,\emptyset)$ and the probability of success depends in some way on the pre-calculated viral load $V_1(a,\emptyset)$.

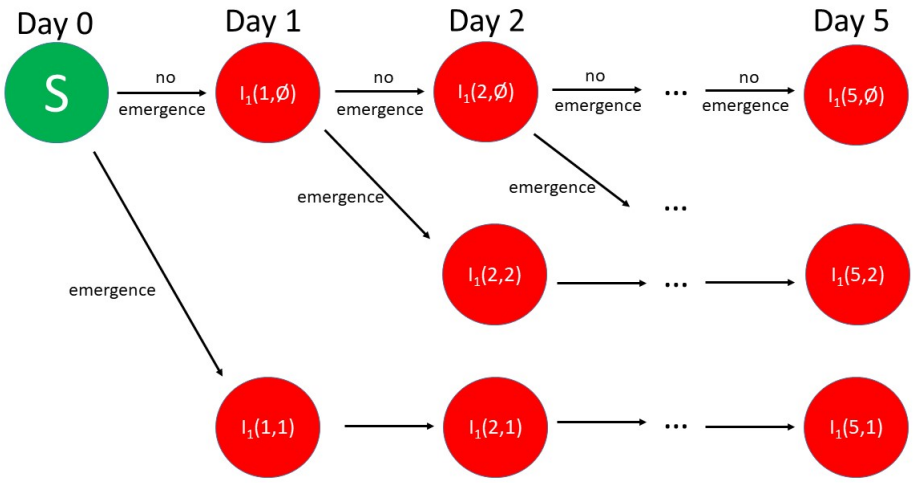

Fig. 4.1 Schematic of the grid implementation of our cross-scale model. This figure represents the possible infection paths of a single infected individual, where we keep track of the age of their infection as well as the time of emergence of the mutant strain within them. Here $I_1(a,\alpha)$ denotes an individual who just finished the a^{th} day of their infection and had the mutant emerge within them at time α. The first row represents the case of an infected individual who did not have the mutant strain emerge within them at any point during their infection. We note that after the 5^{th} day of infection the individual recovers. For the sake of illustration a value of $da = 1$ day was used for this schematic, whereas in our simulations used $da = 0.5$ days.

Figure 4.1 offers a schematic of the grid implementation and describes the possible infection paths of an infected individual. More specifically, we start with an individual

that is infected with the resident strain. If the mutant strain emerges within them by the end of their first day of infection then we save the information that $\alpha = 1$ and the individual moves along the last row of the diagram in figure 4.1 until they recover. No further stochastic tests are needed because we only allow for a single mutant strain to emerge during an individual's infection. If on the other hand the mutant does not emerge during the first day, we save this information by having the individual move to the $I_1(1,\emptyset)$ node in the first row of the diagram, which denotes that their age of infection is 1 day and the mutant has not emerged within them yet. We then follow a similar procedure during the individual's second day of infection, where no emergence will have them continue to the $I_2(2,\emptyset)$ node in the first row while emergence will lead them to the $I_2(2,2)$ node in the second row of the diagram. We note that in this schematic we assumed for the sake of simplicity that $da = dt = 1$ day, which is not true in our simulations as we wanted a finer discretization for the age of infection a. This is because the analysis of our extended *Saenz* model in chapter 3 suggested that there is only a small window for the potential

within-host emergence of the mutant strain early in the infection.

Algorithm 1: Pseudocode for grid model

Initialization : da, $dt > da$, D^p, $P(a)$ ...
for $time = da : da : D^p$ **do**
  day= $\lfloor time \rfloor$
  if *day=*$time$ **then**
    update the ages of infection :
    $I_1^{day}(a,\alpha) \to I_1^{day}(a+da,\alpha)$, $I_2^{day}(a) \to I_2^{day}(a+da)$
    check for emergence :
    $\forall a\ NumTrials(a) = I_1^{day}(a,\emptyset)$
    $NumEmergencies(a) = Binomial(NumTrials(a), P(a))$
    compute new infections :
    $r_1 = \sum_a \sum_\alpha I_1^{day}(a,\alpha)$, $r_2 = \sum_a I_2^{day}(a)$
    $S(day) = \exp(-(r_1+r_2))S(day-dt)$
    $numNewInfs = S(day-dt) - S(day)$
    $numNewI_1 = Binomial(numNewInfs, \frac{r_1}{r_1+r_2})$
    $numNewI_2 = numNewInfs - numNewI_1$
  else
    update the ages of infection
    check for emergence

Algorithm 1 shows the pseudocode for a single simulation of our cross-scale model. In our simulations the real clock $time$ needs to account for the difference in the time scales of the real time t and the age of infection a. Since we set our discretization of a as finer than that of t, we increment $time$ by da to check whether the mutant has emerged within infected individuals between $time - da$ and $time$. When $time$ takes one of the values in our discretization of t, which happens when $time$ and day are equal in algorithm 1, we additionally compute the new infections that arose between $time - dt$ and $time$. This formulation depends on setting $dt = k^\star \times da$, where $k^\star > 1 \in \mathbb{Z}$.

4.6 Results

We will now present the results and analysis of our cross-scale model. The structure of this section is as follows:

- In the first subsection we will investigate how varying some of the within-host model's parameters affects the population-level basic reproduction number of mutant strain.
- In the second subsection we will study our cross-scale model's transmission rates and how they are affected by the age of infection and the within-host time of emergence.
- In the third subsection we will present our cross-scale model's results using the within-host derived emergence density from 3.5 to inform the mutant's within-host probability of emergence.
- In the fourth subsection we will perform a similar analysis of our cross-scale model but instead of the within-host derived emergence density we will assume that the emergence density remains constant throughout an individual's infection. While this means that emergence no longer depends on the results of our within-host model, the resulting framework resembles our population-level model from chapter 2, with the key difference that we have not yet incorporated vaccination to our cross-scale model.
- Finally in the fifth subsection we will study our cross-scale model under the assumption that the within-host emergence follows a scaled Weibull distribution, which we will argue results in emergence dynamics that we originally expected our extended Saenz model to produce. This will further test the sensitivity of our model's results to the assumed form of the within-host emergence density.

4.6.1 The effects of the within-host fitness

In chapter 3 we defined the fitness of the mutant strain, always in relation to the fitness of the parent resident strain, in terms of the death rate of cells infected by the mutant. More specifically we defined a weaker mutant strain as one which results in infected cells dying twice as quickly compared to cells infected with the resident strain, or $\delta_2 = 2\delta_1$ in our notation. Equivalently we defined a fitter mutant strain by setting $\delta_2 = (1/2) \times \delta_2$. Here we review our choice for the fitness of the mutant by varying some of the parameters of our

within-host model and evaluating their impact on the population-level basic reproduction number of the mutant strain $\mathscr{R}_0^{m,p}$. As we showed in section 4.4, we have the following formula for $\mathscr{R}_0^{m,p}$ [equation (4.27)]:

$$\mathscr{R}_0^{m,p} = \int_0^{D^{wh}} bV_2(a)da$$

Therefore by simulating a single-strain infection that is initiated with the mutant strain we can vary all the relevant within-host parameters and examine how they affect $\mathscr{R}_0^{m,p}$ via their effect on the within-host viral load. Since there is no backwards mutation in our model, this process involves no stochastic elements. We note that in order to solve equation (4.27) it is necessary to set a value for the population-level basic reproduction number of the resident strain $\mathscr{R}_0^{r,p}$, as this is necessary to obtain the scaling constant b.

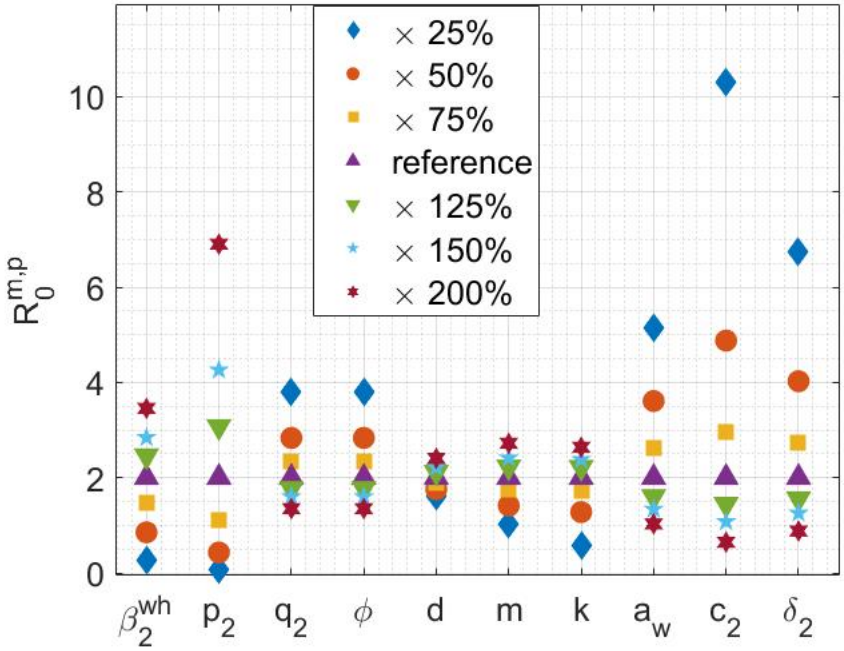

Fig. 4.2 The effects of varying the relevant within-host parameters on the mutant's population-level $\mathscr{R}_0^{m,p}$. When one parameter is varied the rest are kept constant at their reference value from table 4.1. The population-level basic reproduction number of the resident strain is set as $\mathscr{R}_0^{r,p} = 2$.

We can make the following observations based on figure 4.2:

- Doubling the death rate δ_2 of cells infected by the mutant results in $\mathscr{R}_0^{m,p} \approx 0.88$, which makes it impossible for the mutant to spread in the population. Halving the death rate δ_2 leads to $\mathscr{R}_0^{m,p} \approx 4$.

- Decreasing the clearance rate of free virions c_2 has the largest positive effect on $\mathscr{R}_0^{m,p}$, followed by increasing the production rate of progeny virions p_2 and decreasing the death rate δ_2 of infected cells.
- Varying the IFN production rate q_2, the IFN efficiency ϕ, the IFN clearance d, the IFN-reduced infectivity m and the duration of the eclipse phases $1/k_\alpha$ and $1/k_\gamma$ have only a small impact on $\mathscr{R}_0^{m,p}$.
- Increasing the duration of the prerefractory state $1/a_w$ has a significant positive impact on $\mathscr{R}_0^{m,p}$, surpassing that of increasing the mutant's within-host transmission rate β_2^{wh}.

This analysis suggests that we should alter our choice for the fitness of the mutant strain in the context of our cross-scale model. Our previous choice of $\delta_2 = 2\delta_1$ for a deleterious mutation leads to a mutant that has no chance of spreading in the population ($\mathscr{R}_0^{m,p} \approx 0.88$), but we are interested in studying the competition dynamics of an emerging mutant strain both within- and between-host. Therefore, given a resident strain with $\mathscr{R}_0^{r,p} = 2$, we need to choose a value for δ_2 such that in the case of a deleterious mutation we still have $\delta_2 > \delta_1$, but also $\mathscr{R}_0^{m,p} > 1$.

In chapter 3 we studied the resulting within-host viral competition dynamics when varying the mutant's within-host transmission rate β_2^{wh}, the production rate of new virions p_2, the death rate of infected cells δ_2 and the clearance rate of free virions c_2. These are the four mutant-specific within-host parameters that determine the mutant's within-host basic reproduction number $\mathscr{R}_0^{m,wh}$ [equation (4.24)]. We will now further investigate their impact on the mutant's between-host basic reproduction number $\mathscr{R}_0^{m,p}$.

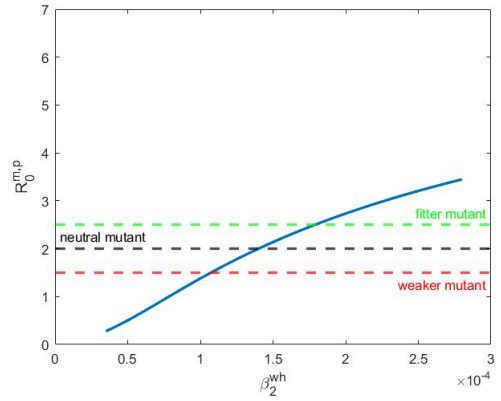

(a) Increasing the within-host transmission β_2^{wh} has the smallest positive effect on $\mathscr{R}_0^{m,p}$

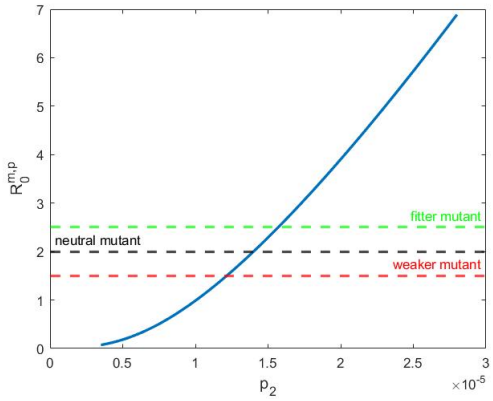

(b) Varying the virion production rate p_2 has an intermediate effect on $\mathscr{R}_0^{m,p}$

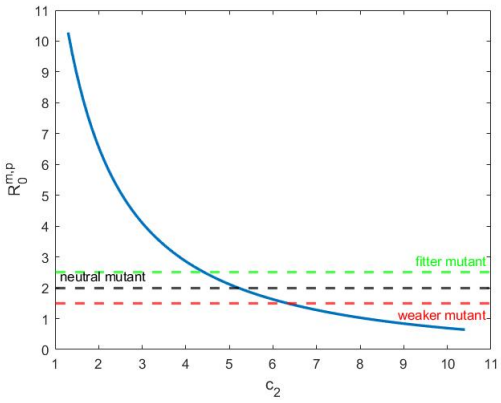

(c) Decreasing the viral clearance rate c_2 has the largest positive effect on $\mathscr{R}_0^{m,p}$. We note that this plot has a different y-axis scale compared to plots (a),(b) and (d). This was chosen only for the sake of illustration.

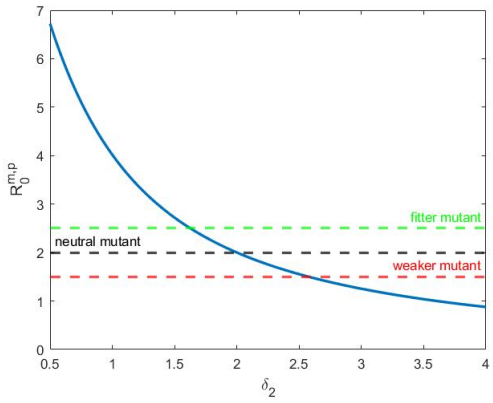

(d) Varying the death rate δ_2 of infected cells has an intermediate effect on $\mathscr{R}_0^{m,p}$.

Fig. 4.3 The effects of varying the mutant-specific within-host parameters on the mutant's population-level basic reproduction number $\mathscr{R}_0^{m,p}$. The parameters were varied between 25% and 200% of their reference values from table 4.1. Whenever the within-host death rate of infected cells δ_2 wasn't varied, we used $\delta_2 = \delta_1 = 2$. The green dashed lines in plots (a)-(d) correspond to a beneficial mutation with $\mathscr{R}_0^{m,p} = 2.5$, the black dashed lines to a neutral mutation with $\mathscr{R}_0^{m,p} = 2$ and finally the red dashed lines to a deleterious mutation with $\mathscr{R}_0^{m,p} = 1.5$. We picked these values in relation to the population-level fitness of the resident strain, for which we set $\mathscr{R}_0^{r,p} = 2$.

Figure 4.3 shows how the mutant's population-level basic reproduction number $\mathscr{R}_0^{m,p}$ is affected when we vary the four mutant-specific within-host parameters: the transmission rate β_2^{wh}, the virion production rate p_2, the viral clearance rate c_2 and the death rate δ_2 of infected cells. We observe that increasing the mutant's within-host transmission rate β_2^{wh} leads to the smallest increase in $\mathscr{R}_0^{m,p}$, while decreasing the clearance rate of free mutant virions c_2 leads to the largest increase in $\mathscr{R}_0^{m,p}$. We therefore expect our model to be more sensitive to changes in c_2 compared to the other within-host parameters studied here. The dashed lines in plots (a)-(d) are at our chosen values for the $\mathscr{R}_0^{m,p}$ of a fitter, a neutral and a weaker mutant strain, always in relation to the fitness of the resident strain for which we set $\mathscr{R}_0^{r,p} = 2$. We note that our choices of $\mathscr{R}_0^{m,p} = 2.5$ for a beneficial

and $\mathscr{R}_0^{m,p} = 1.5$ for a deleterious mutation are semi-arbitrary, as our only criterion was to avoid giving either a very significant advantage or disadvantage to the mutant.

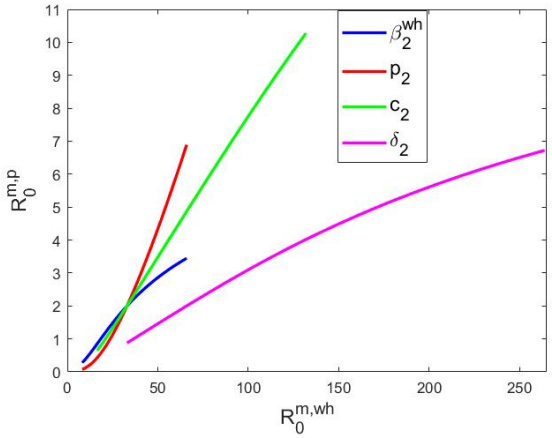

Fig. 4.4 The relation between the mutant's within-host basic reproduction number $\mathscr{R}_0^{m,wh}$ and between-host basic reproduction number $\mathscr{R}_0^{m,p}$. This plot was obtained by varying the mutant-specific within-host parameters and evaluating their impact on $\mathscr{R}_0^{m,wh}$ and $\mathscr{R}_0^{m,p}$. Specifically, he parameters β_2^{wh}, p_2, c_2 and δ_2 were varied between 25% and 200% of their reference values from table 4.1. When one parameter was varied the rest remained constant at their reference value.

Figure 4.4 illustrates how the relation between the mutant's within-host basic reproduction $\mathscr{R}_0^{m,wh}$ and between-host basic reproduction number $\mathscr{R}_0^{m,p}$ changes as we vary the within-host mutant-specific parameters. The parameters we varied here are the ones which appear in our expression for $\mathscr{R}_0^{m,wh}$ [equation (4.24)]: the within-host transmission rate β_2^{wh}, the virion production rate p_2, the viral clearance rate c_2 and the death rate δ_2 of cells infected with the mutant. We may make the following observations:

- Varying β_2^{wh} has the smallest impact on the mutant's relative fitness on both the within- and between-host levels.
- The within-host death rate of infected cells δ_2, which has only an intermediate effect on the mutant's population-level fitness, appears to have the most significant impact on its within-host fitness.
- The relation between $\mathscr{R}_0^{m,wh}$ and $\mathscr{R}_0^{m,p}$ appears to be almost linear as we vary c_2, convex as we vary p_2 and concave as we vary δ_2 and β_2^{wh}. Regrettably I have not been able to find a satisfactory explanation for these relations.

Throughout the rest of this chapter we will use the death rate δ_2 of cells infected with the mutant strain to define the within-host fitness of the mutant, which allows us to remain consistent with our standard definition from chapter 3. Moreover, we will use $\mathscr{R}_0^{m,p} = 2.5$ for a fitter strain and $\mathscr{R}_0^{m,p} = 1.5$ for a weaker strain, unless stated otherwise, while a neutral mutant strain will have $\mathscr{R}_0^{m,p} = 2$ which is the same as the resident strain. From figure 4.3(d) we see that the values of δ_2 which lead to our desired values for $\mathscr{R}_0^{m,p}$ are $\delta_2 = 1.6$, $\delta_2 = \delta_1 = 2$ and $\delta_2 = 2.6$ for a fitter, a neutral and a weaker strain respectively.

4.6.2 The transmission rates

The population-level transmission rates $\beta_{11}(a,\alpha)$, $\beta_{12}(a,\alpha)$ and $\beta_{22}(a,\alpha)$ are very significant for our cross-scale model because they provide the link between the within-host and the population tiers. Therefore they are what differentiates our cross-scale model from population models with constant values for the transmission rate β, such as the model we developed in chapter 2. Considering that one of the principal goals of this thesis is to evaluate the usefulness of a more complex cross-scale model against that of a standard population model in the context of the evolution of influenza, it is crucial to examine the transmission rates of our model very closely.

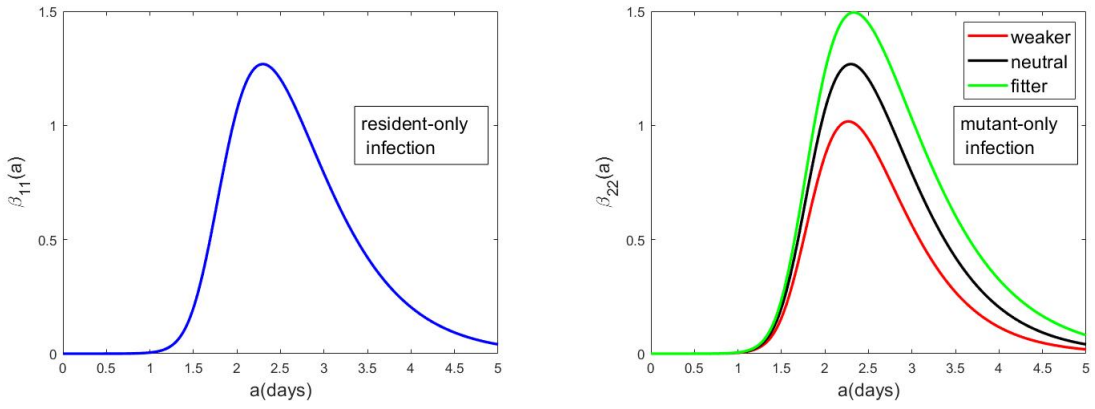

(a) Resident-only infection.

(b) Mutant-only infection.

Fig. 4.5 The transmission rates for single strain infections in our cross-scale model. Their trajectory resembles the within-host viral load curves, which is expected given our assumption that the transmission rates are linear functions of the within-host viral loads. The curve in plot (a) and the black curve in plot (b) are the same because a neutral mutant strain is defined by the same strain-specific parameters as the resident (here $\delta_2 = \delta_1$).

Figure 4.5 shows the transmission rates for single strain infections. Plot (a) describes an infection with only the resident strain present, while plot (b) with only a mutant but

also takes into consideration all three cases for the fitness of the mutant. The blue curve in plot (a) is the same as the black curve in plot (b) because the resident strain and the neutral mutant strain are defined by the same strain-specific within-host parameters. We observe that the trajectories of the transmission rates resemble those of the within-host viral loads. This is expected since we defined the transmission rates to be linear functions of the within-host viral loads, scaled only by a constant. The result is that a host's transmissibility increases as their viral load increases and reaches a peak around the third day of infection, after which the host becomes less infectious. We note that there is no mentioning of the emergence time α in figure 4.5 because we are only considering single strain infections. We also note that in our simulations of the cross-scale model we set the transmission rate equal to zero at the end of the infection (here at $a = 5$ days), but we did not show this here for the sake of illustration.

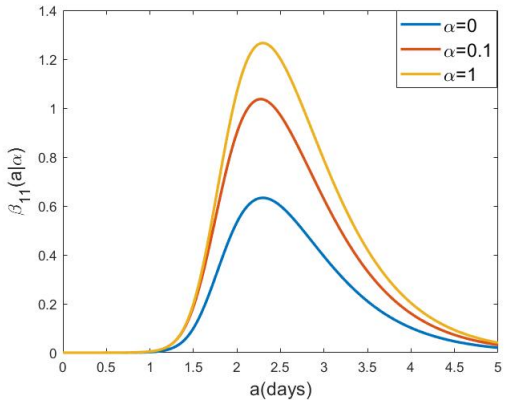

(a) The transmission rate $\beta_{11}(a|\alpha)$ to new infections with the resident strain for three different values of the emergence time α.

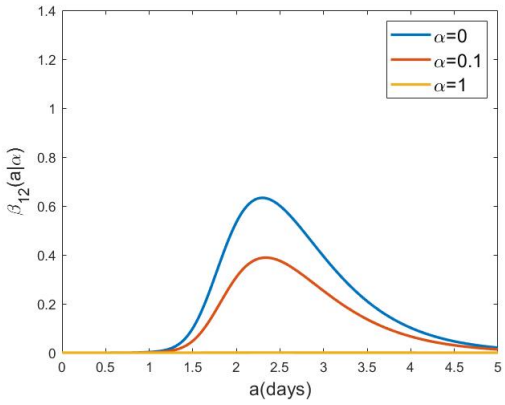

(b) The transmission rate $\beta_{12}(a|\alpha)$ to new infections with the mutant strain for three different values of the emergence time α.

Fig. 4.6 The transmission rates $\beta_{11}(a|\alpha)$ and $\beta_{12}(a|\alpha)$ of a host who was initially infected with the resident strain for three different values of the within-host emergence time α. We note that $\alpha = 0$ describes a coinfection rather than a mutant strain emergence, but we included it here to highlight the positive effects of earlier emergence times on the transmission rate of the mutant. The mutant here is neutral, so we have $\delta_2 = \delta_1$.

Figure 4.6 shows the transmission rates for an individual who was initially infected with the resident strain and had the mutant strain emerge within them at some specified time α during their infection. Plot (a) describes the host's transmission rate to new cases with the resident strain while plot (b) to new cases with the mutant. We observe that a later emergence time has a large negative impact on the transmission rate of the mutant strain, as when $\alpha = 1$ the host transmits almost none of the mutant to new cases [as shown in plot (b)]. This is expected since we assume that the transmission rates are linear functions of the within-host viral load, and as we have demonstrated in chapter 3 a later emergence time significantly hinders the mutant's growth. Given

the within-host competition of the two strains for available resources, it is not surprising that a later emergence time has the opposite, beneficial effect on the transmission rate of the resident strain as plot (a) illustrates. We note that the case $\alpha = 0$ represents a coinfection with two strains rather than a mutant strain emergence, but we included it here to highlight the strong effect of the emergence time on the transmission rates of the two strains.

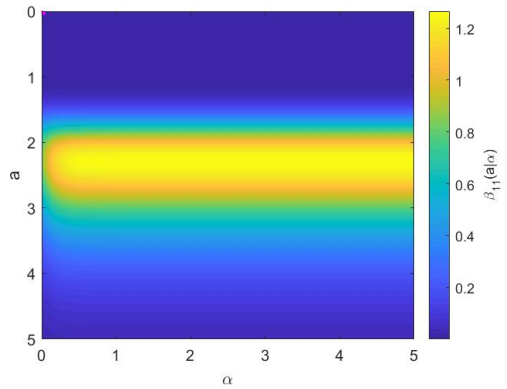

(a) The transmission rate $\beta_{11}(a|\alpha)$ to new infections with the resident strain is almost unaffected by the emergence time α, except when α is very small.

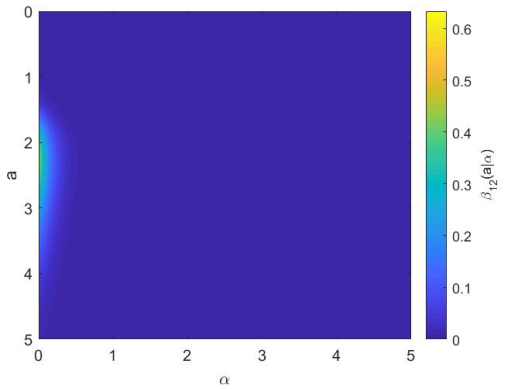

(b) The transmission rate $\beta_{12}(a|\alpha)$ to new infections with the mutant strain attains its largest values when α is very small and is almost 0 for all other values of α.

Fig. 4.7 The transmission rates $\beta_{11}(a|\alpha)$ and $\beta_{12}(a|\alpha)$ of a host who was initially infected with the resident strain functions of the age of infection a and the within-host emergence time of the mutant strain α. The mutant strain is chosen as neutral here, therefore $\delta_2 = \delta_1 = 2$. Here $\alpha = 5$ represents the case that no emergence has taken place during the host's infection. We note that the scale is different between these two plots.

Figure 4.7 shows how the transmission rates vary with the age of infection a and the emergence time α for the specific case of a neutral mutation. Plot (a) describes the transmission rate from an individual who was originally infected with the resident strain, had the mutant emerge within them at some time α, and is now transmitting to new cases with the resident strain. Plot (b) describes the same host's transmission rate to new cases with the mutant strain. We note that in the simulations of our cross-scale model a host at any given time can transmit either the resident or the mutant strain to a new individual, with some probability that depends on the within-host viral loads at the time, but not both. We emphasize that in the context of this figure the emergence of the mutant strain is not stochastic, rather α was used as fixed parameter of our within-host model. As a result, we force a mutant to appear within the host even at times when it cannot grow or survive. The importance of α is evident from plot (b), which shows that the host's transmission of the mutant strain is very close to zero for any emergence time that is not very early in the host's infection. This can also be seen in plot (a), where the

host's transmission rate of the resident strain appears to remain unaffected as α varies, except for very small values of α. We can attribute this to the competition dynamics between the two strains, since as we have shown in chapter 3 even very small increases to α can give a significant disadvantage to the mutant. This is because a later α implies that the resident strain has had more time to circulate within the host and infect target cells, therefore decreasing the pool of target cells available to the mutant. This leads to restricted growth for the mutant, and therefore to smaller viral loads and in turn to smaller transmission rates. We note that this result is dependent on our assumption that a cell may only be infected once and by only one strain. While figure 4.7 illustrates the importance of the within-host emergence time α for the mutant's chances of spreading in the population, it is useful to further examine the relationship between the transmission rates and α.

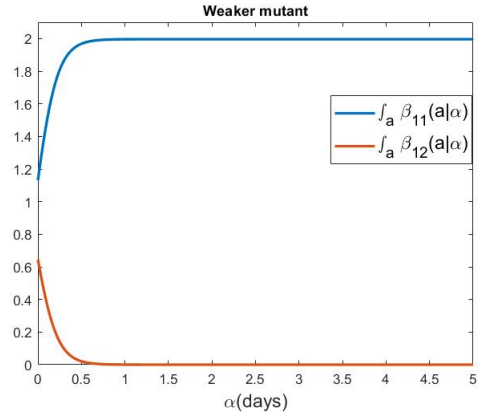

(a) Total conditional transmission potential for a deleterious mutation : $\delta_2 = 2.6$

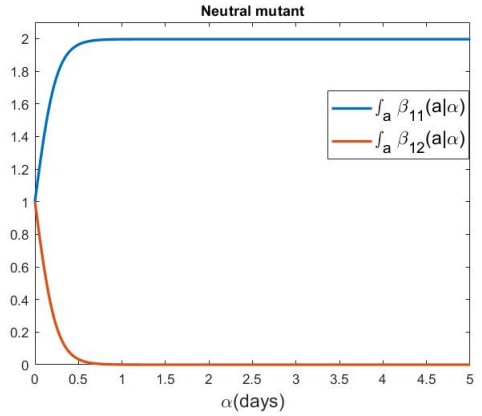

(b) Total conditional transmission potential for a neutral mutation : $\delta_2 = \delta_1 = 2$

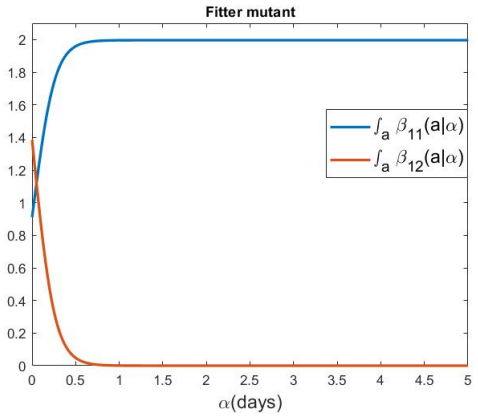

(c) Total conditional transmission potential for a beneficial mutation : $\delta_2 = 1.6$

Fig. 4.8 The total conditional transmission potential $\int_a \beta_{11}(a|\alpha)da$ and $\int_a \beta_{12}(a|\alpha)da$ of hosts who were initially infected with the resident strain as a function of the within-host emergence time α. In all plots the blue curve represents the total conditional transmission potential $\int_a \beta_{11}(a|\alpha)da$ to new cases with the resident strain while the red curve represents the total conditional transmission potential $\int_a \beta_{12}(a|\alpha)da$ to new infections with the mutant strain. Here $\alpha = 5$ describes the case that no emergence has occurred throughout an individual's infection with the resident strain. The case $\alpha = 0$ describes a co-infection, which we do not allow for in our simulations of the epidemic, but we included it here for graphical purposes.

Figure 4.8 shows how the integrals of the conditional transmission rates, which we will refer to as the total conditional transmission potentials, vary with the emergence time α for all three cases for the fitness of the mutant. Due to our choice of the transmission rates being a linear function of the viral load, the total conditional transmission potentials are simply the integral of the conditional viral load multiplied by a scaling constant, namely $\int_a \beta_{11}(a|\alpha)da = b\int_a V_1(a|\alpha)da$ using the conditional transmission of the resident strain to new hosts as an example. We note that the emergence of the mutant here is deterministic, as we are treating α as a parameter of our model for the purposes of this figure. All three plots show that computationally the total conditional transmission potential $\int_a \beta_{11}(a|\alpha)da$ to new cases with the resident strain is a non-decreasing function of the emergence time α, while the total conditional transmission potential $\int_a \beta_{12}(a|\alpha)da$

to new cases with the mutant strain is a non-increasing function of α. This is not surprising given our findings in 3.4.4, which showed that the integrals of the viral loads follow the same trajectories as the ones described here. The reasoning remains the same too: a later α gives an increasingly larger disadvantage to the mutant strain because the resident is depleting its pool of available target cells. After a certain α though, the only factor that contributes to the total viral load of the mutant is the initial number of mutant virions which we introduce to the model at α. This is why the total conditional transmission potential to new cases with the mutant initially decreases but then plateaus as α increases, and equivalently why the total conditional transmission potential to new cases with the resident initially increases but then plateaus with α.

4.6.3 Results using the within-host derived emergence density

In this section we will present our cross-scale model's results under the within-host emergence density function f_{WH} that we derived in section 3.5. We repeat our expression for f_{WH} here:

$$f_{WH}(\alpha) = \lambda(\alpha) \times e^{-\int_0^\alpha \lambda(a)da}$$

where $\lambda(\alpha)$ is the rate of appearance, survival and adequate growth of a mutant strain and is given by:

$$\lambda(\alpha) = (\varepsilon\rho) \times \left(k_\alpha E_\alpha(\alpha) + k_\gamma E_\gamma(\alpha)\right) \times \left(1 - \frac{1}{R_{eff}^{m,wh}(a)}\right) \times \mathbb{1}^n_{(c_2 \int_\alpha^{D^{wh}} (V_2(a)da) \geq s^*)}$$

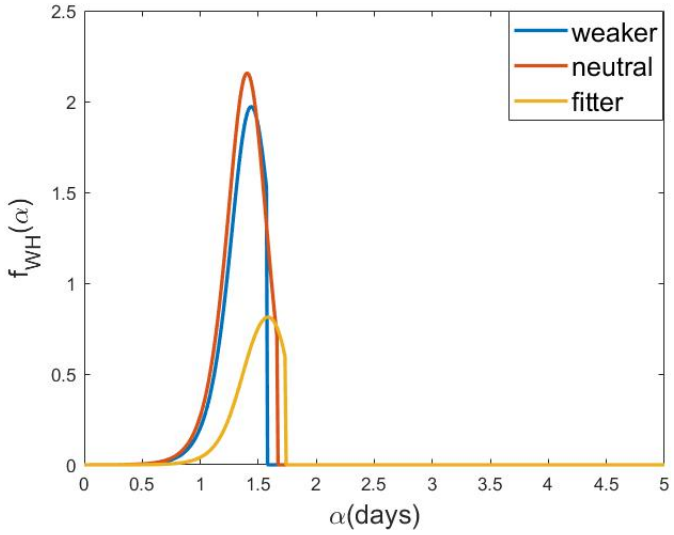

Fig. 4.9 The within-host emergence density function f_{WH} for all three types of mutants.

Figure 4.9 shows how the emergence density f_{WH} changes during an individual's infection. We have already discussed the shape of f_{WH} in 3.5, but we will summarize our relevant conclusions here:

- The mutant's emergence window is very narrow and very early in the infection. This can be attributed to the fast depletion of target cells in our extended *Saenz* model.
- The mutant's cumulative probability of emerging throughout the host's infection, calculated here as $\int_\alpha f_{WH}(\alpha)d\alpha$, can be considered high for all three types of mutants. Specifically, the cumulative within-host emergence probability is 0.73 for a weaker mutant, 0.91 for a neutral and 0.34 for a fitter mutant. The reason for the much smaller cumulative emergence probability for a fitter mutant is that according to Visher *et al.* only 5% of viable mutations lead to a fitter mutant strain [297]. We addressed the large cumulative emergence probabilities in 3.5, and we concluded that they can be attributed to the free mixing of the target cells and virions and to the large number of target cells within the host.

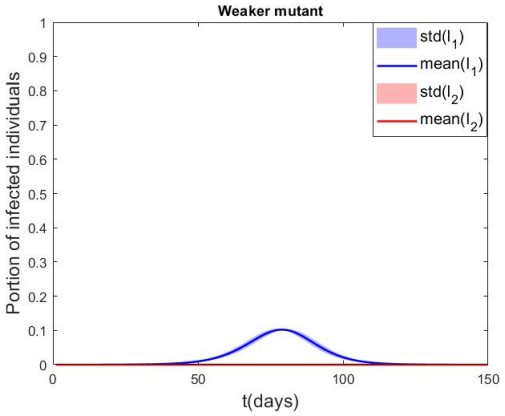

(a) The average portions of individuals originally infected with the resident and mutant strains in 500 simulations of our model. Here the mutant is assumed to be weaker, so we have $\delta_2 = 2.6$ for the within-host death rate of cells infected with the mutant, and $\delta_1 = 2$. At the between-host level this translates to $\mathscr{R}_0^{r,p} = 2$ for the resident and $\mathscr{R}_0^{m,p} = 1.5$ for the weaker mutant strain.

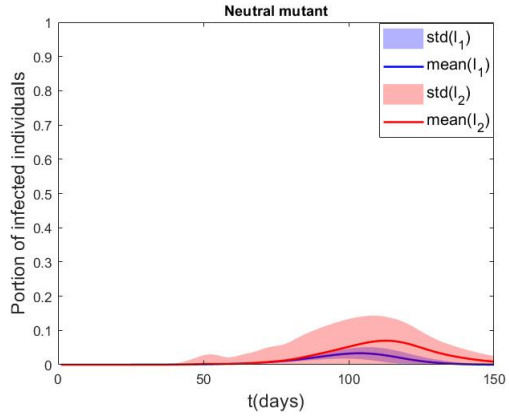

(b) The average portions of individuals originally infected with the resident and mutant strains in 500 simulations of our model. Here the mutant is assumed to be neutral, so we have $\delta_2 = \delta_1 = 2$ and $\mathscr{R}_0^{r,p} = \mathscr{R}_0^{m,p} = 2$.

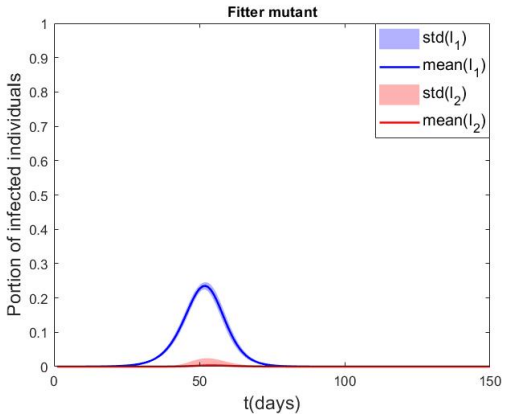

(c) The average portions of individuals originally infected with the resident and mutant strains in 500 simulations of our model. Here the mutant is assumed to be fitter, so we have $\delta_2 = 1.6$, and again $\delta_1 = 2$. At the between-host level this translates to $\mathscr{R}_0^{r,p} = 2$ for the resident and $\mathscr{R}_0^{m,p} = 2.5$ for the fitter mutant strain.

Fig. 4.10 The infectious groups dynamics under the within-host derived f_{WH}. We note that the I_1 compartment refers to the portion of individuals in the population who were originally infected with the resident strain, but could also have had the mutant strain emerge within them. The I_2 compartment refers to hosts who were infected with the mutant strain.

Figure 4.10 shows how the mean portions of individuals originally infected by the resident and mutant strains vary throughout the epidemic for the three cases of a deleterious, neutral and beneficial mutation. We can make the following observations:

- The largest variability in the portion of individuals initially infected with the mutant happens in the case of a neutral mutation [plot (b)]. On the contrary we observe very little variability in the cases of a deleterious mutation [plot(a)] and a beneficial mutation [plot (c)]. For a weaker mutant this can be attributed to the fitness disadvantage that it has compared to the resident strain both at the within- and the between-host levels. For a beneficial mutation we refer back to figure 4.9,

which shows that the fitter mutant's emergence probability attains its maximum and then drops to zero very quickly. Moreover we note that the mutant's chances to emerge during the first day of infection are very small (and lower compared to those of a weaker and a neutral strain). Therefore we expect the fitter mutant to emerge most often around a time when its available resources will be very limited, though still enough for it to survive and reach a minimum final size within-host (by construction of our f_{WH}). This restriction to the mutant's available resources hinders its within-host growth and therefore its transmission to new hosts, even despite the mutant's fitness advantage.

- The peak as well as the duration of the epidemic are affected by the relative fitness of the mutant strain. The case of a neutral mutation leads to the slowest epidemic and the smallest, latest peak. This may be explained by the strong competition between the two strains for available hosts in the population, which allows neither of them to spread quickly. Our assumption of full cross-immunity entails that hosts originally infected by the mutant strain become fully immune to the resident. We also assume though that the mutant strain may emerge within any host that is infected with the resident. These two assumptions, combined with the lack of a fitness disadvantage, the very narrow emergence window early in the infection and the large within-host cumulative emergence probability, can explain why on average the mutant strain dominates the epidemic as plot (b) illustrates. Among the three plots the second slowest epidemic occurs in the case of a deleterious mutation [plot (a)]. Given a weaker strain's fitness disadvantage, it is unsurprising that despite its large within-host cumulative emergence probability, the mutant cannot compete efficiently against the fitter resident strain at either the between- or within-host levels. We note that the case of the beneficial mutation led to the shortest epidemic and the largest peak for the resident strain, suggesting that the fitter mutant's smaller cumulative within-host emergence probability and slightly later emergence window inhibit its within-host growth so much that the mutant has a very small impact on the spread of the resident both within- and between-host .

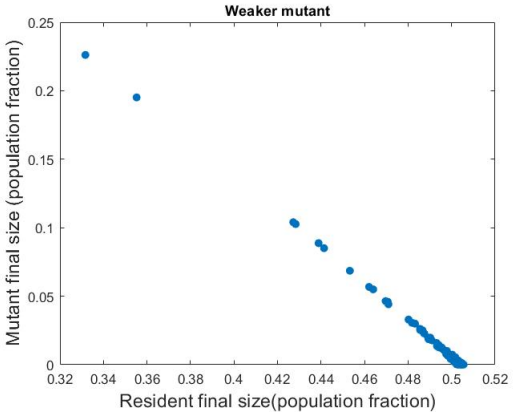

(a) The final sizes of the resident and mutant strain in 500 simulations of our cross-scale model. Here the mutation is assumed to be deleterious. We emphasize that for illustration purposes this plot has a different y-axis scale compared to the other two plots.

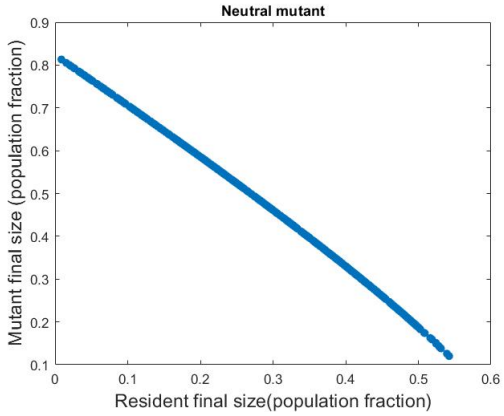

(b) The final sizes of the resident and mutant strain in 500 simulations of our cross-scale model. Here the mutation is assumed to be neutral. We emphasize that for illustration purposes this plot has a different y-axis scale compared to the other two plots.

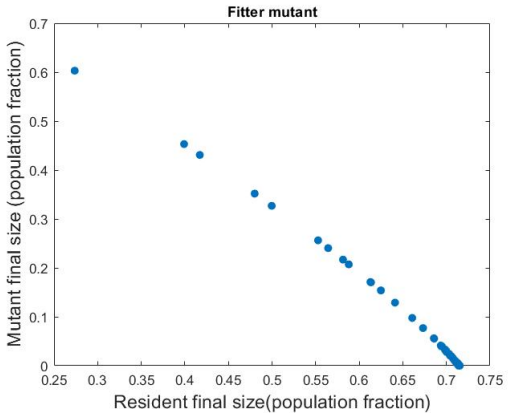

(c) The final sizes of the resident and mutant strain in 500 simulations of our cross-scale model. Here the mutation is assumed to be beneficial. We emphasize that for illustration purposes this plot has a different y-axis scale compared to the other two plots.

Fig. 4.11 The population-level final sizes of the resident and mutant strains in 500 simulations of our cross-scale model for the three different cases of the mutant's relative fitness. We emphasize that for illustration purposes the three plots have different y-axis scales.

Figure 4.11 shows the population-level final sizes of the resident and mutant strains in 500 simulations of our cross-scale model for the three cases of a deleterious, neutral and beneficial mutation. We may make the following observations:

- The final size of the epidemic, defined here as the sum of the final sizes of the resident and mutant strains, is affected by the emergence of a mutant strain at the within-host level. Firstly, we may use Kermack and McKendrick's epidemic final size formula $R_1(\infty) = 1 - \exp(-\mathscr{R}_0^{r,p} \times R_1(\infty))$ from [163] to calculate the final size of a single-strain epidemic with only the resident strain present. We may simulate such an epidemic by assuming that the within-host emergence density of the mutant remains constant at 0, and in that case the epidemic final size is

0.8. All three plots show though that the epidemic final size does not remain at 0.8 when a mutant strain is added to the model. This is true even in cases where the mutant has a very small presence at the between-host level as for instance plot (a) illustrates, where the weaker mutant strain had a final size close to 0 in some of our simulations but the resident never achieved a final size larger than 0.52. Kermack and McKendrick's final size formula assumes a constant between-host transmission rate. But in our model the between-host transmission rate of the resident strain is a function of the resident's within-host viral load and is therefore negatively affected by the within-host emergence of a mutant strain, even if the mutant never transmits to a new host in the population.

- The resident strain achieved larger final sizes when competing against the fitter mutant than the weaker one, as a comparison between plots (a) and (c) shows. This may be attributed to the significantly larger cumulative within-host emergence probability of the weaker mutant strain and the fact that its emergence window comes slightly earlier in the infection. More specifically, a weaker mutant has more chances to emerge during an individual's infection so we expect it to emerge considerably more often than the fitter mutant in our simulations. Moreover the weaker mutant's narrow emergence window comes slightly earlier in the infection and therefore ensures not only that the mutant can grow within-host despite its fitness disadvantage compared to the resident, but also that it has higher chances than the fitter mutant to emerge earlier in the infection and have more resources available to it. As a result we expect the weaker mutant's negative effect on the within-host growth of the resident strain to be more prominent than that of the fitter mutant. Given our assumption that the between-host transmission rates are linear functions of the within-host viral load, this implies a larger decrease in the transmission rates of the resident when it has to compete against a weaker mutant compared to a fitter one. This in turn can account for the smaller population-level final sizes of the resident strain in plot (c) compared to plot (a).

- The most variability in the final size of the mutant occurs in the case of a neutral mutation, as plot (b) illustrates. We can see that in many of our simulations the final size of the mutant strain was significantly larger than that of the resident strain. This can be explained not only by the large cumulative emergence probability of a neutral mutant but also by the narrow and early emergence window that f_{WH} imposes, which guarantees that if the mutant appears it will have enough target and prerefractory cells available to it for infection and its viral load will have the

opportunity to grow within-host. This leads to better chances for the mutant to transmit to new hosts and spread in the population. We note that our use of the word "chances" is because in the implementation of our cross-scale model the decision of which strain transmits to a new host is a random event that depends on the within-host viral load of the two strains at the time of transmission.

4.6.4 Results using a constant emergence density

We will now change our approach regarding the emergence density and instead of deriving it from our within-host model we will assume that it remains constant throughout an individual's infection. This approach has the significant disadvantage that it weakens the link between the two scales of our cross-scale model. As we discussed in chapter 3 though, our within-host derived emergence density comes with the potential drawback that it only allows for a very short emergence window early in the infection. Therefore we want to assess how sensitive our cross-scale model's results are to the assumed form of the within-host emergence density. We choose a constant within-host emergence density because it results in a framework that most closely resembles our between-host model for the evolution of influenza from chapter 2.

We will assume that the within-host emergence density f_{const} follows a uniform distribution in $[0, D^{wh}]$:

$$f_{const}(\alpha) = p \times \frac{1}{D^{wh}} \times \mathbb{1}_{\alpha \in [0, D^{wh}]}$$

where p is the cumulative emergence probability of the mutant during an infection, and is chosen by us.

We will initially use the cumulative emergence probability $\int_\alpha f_{WH}(\alpha) d\alpha$ from the previous section to inform the value of p. We underline though that this initial choice is not particularly important, as later in this section we will vary p and study its impact on our cross-scale model's results. We are interested in contrasting the results of our cross-scale model from this section with the equivalent results from the previous section, where we used the within-host derived emergence density f_{WH}. For this reason we will first assume that the mutation is deleterious and compare how the infectious groups dynamics and the population-level final sizes of the two strains differ between this section

that assumes a constant within-host emergence density and the previous section where the emergence density was informed by our within-host model. We will then repeat the same analysis for the cases of a neutral and a deleterious mutation.

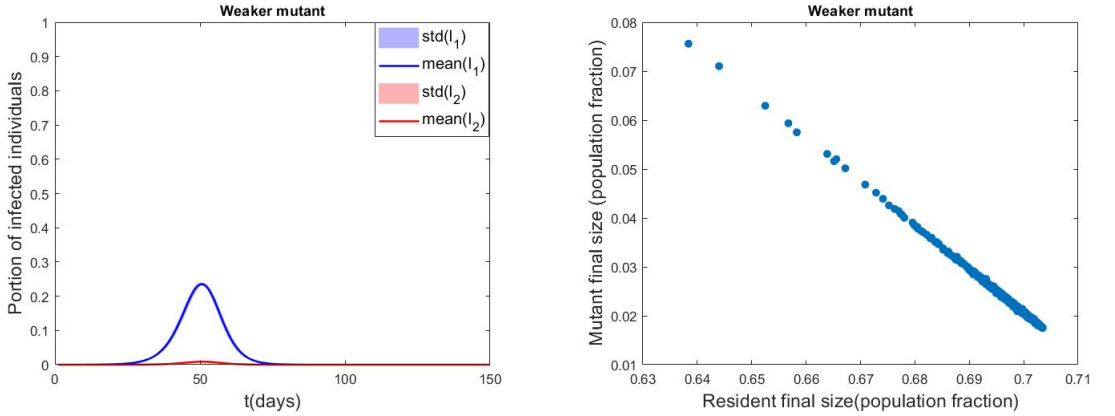

(a) The average portions of individuals originally infected with the resident and mutant strains in 500 simulations of our model.

(b) The final sizes of the resident and mutant strains in 500 simulations of our cross-scale model.

Fig. 4.12 Some key results from 500 simulations of our cross-scale model in the case of a deleterious mutation. Here we assume that the within-host emergence density is constant and the within-host cumulative emergence probability p is 0.73.

Figure 4.12 shows some key results of our cross-scale model under the assumptions that the mutation is deleterious, the within-host emergence density remains constant throughout an individual's infection and the within-host cumulative emergence probability is 0.73.

- Plot (a) shows that the weaker mutant's population-level prevalence throughout the epidemic is very low. Comparing this to the equivalent plot under the within-host derived f_{WH} [figure 4.10(a)], we observe that in the case of f_{WH} the weaker mutant again had a very low population-level prevalence throughout the epidemic but that the epidemic lasted longer and peaked considerably later. It is interesting then that while in both cases the mutant did not spread in the population, in the previous section it still had a considerable impact on the between-host dynamics of the resident strain. Under the assumption that the emergence density remains constant throughout the infection, the mutant's emergence window spans the whole duration of the infection. Therefore there can be many cases where the mutant emerges late in the infection and cannot grow efficiently (or potentially cannot grow at all) because the resident strain has been circulating longer within the host and infecting the target cells. In such cases the mutant's viral load remains so small that the mutant has very low chances of transmitting to new individuals.

Moreover, since the two strains are in competition both within- and between-host, a smaller viral load for the mutant implies a larger viral load (and therefore stronger between-host transmission) for the resident. So the result under f_{const} is a quick epidemic that peaks around 50 days. Contrasting this to the previous section where the emergence density was derived from our within-host model, we first note that f_{WH} imposes a very narrow emergence window early in the infection. This means that whenever the weaker mutant emerges within-host, it emerges early enough to still have available target cells left to it for infection. As a result it can grow more efficiently compared to a weaker mutant strain that appears late in the infection under f_{const}. Therefore the early emergence window under f_{WH} allows the weaker mutant to better compete against the resident within-host, thereby weakening the resident's transmission to new hosts due to our assumption that the between-host transmission rates are linear functions of the within-host viral load. This is why the epidemic is slower under the within-host derived emergence density f_{WH} and peaks later (close to 80 days).

- Plot (b) shows that the weaker mutant never achieved a final size larger than 0.08 at the between-host level, while in the previous section (figure 4.11(a)) it did so for a few of our simulations. This could be again attributed to the fact that a constant emergence density allows for the appearance of a mutant strain throughout the whole duration of a host's infection. As a result the mutant might often appear very late in the infection and be unable to grow efficiently (or at all), which would significantly lower its chances of transmitting to new hosts and therefore decrease its final size in the population.

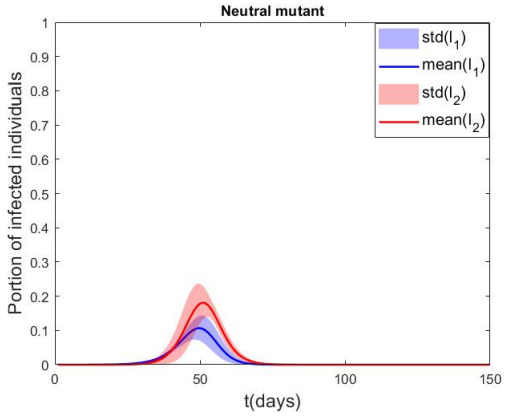

(a) The average portions of individuals originally infected with the resident and mutant strains in 500 simulations of our model.

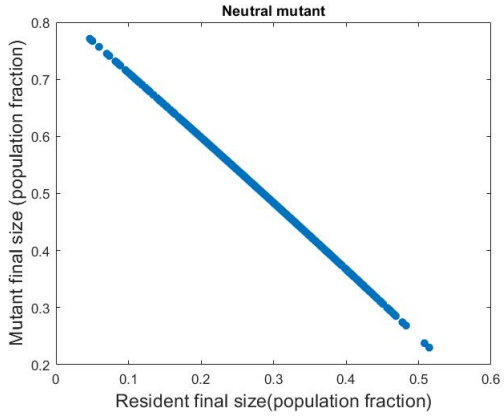

(b) The final sizes of the resident and mutant strain in 500 simulations of our cross-scale model.

Fig. 4.13 Some key results from 500 simulations of our cross-scale model in the case of a neutral mutation. Here we assume that the within-host emergence density is constant and the within-host cumulative emergence probability p is 0.91.

Figure 4.13 shows some key results of our cross-scale model under the assumptions that the mutation is neutral, the within-host emergence density remains constant throughout an individual's infection and the within-host cumulative emergence probability is 0.91.

- Plot (a) shows that the neutral mutant strain has a very strong prevalence throughout the epidemic, and on average even dominates it. A comparison with the equivalent plot under the within-host derived f_{WH} [figure 4.10(b)] shows that, again, under the narrow and early emergence window of f_{WH} the epidemic lasts considerably longer and peaks much later. This is the same observation as in the case of a weaker mutant strain, and can be attributed to similar factors. Under the constant emergence density f_{const} the mutant may appear at any time during a host's infection, even very late in the infection. Such a late emergence impedes the within-host growth of the mutant since it means that there are fewer cells available to it for infection. This offers an advantage to the resident strain, allowing it to spread more efficiently within-host and in turn in the population compared to cases where the mutant emerges early in the infection. The end result is a short epidemic that peaks close to 50 days. Under the within-host derived f_{WH}, the narrow and early emergence window facilitates the within-host growth of the neutral mutant strain and therefore its between-host transmission as well, since that depends linearly on the strain's within-host viral load. The result is an epidemic with two strains which can heavily compete against each other at both the within- and between-host scales, which increases the epidemic's duration as well as the time of its peak (which occurs close to 120 days).

- Plot (b) shows that the neutral strain often achieved larger final sizes than the resident. This is in agreement with the final size results under the within-host derived f_{WH} [figure 4.11(b)].

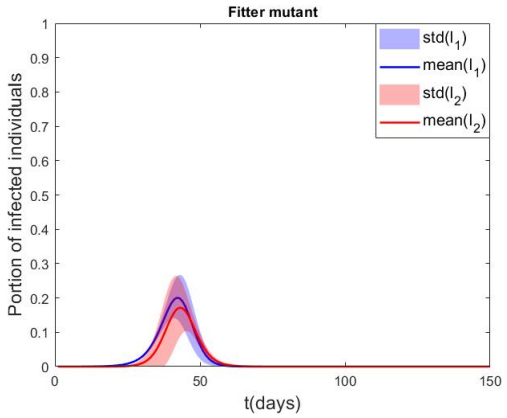

(a) The average portions of individuals originally infected with the resident and mutant strains in 500 simulations of our model. Here the mutant is assumed to be fitter and the within-host emergence density is constant.

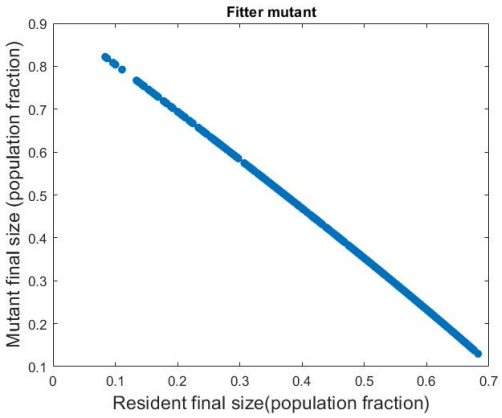

(b) The final sizes of the resident and mutant strain in 500 simulations of our cross-scale model. Here the mutation is assumed to be beneficial.

Fig. 4.14 Some key results from 500 simulations of our cross-scale model in the case of a beneficial mutation. Here we assume that the within-host emergence density is constant and the within-host cumulative emergence probability p is 0.34.

Figure 4.14 shows some key results of our cross-scale model under the assumptions that the mutation is beneficial, the within-host emergence density remains constant throughout an individual's infection and the within-host cumulative emergence probability is 0.34.

- Plot (a) shows that the fitter mutant strain has a strong prevalence in the population throughout the epidemic. It is interesting to compare this to the results under the within-host derived f_{WH} [figure 4.10(c)], where the fitter mutant had a very low prevalence in the population. We may attribute the much higher prevalence of the mutant under f_{const} to the fact that it offers equal chances to the fitter mutant to emerge very early in the infection, while under f_{WH} the fitter mutant is expected to emerge most often very close to its emergence cut-off time. Moreover under f_{WH} no emergence can occur past the second day of infection due to the conditions it imposes, namely that the mutant cannot emerge once its effective reproduction number $\mathscr{R}_{eff}^{m,wh}$ falls below 1 or if it cannot satisfy the minimum within-host final size requirement. On the other hand under f_{const} the mutant may emerge even late in the infection and while that ensures that it will not grow efficiently (or at all), it will

still have a very small but non-zero chance to transmit to new hosts as long as its viral load is positive.

- Plot (b) shows that the fitter mutant often achieved larger final sizes than the resident. This is in contrast with the equivalent results under f_{WH} [figure 4.11(c)], where the fitter mutant reached very small final sizes in the vast majority of our simulations. We may again attribute this difference to the higher chances of the mutant to arise very early in the infection (during the first day) under f_{const} and to the stricter conditions for emergence that our within-host derived f_{WH} imposes.

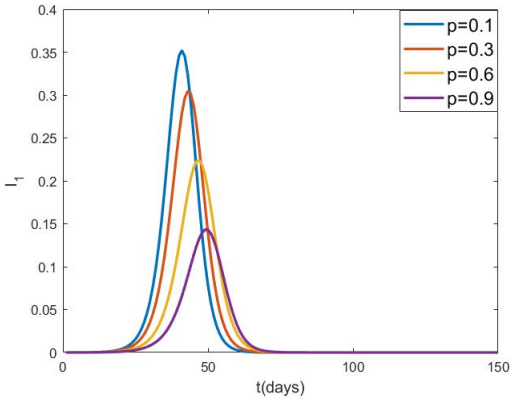

(a) The mean portion of individuals originally infected with the resident strain throughout the epidemic for four different values of the cumulative within-host emergence probability p. For each value of p, the averages were taken over 100 simulations of our cross-scale model.

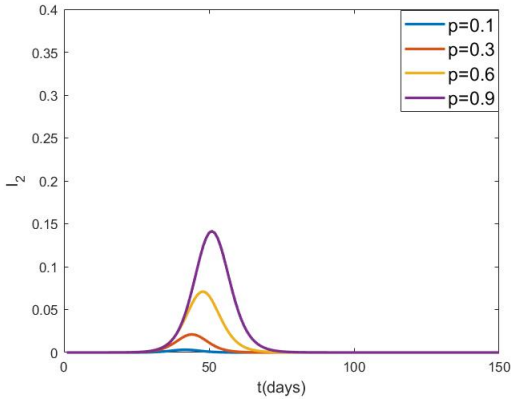

(b) The mean portion of individuals originally infected with the mutant strain throughout the epidemic for four different values of the cumulative within-host emergence probability p. For each value of p, the averages were taken over 100 simulations of our cross-scale model.

Fig. 4.15 The mean portions of individuals originally infected by the resident and mutant strains throughout the epidemic for four different values of the cumulative emergence probability p. The averages were calculated over 100 simulations of our cross-scale model for each value of p. All other values remained fixed at their reference values from tables 4.1 and 4.2 for all simulations, and we assumed that the mutant is neutral.

Figure 4.15 provides some insight into the effects of varying the cumulative within-host emergence probability p on the between-host disease dynamics. It is not surprising that as emergence becomes more probable the prevalence of the mutant strain at the population increases [plot(b)] and equivalently that of the resident strain decreases [plot (a)]. It is interesting that the larger values of p slightly shift the peak of the epidemic later. By peak here we refer to the maximum portion of individuals originally infected with either the resident or the mutant strain (as opposed to the maximum total portion of infected individuals between both strains). This small delay can be attributed to the increasing competition between the two strains at both the within-host and population levels as the cumulative within-host emergence probability of the mutant increases. More specifically, as p increases so does the probability of the mutant strain to emerge within-host at

every time-point of an individual's infection. As a result the mutant has better chances of emerging earlier during a host's infection and achieving larger viral loads. This in turn has a twofold impact: firstly it increases the mutant's chances of transmitting to new hosts due to our assumption that the population-level transmission rates are linear functions of the within-host viral loads, and secondly it hinders the within-host growth of the resident strain due to our assumption that cells can only be infected once and by a single strain. Therefore as the within-host cumulative emergence probability p increases we expect both the within-host viral loads and the population-level prevalence of the mutant strain to increase as well. This results in higher competition between the two strains for available cells at the within-host level and for available hosts at the between-host level, and therefore to the slower spread of the resident strain due to our full-cross immunity assumption. The result is the later epidemic peak that we observe in plot (a).

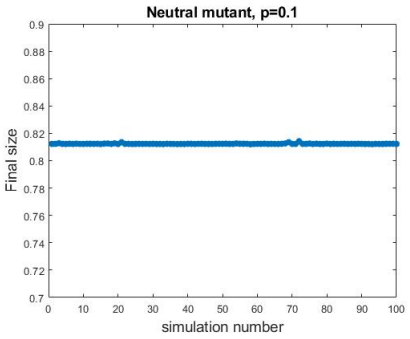

(a) A small within-host cumulative probability, specifically $p = 0.1$ here, has almost no effect on the epidemic final size over 100 distinct simulations of our cross-scale model. We note that the y-axis in plot (a), along with all other plots in this figure, ranges from 0.7 to 0.9

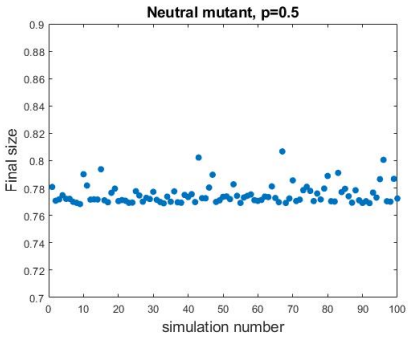

(b) A within-host cumulative probability $p = 0.5$ has a very small effect on the population-level final size.

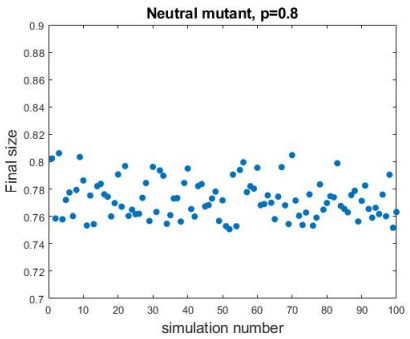

(c) A within-host cumulative probability $p = 0.5$ has a very small effect on the population-level final size, but larger that in the cases of $p = 0.1$ and $p = 0.5$.

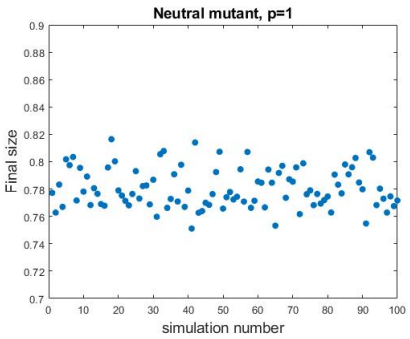

(d) A within-host cumulative probability $p = 0.5$ has a very small effect on the population-level final size, but once again larger that in the cases of $p = 0.1$ and $p = 0.5$.

Fig. 4.16 The epidemic final size in the case of a neutral mutant strain in 100 simulations of our model for four different values of the within-host cumulative emergence probability p under f_{const}. We note that the y-axis in each plot ranges from 0.7 to 0.9, which was done simply for illustration purposes. All other values remained fixed at their reference values from tables 4.1 and 4.2 for all simulations.

Figure 4.16 shows the final size of the epidemic in the case of a neutral mutant strain in 100 distinct simulations of our cross-scale model and for four different values of the within-host cumulative emergence probability p. Here we define the epidemic final size as the sum of the population-level final sizes of the resident and the mutant strains. We observe the following:

- For a very small value of p, specifically $p = 0.1$ in plot (a), there is almost no variability in the epidemic final size among different simulations. A very small p together with our assumption of a uniform distribution for emergence in this section implies that the mutant emerges only rarely within individuals infected with the resident, and even in the cases where it emerges it often does so too late in the infection to efficiently compete with the already circulating resident strain. As a result the resident's within-host growth is hardly impeded by the mutant, which in turn allows its between-host transmission rate to not be affected by the within-host emergence of the mutant. This can explain why in plot (a) we see almost no variability in the epidemic final size, as it is determined almost in its entirety by the spread of the resident strain.

- On the other hand the larger values of p we tested here (specifically $p = 0.8$ and $p = 1$) resulted in some slight variability in the epidemic final size, even though the mutant is assumed to be neutral. We underline though that the y-axis in all plots of figure 4.16 ranges only from 0.7 to 0.9. A larger p implies a higher chance for the neutral mutant to appear within-host early enough that it can compete with the resident for available target cells and grow. Given our assumption that the strain-specific between-host transmission rates are linear functions of the strain-specific within-host viral loads, the within-host spread of the neutral mutant will have a negative impact on the resident's population-level transmission rate. The magnitude of this impact is determined mainly by the within-host appearance time of the mutant, since as we demonstrated in chapter 3 an earlier appearance time implies a larger spread for the mutant and consequently a more inhibited growth for the resident. We may therefore attribute the simulations where the epidemic final size varied (and mostly decreased) in plots (b)-(d) to the neutral mutant growing within a large enough number of hosts originally infected with the resident so as to decrease the resident's between-host transmission rates, but still not growing efficiently enough that its population-level spread can offset the decrease in the epidemic final size that the slower spread of the resident alone would imply. We highlight that this decrease in the resident's transmission rates to new hosts would

still occur even when the neutral mutant only ever managed to attain a very small presence at the population or even if it never transmitted to a new host.

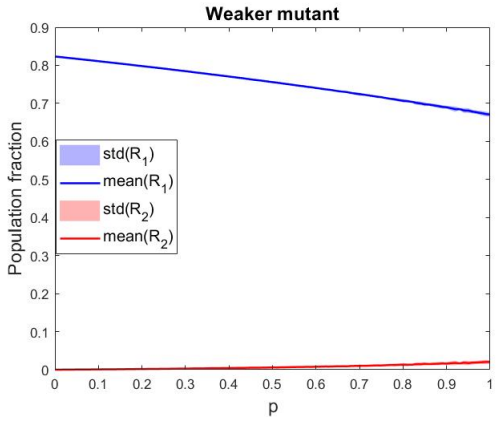

(a) The average final sizes of the resident and mutant strains as a function of the within-host cumulative emergence probability p. Here the mutation is deleterious.

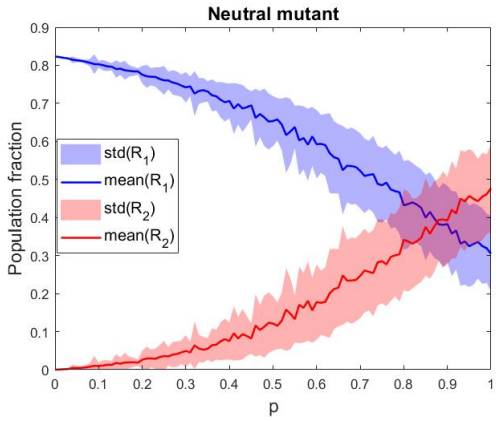

(b) The average final sizes of the resident and mutant strains as a function of the within-host cumulative emergence probability p. Here the mutation is neutral.

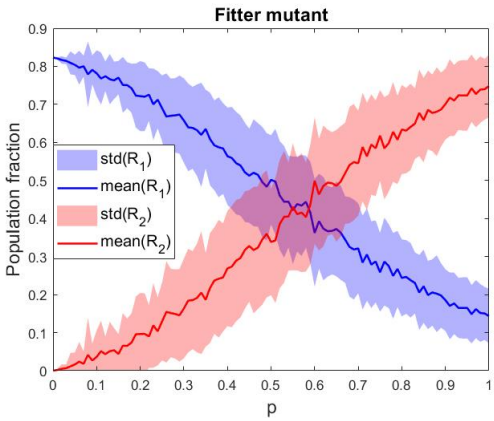

(c) The average final sizes of the resident and mutant strains as a function of the within-host cumulative emergence probability p. Here the mutation is beneficial.

Fig. 4.17 The effects of varying the within-host cumulative emergence probability p on the population-level mean final sizes of the resident and mutant strains in 100 simulations of our cross-scale model and for all three types of mutants. In all cases $\mathscr{R}_0^{r,p} = 2$, while $\mathscr{R}_0^{m,p} = 1.5$, 2 and 2.5 for a weaker, neutral and fitter mutant respectively.

Figure 4.17 illustrates the effects of varying the cumulative within-host emergence probability p on the population-level mean final sizes of the resident and mutant strains for all three types of mutation. For all three cases as the cumulative emergence probability increases so does the mean final size of the mutant strain. In the cases of a neutral and beneficial mutation there is a value of the cumulative emergence probability after which the mean final size of the mutant strain is larger than that of the resident. This happens despite the fact that in all our simulations the outbreak begins only with the resident strain present. It can be attributed though to our assumptions of no coinfection and full cross-immunity. In our model we allow two strains to co-circulate within a single

host only if the host was originally infected with the resident strain and then had the mutant emerge within them. Such a host may then transmit the mutant strain to other susceptible individuals, who will subsequently gain full immunity from the resident as well as the infecting mutant strain. As a result while both the mutant and the resident may only infect fully susceptible individuals at the point of transmission, the mutant has an advantage because it can emerge within several individuals who were originally infected with the resident strain. When the within-host emergence probability is high enough, plots (b) and (c) shows that this advantage can lead to the epidemic being taken over by the mutant strain.

4.6.5 Results using the Weibull distribution

In this section we will present the results of our cross-scale model using a Weibull probability density function for the within-host emergence of the mutant strain. This is because as we will show, a Weibull distribution appears to capture well the emergence dynamics that we expected our within-host model to produce.

The 2-parameter Weibull pdf is given by the following expression:

$$f_{WB}(\alpha) = p \times \frac{\zeta}{\eta}\left(\frac{\alpha}{\eta}\right)^{\zeta-1} e^{-(\alpha/\eta)^{\zeta}}$$

where η is a scale parameter, ζ a shape parameter and p is the cumulative within-host emergence probability of the mutant strain. For the remainder of this chapter we will assume that $\eta = 2$ and $\zeta = 2.5$ unless explicitly stated otherwise.

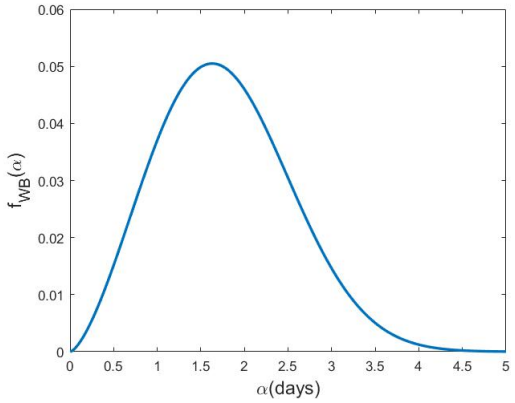

Fig. 4.18 The emergence density f_{WB} throughout the infection for $p = 0.1$.

Figure 4.18 shows how the Weibull within-host emergence density f_{WB} changes throughout an individual's infection. Our reasoning for choosing a Weibull distribution with these specific parameters is that the resulting pdf captures the emergence dynamics that we originally expected our within-host model to produce. We see that under f_{WB} emergence is more likely in the early stages of the infection and becomes very difficult after the third day of infection. This agrees well with the trajectories of the viral load, the eclipse cells and the target cells in our within-host model. Moreover we observe that the window of emergence under f_{WB} is much wider compared to the window of emergence under our within-host derived f_{WH}, which was only a single day. So now we would like to test how the results of our cross-scale model differ when the emergence density is given by a Weibull distribution with these specific shape and scale parameters that allow for such an emergence window.

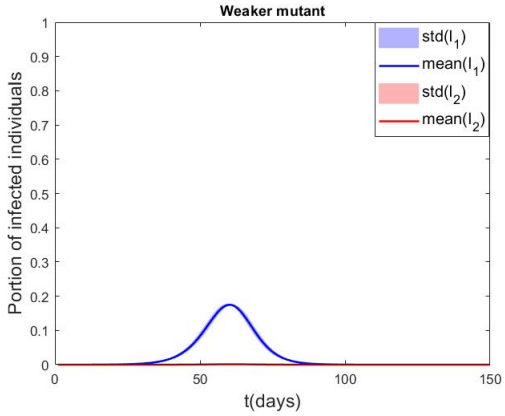

(a) The mean portions of individuals originally infected with the resident and mutant strains throughout the epidemic over 500 simulations of our cross-scale model.

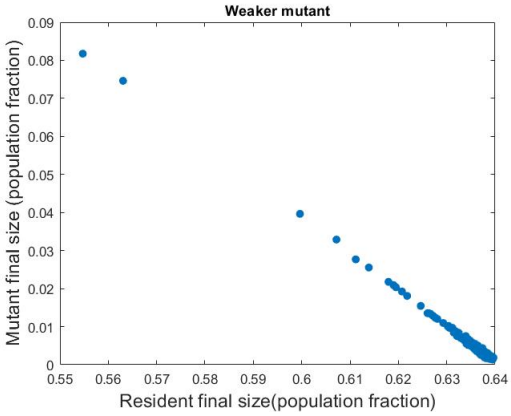

(b) The final sizes of the resident and mutant strains over 500 simulations of our cross-scale model.

Fig. 4.19 Some key results of our cross-scale model under the assumptions that the within-host emergence density is given by f_{WB} and the mutation is deleterious. We assume that the cumulative within-host emergence probability p is 0.73 to facilitate a comparison with our model's results under the within-host derived f_{WH} and the constant f_{const}.

Figure 4.19 shows some of our cross-scale model's results under the assumptions that the within-host emergence of the mutant strain follows a scaled Weibull distribution f_{WB}, the mutation is deleterious and the within-host cumulative emergence probability p is 0.73. We can make the following observations:

- The weaker mutant has a very low prevalence in the population [plot (a)]. This is in agreement with our cross-scale model's results under both the within-host derived f_{WH} and the constant f_{const}.
- The epidemic peak under the f_{WB} shifts earlier compared to f_{WH} [figure 4.10(a)]. The earlier peak under the scaled Weibull emergence density f_{WB} may be explained by the following reasoning: the larger within-host emergence window of f_{WB} allows for the emergence of the mutant later during a host's infection. In such a case the mutant is at a larger disadvantage compared to the resident and cannot grow its viral load as efficiently. As a result, the mutant has lower chances of transmitting to new hosts in the population and also has a smaller negative effect on the within-host viral load of the resident strain. Therefore, the larger emergence window of f_{WB} leads to lower competition between the two strains both at the within- and the between-host levels. The resident strain then can spread more rapidly in the population, leading to the observed earlier epidemic peak in plot (a).
- The epidemic peak under f_{WB} shifts later compared to f_{const} [figure 4.12(a)]. This can be explained by the exact same reasoning as the comparison between f_{WB} and

f_{WH}, since under the constant emergence density f_{const} the window of emergence spans the whole duration of the infection. We may conclude then that between the three forms of the within-host emergence density that we investigated in this chapter, in the case of a deleterious mutation a larger emergence window facilitates the faster spread of the resident strain both within-host and in the population.

- Plot (b) shows that the weaker mutant appeared at the population in all of our simulations, but only reached small final sizes. Despite the large within-host cumulative emergence probability of the mutant ($p = 0.73$), this is not surprising given the fitness disadvantage it has compared to the resident strain. The results illustrated in plot (b) are in agreement with the equivalent results under the within-host derived f_{WB} [figure 4.11(a)] and the constant f_{const} [figure 4.12(a)].

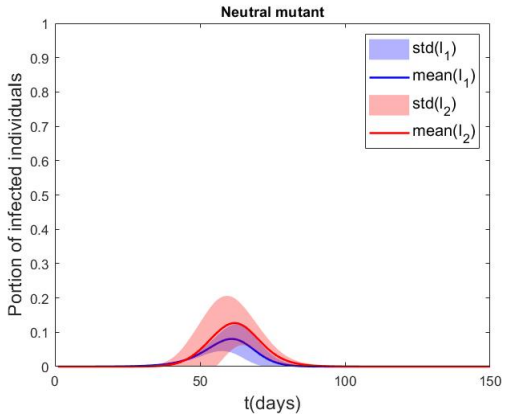

(a) The mean portions of individuals originally infected with the resident and mutant strains throughout the epidemic over 500 simulations of our cross-scale model.

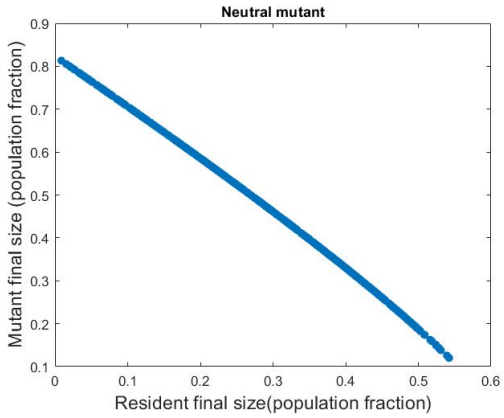

(b) The final sizes of the resident and mutant strains over 500 simulations of our cross-scale model.

Fig. 4.20 Some key results of our cross-scale model under the assumptions that the within-host emergence density is given by f_{WB} and the mutation is neutral. We assume that the cumulative within-host emergence probability p is 0.91.

Figure 4.20 shows some of our cross-scale model's results under the assumptions that the within-host emergence of the mutant strain follows a scaled Weibull distribution f_{WB}, the mutation is neutral and the within-host cumulative emergence probability p is 0.91. We may make the following observations:

- Plot (a) shows that the neutral mutant strain has on average a larger prevalence throughout the epidemic compared to the resident strain. A comparison between plot (a) and the equivalent plots under the within-host derived f_{WH} and the constant f_{const} shows that in the case of a neutral mutation a larger emergence window offers an advantage to the resident strain and facilitates its population-level spread,

resulting in an earlier epidemic peak. This is the same outcome as in the case of a deleterious mutation that we discussed in the previous figure and can be attributed to the same reasons.

- Plot (b) shows that the neutral mutant strain appeared in the population in all 500 simulations of our cross-scale model and often dominated the epidemic and achieved larger final sizes than the resident. This is in agreement with the equivalent results under f_{WH} and f_{const}.

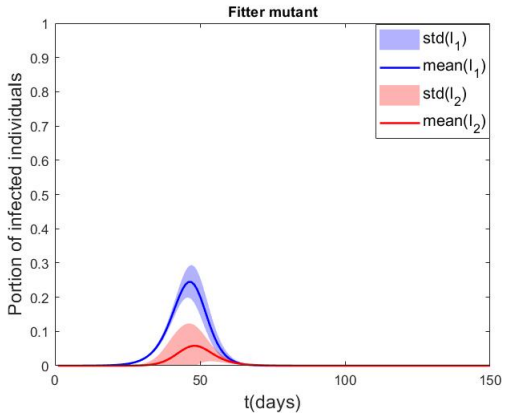

(a) The mean portions of individuals originally infected with the resident and mutant strains throughout the epidemic over 500 simulations of our cross-scale model.

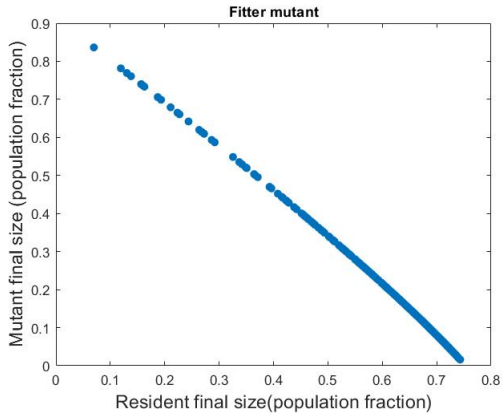

(b) The final sizes of the resident and mutant strains over 500 simulations of our cross-scale model.

Fig. 4.21 Some key results of our cross-scale model under the assumptions that the within-host emergence density is given by f_{WB} and the mutation is beneficial. We assume that the cumulative within-host emergence probability p is 0.34.

Figure 4.21 shows some of our cross-scale model's results under the assumptions that the within-host emergence of the mutant strain follows a scaled Weibull distribution f_{WB}, the mutation is beneficial and the within-host cumulative emergence probability p is 0.34. We may make the following observations:

- Plot (a) shows that the fitter mutant strain has an intermediate prevalence in the population despite its small within-host cumulative emergence probability. A comparison between plot (a) and the equivalent plot under f_{WH} [figure 4.10(c)] highlights the negative effects of the very small emergence chances during the first day of infection and of the strict emergence conditions under our within-host derived f_{WH} on the population-level spread of the mutant. We also observed this when we compared the between-host level prevalence of the fitter mutant strain under f_{WH} and f_{const}.

- Plot (b) shows that the fitter mutant strain appeared in the population in all 500 simulations of our cross-scale model and in a few cases even dominated the epidemic and achieved larger final sizes than the resident. This result is in agreement with the equivalent result under f_{const} [figure 4.14(b)] but is in contrast with the equivalent result under f_{WH} [figure 4.11(c)], where in the majority of our simulations the fitter mutant strain only achieved small final sizes.

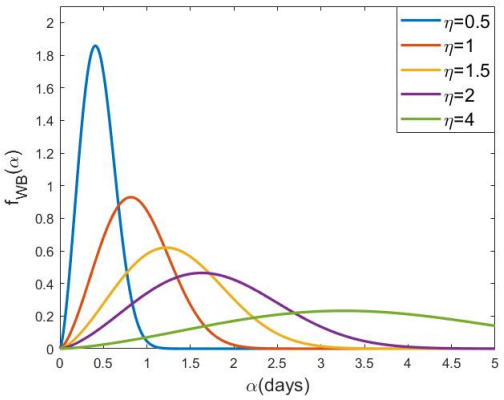

(a) The scaled Weibull distribution f_{WB} for five different values of the scale parameter η. Here $p = 0.91$. We observe that higher values of η lead to a wider emergence window for the mutant.

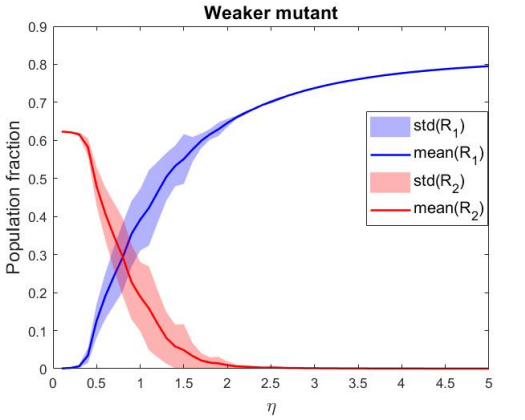

(b) The average final sizes of the resident and mutant strains as a function of η. Here the mutation is deleterious and the within-host cumulative emergence probability p is 0.73.

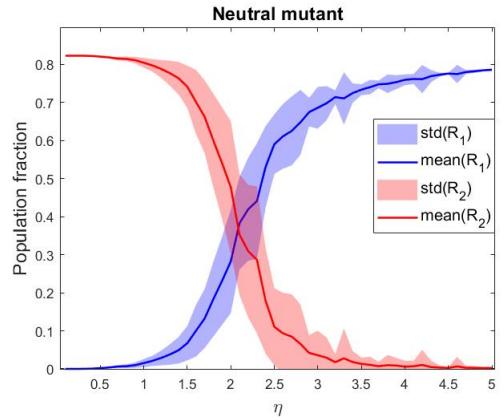

(c) The average final sizes of the resident and mutant strains as a function of η. Here the mutation is neutral $p = 0.91$.

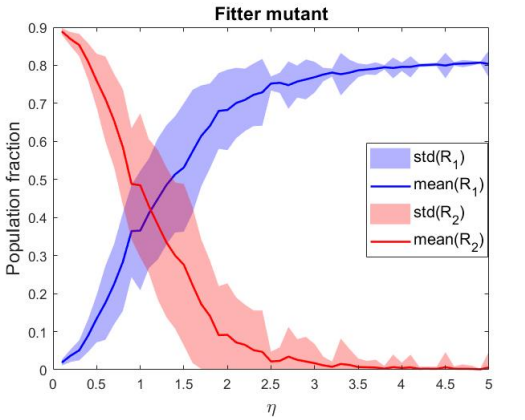

(d) The average final sizes of the resident and mutant strains as a function of η. Here the mutation is beneficial and $p = 0.34$.

Fig. 4.22 The effects of varying the Weibull scale parameter η from 0.1 to 5 on the population-level average final sizes of the resident and the mutant strains. In all plots the mean final sizes were calculated as the average of 100 simulations of our cross-scale model for each value of η. All other parameters remained fixed at their reference values from tables 4.1 and 4.2.

Figure 4.22 illustrates the effects of varying the Weibull scale parameter η on the population-level mean final sizes of the resident and the mutant strains for all three cases of mutant fitness. From plot (a) we can see that varying η may also be thought of as varying the width of the possible emergence window while keeping the cumulative emergence probability constant. For all three types of mutation a short emergence window early in

the infection appears to be more beneficial than a wider window. This can be attributed to the fact that a mutant which arises early in the infection when there is already a resident strain circulating within the host has more resources still available to it compared to a mutant which arises at a later time. This allows for more efficient viral growth within-host and therefore leads to a better chance of being transmitted to new hosts. It is interesting that for very small η, which translates to a very short emergence window very early in the infection, even a weaker mutant can end up taking over the epidemic as plot (a) illustrates. We note that under the within-host derived f_{WH} and the constant emergence density f_{const} the weaker mutant never achieved a higher population-level final size than the resident, despite its high cumulative within-host emergence probability of 0.73. This hightlights the significant advantage of a short and early emergence window, as it allows for more efficient within-host viral growth and therefore better chances of transmission to new hosts.

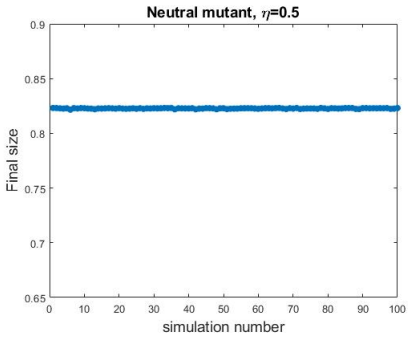

(a) The small value of $\eta = 0.5$ appears to have almost no effect on the variability of the epidemic final size in 100 distinct simulations of our cross-scale model. We note that the y-axis ranges from 0.65 to 0.9 in plots (a)-(d), which was done purely for illustration purposes.

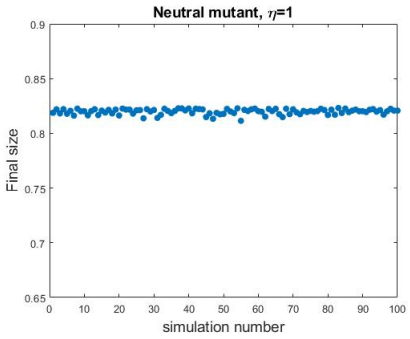

(b) The value of $\eta = 1$ appears to have very little on the variability of the epidemic final size in 100 distinct simulations of our cross-scale model.

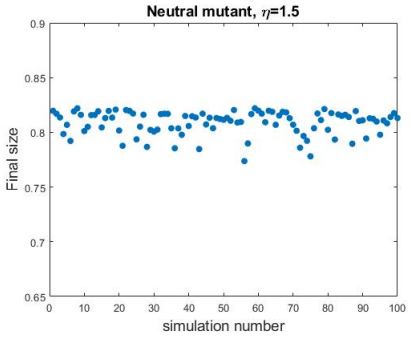

(c) The value of $\eta = 1.5$ appears to have a more prominent effect on the variability of the epidemic final size than the values of $\eta = 0.5$ and $\eta = 1$.

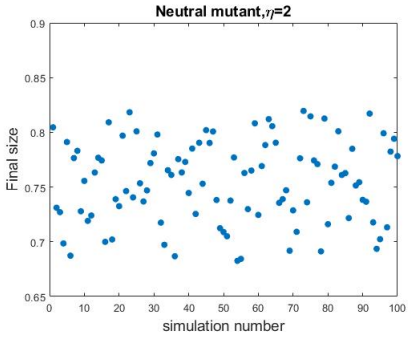

(d) The value of $\eta = 2$ appears to have a more significant effect on the variability of the epidemic final size compared to the values tests in plots (a)-(c), though we highlight that the range still remains between 0.66 and 0.82

Fig. 4.23 The epidemic final size in 100 distinct simulations of our cross scale model for four values of the Weibull scale parameter η and under the assumption of a neutral mutation. The cumulative within-host probability p of the neutral mutant is 0.91. All other parameters remained fixed at their reference values from tables 4.1 and 4.2. We note that the y-axis in all plots ranges from 0.65 to 0.9 for illustration purposes.

Figure 4.23 shows how the epidemic final size varies in 100 distinct simulations of our cross-scale model for four different values of the Weibull scale parameter η, assuming the mutation is neutral. The within-host cumulative emergence probability p here is 0.91 so as to remain consistent with our findings in section 4.6.3. We note that the y-axis in all plots of figure 4.23 ranges from 0.65 to 0.9 for illustration purposes. Plot (a) of figure 4.22 illustrated how the Weibull distribution changes for the same values of the scale parameter η studied here. We observe that for these four values of η, the variability in the final size of the epidemic increases as the value of η increases. We considered the reference value of our Weibull scale parameter to be $\eta = 2$ in this section, which corresponds to plot (d) here. It is then interesting to try and understand why smaller values of η lead to smaller variability in the epidemic final size.

- When $\eta = 0.5$ the window of emergence is very narrow and occurs very early in the infection. This, combined with the high cumulative within-host emergence probability of $p = 0.91$ for the neutral mutant, implies that the mutant emerges very often within hosts originally infected with the resident and it emerges early enough in the infection that it can grow efficiently and transmit to new hosts. Therefore the reduction in the transmission rate of the resident strain to new hosts due to the within-host competition with the neutral is accompanied in this case by the efficient transmission of the mutant to new hosts. Even though within-host the resident has a competitive advantage over the mutant since we do not allow the time of emergence to be $\alpha = 0$, our assumption of total cross immunity gives the mutant a competitive advantage at the population-level. This is because any host originally infected with the mutant is completely immune to the resident, while any host originally infected with the resident may have the mutant emerge within them and then transmit both strains to new hosts. Therefore, the case of $\eta = 0.5$ describes an epidemic where the mutant strain emerges within the majority of hosts infected with the resident, and it emerges early enough in the infection that it can efficiently transmit to new hosts and then spread in the population, thereby contributing significantly to the epidemic final size.

- As η increases in plots (b)-(d) (while p remains constant at 0.91), the window of emergence becomes wider and the chances of the mutant appearing at some later time in the infection where it cannot efficiently grow and then transmit to new hosts increase as well. We emphasize that even in such cases the mutant can still compete with the resident within-host, and therefore reduce the resident's between-host transmission rates. Therefore, the variability in the epidemic final

size which is especially apparent in plots (c) and (d) may be explained by the variability in the mutant's within-host emergence time, where in some cases the mutant emerges early enough within-host that it can grow efficiently and infect new hosts (thereby contributing efficiently to the epidemic final size) while in others the mutant can only have a negative impact on the resident's transmission rate to new hosts but cannot efficiently spread in the population.

4.7 Discussion

In this chapter we developed a two-strain cross-scale model for the epidemiological and evolutionary dynamics of influenza that explicitly links the within- and between-host scales. The links were the population-level transmission rates of two strains, which we assumed are linear functions of each strain's within-host viral load. One of our main goals was to investigate the emergence and subsequent competition dynamics between a mutant strain and its parent resident strain both at the between- and within-host scales. We first studied the results of our cross-scale model using the within-host emergence density that we originally derived from our within-host model in section 3.5.1, which imposes a very narrow window of emergence early in the infection. Our analysis showed that under these conditions a neutral mutant strain has the best chances of emerging within-host and subsequently spreading in the population. On the contrary a weaker mutant strain had a significant fitness disadvantage which limited its spread at both scales due to the competition with the resident, while a fitter mutant strain had a very low prevalence in the population because of its significantly smaller within-host cumulative emergence probability and its slightly later emergence window (in comparison to the neutral and weaker strains). In order to test the sensitivity of our model's results, we then repeated the analysis of our cross-scale model first by assuming that the within-host emergence density remains constant throughout an individual's infection and then by assuming that it follows a scaled Weibull distribution. Our results highlighted the importance of the within-host emergence window for the population-level spread of the mutant, as extending the width of the emergence window while keeping the within-host cumulative emergence probability fixed had a negative effect on the between-host final size of the mutant strain in all cases. On the contrary, our analysis showed that a very narrow emergence window early in the infection provides the best opportunity for the mutant to emerge and grow within-host and then spread in the population.

One of the most important assumptions of our cross-scale model is that the between-host transmission rates are linear functions of the within-host viral load. Considering that these transmission rates provide the explicit link between the two tiers of our model, we need to carefully consider the multi-faceted impact of this assumption. In a paper published in 2019, Almocera and Hernandez-Vargas report that an acceptable form for the population transmission rate as a function of the within-host viral load is still open to discussion due to insufficient empirical data [7]. We will expand on this in the next paragraph by first discussing some papers that assumed a linear relation between host infectiousness and viral load, then by presenting a paper which assumed a logarithmic relation and finally by discussing a paper that compared several approaches.

In 2009 Chen *et al*. published a paper in which they investigated the effects of within-host viral kinetics and exhaled droplet size on the indoor transmission of influenza [63]. Using empirical data on the amount of a host's exhaled virus-carrying bioaerosol droplets per time, the authors found that a linear dependence on the within-host viral load captured the dataset well. As they pointed out though, their results are difficult to validate due to the scarcity of experimental data on the amount of exhaled virus-carrying droplets in indoor environments. A similar breath plume model published by Halloran *et al*. in 2012 also found that a linear relation between the viral load and the concentration of exhaled pathogens per unit volume of air could capture well a different empirical dataset [134]. In 2007 Handel *et al*. published a paper in which they investigated the generation and spread of neuraminidase inhibitor (NI) resistance in influenza [140]. Part of their modelling framework included developing a function for the amount of viral shedding that depended on the within-host viral load. The authors used viral load and nasal discharge weight data from previously published volunteer studies and found that a sigmoid relation between viral shedding and the logarithm of the viral load provided the best fit. To connect this with infectiousness, the authors then assumed a direct proportionality relation between the total amount of shedding and the basic reproduction number $\mathscr{R}_0$. Finally, Tsang *et al*. published a paper in 2015 in which they mapped influenza A viral shedding to infectiousness in households [294]. The authors studied four different models based on the assumed relation between viral shedding and infectivity: infectivity being proportional to the viral load V, to $\log(V)$ and to a power of these variables. Their results showed that the model which assumed that infectivity was proportional to the viral load V gave the worst fit to the household data because it led to most transmission occurring very early in the infection. The rest of the models resulted in better fits, but still overestimated the proportion of transmission occurring more than three days since

symptom onset. Our main conclusion after reviewing these published studies is that there is not enough empirical data to inform the exact nature of the relationship between the within-host viral load and the population-level transmission rate of influenza. Therefore an important future research project would be to repeat the analysis of our cross-scale model assuming different functional relations between the population-level transmission rates and the within-host viral load.

The analysis of our model highlights the significant advantage of cross-scale models to allow for the direct comparison of competing selection pressures from different scales. In section 4.6.3 we demonstrated that even a fitter mutant strain may fail to spread in the population if it consistently emerges during a time in a host's infection that it can survive and grow but still has relatively limited resources available to it. More specifically, under our within-host derived emergence density f_{WH} we showed that the fitter mutant strain is expected to emerge most often very close to its emergence cut-off value. As a result its pool of available target and prerefractory cells is limited due to depletion by the already circulating resident strain. This inhibits the within-host growth of the fitter mutant and has a large negative impact on its transmission to new hosts, even despite the mutant's fitness advantage.

Special consideration needs to be given to the case of a neutral mutant strain. Even though a neutral strain is characterized in our cross-scale model by the same values for the strain-specific within-host parameters as the resident, the two strains are not structurally indistinguishable. We may attribute this to the combined effect of some key assumptions of our model. The first is the total cross-immunity assumption, which dictates that an individual infected with either strain gains full immunity not only to the infecting strain but to the other one as well. As a result, individuals originally infected with the mutant strain have complete protection against the resident strain. But we further assume that any individual originally infected with the resident strain might have the mutant strain emerge within them, making it possible for the host to then transmit either strain to new hosts. We note that in the implementation of our model the decision of which strain is transmitted at every transmission event is made stochastically, with a probability based on the viral loads of the two strains at the time of transmission. We further emphasize that when the mutant strain emerges within-host it competes with the resident for target and prerefractory cells, which has a negative effect on the growth of the resident within-host and in turn on its between-host transmission (since we assume

that the strain-specific between-host transmission rates are linear functions of the strain-specific within-host viral load). Therefore by construction of our model we can make the following observations:

- The mutant strain has an advantage over the resident because it may emerge within individuals originally infected with the resident, while individuals originally infected with the mutant have total immunity to the resident strain.
- The emergence of a mutant strain within a host infected with the resident can slow down the within-host growth of the resident and therefore decrease its transmission rate to new hosts. This is independent of whether the mutant successfully transmits to new hosts. The asymmetry between the neutral mutant and its parent resident strain then also lies in the fact that in a host originally infected with the mutant strain, the transmission rate to new cases with the mutant cannot be affected in any way by within-host processes involving the resident strain.

These observations together lead to a problematic scenario in the case of a neutral mutant strain, which could be the result of a silent mutation and biologically indistinguishable from the parent resident. In that case we would expect the strains to be competitively neutral, and the existence of the neutral mutant to have no impact on the epidemic final size. But in figures 4.16 and 4.23 we have shown that a neutral mutant can indeed have an effect on the final size of the epidemic. The conditions we have identified for such an outcome are that the within-host cumulative emergence probability should be high enough that the neutral mutant emerges within a large portion of the hosts infected with the resident, and that the mutant should arise late enough in the infection that it cannot grow and spread to new hosts efficiently. The mere presence of the mutant within-host though will still have a negative impact on the resident's transmission to new hosts due to the within-host competition of the two strains for available target and prerefractory cells. Therefore these conditions create an epidemic where the mutant emerges within many hosts, fails to have a significant presence at the population-level (and therefore fails to contribute efficiently to the epidemic final size) but still slows down the transmission of the resident strain to new hosts. In contrast, the situations we identified where the neutral mutant has no effect on the epidemic final size can be divided into two different cases. Firstly, under the assumption of a small within-host cumulative probability and a uniform emergence distribution the mutant emerges very rarely within infected hosts and when it does, there is a significant chance that it appears too late in the infection to compete efficiently with the resident at either the within- or between-host levels. The result is an epidemic that is dominated by the resident strain, therefore it is not surprising that the

epidemic final size would not be affected by the neutral mutant. The second case is when the within-host cumulative probability is so high that the mutant emerges very often, and the emergence window is narrow and occurs early in the infection. Under these conditions the mutant emerges in the majority of hosts infected with the resident and it emerges early enough in the infection that it can spread efficiently both at the within- and the between-host levels. The result is an epidemic where both strains contribute significantly to the final size and the neutral mutant has almost no effect on the overall dynamics. While this analysis may explain why a neutral mutant can sometimes have an effect on the epidemic final size, it still does not resolve the pathological outcome that two biologically indistinguishable strains are not structurally indistinguishable in our mutation model. We have already argued that this is an inherent issue with our model by its construction, but it is important to understand then to what extent it might invalidate our conclusions. We refer to a 2009 paper published by Lipsitch *et al*. [193] where the authors introduced the concept of "neutral null models", which are transmission models of strain coexistence that meet the following two criteria when applied to functionally indistinguishable strains: ecological dynamics should be independent of strain identities and there should be no stable equilibrium frequency of the strains. The authors mention that models which meet their null neutrality criteria cannot include mutation. They also repeatedly emphasize though that there is nothing intrinsically wrong with non-neutral null models, rather such models should simply be cautious when identifying mechanisms that promote stable coexistence. With this in mind then we posit that the structural asymmetry between the resident and the neutral mutant in our cross-scale model does not invalidate our conclusions (especially since they are not quantitative) but rather makes it crucial to identify the mechanisms by which this asymmetry affects our model's results, as we have done in the analyses of figures 4.16 and 4.23. We note that some ways we could alter or extend our cross-scale model specifically to counteract the effects of the structural asymmetry between the resident and mutant strains (of any fitness level) are:

- To increase the transmission bottleneck to include up to two strains. This would lead to fewer cases where a mutant emerges within a host and fails to transmit to new hosts but is still negatively affecting the between-host transmission rate of the resident.
- To allow for backwards mutation. This would imply that individuals originally infected with the mutant strain may have the resident strain emerge within them, thereby negating the competition advantage that the mutant strain has in our current model with total cross-immunity.

4.8 Summary

In this chapter we developed a cross-scale model to describe the epidemiological and evolutionary dynamics of influenza within a single season. Our model takes explicitly into account processes that occur at the within-host level. The main links between the within-host and population-level tiers of our cross-scale model are the between-host transmission rates, which we assumed are linear functions of the within-host viral load. We studied our model's results under different forms for the within-host emergence density of the mutant strain and showed that given a fixed within-host cumulative emergence probability, a narrower emergence window earlier in the infection is the most beneficial for the spread of a mutant strain both within-host and in the population.

Chapter 5

A cross-scale vaccination model for the evolution of influenza

5.1 Introduction

In this chapter we develop a cross-scale vaccination model to describe the epidemiological and evolutionary dynamics of influenza within a single season. Our model takes explicitly into account dynamical processes that occur at the within-host level. The main links between the two scales are the between-host transmission rates, which we assume are linear functions of the within-host viral load. The effects of vaccination are captured as an increase in the within-host viral clearance rates and affect the transmissibility of the virus to new hosts. We will first examine the results of our cross-scale vaccination model under the within-host derived emergence density that we formulated in section 3.5.1. In order to test the sensitivity of our results, we will then repeat our analysis using two different functional forms for the within-host emergence density. One of our main goals is to compare the results of our cross-scale vaccination model with those of our population-level vaccination model from chapter 2 in order to gain a better understanding of the advantages, disadvantages and potential necessity of explicitly linking the scales when studying the spread and evolution of influenza in a single season.

5.2 Background

We will base our cross-scale vaccination model on the *Coombs model*, which was published by Coombs *et al*. in 2007 [68] and which we have already discussed in chapter 4. Since our cross-scale model requires input from a dynamical within-host model, we will pair it with our extension of the *Saenz model* that includes vaccination. We originally discussed and analyzed this model in 3.6.1. It is defined by the same of ODEs that define our extended *Saenz* model, and vaccination is incorporated simply as an increase in the clearance rate of the virus (c_1 or c_2 in our notation) in vaccinated individuals. Therefore by construction vaccination reduces only the transmissibility of the infection but has no impact on the susceptibility of vaccinated individuals. A vaccine that targets the resident strain increases c_1 from its reference value. The higher the increase, the more efficient the vaccine is against the resident. The equivalent holds for a vaccine that targets only the mutant or both strains.

We note that since we will need to refer to vaccinated individuals both at the within- and between-host scales, we will slightly change the notation of our extended *Saenz* model where V_i used to denote the within-host viral load of the ith strain. Instead we will use the following notation:

- S: the class of fully-susceptible individuals at the between-host level
- V: the class of vaccinated individuals at the between-host level
- $\bar{V}_i^S$: the within-host viral load of the ith strain in an individual who used to be fully susceptible and then became infected
- $\bar{V}_i^V$: the within-host viral load of the ith strain in an individual who was vaccinated but became infected

5.3 Model Presentation

We will now present our cross-scale vaccination model for the epidemiological and evolutionary dynamics of influenza within a single season. We will first motivate our model and then present the equations that define it.

Given the way in which we incorporated vaccination to our within-host model, our cross-scale model assumes by construction that vaccination reduces infectiousness. This stems from our assumption that vaccination increases the within-host viral clearance rate, which leads to smaller viral loads throughout an individual's infection. This in turn leads to lower infectiousness due to our assumption that the population transmission rates depend linearly on the within-host viral load. We will discuss this effect of the within-host viral clearance rates on the population transmission rates in more detail in section 5.7.1 of this chapter. To capture the population heterogeneity due to vaccination status, we have the following definitions:

- β_{ij}^S : the transmission rate from an individual who used to be fully susceptible and became infected with strain i to new cases with strain j, where $i, j \in 1, 2$. We note that this is a function of the age of infection a and the within-host emergence time α, but we omit writing this explicitly for now.
- β_{ij}^V : the transmission rate from an individual who was vaccinated and became infected with strain i to new cases with strain j, where $i, j \in 1, 2$.
- I_1^S : the class of individuals who used to be fully susceptible and then became infected with the resident strain (strain 1). We note that hosts in this class might have the mutant strain (strain 2) emerge within them, which would result in two strains circulating within them.
- I_1^V : the class of individuals who were vaccinated and then became infected with the resident strain. We note again that hosts in this class might have the mutant strain emerge within them.
- I_2^S : the class of individuals who used to be fully susceptible and then became infected with the mutant strain. We note that hosts in this class can only have the mutant strain circulating within them, because we do not allow for backwards mutation in our model (mutation from strain 2 back to strain 1).
- I_2^V : the class of individuals who were vaccinated and then became infected with the mutant strain. We note again that hosts in this class can only have the mutant strain circulating within them.

The key difference between these four infected classes as far as vaccination is concerned is that the previously fully susceptible individuals in I_1^S and I_2^S will transmit the virus at

a rate β_{1j}^S and β_{2j}^S respectively, while the infected individuals in I_1^V and I_2^V who have received the vaccine will transmit the virus at a rate β_{1j}^V and β_{2j}^V respectively, where $j \in 1,2$.

We make some final observations before we present our cross-scale vaccination model:

- Fully susceptible and healthy vaccinated individuals are available to both the resident and mutant strains for infection.
- Vaccinated individuals may be either healthy, in which case they are in the V compartment, or infected, in which case they can be in the I_1^V or I_2^V compartments.
- A fully-susceptible individual can enter the I_1^S compartment by being infected with the resident strain either by a previously fully susceptible individual already in I_1^S at a rate β_{11}^S or by a vaccinated infected individual in I_1^V at a rate β_{11}^V. The same holds with regards to how a healthy vaccinated individual can enter the I_1^V compartment.
- A fully-susceptible individual can enter the I_2^S compartment via four different ways. The first is due to infection with the mutant strain by a previously fully susceptible individual currently in I_1^S who was originally infected with the resident strain but then had the mutant emerge within them and is now transmitting both strains. This occurs at a rate β_{12}^S. The second way is equivalent to the first but assumes instead that the infecting individual is vaccinated and currently in I_1^V and is transmitting the mutant at a rate β_{12}^V. The third way is due to infection with the mutant strain by a previously fully susceptible individual currently in I_2^S who was infected with the mutant strain and is now transmitting it at a rate β_{22}^S. Finally the fourth way is the same as the third but instead assumes that the infecting individual is vaccinated and currently in I_2^V and is transmitting the mutant at a rate β_{22}^V. The equivalent four ways also hold with regards to how a healthy vaccinated individual can enter the I_2^V compartment. These infection pathways are illustrated in figure 5.1.

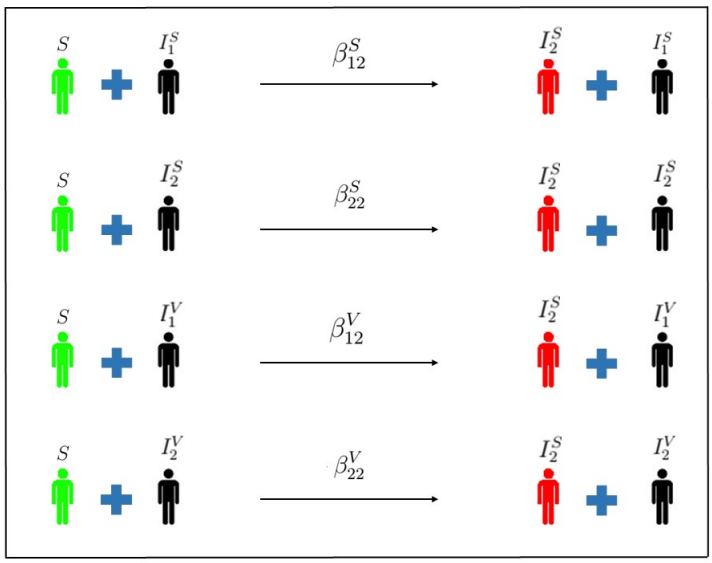

Fig. 5.1 The different ways in which a fully susceptible individual can become infected with the mutant strain in our cross-scale vaccination model.

We define the force of infection of the resident strain as:

$$\Lambda_1(t) = \int_0^\infty \left[\beta_{11}^S(a) I_1^S(t-a,0) + \beta_{11}^V(a) I_1^V(t-a,0)\right] da \tag{5.1}$$

Similarly we define the force of infection of the mutant strain as:

$$\Lambda_2(t) = \int_0^\infty \Big\{ \left[\beta_{12}^S(a) I_1^S(t-a,0) + \beta_{22}^S(a) I_2^S(t-a,0)\right] + \left[\beta_{12}^V(a) I_1^V(t-a,0) + \beta_{22}^V(a) I_2^V(t-a,0)\right] \Big\} da \tag{5.2}$$

We will now present the equations of our cross-scale vaccination model in the case of only two strains, a resident (strain 1) and a mutant (strain 2):

$$\frac{dS}{dt} = -S(\Lambda_1 + \Lambda_2) \tag{5.3}$$

$$\frac{dV}{dt} = -V(\Lambda_1 + \Lambda_2) \tag{5.4}$$

$$kI_1^S(t,0) = S\Lambda_1 \tag{5.5}$$

$$kI_2^S(t,0) = S\Lambda_2 \tag{5.6}$$

$$kI_1^V(t,0) = V\Lambda_1 \tag{5.7}$$

$$kI_2^V(t,0) = V\Lambda_2 \tag{5.8}$$

where:

- $S(t)$ denotes the number of susceptible individuals at time t of the epidemic.
- $V(t)$ denotes the number of susceptible individuals at time t of the epidemic.
- $I_i^S(t-a,0)$ represents the density (in a) of previously fully-susceptible individuals who became infected with strain i at time $t-a$.
- $I_i^V(t-a,0)$ represents the density (in a) of vaccinated individuals who became infected with strain i at time $t-a$.
- The constant k is such that $da = kdt$. This accounts for the fact that $I_i^S(t,a)$ and $I_i^V(t,a)$ are densities in a whereas the right hand side of equations (5.5)-(5.8) are numbers.

- The parameter $\beta_{ij}^{S}(a)$ is the transmission rate from previously fully-susceptible individuals who were infected with the ith strain a time units ago to new infections with strain j.
- The parameter $\beta_{ij}^{V}(a)$ is the transmission rate from vaccinated individuals who were infected with the ith strain a time units ago to new infections with strain j.

Equation (5.3) is an integro-differential equation that describes how the number of fully-susceptible individuals in the population varies over time. It needs to account for the new infections generated by both vaccinated as well as previously fully-susceptible hosts of all possible infection ages $a \in [0, \infty)$ who were initially infected with the ith strain and are now infecting new cases with the jth strain, where $i, j \in 1, 2$. The equivalent holds for equation (5.4), which describes how the number of uninfected vaccinated individuals varies over time. Equations (5.5)-(5.8) are renewal conditions which describe how new infected cases of the jth strain are generated. They take into account the contact of both fully-susceptible as well as healthy vaccinated individuals with infected hosts of all possible infection ages and vaccination statuses who were initially infected with either strain, but are now transmitting specifically the jth strain.

It is important to emphasize that while equations (5.3)-(5.8) describe the population disease dynamics, they depend on the viral dynamics within infected hosts via the transmission rates $\beta_{ij}^{S}(a)$ and $\beta_{ij}^{V}(a)$. More specifically, we assume that the transmission rates are linear functions of the within-host viral load. We will discuss this in more detail in the next section, in which we will go over our model's assumptions. Since our cross-scale model requires an explicit within-host dynamical model, we pair it with our extended *Saenz* vaccination model from 3.6.1.

5.4 Model Assumptions

We will now discuss all the assumptions of our cross-scale vaccination model, and for each one we will specify whether it originated from published work or if it is our own addition.

Assumptions taken from Saenz *et al*. [262]:

- On a cellular level infection always leads to death.
- Refractory cells are completely immune to infection. Once a cell becomes refractory it remains in this antiviral state for the duration of the infection.

Assumptions taken from Coombs *et al*. [68]:

- Cells can be infected only by a single strain. We note that this combined with the Saenz assumption that infection always results in the death of the infected cell means that target cells can only be infected once.
- The competition between the two strains is mediated purely through the availability of resources such as the target and prerefractory cells within-host and the susceptible individuals at the population-level.
- The population transmission rates depend linearly on the viral load of the host. Specifically

$$\beta_{ij}(a) = b\bar{V}_j(a)$$

where b is a scaling constant, and $i, j \in \{1,2\}$. We adapt this assumption to our model, in which we have different transmission rates for vaccinated and unvaccinated individuals. So we set

$$\beta_{ij}^S(a,\alpha) = b\bar{V}_j^S(a,\alpha) \tag{5.9}$$

$$\beta_{ij}^V(a,\alpha) = b\bar{V}_j^V(a,\alpha) \tag{5.10}$$

where $\bar{V}^S$ denotes the viral load of an infected individual who used to be fully susceptible, $\bar{V}^V$ that of a vaccinated individual who became infected, b is a scaling constant, a denotes the age of infection and α is the within-host emergence time of the mutant strain. As we have previously demonstrated with the analysis of our within-host model in chapter 3, the emergence time a has a significant impact on the viral load of both strains. As a result α also has an effect on the population transmission rates, given our definition of β^S and β^V in equations (5.9) and (5.10). This linear dependence of the between-host transmission rates on the within-host

viral load is a key assumption of our cross-scale vaccination model. We note that we used the same assumption for our cross-scale model in chapter 4, and we discussed its significance and implications in the Discussion section of that chapter.

Our own additional assumptions:

- Backwards mutation (from the mutant to the resident strain) is not possible. Therefore $\beta_{21}(a, \alpha) = 0 \; \forall a, \alpha$.
- Vaccination acts within-host by increasing the viral clearance rate(s). As we assume that the vaccine is homologous to the resident strain, vaccination mainly acts by increasing c_1. We emphasize though that the vaccine can still have an impact on the mutant too, so we will also investigate the effects of varying c_2. In section 3.6.1 we discussed that our decision to incorporate vaccination in such a simplistic way was motivated by the complicated nature and computational challenges of cross-scale models. Moreover, using the results of our extended *Saenz* model's parameter sensitivity analysis, we showed that our decision to use c_i instead of another within-host strain-specific parameter should not affect our model's results in any fundamental way.
- On a population level infection leads to recovery. This is a simplifying assumption, but applicable to seasonal influenza. It is why there is no disease-related mortality rate in our model, as opposed to the *Coombs model* from [68] which focuses primarily on HIV.
- Each individual can be initially infected by exactly one strain. No co-infection can occur. The only case where more than one strains may co-circulate within a single host is if the host was initially infected with the resident strain and then had the mutant strain emerge during their infection.
- Vaccination occurs only prior to the onset of the outbreak. Once the epidemic starts no further vaccination may take place. This is merely a simplifying assumption.

5.5 Basic Properties

The population-level basic reproduction number $\mathscr{R}_0^{r,p}$ of the resident strain in our cross-scale model can be expressed as:

$$\mathscr{R}_0^{r,p} = \int_0^{D^{wh}} \beta_{11}^S(a)da \tag{5.11}$$

where $\beta_{11}^S(a)$ is the rate at which previously fully-susceptible individuals who were initially infected with the resident strain a time units ago and never had the mutant strain emerge within them infect new individuals. Here D^{wh} denotes the duration of the infection. Similarly, we may express the population-level basic reproduction number of the mutant strain as:

$$\mathscr{R}_0^{m,p} = \int_0^{D^{wh}} \beta_{22}^S(a)da \tag{5.12}$$

Since in our model vaccination reduces infectiousness and introduces heterogeneity in the host population, it is important to also consider the control reproduction number of the disease $\mathscr{R}_c$ which is simply the reproduction number with control measures in place [296]. For the resident strain we can express:

$$\mathscr{R}_c^{r,p} = \left[S(0)\int_0^{D^{wh}} \beta_{11}^S(a)da\right] + \left[V(0)\int_0^{D^{wh}} \beta_{11}^V(a)da\right] \tag{5.13}$$

where $\beta_{11}^V(a)$ is the rate at which vaccinated individuals who were initially infected with the resident strain a time units ago and never had the mutant strain emerge within them infect new individuals. Here $S(0)$ and $V(0)$ denote respectively the initial portion of fully-susceptible and vaccinated individuals, and we have $S(0)+V(0) \approx 1$. We note that $V(0)$ is also the same as the vaccination coverage c in our model. Similarly the control reproduction number of the mutant strain is given by:

$$\mathscr{R}_c^{m,p} = \left[S(0)\int_0^{D^{wh}} \beta_{22}^S(a)da\right] + \left[V(0)\int_0^{D^{wh}} \beta_{22}^V(a)da\right] \tag{5.14}$$

As we mentioned in the previous section, we assume that infectiousness scales linearly with the viral load. More specifically we defined

$$\beta_{ij}^{S}(a,\alpha) = b\bar{V}_{j}^{S}(a,\alpha)$$

where $\bar{V}^{S}$ denotes the viral load of an infected individual who used to be fully susceptible, b is a scaling constant and $i,j \in \{1,2\}$. If we substitute this into equation (5.11) for the basic reproduction number of the resident strain and then solve for the scaling constant b we obtain

$$b = \frac{\mathscr{R}_{0}^{r,p}}{\int_{0}^{D^{wh}} \bar{V}_{1}^{S}(a,\emptyset)da} \tag{5.15}$$

where $\bar{V}_{1}^{S}(a,\emptyset)$ denotes the viral load of a previously fully-susceptible individual who was infected with the resident strain and never had the mutant strain emerge within them.

5.6 Methods

We are interested in studying the emergence dynamics of a mutant strain in the population, so we assume that initially there is only a resident strain causing the epidemic. We further assume that some portion of the population has been vaccinated against the resident strain prior to the onset of the outbreak. When an individual becomes infected with the resident strain we keep track of the age of their infection because variations in their within-host viral load will affect their population-level transmission rate. Similarly to the implementation of our within-host model from chapter 3, we assume that when an individual is infected with the resident strain there is a chance that errors will occur during the within-host viral replication process which will lead to the emergence of a mutant strain within that host. At the between-host level the consequence of this within-host emergence is that the host may transmit either the resident or the newly emerged mutant whenever they infect a new host, with a probability that depends on each strain's viral load at the time of transmission. This in turn can lead to two strains, a mutant and its parent resident, circulating in the population and competing for hosts either until the end of the epidemic or until one of them disappears.

Our model has the following initial conditions:

- $N = 1$ is the total size of our population and we assume it remains fixed throughout the outbreak.
- $c = V(0) = 0.63$ is the vaccination coverage. This matches the vaccination coverage of our population-only vaccination model from chapter 2. It was taken from a report published by Public Health England on the seasonal influenza vaccine uptake in GP patients from the winter season 2017 up to 2018 [240].
- $I_1^S(0) = 10^{-5}$ individuals.
- $I_1^V(0) = 0$.
- $I_2^S(0) = I_2^V(0) = 0$. This is because we assume that the outbreak is initiated only by the resident strain.
- $D^p = 150$ days. This is the duration of the outbreak, and we set it as 150 days to cover the main winter season of influenza in the Northern hemisphere, namely December-February, together with a month leading up to it and a month right after it.
- $D^{wh} = 5$ days. This is the duration of the infection within a host.
- $\mathscr{R}_0^{r,p} = 2$. This was chosen simply to satisfy reported values of the population-level $\mathscr{R}_0$ of influenza. More specifically Cauchemez *et al*. report in [55] that $\mathscr{R}_0$ ranges from 1.4 to 2.2.

Within-host model				
Parameter	**Description**	**Value**	**Units**	**Source**
β_i^{wh}	Infectivity rate of ith strain	1.4×10^{-4}	(RNA copies)$^{-1}$ ml NS day^{-1}	[262]
p_i	Virus production rate for ith strain	1.4×10^{-5}	RNA copies (ml NS)$^{-1}$ day^{-1} cell^{-1}	[262]
q_i	IFN production by cells in I_i	5×10^{-10}	IFN fold change day^{-1} cell^{-1}	[262]
c_i	Free virus clearance rate for ith strain	5.2	Rate of virus clearance day^{-1}	[262]
$\frac{1}{k_\alpha}$, $\frac{1}{k_\gamma}$	Average duration of eclipse phases	$1/2$	Days	[262]
ε	Mutation rate	1.08×10^{-10}	s/n/c	chosen by us
$1/a_w$	Average duration of prerefractory phase	$1/4$	Days	[262]
$1/\delta_1$	Average lifespan of cells infected with resident strain	$1/2$	Days	[262]
$1/\delta_2$	Average lifespan of cells infected with mutant strain	Varies	Days	
d	IFN clearance	6.8	Rate of IFN clearance day^{-1}	[262]
ϕ	IFN efficiency	56	(IFN fold change)$^{-1}$ day^{-1}	[262]
m	IFN-reduced infectivity	0.9		
α	Time of emergence of mutant strain	Varies	Days	
D^{wh}	Infection duration	5	Days	

Table 5.1 Parameters of the within-host tier of our cross-scale vaccination model.

Between-host model				
Parameter	**Description**	**Value**	**Units**	**Source**
D^p	outbreak duration	150	days	
$\mathscr{R}_0^{r,p}$	resident basic reproduction number (population-level)	2		[55]
b	virus transmission scaling factor	1.63×10^{-11}		chosen to satisfy $\mathscr{R}_0^{r,p} = 2$
c	vaccination coverage	0.63		[240]

Table 5.2 Parameters of the between-host tier of our cross-scale vaccination model.

5.6.1 Implementation

The implementation of our cross-scale vaccination model is the same as the implementation of our cross-scale model, which we described in detail in section 4.5.1, with the only difference being that we now need to account for vaccinated individuals. This is the

pseudocode for our cross-scale vaccination model:

Algorithm 2: Pseudocode for cross-scale vaccination model

Initialization : c, da, $dt > da$, D^p, D^{wh}, $P^S(a)$,$P^V(a)$ ...

for $time = da : da : D^p$ **do**

day= $\lfloor time \rfloor$

if *day=time* **then**

update the ages of infection :

$I_1^{S,day}(a,\alpha) \to I_1^{S,day}(a+da,\alpha)$, $I_2^{S,day}(a) \to I_2^{S,day}(a+da)$

$I_1^{V,day}(a,\alpha) \to I_1^{V,day}(a+da,\alpha)$, $I_2^{V,day}(a) \to I_2^{V,day}(a+da)$

check for emergence :

$\forall a\ NumTrialsS(a) = I_1^{S,day}(a,\emptyset)$

$\forall a\ NumTrialsV(a) = I_1^{V,day}(a,\emptyset)$

$NumEmergencies(a) =$

$Binomial(NumTrialsS(a), P^S(a)) + Binomial(NumTrialsV(a), P^V(a))$

compute new infections :

$r_1 = \sum_a \sum_\alpha \beta_{11}^S(a,\alpha) I_1^{S,day}(a,\alpha) + \sum_a \sum_\alpha \beta_{11}^V(a,\alpha) I_1^{V,day}(a,\alpha)$

$r_2 = \sum_a [\beta_{12}^S(a,\alpha) + \beta_{22}^S(a)] I_2^{S,day}(a)$
$\quad + \sum_a [\beta_{12}^V(a,\alpha) + \beta_{22}^V(a)] I_2^{V,day}(a)$

$(S+V)(day) = \exp(-(r_1+r_2)) \times (S+V)(day-dt)$

$s = \frac{S(day-dt)}{(S+V)(day-dt)}$

$numNewInfs = (S+V)(day-dt) - (S+V)(day)$

$numNewSInfs = Binomial(numNewSInfs, s)$

$numNewVinfs = numNewInfs - numNewSInfs$

$S(day) = S(day-dt) - numNewSInfs$

$V(day) = V(day-dt) - numNewVInfs$

$numNewI_1^S = Binomial(numNewSInfs, \frac{r_1}{r_1+r_2})$

$numNewI_1^V = Binomial(numNewVInfs, \frac{r_1}{r_1+r_2})$

$numNewI_2^S = numNewSInfs - numNewI_2^S$

$numNewI_2^V = numNewVInfs - numNewI_2^V$

else

update the ages of infection

check for emergence

5.7 Results

We will now present the results of our cross-scale vaccination model. We underline that all of our results assume a neutral mutant strain ($\delta_2 = \delta_1 = 2$), unless explicitly stated otherwise. We divide our results into different sections depending on the assumed form of the within-host emergence density. This is because, as we will discuss in more detail in the following sections, our within-host derived emergence density comes with some strict limitations. We are also interested in assessing the sensitivity of our model's results to the assumed form of the emergence density.

The structure of our Results section is as follows:

- In the first subsection we will present some of our model's results that do not depend in any way on the within-host emergence density.
- In the second subsection we will analyze our cross-scale vaccination model under the the within-host derived emergence density f_{WH} from 3.5.1.
- In the third subsection we will assume that the within-host emergence density f_{const} remains constant throughout an individual's infection. This means that our within-host model no longer informs the emergence density, but the resulting framework most closely resembles that of our population-level vaccination model from chapter 2.
- In the final subsection we will assume that the emergence density f_{WB} is given by a Weibull distribution. This is because the resulting density appears to capture well the emergence dynamics that we originally expected our extended *Saenz* model to produce.

5.7.1 The effects of the viral clearance rates

We first present some of our cross-scale vaccination model's results that do not depend on our choice of the within-host emergence density.

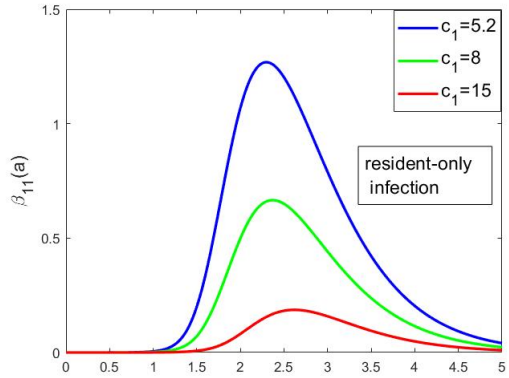

Fig. 5.2 The transmission rates for a resident-only infection in our cross-scale vaccination model for different values of the clearance rate c_1. Their trajectory resembles the within-host viral load curves, which is expected given our assumption that the transmission rates are linear functions of the within-host viral loads.

Figure 5.2 shows the between-host transmission rates in the case of a resident-only infection for three different values of the viral clearance rate c_1. Since we assume that vaccination acts at the within-host level by increasing the viral clearance rate(s), this figure illustrates the reduction in infectiousness of a vaccinated individual who has acquired the infection. More specifically, the vaccine initially acts within-host by increasing c_1. This reduces the viral load of the resident strain throughout the infection. Since we assume though that the population-level transmission rates are linear functions of the within-host viral load, this reduction in the viral load implies a reduction in the between-host transmission rates. This is the mechanism via which vaccination has an effect both at the within- and the between-host tiers of our cross-scale model. The reason we focus on c_1 instead of c_2 is because we assume that the vaccine is homologous to the resident strain, so in our framework it should mainly act by increasing c_1. We note though that the vaccine may still exert some pressure on the mutant strain by increasing c_2 as well, but we will examine this scenario in the next sections because its outcomes depend on the form of the within-host emergence density.

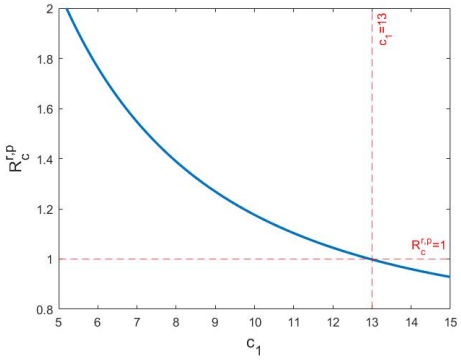

(a) The first value of c_1 for which $\mathscr{R}_c^{r,p}$ becomes smaller than 1 is 13.

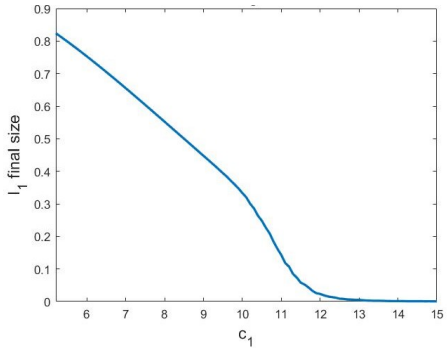

(b) The final size of the resident strain is computationally a non-increasing function of c_1. We note that for $c_1 \geq 13$ we have $\mathscr{R}_c^{r,p} < 1$ but we still ran the simulations of our cross-scale vaccination model to obtain a final size.

Fig. 5.3 The effects of the viral clearance rate c_1 on the resident's control reproduction number $\mathscr{R}_c^{r,p}$ and the the final size in a resident-only epidemic. Here c_1 ranges from its reference value 5.2 up to 15 in vaccinated individuals. In fully-susceptible individuals it remains fixed at its reference value across all simulations. All other relevant parameters were fixed at their reference values from Tables 5.1 and 5.2.

Figure 5.3 shows the effects of varying the viral clearance rate c_1 on the the resident's control reproduction number $\mathscr{R}_c^{r,p}$ and the final size of the resident strain in a resident-only epidemic. An epidemic with only the resident strain was achieved by simply setting the within-host emergence density to 0. Since we assume that vaccination acts by increasing the viral clearance rate within-host, we may think of varying c_1 as varying the efficacy of the vaccine against the resident. This is why our initial value for c_1 is its reference value of 5.2 (from Table 5.1). We note that the increase in c_1 is only reflected in vaccinated individuals. Fully-susceptible individuals who become infected have a clearance rate of $c_1 = 5.2$. This will apply to all our results that depend on varying the clearance rates c_1 and c_2 in the following sections as well. We can see in plot(a) that for any c_1 larger than 13 the virus cannot invade the population. This helps inform our choice for the upper limit of c_1 that we will use in all our subsequent simulations of two-strain epidemics.

5.7.2 Results using the original within-host derived emergence density

We will now present some of our model's results which depend on the choice of the within-host emergence density. We start by using our within-host derived f_{WH} as the emergence density:

$$f_{WH}(\alpha) = \lambda(\alpha) \times e^{-\int_0^\alpha \lambda(a)da}$$

where $\lambda(\alpha)$ is the rate of appearance, survival and adequate growth of a mutant strain and is given by:

$$\lambda(\alpha) = (\varepsilon\rho) \times \left(k_\alpha E_\alpha(\alpha) + k_\gamma E_\gamma(\alpha)\right) \times \left(1 - \frac{1}{R_{eff}^{m,wh}(a)}\right) \times \mathbb{1}^n_{(c_2 \int_\alpha^{D^{wh}} (\bar{V}_2(a)da) \geq s^*)}$$

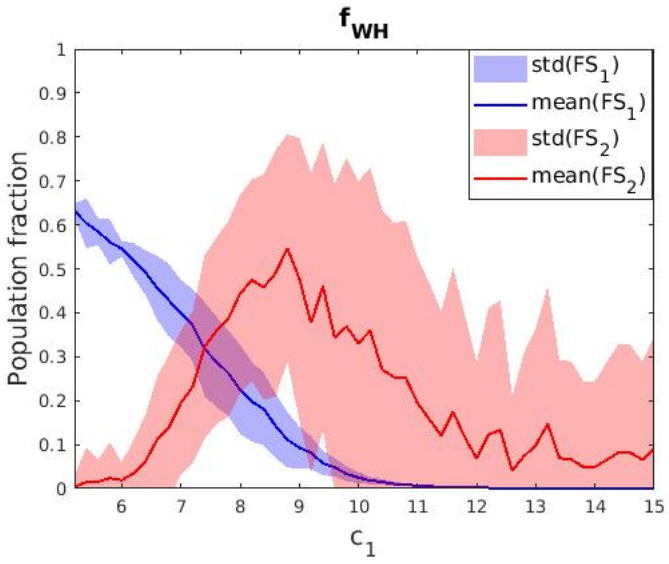

Fig. 5.4 The effects of the viral clearance rate c_1 on the average final sizes of the two strains. The mean final sizes were obtained by running 100 simulations of our cross-scale vaccination model for each value of c_1. All other parameters were fixed at their reference values from Tables 5.1 and 5.2. We underline that the increase in c_1 is reflected only in vaccinated individuals, who make up 63% of the population.

Figure 5.4 shows how the average final sizes of the two strains change as we vary the viral clearance rate c_1. We note again that our initial value for c_1 is its reference value 5.2, which describes a vaccine that is completely ineffective against the resident strain because $c_1 = 5.2$ is also the viral clearance rate in fully-susceptible individuals. Increasing c_1 past its reference value then denotes a vaccine that is increasingly efficient in clearing the resident strain within-host. Figure 5.4 provides some interesting insight into the conflicting effects of the within-host clearance rate c_1 on the population-level final size of the mutant strain. We see that initially as c_1 increases so does the average

final size of the mutant. We can attribute this to the advantage that the mutant gains due to the action of a vaccine that is putting increasingly more pressure on the resident strain both at the within- and between-host scales. After a certain value of c_1 though the vaccine-induced inhibition on the spread of the resident becomes so large that the mutant has significantly fewer opportunities to emerge. This can explain the decreasing portion of the mutant's mean final size curve. We underline that this figure provides some initial evidence that intermediate levels of immuno-protection are the most beneficial for the emergence and spread of a mutant strain in our cross-scale vaccination model, which was also the main result of our population-level vaccination model from chapter 2.

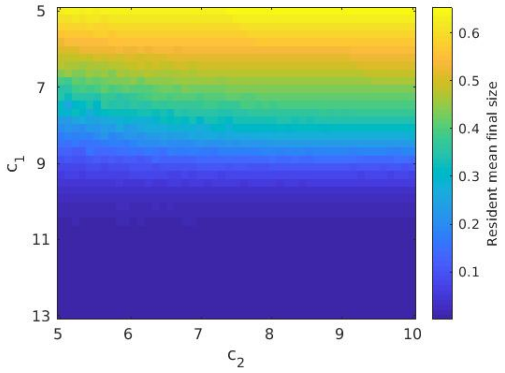

(a) Cross-scale vaccination model : the mean final size of the resident strain as we vary the viral clearance rates c_1 and c_2.

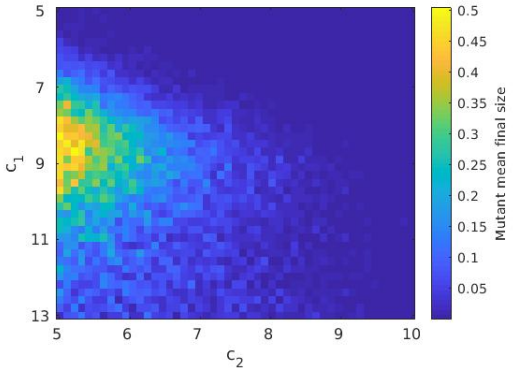

(b) Cross-scale vaccination model : the mean final size of the mutant strain as we vary the viral clearance rates c_1 and c_2. We note that plots (a) and (b) are on different scales.

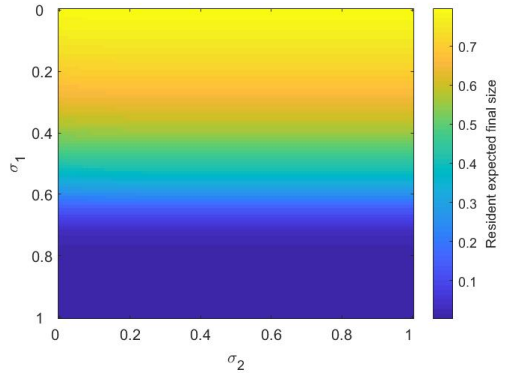

(c) Population-level vaccination model : the expected final size of the resident strain as a function of the vaccine efficacy σ_i against each strain.

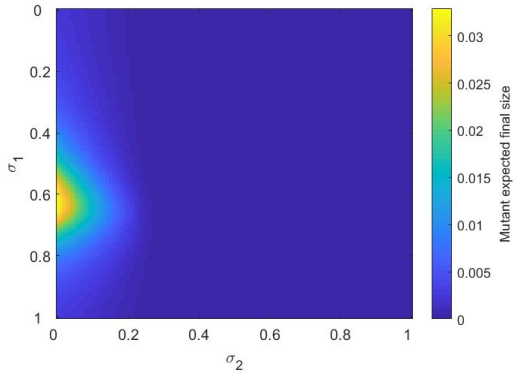

(d) Population-level vaccination model : the expected final size of the mutant strain as a function of the vaccine efficacy σ_i against each strain. We note that plots (c) and (d) are on different scales.

Fig. 5.5 The effects of varying the viral clearance rates c_1 and c_2 on the average final sizes of the two strains in our cross-scale vaccination model [plots (a) and (b)]. The mean final sizes were calculated by running 50 simulations of our cross-scale model for each value of c_1 and c_2. All other parameters remained fixed at their reference values from Tables 5.1 and 5.2. Plots (c) and (d) are the equivalent results from our population-level vaccination model from chapter 2, where σ_i denotes the portion by which the vaccine reduces susceptibility to the ith strain.

Figure 5.5 shows the effects of varying the viral clearance rates c_1 and c_2 on the average final sizes of the two strains in our cross-scale vaccination model [plots (a) and (b)], and then contrasts them with the equivalent results from our population-level vaccination model from chapter 2 [plots (c) and (d)]. We can make the following observations:

- Varying the viral clearance rate c_2 has very little effect on the mean final size of the resident strain, as plot (a) shows. This is not surprising given our assumption that the resident strain alone initiates the epidemic and therefore has some time to circulate in the population without any competition. This gives it a significant advantage over the mutant, which is then only slightly strengthened as the vaccine becomes more efficient at clearing the mutant strain within-host (or equivalently as c_2 increases). Plot (c) shows that the same is true for the effects of the vaccine efficacy σ_2 against the mutant strain on the expected final size of the resident in our population-level vaccination model.

- Plot (b) shows that intermediate values of the viral clearance rate c_1 are the most beneficial for the emergence and spread of the mutant in the population. As c_1 increases vaccinated individuals who have acquired the infection become more efficient in clearing it. This has a negative impact on the within-host viral load of the resident, which translates to a reduction in the population-level transmission of the resident due to our assumption that the between-host transmission rates are linear functions of the within-host viral load. This inhibition to the resident strain provides an advantage to the mutant, as the two strains are competing for available resources both within- and between-host. This explains the increasing portion of the mutant's mean final size along the c_1 axis. After a certain value of c_1 though, and more specifically the value which corresponds to the peak of the mutant's final size as c_1 increases, the vaccine-induced pressure against the resident strain is too large for it to spread efficiently. As a result there are fewer opportunities for the mutant strain to emerge within infected individuals, leading to the decreasing portion of its mean final size along the c_1 axis that we see in plot (b). We note that this pattern agrees with the equivalent result from our population-level vaccination model, as a comparison with plot (d) shows.

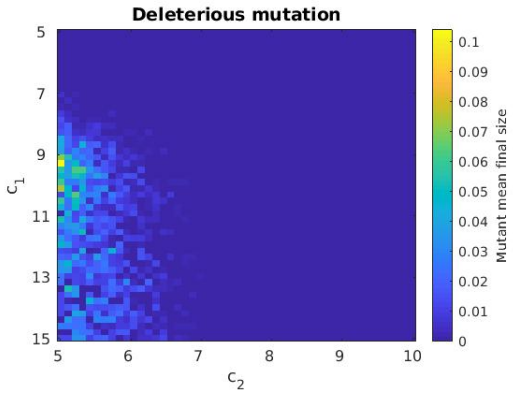

(a) Cross-scale vaccination model: the average final size of a weaker mutant strain as a function of the viral clearance rates c_1 and c_2. A deleterious mutation is defined in our model by $\delta_2 = 2.6$, where δ_2 is the death rate of cells infected with the mutant. We have shown that for such a mutant $\mathscr{R}_0^{m,p} = 1.5$.

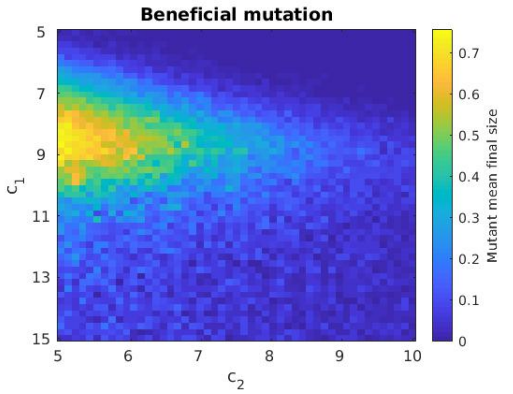

(b) Cross-scale vaccination model: the average final size of a fitter mutant strain as a function of the viral clearance rates c_1 and c_2. A beneficial mutation is defined in our model by $\delta_2 = 1.6$. We have shown that for such a mutant $\mathscr{R}_0^{m,p} = 2.5$. We note that the scales between plots (a) and (b) are different.

Fig. 5.6 The effects of varying the viral clearance rates c_1 and c_2 on the average final size of the mutant strain for two cases: a deleterious mutation in plot (a) and a beneficial mutation in plot (b). A weaker mutant is characterized by $\delta_2 = 2.6$, which leads to $\mathscr{R}_0^{m,p} = 1.5$. A fitter mutant is defined by $\delta_2 = 1.6$, which leads to $\mathscr{R}_0^{m,p} = 2.5$. We note that the resident strain remained at $\mathscr{R}_0^{r,p} = 2$ for both plots. The mean final sizes were calculated by running 50 simulations of our cross-scale model for each value of c_1 and c_2. All other parameters remained fixed at their reference values from Tables 5.1 and 5.2.

Figure 5.6 shows how the average final size of the mutant strain changes as we vary the viral clearance rates c_1 and c_2 in two cases: a deleterious mutation in plot (a) and a beneficial mutation in plot (b). We emphasize that for both these plots the parameters that define the resident strain remained fixed at their reference values. We observe the following:

- Plot (a) shows that our previous conclusion that intermediate values of c_1 are the most beneficial for the emergence and spread of a neutral mutant strain is not as prominent in the case of a weaker mutant. While we still observe that the weaker mutant reaches its largest final size for some intermediate values of c_1, we can also see that for small values of c_2 varying c_1 from intermediate up to large values does not appear to have a significant effect on the final size of the mutant. This does not agree with the pattern we observed in the case of a neutral mutant, but it could be attributed to the fitness disadvantage of the weaker mutant. Our reasoning for the decreasing portion of the average final size of the neutral mutant strain along the c_1 axis was that the vaccine-induced inhibition on the spread of the resident significantly lowered the mutant's chances of emerging at a population-level. But in the case of a deleterious mutation the mutant's chances of emerging within-host and then spreading in the population while competing with the resident at both scales are smaller compared to those of a neutral mutant. Therefore it is not surprising that the efficacy of the vaccine against the resident strain has a less

prominent impact on the final size of a weaker mutant strain as opposed to that of a neutral mutant strain.

- Plot (b) shows that intermediate values of c_1 are the most beneficial for the emergence and spread of a fitter mutant strain in the population. We observe that the fitter mutant can spread even at large values of c_2, which was not the case for either the weaker or the neutral strain.

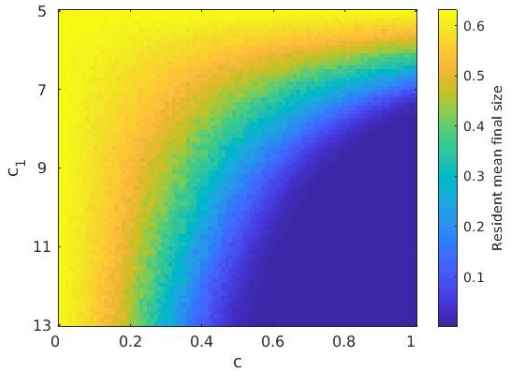

(a) Cross-scale vaccination model: the average final size of the resident strain against the vaccination coverage c and the viral clearance rate c_1.

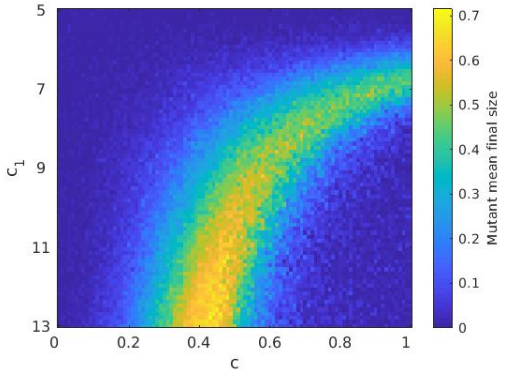

(b) Cross-scale vaccination model: the average final size of the mutant strain against the vaccination coverage c and the viral clearance rate c_1. We note that the scales between plots (a) and (b) are different.

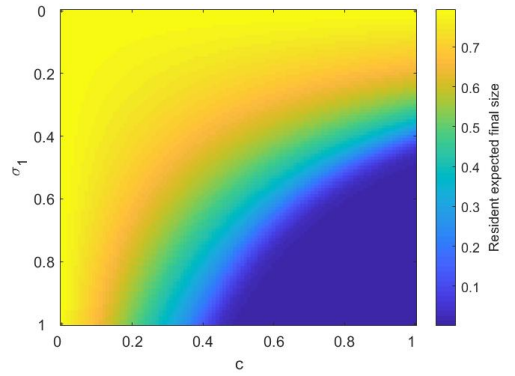

(c) Population-level vaccination model: the expected final size $\mathbb{E}(FS_1)$ of the resident strain against the vaccine efficacy σ_1 and the vaccination coverage c.

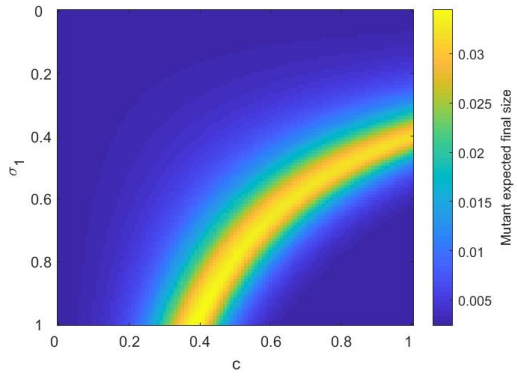

(d) Population-level vaccination model : the expected final size $\mathbb{E}(FS_2)$ of the mutant strain against the vaccine efficacy σ_1 and the vaccination coverage c. We note that the scales between plots (c) and (d) are different.

Fig. 5.7 The effects of varying the viral clearance rate c_1 and the vaccination coverage c on the average final sizes of the two strains in our cross-scale vaccination model [plots (a) and (b)]. The mean final sizes were calculated by running 50 simulations of our cross-scale model for each value of c_1 and c. All other parameters remained fixed at their reference values from Tables 5.1 and 5.2. Plots (c) and (d) are the equivalent results from our population-level vaccination model from chapter 2, where σ_1 denotes the portion by which the vaccine reduces susceptibility to the resident strain.

Figure 5.7 illustrates the impact of varying the viral clearance rate c_1 and the vaccination coverage c on the mean final sizes of the two strains. Plot (a) shows that the mean final size of the resident is computationally a decreasing function of c and c_1, as expected. Plot (b) on the other hand provides some interesting information as to the conditions

which are most inducive to the emergence and spread of a mutant strain in the population. We can identify three such scenarios:

- When both c and c_1 have intermediate values.
- When c is intermediate and c_1 is large.
- When c is large and c_1 is small or intermediate.

These results highlight the key role of the vaccination coverage in reducing the burden of influenza epidemics. They also show that a high vaccine-induced immune pressure against the homologous resident strain is important not only because of its direct effects in limiting the spread of the resident, but also because it inhibits the chances of a mutant strain emerging and growing in the population. We note that these results are qualitatively very similar to the equivalent results of our population-level vaccination model from chapter 2, as plots (c) and (d) illustrate.

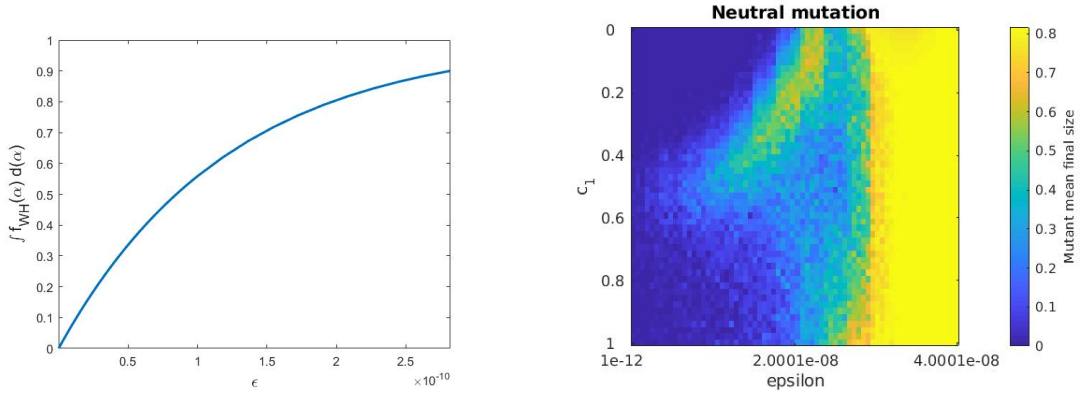

(a) The cumulative within-host emergence probability $\int f(\alpha)d\alpha$ as a function of the within-host mutation rate ε. Here the largest value of ε that we tested is $\varepsilon = 2.82 \times 10^{-10}$ and it leads to a cumulative within-host emergence probability of 0.9.

(b) Cross-scale vaccination model: the average final size of a mutant strain as a function of the viral clearance rate c_1 and the within-host mutation rate ε.

Fig. 5.8 The effects of the within-host mutation rate ε on the within-host cumulative emergence probability and on the population-level average final size of the mutant strain. The mean final size was calculated by running 50 simulations of our cross-scale model for each value of c_1 and ε. All other parameters remained fixed at their reference values from Tables 5.1 and 5.2.

Figure 5.8 illustrates the effects of the within-host mutation rate ε on the within-host cumulative emergence probability $\int_0^{D^{wh}} f(\alpha)d\alpha$ and on the population-level average final size of a neutral mutant strain. We first discussed the mutation rate ε in section 3.5.1, where we defined it as the number of substitutions per nucleotide per cell infection that lead to an an antigenic change. We restricted our definition to only take into account the HA- and NA-coding nucleotides and further assumed that only 10% of those nucleotides can potentially generate an antigenic change and that the probability that they do is

0.0005 per substitution. These values though were chosen semi-arbitrarily and led to a within-host cumulative emergence probability of 0.73 for a weaker mutant, 0.91 for a neutral mutant and 0.34 for a fitter mutant. Here, using plot (a) as a guide, we chose values of ε ranging from 10^{-12} up to 5×10^{-8} and varied them against the viral clearance rate c_1 to study their effects on the mutant's population-level final size. The results are displayed in plot (b). We can see that for most values of ε which allow the mutant to emerge and spread in the population, intermediate values of c_1 lead to the largest final sizes for the mutant. Plot (b) shows that as ε increases the interval of c_1 values that benefit the mutant increases as well. This is not surprising since a larger ε implies a larger cumulative emergence probability. We also note that the very narrow emergence window under f_{WH} guarantees that if the mutant emerges it will emerge early enough during an individual's infection to still have plenty of resources available to it to grow within-host. In our model this translates to high between-host transmission rates due to their linear dependence on the viral load. Therefore as ε increases the mutant strain gains a considerable competitive advantage against the resident strain. We see that if ε is large enough then the mutant can emerge and spread in the population even for very large values of c_1 and even dominate the epidemic.

5.7.3 Results using a constant emergence density

We will now change our approach regarding the emergence density and instead of deriving it from our within-host model we will assume that it remains constant throughout an individual's infection. This means that our within-host model no longer directly informs the emergence probability. Nevertheless we are still interested in assessing the results of our cross-scale vaccination model using a constant emergence density because it most closely resembles the framework of our population-only vaccination model for the evolution of influenza from chapter 2.

We assume that f_{const} follows a scaled uniform distribution in $[0, D^{wh}]$:

$$f_{const}(\alpha) = p \times \frac{1}{D^{wh}} \times \mathbb{1}_{\alpha \in [0, D^{wh}]}$$

where p refers to the within-host cumulative emergence probability.

Given our new definition for the emergence density f_{const} and its lack of dependence on our within-host model, we need to redefine the way in which vaccination affects the within-host emergence density. Let $c_1 \in [c_{1,ref}, C]$, where $c_{1,ref}$ denotes the reference value for c_1 (in our case 5.2). As $c_1 = c_{1,ref}$ leads to a completely ineffective vaccine, we want it to have no effect on f_{const}. On the other hand we set up $c_1 = C$ to lead to a zero emergence density in vaccinated individuals. So we set:

$$f^V_{const}(\alpha|c_1) = f^S_{const}(\alpha) \times \left(1 - \frac{c_1 - c_{1,ref}}{C - c_{1,ref}}\right) \tag{5.16}$$

where f^S_{const} and f^V_{const} denote the emergence densities in fully-susceptible and vaccinated individuals respectively. We set $C = 15$ for the rest of our simulations. We have already demonstrated that the resident strain cannot initiate an epidemic when $c_1 = 13$ in a single-strain epidemic, but we use $c_1 = 15$ to investigate whether that could give such a large competitive advantage to the mutant strain that the mutant alone could drive the epidemic.

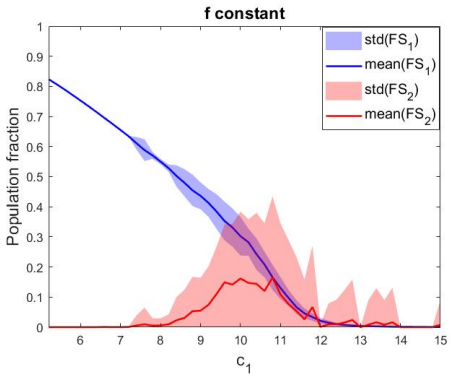

(a) The average final sizes of the resident and mutant strains as a function of c_1 when $p = 0.003$.

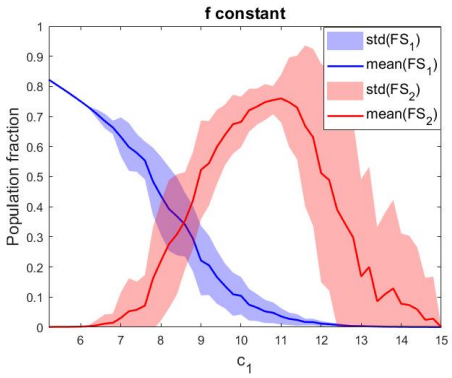

(b) The average final sizes of the resident and mutant strains as a function of c_1 when $p = 0.05$.

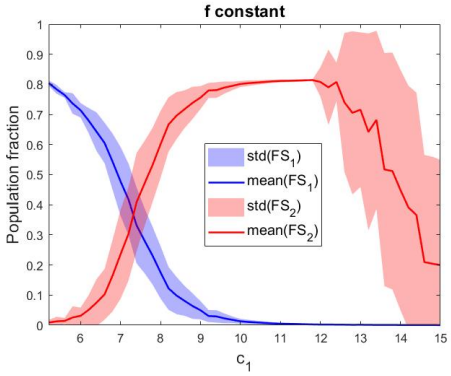

(c) The average final sizes of the resident and mutant strains as a function of c_1 when $p = 0.1$.

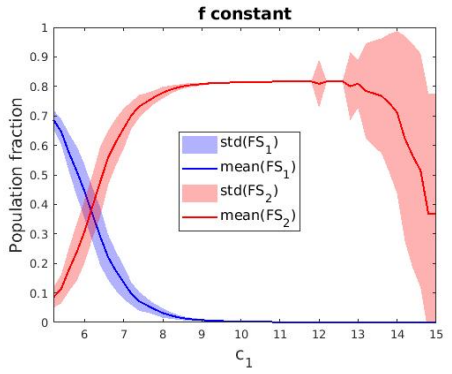

(d) The average final sizes of the resident and mutant strains as a function of c_1 when $p = 0.5$.

Fig. 5.9 The average final sizes of the resident and mutant strains when varying the viral clearance rate c_1 for four different values of the within-host cumulative emergence probability p. The average sizes were obtained after running 100 simulations of our cross-scale vaccination model for each value of c_1. We note that the mean final size of the resident strain is very small but still non-zero for all values of c_1 and p tested here. We underline that the changes in c_1 are only reflected in vaccinated individuals, which make up 63% of our population. All non-varying parameters remained fixed at their reference values from Tables 5.1 and 5.2.

Figure 5.9 illustrates the effects of varying the viral clearance rate c_1 on the mean final sizes of the two strains for four different values of the within-host cumulative emergence probability p. We see that p appears to have a significant effect on the final size of the mutant strain. Interestingly a pattern that remains constant among these four plots is the general shape of the final size of the mutant as a function of c_1, which appears to indicate again that intermediate values of immuno-protection are the most inducive to the emergence and spread of a mutant strain in a population.

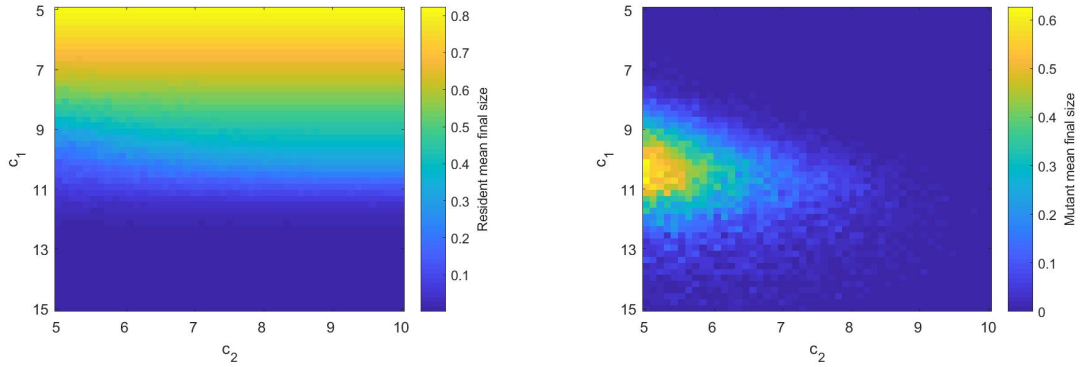

(a) The average final size of the resident strain as a function of c_1 and c_2.

(b) The average final size of the mutant strain as a function of c_1 and c_2.

Fig. 5.10 The average final sizes of the resident and the mutant strains when we vary the viral clearance rates c_1 and c_2. The average sizes were obtained after running 50 simulations of our cross-scale vaccination model for each value of c_1 and c_2. The within-host cumulative emergence probability was $p = 0.003$ for all simulations and the mutant was assumed to be neutral. All other parameters remained fixed at their reference values from Tables 5.1 and 5.2.

Figure 5.10 shows how the average final sizes of the two strains change as we vary the viral clearance rates c_1 and c_2. We chose $p = 0.003$ for the within-host cumulative emergence probability of the mutant. This comes into contrast with our values for p from chapter 4 which were significantly higher, but here we need to also account for the detrimental effects of the homologous vaccine against the resident strain. We emphasize though that our choice of p is not very important here, since we are interested in studying the changes in the final size of the mutant as we vary c_1 and c_2, rather than its actual prevalences. Figure 5.10 shows that the end results for both strains are qualitatively very similar to the equivalent results of our cross-scale vaccination model in the previous section, where we used the within-host derived emergence density f_{WH} instead of f_{const}. They are also very similar to the equivalent results of our population-level vaccination model.

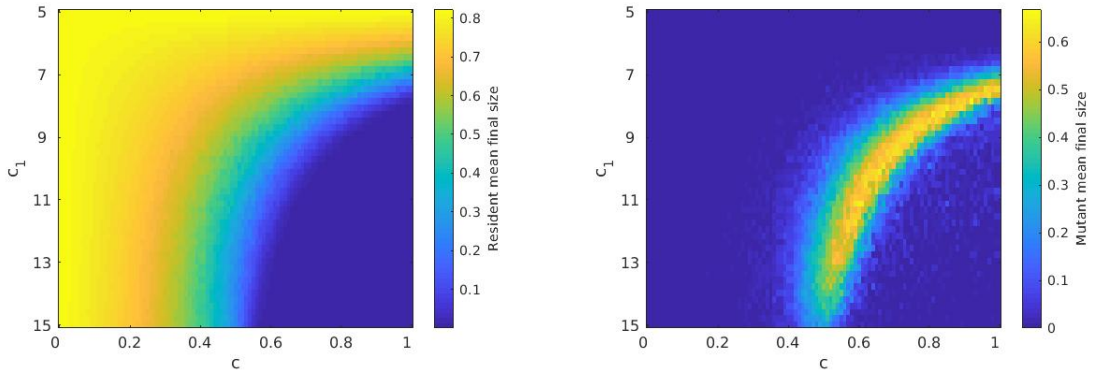

(a) The average final size of the resident strain as a function of c and c_1.

(b) The average final size of the mutant strain as a function of c and c_1. We note that plots (a) and (b) are on different scales.

Fig. 5.11 The average final sizes of the resident and the mutant strains as we vary the vaccination coverage c and the viral clearance rate against the resident c_1. The average sizes were obtained after running 50 simulations of our cross-scale vaccination model for each value of c and c_1. The within-host cumulative emergence probability was $p = 0.003$ for all simulations. All other parameters remained fixed at their reference values from Tables 5.1 and 5.2.

Figure 5.11 illustrates the effects of varying the vaccination coverage c and the within-host viral clearance rate c_1 on the average final sizes of the two strains, under the assumption that the within-host emergence density is constant. Once again, our results are qualitatively very similar to the equivalent results from our cross-scale vaccination model when the emergence density is given by f_{WH} and to the equivalent results from our population-only vaccination model from chapter 2.

5.7.4 Results using the Weibull distribution

We will now choose a different functional form for the within-host emergence density f. We will assume that f follows a Weibull distribution with scale parameter $\eta = 2$ and shape parameter $\zeta = 2.5$. The resulting pdf is given by the following expression:

$$f_{WB}(\alpha) = p \times \frac{\zeta}{\eta}\left(\frac{\alpha}{\eta}\right)^{\zeta-1} e^{-(\alpha/\eta)^{\zeta}}$$

where p again denotes the within-host cumulative emergence probability of the mutant strain. We note that this is the same scaled Weibull distribution as in section 4.6.5.

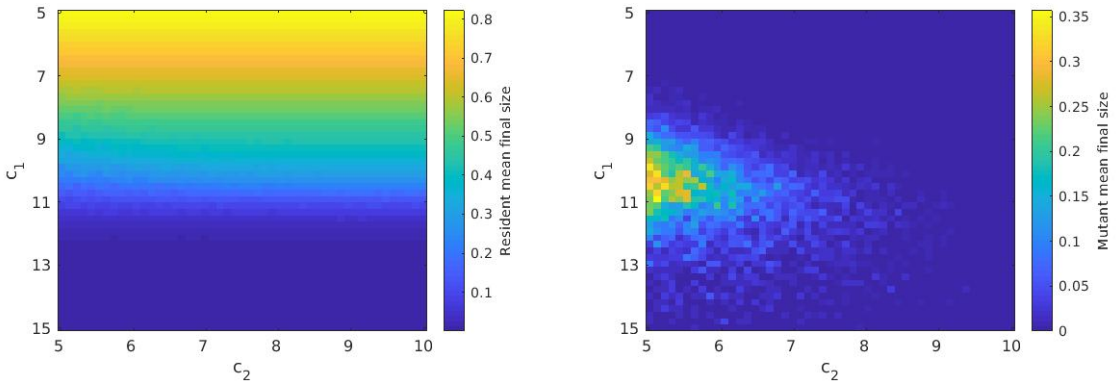

(a) The average final size of the resident strain as a function of c_1 and c_2.

(b) The average final size of the mutant strain as a function of c_1 and c_2. We note that plots (a) and (b) have different scales.

Fig. 5.12 The average final sizes of the resident and the mutant strains when we vary the viral clearance rates c_1 and c_2 assuming that the emergence density is given by f_{WB}. The average sizes were obtained after running 50 simulations of our cross-scale vaccination model for each value of c_1 and c_2. The within-host cumulative emergence probability was $p = 0.003$ and the mutant was assumed to be neutral for all simulations. All other parameters remained fixed at their reference values from Tables 5.1 and 5.2.

Figure 5.12 illustrates how the average final sizes of the two strains change as we vary the viral clearance rates c_1 and c_2, under the assumption that the within-host emergence density is given by f_{WB}. Plot (a) shows that the viral clearance rate against the mutant strain c_2 has very little effect on the mean final size of the resident strain. This is not surprising given our assumption that the resident strain alone initiates the epidemic and therefore has some time to circulate in the population without any competition. Plot (b) on the other hand illustrates again the interesting and conflicting effects of the viral clearance rate c_1 on the average final size of the mutant. We see that intermediate values of c_1 are the most beneficial for the emergence and spread of the mutant in the population. This is a pattern that we also have observed in the previous sections where we assumed different forms for the emergence density, and it can be attributed to the same factors. The increasing portion of the mutant's mean final size can be explained by the inhibition in both the within-host and the population-level spread of the resident that a higher c_1 entails. After some value of c_1 though, the resident strain cannot spread efficiently anymore, giving fewer opportunities to the mutant strain to emerge. This can explain the decreasing portion of the plot along the c_1 axis.

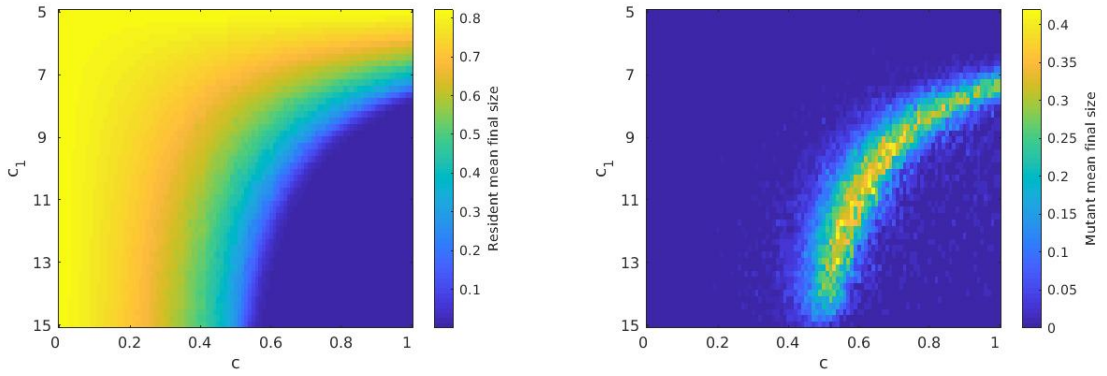

(a) The average final size of the resident strain as a function of c and c_1.

(b) The average final size of the mutant strain as a function of c and c_1. We note that plots (a) and (b) are on different scales.

Fig. 5.13 The average final sizes of the resident and the mutant strains against the viral clearance rate c_1 and the vaccination coverage c, assuming that the emergence density is given by f_{WB}. The average sizes were obtained after running 50 simulations of our cross-scale vaccination model for each value of c and c_1. The within-host cumulative emergence probability was $p = 0.003$ for all simulations. All other parameters remained fixed at their reference values from Tables 5.1 and 5.2.

Figure 5.13 shows how the average final sizes of the two strains change as we vary the vaccination coverage c and the viral clearance rate c_1 under the assumption that the emergence density is given by f_{WB}. The results are very similar from a qualitative perspective to the equivalent results of our cross-scale vaccination model under f_{WH} and under f_{const} as well as to the results of our population-level vaccination model from chapter 2.

Overall, we studied the results of our cross-scale vaccination model under three different scenarios: one where the emergence density is derived from our within-host model, one where it remains constant throughout the duration of the infection and finally one where it is given by a Weibull distribution. In all three cases varying the efficacy of the vaccine against the resident strain (captured here via varying the within-host viral clearance rate c_1) led to the same conclusion: intermediate values of immuno-protection are the most beneficial for the emergence and growth of a mutant strain in the population. This is also the main result of the analysis of our population-level vaccination model from chapter 2. In the next section we will discuss at length the implications of these findings with regards to the advantages and disadvantages of our cross-scale model compared to our simpler population-level model.

5.8 Discussion

In this chapter we developed a cross-scale model to study the epidemiological and evolutionary dynamics of influenza within a single season that also incorporated the effects of vaccination. Our cross-scale vaccination model is the same as the Coombs-based cross-scale model that we presented in chapter 4, with the only difference that we increased the within-host viral clearance rates in individuals who were assumed to have received a vaccine prior to the onset of the epidemic. We again assumed that the between-host transmission rates are linear functions of the within-host viral load and used three different forms for the within-host emergence density of the mutant strain: our within-host derived emergence density from 3.5.1, a constant emergence density and finally a scaled Weibull emergence density. By varying the efficacy of the vaccine we demonstrated that in all cases intermediate values of immuno-protection are the most inducive to the emergence and subsequent spread of a mutant strain in the population. We emphasize that this is the same conclusion that we reached using our population-level vaccination model from chapter 2.

One of the main research questions that we wanted to answer via this thesis was whether the explicit linking of the scales is essential to describe the effects of vaccination on the single-season evolutionary dynamics of influenza, modelled here as the emergence and spread of a mutant strain in the population. The analysis of our cross-scale vaccination model combined with a comparison to the results of our population-level vaccination model reveals that the two models produce qualitatively very similar results with regard to the conditions which facilitate the growth of a mutant strain in the population. Therefore we may conclude that if we only limit our focus to the question of how vaccination affects the population-level final size of an emerging mutant strain then explicitly linking the between- and within-host scales is not necessary. We emphasize though that using a cross-scale model allows for research questions which cannot be answered from a single-scale perspective, such as how the within-host mutation rate affects the between-host spread of a mutant strain in the presence of a vaccine that is homologous to the resident strain and has no effect on the mutant.

We incorporated the effects of vaccination in our model simply as an increase in the within-host viral clearance rates. We first presented and analysed this within-host vaccination model in section 3.6.1. We note that this is a very simplistic way to account

for the effects of vaccination, but given the complicated nature and computational intensity of cross-scale models we wanted to include vaccination in a very simple way. We have already discussed in 3.6.1 our decision to have vaccination affect specifically the within-host viral clearance rates, as opposed to other within-host strain-specific parameters such as the death rate of infected cells, and demonstrated that varying the different strain-specific parameters has similar effects on the results of our within-host model. Therefore we expect the results of our cross-scale vaccination model to remain qualitatively similar if we use a different within-host strain-specific parameter to capture the effects of vaccination.

An important future research project is repeating the analysis of our cross-scale vaccination model assuming different functional forms for the relationship between the population-level transmission rates and the within-host viral load. We have already addressed the lack of empirical data that could accurately define this relationship in the Discussion section of chapter 4. Since the transmission rates are the main links of the two scales in our model, testing the sensitivity of our model's results to the assumed form of the dependence of the transmission rates on the viral loads is of particular importance.

5.9 Summary

In this chapter we developed a cross-scale model for the epidemiological and evolutionary dynamics of influenza within a single season that took into consideration the effects of vaccination. We modelled the evolution of influenza as the emergence of a mutant strain within hosts already infected by a resident strain, combined with the mutant's subsequent spread in the population. Our cross-scale model explicitly linked the between- and within-host scales via the population-level transmission rates, which we assumed are linear functions of the within-host viral load. The effects of vaccination were captured simply as an increase in the within-host clearance rate of the virus. We varied the assumed form of the within-host emergence density as well as the fitness of the mutant strain and the efficacy of vaccination and illustrated that in all cases intermediate values of immuno-protection were the most inducive to the emergence and spread of a mutant strain in the population.

Chapter 6

Conclusion

The main research question that drove this thesis is how vaccination affects the emergence dynamics of a mutant strain and the subsequent competition dynamics with its parent resident strain within-host, between-host and across-scales. We developed a within-host, a between-host and a cross-scale model to investigate this and here we will summarize some of our most important insights and conclusions:

Insights from the between-host model

Using our population-level vaccination model we showed that intermediate values of immuno-protection are the most inducive to the emergence and spread of a mutant strain in the population. We measured the efficacy of the vaccine using the proportion by which it lowers susceptibility to infection. Our results showed that intermediate values of the vaccine efficacy against the resident strain lead to the highest expected final size for the mutant. We also showed that a small or intermediate vaccine coverage also facilitates the between-host growth of an emerging mutant strain, even in the case that the efficacy of the vaccine is large. Therefore the analysis of our between-host vaccination model underlines the significance of not only having a vaccine that is very efficient in preventing infection, but also of vaccinating large portions of the population.

The analysis of our between-host model also highlighted that the time of appearance of the mutant strain is crucial in determining its survival and growth in the population. A later emergence time implies that the already circulating resident strain has had more

time to infect susceptible individuals and therefore deplete the emerging mutant's pool of potential resources. This is certainly not a surprising result, but it is linked to our assumptions of no co-infection and full cross-immunity. More specifically, we assumed that individuals can only be infected by a single strain and that a recovered individual gains full immunity both from the infecting strain and the other circulating one. As we argued in the Discussion section of chapter 2 though, both of these assumptions can be justified within the scope of our model with empirical data as well as previously published work.

Insights from the within-host model

The within-host appearance time of a mutant strain is very important in determining its viability and growth. This is linked to our assumptions of no co-infection at the cellular level and cell death following infection, and can be explained by the depletion of available resources due to infection by the already circulating resident strain. In the context of our extended *Saenz* model the resources that a mutant strain requires to grow are susceptible target and prerefractory cells.

In chapter 3 we showed that the explicit inclusion of the innate immune response via the action of type I interferon (IFN) as well as the inclusion of the cell eclipse phase are important in determining the emergence window of a mutant strain. In our simple two-strain TIV model the mutant's effective reproduction number becomes smaller than 1 at 0.76 days at the latest. Therefore in that model emergence is not possible after the first approximately 18 hours of infection. This is a very restrictive condition, and we attributed it to the very fast depletion of target cells due to infection. The extended *Saenz* model can partially mitigate this as it slows down viral kinetics via the inclusion of the eclipse phase and the protective action of IFN which reduces the infectivity rate of the virus towards prerefractory cells. The result is a wider emergence window that extends up to the second day of infection, specifically up to the first 46.5 hours of infection. We showed that this later emergence cutoff time can be attributed primarily to the slower depletion of target cells in the extended *Saenz* model. We may argue though that even in our two-strain *Saenz* model the population of target cells decreases very quickly, which we attributed to the free mixing of virions with target cells. Therefore, while we underline that explicitly incorporating the immune response is important when investigating the mutant's

emergence window, we posit that adding spatial structure to the extended *Saenz* model will allow for a wider emergence window. More specifically if we adapt the framework of Reperant *et al*. from [253] and break down the respiratory tract into three distinct compartments, each with its own within-host model and initial population of target cells and assume that infection begins in one compartment and can then slowly spread to the other two, then the overall population of target cells should decrease more slowly compared to our extended *Saenz* model.

Insights from the cross-scale model

The explicit linking of the scales is not necessary to capture the conflicting effects of vaccination at the within- and between-host levels. As we have demonstrated, both our between-host vaccination model from chapter 2 and our cross-scale vaccination model from chapter 5 show that intermediate values of immuno-protection are the most inducive for the emergence and spread of a mutant strain in the population. While the between-host tier of our cross-scale model was explicitly informed by the emergence dynamics of a mutant strain within-host, our population-level model considered only implicitly the within-host processes that give rise to mutant strains via a parameter for the mutation rate per infection, which was either varied or chosen by us. Both models though illustrated that initially as the vaccine efficacy against the resident strain increases the expected final size of the mutant strain increases as well due to the advantage that the mutant gains from a vaccine that is hindering the growth of its competitor resident strain. And both models then showed that there is a value for the vaccine efficacy after which the vaccine-induced pressure on the resident strain is so large that the resident cannot spread efficiently anymore, allowing significantly fewer opportunities for the mutant strain to emerge and negatively impacting its expected final size. Therefore, we concluded that explicitly linking the within- and between-host scales is not necessary in order to answer the main driving question of this thesis, which is how vaccination affects the epidemiological and evolutionary dynamics of influenza within a single season. As Mideo *et al*. report in [210] though, "Almost all of the studies that have used nested models of disease dynamics to date (2008) have not actually required nesting to accomplish their goals. Despite this, these models have provided important insights about pathogen evolution". We argue that the same holds for our cross-scale vaccination model, as it still provided useful insights into how the within-host time of emergence affects the population-level final size of both strains and how the within-host fitness of the two strains translates into

their population-level fitness as captured by their basic reproduction numbers.

References

[1] (1971). A revised system of nomenclature for influenza viruses. *Bulletin of the World Health Organization*, 45(1):119 – 124.

[2] (1980). A revision of the system of nomenclature for influenza viruses: a WHO memorandum. *Bulletin of the World Health Organization*, 58(4):585–91.

[3] Alexander, M., Bowman, C., Moghadas, S., Summers, R., Gumel, A., and Sahai, B. (2004). A vaccination model for transmission dynamics of influenza. *SIAM Journal on Applied Dynamical Systems*, 3(4):503–524.

[4] Alexopoulou, L., Holt, A. C., Medzhitov, R., and Flavell, R. A. (2001). Recognition of double-stranded RNA and activation of NF-B by Toll-like receptor 3. *Nature*, 413(6857):732–738.

[5] Alizon, S., Luciani, F., and Regoes, R. R. (2011). Epidemiological and clinical consequences of within-host evolution. *Trends in Microbiology*, 19(1):24–32.

[6] Allen, L. J. S., Brauer, F., Van den Driessche, P., and Wu, J. (2008). *An Introduction to Stochastic Epidemic Models*. Springer-Verlag.

[7] Almocera, A. E. S. and Hernandez-Vargas, E. A. (2019). Coupling multiscale within-host dynamics and between-host transmission with recovery (SIR) dynamics. *Mathematical Biosciences*, 309:34–41.

[8] Almocera, A. E. S., Nguyen, V. K., and Hernandez-Vargas, E. A. (2018). Multiscale model within-host and between-host for viral infectious diseases. *Journal of Mathematical Biology*, 77(4):1035–1057.

[9] Anderson, R. M. and May, R. M. (1985). Vaccination and herd immunity to infectious diseases. *Nature*, 318(6044):323–329.

[10] Andreasen, V. (2003). Dynamics of annual influenza a epidemics with immuno-selection. *Journal of Mathematical Biology*, 46(6):504–536.

[11] Andreasen, V. (2011). The final size of an epidemic and its relation to the Basic Reproduction Number. *Bulletin of Mathematical Biology*, 73(10):2305–2321.

[12] Andreasen, V. (2018). Epidemics in competition: Partial cross-immunity. *Bulletin of Mathematical Biology*, 80(11):2957–2977.

[13] Andreasen, V. and Gog, J. R. (2020). Pease (1987): The evolutionary epidemiology of influenza A. *Theoretical Population Biology*.

[14] Andreasen, V., Lin, J., and Levin, S. A. (1997). The dynamics of cocirculating influenza strains conferring partial cross-immunity. *Journal of Mathematical Biology*, 35(7):825–842.

[15] Appiah, G. D., Blanton, L., D'Mello, T., Kniss, K., Smith, S., Mustaquim, D., Steffens, C., Dhara, R., Cohen, J., Chaves, S. S., Bresee, J., Wallis, T., Xu, X., Elal, A. I. A., Gubareva, L., Wentworth, D. E., Katz, J., Jernigan, D., Brammer, L., (CDC), C. f. D. C., and Prevention (2015). Influenza activity - United States, 2014-15 season and composition of the 2015-16 influenza vaccine. *MMWR. Morbidity and mortality weekly report*, 64(21):583–90.

[16] Arinaminpathy, N., Kim, I. K., Gargiullo, P., Haber, M., Foppa, I. M., Gambhir, M., and Bresee, J. (2017). Estimating Direct and Indirect Protective Effect of Influenza Vaccination in the United States. *American Journal of Epidemiology*, 186(1):92–100.

[17] Arinaminpathy, N., Ratmann, O., Koelle, K., Epstein, S., Price, G., Viboud, C., Miller, M., and Grenfell, B. (2012). Impact of cross-protective vaccines on epidemiological and evolutionary dynamics of influenza. *Proceedings of the National Academy of Sciences*, 109(8):3173–3177.

[18] Arinaminpathy, N., Riley, S., Barclay, W. S., Saad-Roy, C., and Grenfell, B. (2020). Population implications of the deployment of novel universal vaccines against epidemic and pandemic influenza. *Journal of the Royal Society Interface*, 17(164):20190879.

[19] Arino, J., Brauer, F., Driessche, P., Watmough, J., and Wu, J. (2006). Simple models for containment of a pandemic. *Journal of the Royal Society Interface*, 3(8):453–457.

[20] Arino, J., C, M., and Driessche, P. (2003). Global results for an epidemic model with vaccination that exhibits backward bifurcation. *SIAM Journal on Applied Mathematics*, 64(1):260–276.

[21] Asahi, Y., Yoshikawa, T., Watanabe, I., Iwasaki, T., Hasegawa, H., Sato, Y., Shimada, S.-i., Nanno, M., Matsuoka, Y., Ohwaki, M., Iwakura, Y., Suzuki, Y., Aizawa, C., Sata, T., Kurata, T., and Tamura, S.-i. (2002). Protection Against Influenza Virus Infection in Polymeric Ig Receptor Knockout Mice Immunized Intranasally with Adjuvant-Combined Vaccines. *The Journal of Immunology*, 168(6):2930–2938.

[22] Baalen, M. v. and Sabelis, M. W. (1995). The Dynamics of Multiple Infection and the Evolution of Virulence. *The American Naturalist*, 146(6):881–910.

[23] Bacaër, N. (2011). *Ross and malaria (1911)*, pages 65–69. Springer London, London.

[24] Baccam, P., Beauchemin, C., Macken, C. A., Hayden, F. G., and Perelson, A. S. (2006). Kinetics of influenza a virus infection in humans. *Journal of Virology*, 80(15):7590–7599.

[25] Ball, F. G. and Britton, T. (2007). An epidemic model with infector-dependent severity. *Advances in Applied Probability*, 39(4):949–972.

[26] Barberis, I., Myles, P., Ault, S. K., Bragazzi, N. L., and Martini, M. (2016). History and evolution of influenza control through vaccination: from the first monovalent vaccine to universal vaccines. *Journal of Preventive Medicine and Hygiene*, 57(3):E115–E120.

[27] Beauchemin, C., Samuel, J., and Tuszynski, J. (2005). A simple cellular automaton model for influenza a viral infections. *Journal of Theoretical Biology*, 232(2):223–234.

[28] Beauchemin, C. A. and Handel, A. (2011). A review of mathematical models of influenza a infections within a host or cell culture: lessons learned and challenges ahead. *BMC Public Health*, 11(Suppl 1):S7.

[29] Beauchemin, C. A., McSharry, J. J., Drusano, G. L., Nguyen, J. T., Went, G. T., Ribeiro, R. M., and Perelson, A. S. (2008). Modeling amantadine treatment of influenza a virus in vitro. *Journal of Theoretical Biology*, 254(2):439–451.

[30] Bedford, T., Rambaut, A., and Pascual, M. (2012). Canalization of the evolutionary trajectory of the human influenza virus. *BMC Biology*, 10(1):38.

[31] Ben-Shachar, R. and Koelle, K. (2014). Minimal within-host dengue models highlight the specific roles of the immune response in primary and secondary dengue infections. *Journal of The Royal Society Interface*, 12.

[32] Bergmann, M., Garcia-Sastre, A., Carnero, E., Pehamberger, H., Wolff, K., Palese, P., and Muster, T. (2000). Influenza Virus NS1 Protein Counteracts PKR-Mediated Inhibition of Replication. *Journal of Virology*, 74(13):6203–6206.

[33] Bernoulli, D. (1760). Essai d'une nouvelle analyse de la mortalité causée par la petite vérole et des avantages de l'inoculation pour la prévenir. *Mém. Math. Phys. Acad. Roy. Sci.*, pages 1–45.

[34] Berthoud, T. K., Hamill, M., Lillie, P. J., Hwenda, L., Collins, K. A., Ewer, K. J., Milicic, A., Poyntz, H. C., Lambe, T., Fletcher, H. A., Hill, A. V. S., and Gilbert, S. C. (2011). Potent CD8+ T-Cell Immunogenicity in Humans of a Novel Heterosubtypic Influenza A Vaccine, MVA–NP+M1. *Clinical Infectious Diseases*, 52(1):1–7.

[35] Blanton, L., Alabi, N., Mustaquim, D., Taylor, C., Kniss, K., Kramer, N., Budd, A., Garg, S., Cummings, C. N., Chung, J., Flannery, B., Fry, A. M., Sessions, W., Garten, R., Xu, X., Elal, A. I. A., Gubareva, L., Barnes, J., Dugan, V., Wentworth, D. E., Burns, E., Katz, J., Jernigan, D., and Brammer, L. (2017). Update: Influenza Activity in the United States During the 2016–17 Season and Composition of the 2017–18 Influenza Vaccine. *MMWR. Morbidity and Mortality Weekly Report*, 66(25):668–676.

[36] Bocharov, G. A. and Romanyukha, A. A. (1994). Mathematical model of antiviral immune response iii. influenza a virus infection. *Journal of Theoretical Biology*, 167:323–360.

[37] Bodewes, R., Kreijtz, J. H. C. M., Geelhoed-Mieras, M. M., van Amerongen, G., Verburgh, R. J., van Trierum, S. E., Kuiken, T., Fouchier, R. A. M., Osterhaus, A. D. M. E., and Rimmelzwaan, G. F. (2011). Vaccination against seasonal influenza a/h3n2 virus reduces the induction of heterosubtypic immunity against influenza a/h5n1 virus infection in ferrets. *Journal of Virology*, 85(6):2695–2702.

[38] Bodewes, R., Morick, D., Mutsert, G. d., Osinga, N., Bestebroer, T., Vliet, S. v. d., Smits, S. L., Kuiken, T., Rimmelzwaan, G. F., Fouchier, R. A., and Osterhaus, A. D. (2013). Recurring Influenza B Virus Infections in Seals. *Emerging Infectious Diseases*, 19(3):511–512.

[39] Boni, M., Gog, J., Andreasen, V., and Feldman, M. (2006). Epidemic dynamics and antigenic evolution in a single season of influenza a. *Proceedings of the Royal Society B: Biological Sciences*, 273(1592):1307–1316.

[40] Boni, M. F. (2008). Vaccination and antigenic drift in influenza. *Vaccine*, 26:C8–C14.

[41] Boni, M. F., Gog, J. R., Andreasen, V., and Christiansen, F. B. (2004). Influenza drift and epidemic size: the race between generating and escaping immunity. *Theoretical Population Biology*, 65(2):179–191.

[42] Bourret, V., Croville, G., Mariette, J., Klopp, C., Bouchez, O., Tiley, L., and Guérin, J.-L. (2013). Whole-genome, deep pyrosequencing analysis of a duck influenza A virus evolution in swine cells. *Infection, Genetics and Evolution*, 18:31–41.

[43] Bourret, V., Lyall, J., Frost, S. D. W., Teillaud, A., Smith, C. A., Leclaire, S., Fu, J., Gandon, S., Guérin, J.-L., and Tiley, L. S. (2017). Adaptation of avian influenza virus to a swine host. *Virus Evolution*, 3(1):vex007.

[44] Bouvier, N. M. and Palese, P. (2008). The Biology of Influenza Viruses. *Vaccine*, 26:D49–D53.

[45] Brass, A. L., Huang, I.-C., Benita, Y., John, S. P., Krishnan, M. N., Feeley, E. M., Ryan, B. J., Weyer, J. L., Weyden, L. v. d., Fikrig, E., Adams, D. J., Xavier, R. J., Farzan, M., and Elledge, S. J. (2009). The IFITM Proteins Mediate Cellular Resistance to Influenza A H1N1 Virus, West Nile Virus, and Dengue Virus. *Cell*, 139(7):1243–1254.

[46] Brauer, F. (2005). The kermack–mckendrick epidemic model revisited. *Mathematical Biosciences*, 198(2):119–131.

[47] Brauer, F. (2008). Epidemic models with heterogeneous mixing and treatment. *B Math Biol*, 70(7):1869–1885.

[48] Brauer, F. (2017a). Mathematical epidemiology: Past, present, and future. *Infectious Disease Modelling*, 2(2):113 – 127.

[49] Brauer, F. (2017b). Mathematical epidemiology: Past, present, and future. *Infectious Disease Modelling*, 2(2):113 – 127.

[50] Bush, R. M., Bender, C. A., Subbarao, K., Cox, N. J., and Fitch, W. M. (1999). Predicting the evolution of human influenza a. *Science*, 286(5446):1921–1925.

[51] Cao, P., Wang, Z., Yan, A. W. C., McVernon, J., Xu, J., Heffernan, J. M., Kedzierska, K., and McCaw, J. M. (2016). On the role of cd8+ t cells in determining recovery time from influenza virus infection. *Frontiers in Immunology*, 7:611.

[52] Carrat, F., Vergu, E., Ferguson, N. M., Lemaitre, M., Cauchemez, S., Leach, S., and Valleron, A.-J. (2008). Time Lines of Infection and Disease in Human Influenza: A Review of Volunteer Challenge Studies. *American Journal of Epidemiology*, 167(7):775–785.

[53] Casagrandi, R., Bolzoni, L., Levin, S. A., and Andreasen, V. (2006). The SIRC model and influenza A. *Mathematical Biosciences*, 200(2):152–169.

[54] Castillo-Chavez, C., Hethcote, H. W., Andreasen, V., Levin, S. A., and Liu, W. M. (1989). Epidemiological models with age structure, proportionate mixing, and cross-immunity. *Journal of Mathematical Biology*, 27(3):233–258.

[55] Cauchemez, S., Valleron, A.-J., Boëlle, P.-Y., Flahault, A., and Ferguson, N. M. (2008). Estimating the impact of school closure on influenza transmission from sentinel data. *Nature*, 452(7188):750.

[56] CDC (2015). Flu vaccination coverage: United States 2014-15 Influenza Season. Technical report.

[57] CDC (2016). Flu vaccination coverage: United States 2015-16 Influenza Season. Technical report.

[58] CDC (2017). Flu vaccination coverage: United States 2016-17 Influenza Season. Technical report.

[59] (CDC), C. f. D. C. and Prevention (2011). Update: influenza activity–United States, 2010-11 season, and composition of the 2011-12 influenza vaccine. *MMWR. Morbidity and mortality weekly report*, 60(21):705–12.

[60] (CDC), C. f. D. C. and Prevention (2012). Update: influenza activity - United States, 2011-12 season and composition of the 2012-13 influenza vaccine. *MMWR. Morbidity and mortality weekly report*, 61(22):414–20.

[61] (CDC), C. f. D. C. and Prevention (2013). Influenza activity–United States, 2012-13 season and composition of the 2013-14 influenza vaccine. *MMWR. Morbidity and mortality weekly report*, 62(23):473–9.

[62] Cella, M., F. F. L. A. . C. M. (2000). Plasmacytoid dendritic cells activated by influenza virus and cd40l drive a potent th1 polarization. *Infectious Disease Modelling*, 1(4):305–310.

[63] Chen, S. C., Chio, C. P., Jou, L. J., and Liao, C. M. (2009). Viral kinetics and exhaled droplet size affect indoor transmission dynamics of influenza infection. *Indoor Air*, 19(5):401–413.

[64] Cifuentes-Muñoz, N., Dutch, R. E., and Cattaneo, R. (2018). Direct cell-to-cell transmission of respiratory viruses: The fast lanes. *PLOS Pathogens*, 14(6):e1007015.

[65] Ciupe, S. M. and Heffernan, J. M. (2017). In-host modeling. *Infectious Disease Modelling*, 2(2):188–202.

[66] Clapham, H. E., Tricou, V., Chau, N. V. V., Simmons, C. P., and Ferguson, N. M. (2014). Within-host viral dynamics of dengue serotype 1 infection. *Journal of The Royal Society Interface*, 11:20140094–20140094.

[67] Conenello, G. M., Zamarin, D., Perrone, L. A., Tumpey, T., and Palese, P. (2007). A single mutation in the PB1-F2 of H5N1 (HK/97) and 1918 influenza A viruses contributes to increased virulence. *PLoS Pathogens*, 3(10):e141.

[68] Coombs, D., Gilchrist, M. A., and Ball, C. L. (2007). Evaluating the importance of within- and between-host selection pressures on the evolution of chronic pathogens. *Theoretical Population Biology*, 72(4):576–591.

[69] Cox, R. J., Brokstad, K. A., and Ogra, P. (2004). Influenza Virus: Immunity and Vaccination Strategies. Comparison of the Immune Response to Inactivated and Live, Attenuated Influenza Vaccines. *Scandinavian Journal of Immunology*, 59(1):1–15.

[70] Crotta, S., Davidson, S., Mahlakoiv, T., Desmet, C. J., Buckwalter, M. R., Albert, M. L., Staeheli, P., and Wack, A. (2013). Type I and Type III Interferons Drive Redundant Amplification Loops to Induce a Transcriptional Signature in Influenza-Infected Airway Epithelia. *PLoS Pathogens*, 9(11):e1003773.

[71] Davlin, S. L., Blanton, L., Kniss, K., Mustaquim, D., Smith, S., Kramer, N., Cohen, J., Cummings, C. N., Garg, S., Flannery, B., Fry, A. M., Grohskopf, L. A., Bresee, J., Wallis, T., Sessions, W., Garten, R., Xu, X., Elal, A. I. A., Gubareva, L., Barnes, J., Wentworth, D. E., Burns, E., Katz, J., Jernigan, D., and Brammer, L. (2016). Influenza Activity - United States, 2015-16 Season and Composition of the 2016-17 Influenza Vaccine. *MMWR. Morbidity and mortality weekly report*, 65(22):567–75.

[72] Deng, Y.-M., Caldwell, N., and Barr, I. G. (2011). Rapid Detection and Subtyping of Human Influenza A Viruses and Reassortants by Pyrosequencing. *PLoS ONE*, 6(8):e23400.

[73] Diebold, S. S., Kaisho, T., Hemmi, H., Akira, S., and Reis e Sousa, C. (2004). Innate antiviral responses by means of tlr7-mediated recognition of single-stranded rna. *Science*, 303(5663):1529–1531.

[74] Diebold, S. S., Montoya, M., Unger, H., Alexopoulou, L., Roy, P., Haswell, L. E., Al-Shamkhani, A., Flavell, R., Borrow, P., and Sousa, C. R. e. (2003). Viral infection switches non-plasmacytoid dendritic cells into high interferon producers. *Nature*, 424(6946):324–328.

[75] Diekman, O. and Heesterbeek, J. A. (2000). Mathematical epidemiology of infectious diseases: model building, analysis and interpretation.

[76] Diekmann, O., Heesterbeek, J. A. P., and Metz, J. A. J. (1990). On the definition and the computation of the basic reproduction ratio R 0 in models for infectious diseases in heterogeneous populations. *Journal of Mathematical Biology*, 28(4):365–382.

[77] Dietz, K. (1974). Transmission and control of arbovirus diseases. *In Proceedings of the Society for Industrial and Applied Mathematics, Epidemiology: Philadelphia*, pages 104–121.

[78] Dietz, K. (1979). Epidemiologic interference of virus populations. *Journal of Mathematical Biology*, 8(3):291–300.

[79] Dietz, K. (1993). The estimation of the basic reproduction number for infectious diseases. *Statistical Methods in Medical Research*, 2(1):23–41.

[80] Dietz, K. and Schenzle, D. (1985). Proportionate mixing models for age-dependent infection transmission. *Journal of Mathematical Biology*, 22(1):117–120.

[81] Diggle, M. A. and Clarke, S. C. (2004). Pyrosequencing™. *Molecular Biotechnology*, 28(2):129–137.

[82] Dixit, N. M. and Perelson, A. S. (2004). Multiplicity of Human Immunodeficiency Virus Infections in Lymphoid Tissue. *Journal of Virology*, 78(16):8942–8945.

[83] Dobrovolny, H. M., Baron, M. J., Gieschke, R., Davies, B. E., Jumbe, N. L., and Beauchemin, C. A. A. (2010). Exploring Cell Tropism as a Possible Contributor to Influenza Infection Severity. *PLoS ONE*, 5(11):e13811.

[84] Dobrovolny, H. M., Reddy, M. B., Kamal, M. A., Rayner, C. R., and Beauchemin, C. A. A. (2013). Assessing mathematical models of influenza infections using features of the immune response. *PLoS ONE*, 8(2):e57088.

[85] Dou, D., Revol, R., Östbye, H., Wang, H., and Daniels, R. (2018). Influenza a virus cell entry, replication, virion assembly and movement. *Frontiers in Immunology*, 9:1581.

[86] Doud, M. B., Lee, J. M., and Bloom, J. D. (2018). How single mutations affect viral escape from broad and narrow antibodies to H1 influenza hemagglutinin. *Nature Communications*, 9(1):1386.

[87] Dowdle, W. R., Galphin, J. C., Coleman, M. T., and Schild, G. C. (1974). A simple double immunodiffusion test for typing influenza viruses. *Bulletin of the World Health Organization*, 51(3):213–5.

[88] Driessche, P. v. d. (2017). Reproduction numbers of infectious disease models. *Infectious Disease Modelling*, 2(3):288–303.

[89] Driessche, P. v. d. and Watmough, J. (2002). Reproduction numbers and subthreshold endemic equilibria for compartmental models of disease transmission. *Mathematical Biosciences*, 180(1-2):29–48.

[90] Earn, D., Dushoff, J., and Levin, S. (2002). Ecology and evolution of the flu. *Trends in Ecology & Evolution*, 17(7):334–340.

[91] Edenborough, K. M., Gilbertson, B. P., and Brown, L. E. (2012). A Mouse Model for the Study of Contact-Dependent Transmission of Influenza A Virus and the Factors That Govern Transmissibility. *Journal of Virology*, 86(23):12544–12551.

[92] El Ramahi, R. and Freifeld, A. (2019). Epidemiology, diagnosis, treatment, and prevention of influenza infection in oncology patients. *Journal of Oncology Practice*, 15(4):177–184.

[93] Elveback, L., Fox, J. P., and Varma, A. (1964). An extension of the reed-frost epidemic model for the study of competition between viral agents in the presence of interference. *American Journal of Epidemiology*, 80(3):356–364.

[94] Engel, D. A. (2013). The influenza virus NS1 protein as a therapeutic target. *Antiviral Research*, 99(3):409–416.

[95] Ennis, F., Yi-Hua, Q., Riley, D., Rook, A., Schild, G., Pratt, R., and Potter, C. (1981). HLA-restricted virus-specific cytotoxic T-lymphocyte responses to live and inactivated influenza vaccines. *The Lancet*, 318(8252):887–891.

[96] Epperson, S., Blanton, L., Kniss, K., Mustaquim, D., Steffens, C., Wallis, T., Dhara, R., Leon, M., Perez, A., Chaves, S. S., Elal, A. A., Gubareva, L., Xu, X., Villanueva, J., Bresee, J., Cox, N., Finelli, L., Brammer, L., CDC, Influenza Division, N. C. f. I., and Diseases, R. (2014). Influenza activity - United States, 2013-14 season and composition of the 2014-15 influenza vaccines. *MMWR. Morbidity and mortality weekly report*, 63(22):483–90.

[97] Feeley, E. M., Sims, J. S., John, S. P., Chin, C. R., Pertel, T., Chen, L.-M., Gaiha, G. D., Ryan, B. J., Donis, R. O., Elledge, S. J., and Brass, A. L. (2011). IFITM3 Inhibits Influenza A Virus Infection by Preventing Cytosolic Entry. *PLoS Pathogens*, 7(10):e1002337.

[98] Ferguson, N. M., Galvani, A. P., and Bush, R. M. (2003). Ecological and immunological determinants of influenza evolution. *Nature*, 422(6930):428.

[99] Fine, P., Eames, K., and Heymann, D. (2011). "Herd immunity": A rough guide. *Clinical Infectious Diseases*, 52(7):911–916.

[100] Flannery, B., Zimmerman, R. K., Gubareva, L. V., Garten, R. J., Chung, J. R., Nowalk, M. P., Jackson, M. L., Jackson, L. A., Monto, A. S., Ohmit, S. E., Belongia, E. A., McLean, H. Q., Gaglani, M., Piedra, P. A., Mishin, V. P., Chesnokov, A. P., Spencer, S., Thaker, S. N., Barnes, J. R., Foust, A., Sessions, W., Xu, X., Katz, J., and Fry, A. M. (2016). Enhanced genetic characterization of influenza a(h3n2) viruses and vaccine effectiveness by genetic group, 2014–2015. *The Journal of Infectious Diseases*, 214(7):1010–1019.

[101] FM, B. (1937). Influenza Virus on the Developing Egg. IV The Pathogenicity and Immunizing Power of Egg Virus for Ferrets and Mice. *Br J Exp Pathol*, 18(1):37–43.

[102] Fonville, J. M., Wilks, S. H., James, S. L., Fox, A., Ventresca, M., Aban, M., Xue, L., Jones, T. C., H, L. N. M., T, P. Q., D, T. N., Wong, Y., Mosterin, A., Katzelnick, L. C., Labonte, D., T, L. T., Net, G. v. d., Skepner, E., Russell, C. A., Kaplan, T. D., Rimmelzwaan, G. F., Masurel, N., Jong, J. C. d., Palache, A., Beyer, W. E. P., M, L. Q., H, N. T., Wertheim, H. F. L., Hurt, A. C., Osterhaus, A. D. M. E., Barr, I. G., Fouchier, R. A. M., Horby, P. W., and Smith, D. J. (2014). Antibody landscapes after influenza virus infection or vaccination. *Science*, 346(6212):996–1000.

[103] Foppa, I. M., Haber, M., Ferdinands, J. M., and Shay, D. K. (2013). The case test-negative design for studies of the effectiveness of influenza vaccine. *Vaccine*, 31(30):3104–3109.

[104] Fouchier, R. A. M., Munster, V., Wallensten, A., Bestebroer, T. M., Herfst, S., Smith, D., Rimmelzwaan, G. F., Olsen, B., and Osterhaus, A. D. M. E. (2005). Characterization of a Novel Influenza A Virus Hemagglutinin Subtype (H16) Obtained from Black-Headed Gulls. *Journal of Virology*, 79(5):2814–2822.

[105] Francis, M. E., King, M. L., and Kelvin, A. A. (2019). Back to the Future for Influenza Preimmunity—Looking Back at Influenza Virus History to Infer the Outcome of Future Infections. *Viruses*, 11(2):122.

[106] Francis, T. and Getting, V. A. (1947). The present status of vaccination against influenza. *American Journal of Public Health and the Nation's Health*, 37(9):1109–12.

[107] Francis Thomas, J. and Magill, T. P. (1936). Vaccination of human subjects with virus of human influenza. *Proceedings of the Society for Experimental Biology and Medicine*, 33(4):604–606.

[108] Frost, S. D., Pybus, O. G., Gog, J. R., Viboud, C., Bonhoeffer, S., and Bedford, T. (2014). Eight challenges in phylodynamic inference. *Epidemics*.

[109] Fukushima, W. and Hirota, Y. (2017). Basic principles of test-negative design in evaluating influenza vaccine effectiveness. *Vaccine*, 35(36):4796–4800.

[110] Fukuyama, S., Katsura, H., Zhao, D., Ozawa, M., Ando, T., Shoemaker, J. E., Ishikawa, I., Yamada, S., Neumann, G., Watanabe, S., Kitano, H., and Kawaoka, Y. (2015). Multi-spectral fluorescent reporter influenza viruses (color-flu) as powerful tools for in vivo studies. *Nature Communications*, 6(1):6600.

[111] Gallagher, M. E., Brooke, C. B., Ke, R., and Koelle, K. (2018). Causes and consequences of spatial within-host viral spread. *Viruses*, 10(11):627.

[112] Ganti, K., Bagga, A., DaSilva, J., Shepard, S. S., Barnes, J. R., Shriner, S., Koelle, K., and Lowen, A. C. (2021). Avian Influenza A Viruses Reassort and Diversify Differently in Mallards and Mammals. *Viruses*, 13(3):509.

[113] García-Sastre, A. (2002). Mechanisms of inhibition of the host interferon /-mediated antiviral responses by viruses. *Microbes and Infection*, 4(6):647–655.

[114] García-Sastre, A., Egorov, A., Matassov, D., Brandt, S., Levy, D. E., Durbin, J. E., Palese, P., and Muster, T. (1998). Influenza A Virus Lacking the NS1 Gene Replicates in Interferon-Deficient Systems. *Virology*, 252(2):324–330.

[115] Garira, W. (2017). A complete categorization of multiscale models of infectious disease systems. *Journal of Biological Dynamics*, 11(1):378–435.

[116] Garten, R., Blanton, L., Elal, A. I. A., Alabi, N., Barnes, J., Biggerstaff, M., Brammer, L., Budd, A. P., Burns, E., Cummings, C. N., Davis, T., Garg, S., Gubareva, L., Jang, Y., Kniss, K., Kramer, N., Lindstrom, S., Mustaquim, D., O'Halloran, A., Sessions, W., Taylor, C., Xu, X., Dugan, V. G., Fry, A. M., Wentworth, D. E., Katz, J., and Jernigan, D. (2018). Update: Influenza Activity in the United States During the 2017–18 Season and Composition of the 2018–19 Influenza Vaccine. *Morbidity and Mortality Weekly Report*, 67(22):634–642.

[117] Gerhard, W., Yewdell, J., Frankel, M. E., and Webster, R. (1981). Antigenic structure of influenza virus haemagglutinin defined by hybridoma antibodies. *Nature*, 290(5808):713–717.

[118] Ghedin, E., Fitch, A., Boyne, A., Griesemer, S., DePasse, J., Bera, J., Zhang, X., Halpin, R. A., Smit, M., Jennings, L., George, K. S., Holmes, E. C., and Spiro, D. J. (2009). Mixed infection and the genesis of influenza virus diversity. *Journal of Virology*, 83(17):8832–8841.

[119] Gilchrist, M. A. and Coombs, D. (2006). Evolution of virulence: Interdependence, constraints, and selection using nested models. *Theoretical Population Biology*, 69(2):145–153.

[120] Gog, J. (2008). The impact of evolutionary constraints on influenza dynamics. *Vaccine*, 26:C15–C24.

[121] Gog, J. R. and Grenfell, B. T. (2002). Dynamics and selection of many-strain pathogens. *Proceedings of the National Academy of Sciences*, 99(26):17209–14.

[122] Gog, J. R., Pellis, L., Wood, J. L., McLean, A. R., Arinaminpathy, N., and Lloyd-Smith, J. O. (2015). Seven challenges in modeling pathogen dynamics within-host and across scales. *Epidemics*, 10:45–48.

[123] Gregory, V., Bennett, M., Orkhan, M., Hajjar, S. A., Varsano, N., Mendelson, E., Zambon, M., Ellis, J., Hay, A., and Lin, Y. (2002). Emergence of Influenza A H1N2 Reassortant Viruses in the Human Population during 2001. *Virology*, 300(1):1–7.

[124] Grenfell, B. and Harwood, J. (1997). (Meta)population dynamics of infectious diseases. *Trends in Ecology & Evolution*, 12(10).

[125] Grenfell, B. T., Pybus, O. G., Gog, J. R., Wood, J. L., Daly, J. M., Mumford, J. A., and Holmes, E. C. (2004). Unifying the epidemiological and evolutionary dynamics of pathogens. *Science*, 303(5656):327–332.

[126] Gupta, S. and Day, K. (1994). A strain theory of malaria transmission. *Parasitology Today*, 10(12):476–481.

[127] Gupta, S., Ferguson, N., and Anderson, R. (1998). Chaos, Persistence, and Evolution of Strain Structure in Antigenically Diverse Infectious Agents. *Science*, 280(5365):912–915.

[128] Gupta, S., Maiden, M. C. J., Feavers, I. M., Nee, S., May, R. M., and Anderson, R. M. (1996). The maintenance of strain structure in populations of recombining infectious agents. *Nature Medicine*, 2(4):437–442.

[129] Gupta, S., Trenholme, K., Anderson, R., and Day, K. (1994). Antigenic diversity and the transmission dynamics of Plasmodium falciparum. *Science*, 263(5149):961–963.

[130] Gutierrez, J. B., Galinski, M. R., Cantrell, S., and Voit, E. O. (2015). From within host dynamics to the epidemiology of infectious disease: Scientific overview and challenges. *Mathematical Biosciences*, 270(Pt B):143–155.

[131] Hadjichrysanthou, C., Cauet, E., Lawrence, E., Vegvari, C., de Wolf, F., and Anderson, R. M. (2005). Understanding the within-host dynamics of influenza a virus: from theory to clinical implications. *Journal of The Royal Society Interface*, 13(19).

[132] Hak, E., Hoes, A., and Verheij, T. (2002). Influenza vaccinations. *Drugs*, 62(17):2413–2420.

[133] Haller, O., Arnheiter, H., Lindenmann, J., and Gresser, I. (1980). Host gene influences sensitivity to interferon action selectively for influenza virus. *Nature*, 283(5748):660–662.

[134] Halloran, S. K., Wexler, A. S., and Ristenpart, W. D. (2012). A Comprehensive Breath Plume Model for Disease Transmission via Expiratory Aerosols. *PLoS ONE*, 7(5):e37088.

[135] Hamilton, J. R., Sachs, D., Lim, J. K., Langlois, R. A., Palese, P., and Heaton, N. S. (2016). Club cells surviving influenza a virus infection induce temporary nonspecific antiviral immunity. *Proceedings of the National Academy of Sciences*, 113(14):3861–3866.

[136] Hancioglu, B., Swigon, D., and Clermont, G. (2007). A dynamical model of human immune response to influenza A virus infection. *Journal of Theoretical Biology*, 246(1):70–86.

[137] Handel, A., Brown, J., Stallknecht, D., and Rohani, P. (2013). A multi-scale analysis of influenza a virus fitness trade-offs due to temperature-dependent virus persistence. *PLoS Computational Biology*, 9(3):e1002989.

[138] Handel, A., Lebarbenchon, C., Stallknecht, D., and Rohani, P. (2014). Trade-offs between and within scales: environmental persistence and within-host fitness of avian influenza viruses. *Proceedings of the Royal Society B: Biological Sciences*, 281(1787):20133051.

[139] Handel, A., Li, Y., McKay, B., Pawelek, K. A., Zarnitsyna, V., and Antia, R. (2018). Exploring the impact of inoculum dose on host immunity and morbidity to inform model-based vaccine design. *PLOS Computational Biology*, 14(10):e1006505.

[140] Handel, A., Longini, I. M., and Antia, R. (2007). Neuraminidase Inhibitor Resistance in Influenza: Assessing the Danger of Its Generation and Spread. *PLoS Computational Biology*, 3(12):e240.

[141] Handel, A., Longini, I. M., and Antia, R. (2010). Towards a quantitative understanding of the within-host dynamics of influenza A infections. *Journal of The Royal Society Interface*, 7(42):35–47.

[142] Handel, A. and Rohani, P. (2015). Crossing the scale from within-host infection dynamics to between-host transmission fitness: a discussion of current assumptions and knowledge. *Philosophical Transactions of the Royal Society B*, 370.

[143] Hartfield, M. and Alizon, S. (2014). Epidemiological feedbacks affect evolutionary emergence of pathogens. *The American Naturalist*, 183(4):E105–E117.

[144] Hartfield, M. and Alizon, S. (2015). Within-host stochastic emergence dynamics of immune-escape mutants. *PLOS Computational Biology*, 11(3):e1004149.

[145] Hatada, E. and Fukuda, R. (1992). Binding of influenza A virus NS1 protein to dsRNA in vitro. *Journal of General Virology*, (73):3325–3329.

[146] Hause, B. M., Ducatez, M., Collin, E. A., Ran, Z., Liu, R., Sheng, Z., Armien, A., Kaplan, B., Chakravarty, S., Hoppe, A. D., Webby, R. J., Simonson, R. R., and Li, F. (2013). Isolation of a Novel Swine Influenza Virus from Oklahoma in 2011 Which Is Distantly Related to Human Influenza C Viruses. *PLoS Pathogens*, 9(2):e1003176.

[147] Hayward, A. C., Wang, L., Goonetilleke, N., Fragaszy, E. B., Bermingham, A., Copas, A., Dukes, O., Millett, E. R. C., Nazareth, I., Nguyen-Van-Tam, J. S., Watson, J. M., Zambon, M., Group, F. W., Johnson, A. M., and McMichael, A. J. (2015). Natural T Cell–mediated Protection against Seasonal and Pandemic Influenza. Results of the Flu Watch Cohort Study. *American Journal of Respiratory and Critical Care Medicine*, 191(12):1422–1431.

[148] Heesterbeek, J. (2002). A Brief History of <Emphasis Type= Italic >R</Emphasis> <Subscript>0</Subscript> and a Recipe for its Calculation. *Acta Biotheoretica*, 50(3):189–204.

[149] Heesterbeek, J. A. P. and Dietz, K. (1996). The concept of Ro in epidemic theory. *Statistica Neerlandica*, 50(1):89–110.

[150] Hirst, G. K. (1943). Studies of antigenic differences among strains of influenza A by means of red cell agglutination . *Journal of Experimental Medicine*, 78(5):407–423.

[151] Holmes, E. C., Ghedin, E., Miller, N., Taylor, J., Bao, Y., George, K. S., Grenfell, B. T., Salzberg, S. L., Fraser, C. M., Lipman, D. J., and Taubenberger, J. K. (2005). Whole-Genome Analysis of Human Influenza A Virus Reveals Multiple Persistent Lineages and Reassortment among Recent H3N2 Viruses. *PLoS Biology*, 3(9):e300.

[152] Hutchinson, E. C., Charles, P. D., Hester, S. S., Thomas, B., Trudgian, D., Martínez-Alonso, M., and Fodor, E. (2014). Conserved and host-specific features of influenza virion architecture. *Nature Communications*, 5(1):4816.

[153] Isaacs, A. and Lindenmann, J. (1957). Virus Interference. I. The interferon. *Proceedings of the Royal Society B: Biological Sciences*, 147(927):258–267.

[154] Ivashkiv, L. B. and Donlin, L. T. (2014). Regulation of type I interferon responses. *Nature Reviews Immunology*, 14(1):36–49.

[155] Jacobs, B. L. and O, L. J. (1996). When two strands are better than one: The mediators and modulators of the cellular responses to double-stranded rna. *Virology*, 219(2):339–349.

[156] Jego, G., Palucka, A., Blanck, J.-P., Chalouni, C., Pascual, V., and Banchereau, J. (2003). Plasmacytoid Dendritic Cells Induce Plasma Cell Differentiation through Type I Interferon and Interleukin 6. *Immunity*, 19(2):225–234.

[157] Jin, H. and Chen, Z. (2014). Production of live attenuated influenza vaccines against seasonal and potential pandemic influenza viruses. *Current Opinion in Virology*, 6:34–39.

[158] Johnson, N. P. A. S. and Mueller, J. (2002). Updating the Accounts: Global Mortality of the 1918-1920 "Spanish" Influenza Pandemic. *Bulletin of the History of Medicine*, 76(1):105–115.

[159] Julkunen, I., Melén, K., Nyqvist, M., Pirhonen, J., Sareneva, T., and Matikainen, S. (2000). Inflammatory responses in influenza a virus infection. *Vaccine*, 19:S32–S37.

[160] Keeling, M. and Shattock, A. (2012). Optimal but unequitable prophylactic distribution of vaccine. *Epidemics*, 4(2):78–85.

[161] Keeling, M. J. and Rohani, P. (2007). *Modeling Infectious Diseases in Humans and Animals*. Princeton University Press.

[162] Kendall, W. S. and Saunders, I. W. (1983). Epidemics in competition II: the general epidemic. *Journal of the Royal Statistical Society Series B*, 45(2):238–244.

[163] Kermack, W. O. and McKendrick, A. G. (1927). A contribution to the mathematical theory of epidemics. *Proceedings of the Royal Society A*, 115(772):700–721.

[164] Kermack, W. O. and McKendrick, A. G. (1932). Contributions to the mathematical theory of epidemics. ii. —the problem of endemicity. *Proceedings of the Royal Society A*, 138(834):55–83.

[165] Kermack, W. O. and McKendrick, A. G. (1933). Contributions to the mathematical theory of epidemics. iii.—further studies of the problem of endemicity. *Proceedings of the Royal Society A*, 141(843):94–122.

[166] Kilbourne, E. D. (2006). Influenza pandemics of the 20th century. *Emerging Infectious Diseases*, 12(1):9–14.

[167] Killip, M. J., Fodor, E., and Randall, R. E. (2015). Influenza virus activation of the interferon system. *Virus Research*, 209:11–22.

[168] Koel, B. F., Mögling, R., Chutinimitkul, S., Fraaij, P. L., Burke, D. F., Vliet, S. v. d., Wit, E. d., Bestebroer, T. M., Rimmelzwaan, G. F., Osterhaus, A. D. M. E., Smith, D. J., Fouchier, R. A. M., and Graaf, M. d. (2015). Identification of Amino Acid Substitutions Supporting Antigenic Change of Influenza A(H1N1)pdm09 Viruses. *Journal of Virology*, 89(7):3763–3775.

[169] Koelle, K., Cobey, S., Grenfell, B., and Pascual, M. (2006). Epochal Evolution Shapes the Phylodynamics of Interpandemic Influenza A (H3N2) in Humans. *Science*, 314(5807):1898–1903.

[170] Koelle, K., Farrell, A. P., Brooke, C. B., and Ke, R. (2019). Within-host infectious disease models accommodating cellular coinfection, with an application to influenza. *Virus Evolution*, 5(2):vez018.

[171] Koelle, K., Khatri, P., Kamradt, M., and Kepler, T. B. (2010). A two-tiered model for simulating the ecological and evolutionary dynamics of rapidly evolving viruses, with an application to influenza. *Journal of The Royal Society Interface*, 7(50):1257–1274.

[172] Koelle, K. and Rasmussen, D. A. (2015). The effects of a deleterious mutation load on patterns of influenza A/H3N2's antigenic evolution in humans. *eLife*, 4:e07361.

[173] Komarova, N. L., Levy, D. N., and Wodarz, D. (2012). Effect of Synaptic Transmission on Viral Fitness in HIV Infection. *PLoS ONE*, 7(11):e48361.

[174] Korenkov, D., Isakova-Sivak, I., and Rudenko, L. (2018). Basics of CD8 T-cell immune responses after influenza infection and vaccination with inactivated or live attenuated influenza vaccine. *Expert Review of Vaccines*, 17(11).

[175] Koyama, S., Ishii, K. J., Kumar, H., Tanimoto, T., Coban, C., Uematsu, S., Kawai, T., and Akira, S. (2007). Differential Role of TLR- and RLR-Signaling in the Immune Responses to Influenza A Virus Infection and Vaccination. *The Journal of Immunology*, 179(7):4711–4720.

[176] Kribs-Zaleta, C. and Velasco-Hernández, J. (2000). A simple vaccination model with multiple endemic states. *Mathematical Biosciences*, 164(2):183–201.

[177] Kucharski, A. J., Andreasen, V., and Gog, J. R. (2016). Capturing the dynamics of pathogens with many strains. *Journal of Mathematical Biology*, 72:1–24.

[178] Kucharski, A. J. and Baguelin, M. (2017). The role of human immunity and social behavior in shaping influenza evolution. *PLOS Pathogens*, 13(8):e1006432.

[179] Kunisaki, K. M. and Janoff, E. N. (2009). Influenza in immunosuppressed populations: a review of infection frequency, morbidity, mortality, and vaccine responses. *The Lancet. Infectious diseases*, 9(8):493–504.

[180] Lambert, L. C. and Fauci, A. S. (2010). Influenza Vaccines for the Future. *New England Journal of Medicine*, 363(21):2036–2044.

[181] Lampson, G. P., Tytell, A. A., Field, A. K., Nemes, M. M., and Hilleman, M. R. (1967). Inducers of interferon and host resistance. I. Double-stranded RNA from extracts of Penicillium funiculosum. *Proceedings of the National Academy of Sciences*, 58(2):782–789.

[182] Larson, E. W., Dominik, J. W., Rowberg, A. H., and Higbee, G. A. (1976). Influenza virus population dynamics in the respiratory tract of experimentally infected mice. *Infection and immunity*, 13(2):438–47.

[183] Laurie, K. L., Guarnaccia, T. A., Carolan, L. A., Yan, A. W. C., Aban, M., Petrie, S., Cao, P., Heffernan, J. M., McVernon, J., Mosse, J., Kelso, A., McCaw, J. M., and Barr, I. G. (2015). Interval Between Infections and Viral Hierarchy Are Determinants of Viral Interference Following Influenza Virus Infection in a Ferret Model. *Journal of Infectious Diseases*, 212(11):1701–1710.

[184] Laver, W. G., Air, G. M., Webster, R. G., Gerhard, W., Ward, C. W., and Dopheide, T. A. A. (1979). Antigenic drift in type A influenza virus: Sequence differences in the hemagglutinin of Hong Kong (H3N2) variants selected with monoclonal hybridoma antibodies. *Virology*, 98(1):226–237.

[185] Lee, H. Y., Topham, D. J., Park, S. Y., Hollenbaugh, J., Treanor, J., Mosmann, T. R., Jin, X., Ward, B. M., Miao, H., Holden-Wiltse, J., Perelson, A. S., Zand, M., and Wu, H. (2009a). Simulation and Prediction of the Adaptive Immune Response to Influenza A Virus Infection. *Journal of Virology*, 83(14):7151–7165.

[186] Lee, N., Chan, P. K. S., Hui, D. S. C., Rainer, T. H., Wong, E., Choi, K., Lui, G. C. Y., Wong, B. C. K., Wong, R. Y. K., Lam, W., Chu, I. M. T., Lai, R. W. M., Cockram, C. S., and Sung, J. J. Y. (2009b). Viral Loads and Duration of Viral Shedding in Adult Patients Hospitalized with Influenza. *The Journal of Infectious Diseases*, 200(4):492–500.

[187] Leung, N. H. L., Chu, D. K. W., Shiu, E. Y. C., Chan, K.-H., McDevitt, J. J., Hau, B. J. P., Yen, H.-L., Li, Y., Ip, D. K. M., Peiris, J. S. M., Seto, W.-H., Leung, G. M., Milton, D. K., and Cowling, B. J. (2020). Respiratory virus shedding in exhaled breath and efficacy of face masks. *Nature Medicine*, pages 1–5.

[188] Levin, S. and Pimentel, D. (1981). Selection of Intermediate Rates of Increase in Parasite-Host Systems. *The American Naturalist*, 117(3):308–315.

[189] Lillie, P. J., Berthoud, T. K., Powell, T. J., Lambe, T., Mullarkey, C., Spencer, A. J., Hamill, M., Peng, Y., Blais, M.-E., Duncan, C. J. A., Sheehy, S. H., Havelock, T., Faust, S. N., Williams, R. L., Gilbert, A., Oxford, J., Dong, T., Hill, A. V. S., and Gilbert, S. C. (2012). Preliminary Assessment of the Efficacy of a T-Cell–Based Influenza Vaccine, MVA-NP+M1, in Humans. *Clinical Infectious Diseases*, 55(1):19–25.

[190] Lin, J., Andreasen, V., and Levin, S. A. (1999a). Dynamics of influenza A drift: the linear three-strain model. *Mathematical Biosciences*, 162(1-2):33–51.

[191] Lin, J., Andreasen, V., and Levin, S. A. (1999b). Dynamics of influenza A drift: the linear three-strain model. *Mathematical Biosciences*, 162(1-2):33–51.

[192] Lipsitch, M. (2001). The rise and fall of antimicrobial resistance. *Trends in Microbiology*, 9(9):438–444.

[193] Lipsitch, M., Colijn, C., Cohen, T., Hanage, W. P., and Fraser, C. (2009). No coexistence for free: Neutral null models for multistrain pathogens. *Epidemics*, 1(1):2–13.

[194] Liu, X., Takeuchi, Y., and Iwami, S. (2008). SVIR epidemic models with vaccination strategies. *Journal of Theoretical Biology*, 253(1):1 – 11.

[195] Lloyd, A. L. (2001). The dependence of viral parameter estimates on the assumed viral life cycle: limitations of studies of viral load data. *Proceedings of the Royal Society of London. Series B: Biological Sciences*, 268(1469):847–854.

[196] Lofgren, E., Fefferman, N., Naumov, Y., Gorski, J., and Naumova, E. (2007). Influenza seasonality: Underlying causes and modeling theories. *Journal of Virology*, 81(11):5429–5436.

[197] Lorenzo, M. M. G. and Fenton, M. J. (2013). Immunobiology of Influenza Vaccines. *Chest*, 143(2):502–510.

[198] Luciani, F. and Alizon, S. (2009). The evolutionary dynamics of a rapidly mutating virus within and between hosts: The case of hepatitis c virus. *PLoS Computational Biology*, 5(11):e1000565.

[199] Luo, S., Reed, M., Mattingly, J. C., and Koelle, K. (2012). The impact of host immune status on the within-host and population dynamics of antigenic immune escape. *Journal of The Royal Society Interface*, 9(75):2603–2613.

[200] Lyons, D. M. and Lauring, A. S. (2018). Mutation and epistasis in influenza virus evolution. *Viruses*, 10(8):407.

[201] Lythgoe, K. A., Pellis, L., and Fraser, C. (2013). Is HIV short-sighted? Insights from a multistrain nested model. *Evolution*, 67(10):2769–2782.

[202] Macdonald, G. (1952). The analysis of equilibrium in malaria. *Tropical Diseases Bulletin*, 49(9):813–29.

[203] Mameli, C., Cocchi, I., Fumagalli, M., and Zuccotti, G. (2019). Influenza Vaccination: Effectiveness, Indications, and Limits in the Pediatric Population. *Frontiers in Pediatrics*, 7:317.

[204] Margine, I., Krammer, F., Hai, R., Heaton, N. S., Tan, G. S., Andrews, S. A., Runstadler, J. A., Wilson, P. C., Albrecht, R. A., García-Sastre, A., and Palese, P. (2013). Hemagglutinin Stalk-Based Universal Vaccine Constructs Protect against Group 2 Influenza A Viruses. *Journal of Virology*, 87(19):10435–10446.

[205] Martcheva, M., Lenhart, S., Eda, S., Klinkenberg, D., Momotani, E., and Stabel, J. (2015). An immuno-epidemiological model for Johne's disease in cattle. *Veterinary Research*, 46(1):69.

[206] May, R. M. and Nowak, M. A. (1995). Coinfection and the evolution of parasite virulence. *Proceedings. Biological sciences / The Royal Society*, 261(1361):209–15.

[207] McAuley, J. L., Gilbertson, B. P., Trifkovic, S., Brown, L. E., and McKimm-Breschkin, J. L. (2019). Influenza virus neuraminidase structure and functions. *Frontiers in Microbiology*, 10:39.

[208] McCrone, J. T., Woods, R. J., Martin, E. T., Malosh, R. E., Monto, A. S., and Lauring, A. S. (2018). Stochastic processes constrain the within and between host evolution of influenza virus. *eLife*, 7:e35962.

[209] Mcmichael, A., Dongworth, D., Gotch, F., Clark, A., and Potter, C. (1983). Declining t-cell immunity to influenza, 1977-82. *The Lancet*, 322(8353):762–764. Originally published as Volume 2, Issue 8353.

[210] Mideo, N., Alizon, S., and Day, T. (2008). Linking within- and between-host dynamics in the evolutionary epidemiology of infectious diseases. *Trends in Ecology & Evolution*, 23(9):511–517.

[211] Mohler, L., Flockerzi, D., Sann, H., and Reichl, U. (2005). Mathematical model of influenza a virus production in large-scale microcarrier culture. *Biotechnology and Bioengineering*, 90(1):46–58.

[212] Morens, D., Taubenberger, J., Harvey, H., and Memoli, M. (2010). The 1918 influenza pandemic: Lessons for 2009 and the future. *Critical Care Medicine*, 38:e10.

[213] Murillo, L. N., Murillo, M. S., and Perelson, A. S. (2013). Towards multiscale modeling of influenza infection. *Journal of Theoretical Biology*, 332:267–90.

[214] Nelson, M. I., Simonsen, L., Viboud, C., Miller, M. A., Taylor, J., George, K. S., Griesemer, S. B., Ghedin, E., Sengamalay, N. A., Spiro, D. J., Volkov, I., Grenfell, B. T., Lipman, D. J., Taubenberger, J. K., and Holmes, E. C. (2006). Stochastic processes are key determinants of short-term evolution in influenza a virus. *PLoS Pathogens*, 2(12):e125.

[215] Nichol, K. L., Nordin, J. D., Nelson, D. B., Mullooly, J. P., and Hak, E. (2007). Effectiveness of Influenza Vaccine in the Community-Dwelling Elderly. *The New England Journal of Medicine*, 357(14):1373–1381.

[216] Nobusawa, E. and Sato, K. (2006). Comparison of the Mutation Rates of Human Influenza A and B Viruses. *Journal of Virology*, 80(7):3675–3678.

[217] Noda, T. and Kawaoka, Y. (2010). Structure of influenza virus ribonucleoprotein complexes and their packaging into virions. *Reviews in Medical Virology*, 20(6):380–391.

[218] Nowak, M. A., Bonhoeffer, S., Hill, A. M., Boehme, R., Thomas, H. C., and McDade, H. (1996). Viral dynamics in hepatitis b virus infection. *Proceedings of the National Academy of Sciences*, 93(9):4398–4402.

[219] Nowak, M. A. and May, R. M. (1994). Superinfection and the evolution of parasite virulence. *Proceedings. Biological sciences / The Royal Society*, 255(1342):81–9.

[220] Oslund, K. L. and Baumgarth, N. (2011). Influenza-induced innate immunity: regulators of viral replication, respiratory tract pathology and adaptive immunity. *Future Virology*, 8(6):951–962.

[221] Osterholm, M. T., Kelley, N. S., Sommer, A., and Belongia, E. A. (2012). Efficacy and effectiveness of influenza vaccines: a systematic review and meta-analysis. *The Lancet Infectious Diseases*, 12(1):36–44.

[222] Padilla-Quirarte, H. O., Lopez-Guerrero, D. V., Gutierrez-Xicotencatl, L., and Esquivel-Guadarrama, F. (2019). Protective Antibodies Against Influenza Proteins. *Frontiers in Immunology*, 10:1677.

[223] Panda, S. and Ding, J. L. (2015). Natural antibodies bridge innate and adaptive immunity. *The Journal of Immunology*, 194(1):13–20.

[224] Park, M., Loverdo, C., Schreiber, S. J., and Lloyd-Smith, J. O. (2013). Multiple scales of selection influence the evolutionary emergence of novel pathogens. *Philosophical Transactions of the Royal Society B: Biological Sciences*, 368(1614):20120333.

[225] Parvin, J. D., Moscona, A., Pan, W. T., Leider, J. M., and Palese, P. (1986). Measurement of the mutation rates of animal viruses: influenza A virus and poliovirus type 1. *Journal of virology*, 59(2):377–83.

[226] Pawelek, K. A., Huynh, G. T., Quinlivan, M., Cullinane, A., Rong, L., and Perelson, A. S. (2012). Modeling within-host dynamics of influenza virus infection including immune responses. *PLoS Computational Biology*, 8(6):e1002588.

[227] Pearson, J. E., Krapivsky, P., and Perelson, A. S. (2011). Stochastic theory of early viral infection: Continuous versus burst production of virions. *PLoS Computational Biology*, 7(2):e1001058.

[228] Pease, C. M. (1987). An evolutionary epidemiological mechanism, with applications to type a influenza. *Theoretical Population Biology*, 31(3):422 – 452.

[229] Peck, K. M., Chan, C. H. S., and Tanaka, M. M. (2015). Connecting within-host dynamics to the rate of viral molecular evolution. *Virus Evolution*, 1(1):vev013.

[230] Perelson, A. S., Kirschner, D. E., and Boer, R. D. (1993). Dynamics of HIV infection of CD4+ T cells. *Mathematical Biosciences*, 114:81–125.

[231] Perelson, A. S. and Ribeiro, R. M. (2013). Modeling the within-host dynamics of hiv infection. *BMC Biology*, 11(1):96.

[232] Petrie, S. M., Butler, J., Barr, I. G., McVernon, J., Hurt, A. C., and McCaw, J. M. (2015). Quantifying relative within-host replication fitness in influenza virus competition experiments. *Journal of Theoretical Biology*, 382(J. Virol. 76 18 2002):259–271.

[233] Phan, D. and Wodarz, D. (2015). Modeling multiple infection of cells by viruses: Challenges and insights. *Mathematical Biosciences*, 264:21–28.

[234] Pichlmair, A., Schulz, O., Tan, C. P., Näslund, T. I., Liljeström, P., Weber, F., and Sousa, C. R. e. (2006). RIG-I-Mediated Antiviral Responses to Single-Stranded RNA Bearing 59-Phosphates. *Science*, 314(5801):997–1001.

[235] Pinky, L. and Dobrovolny, H. M. (2016). Coinfections of the Respiratory Tract: Viral Competition for Resources. *PLOS One*, 11(5):e0155589.

[236] Pompei, S., Loreto, V., and Tria, F. (2012). Phylogenetic properties of RNA viruses. *PLOS One*, 7(9):e44849.

[237] Poon, L. L. M., Song, T., Rosenfeld, R., Lin, X., Rogers, M. B., Zhou, B., Sebra, R., Halpin, R. A., Guan, Y., Twaddle, A., DePasse, J. V., Stockwell, T. B., Wentworth, D. E., Holmes, E. C., Greenbaum, B., Peiris, J. S. M., Cowling, B. J., and Ghedin, E. (2016). Quantifying influenza virus diversity and transmission in humans. *Nature Genetics*, 48(2):195–200.

[238] Price, G. E., Lo, C.-Y., Misplon, J. A., and Epstein, S. L. (2014). Mucosal Immunization with a Candidate Universal Influenza Vaccine Reduces Virus Transmission in a Mouse Model. *Journal of Virology*, 88(11):6019–6030.

[239] Price, G. E., Soboleski, M. R., Lo, C.-Y., Misplon, J. A., Pappas, C., Houser, K. V., Tumpey, T. M., and Epstein, S. L. (2009). Vaccination focusing immunity on conserved antigens protects mice and ferrets against virulent H1N1 and H5N1 influenza A viruses. *Vaccine*, 27(47):6512–6521.

[240] Public Health England (2018). Seasonal influenza vaccine uptake in GP patients -Winter 2018 to 2019. Technical report.

[241] Public Health England (2019). Surveillance of influenza and other respiratory viruses in the UK-Winter 2018 to 2019. Technical report.

[242] Public Health England (2020a). Seasonal influenza vaccine uptake in children of primary school age -Winter 2018 to 2019. Technical report.

[243] Public Health England (2020b). Seasonal influenza vaccine uptake in GP patients: winter 2019 to 2020. Technical report.

[244] Public Health England (2020c). Seasonal influenza vaccine uptake in healthcare workers (HCWs) in england: winter season 2019 to 2020. Technical report.

[245] Rahman, S. and Zou, X. (2011). Flu epidemics: a two-strain flu model with a single vaccination. *Journal of Biological Dynamics*, 5(5):376–390.

[246] Rambaut, A., Pybus, O. G., Nelson, M. I., Viboud, C., Taubenberger, J. K., and Holmes, E. C. (2008). The genomic and epidemiological dynamics of human influenza A virus. *Nature*, 453(7195):615–619.

[247] Randall, R. E. and Goodbourn, S. (2008). Interferons and viruses: an interplay between induction, signalling, antiviral responses and virus countermeasures. *Journal of General Virology*, 89(1):1–47.

[248] Read, J. M. and Keeling, M. J. (2006). Disease evolution across a range of spatio-temporal scales. *Theoretical Population Biology*, 70(2):201–213.

[249] Recker, M., Pybus, O. G., Nee, S., and Gupta, S. (2007). The generation of influenza outbreaks by a network of host immune responses against a limited set of antigenic types. *Proceedings of the National Academy of Sciences*, 104(18):7711–7716.

[250] Regenmortel, M. V. (2007). Virus species and virus identification: Past and current controversies. *Infection, Genetics and Evolution*, 7(1):133–144.

[251] Reperant, L. A., Grenfell, B. T., and Osterhaus, A. D. (2015). Quantifying the risk of pandemic influenza virus evolution by mutation and re-assortment. *Vaccine*, 33(49):6955–6966.

[252] Reperant, L. A., Kuiken, T., Grenfell, B. T., and Osterhaus, A. D. M. E. (2014). The immune response and within-host emergence of pandemic influenza virus. *The Lancet*, 384(9959):2077–2081.

[253] Reperant, L. A., Kuiken, T., Grenfell, B. T., Osterhaus, A. D. M. E., and Dobson, A. P. (2012). Linking influenza virus tissue tropism to population-level reproductive fitness. *PLOS One*, 7(8):e43115.

[254] Restif, O. (2009). Evolutionary epidemiology 20 years on: Challenges and prospects. *Infection, Genetics and Evolution*, 9(1):108–123.

[255] Restif, O. and Grenfell, B. T. (2006). Integrating life history and cross-immunity into the evolutionary dynamics of pathogens. *Proceedings of the Royal Society B: Biological Sciences*, 273(1585):409–416.

[256] Roberts, K. L., Manicassamy, B., Lamb, R. A., and Lyles, D. S. (2015). Influenza a virus uses intercellular connections to spread to neighboring cells. *Journal of Virology*, 89(3):1537–1549.

[257] Rodriguez, L., Blanco-Lobo, P., Reilly, E. C., Maehigashi, T., Nogales, A., Smith, A., Topham, D. J., Dewhurst, S., Kim, B., and Martínez-Sobrido, L. (2019). Comparative Study of the Temperature Sensitive, Cold Adapted and Attenuated Mutations Present in the Master Donor Viruses of the Two Commercial Human Live Attenuated Influenza Vaccines. *Viruses*, 11(10):928.

[258] Ronaghi, M. (2001). Pyrosequencing Sheds Light on DNA Sequencing. *Genome Research*, 11(1):3–11.

[259] Ross, R. (1916). An application of the theory of probabilities to the study of a priori pathometry. part i. *Proceedings of the Royal Society A*, 92(638):204–230.

[260] Ross, R. and Hudson, H. P. (1917). An application of the theory of probabilities to the study of a priori pathometry.—Part III. *Proceedings of the Royal Society of London. Series A, Containing Papers of a Mathematical and Physical Character*, 93(650):225–240.

[261] Rubio, A. P. and Eiros, J. M. (2018). Cell culture-derived flu vaccine: Present and future. *Human Vaccines & Immunotherapeutics*, pages 1–25.

[262] Saenz, R. A., Quinlivan, M., Elton, D., MacRae, S., Blunden, A. S., Mumford, J. A., Daly, J. M., Digard, P., Cullinane, A., Grenfell, B. T., McCauley, J. W., Wood, J. L. N., and Gog, J. R. (2010). Dynamics of influenza virus infection and pathology. *Journal of Virology*, 84(8):3974–3983.

[263] Sandt, C. E. v. d., Hillaire, M. L. B., Geelhoed-Mieras, M. M., Osterhaus, A. D. M. E., Fouchier, R. A. M., and Rimmelzwaan, G. F. (2015). Human Influenza A Virus–Specific CD8+ T-Cell Response Is Long-lived. *The Journal of Infectious Diseases*, 212(1):81–85.

[264] Sanjuán, R., Nebot, M. R., Chirico, N., Mansky, L. M., and Belshaw, R. (2010). Viral mutation rates. *Journal of Virology*, 84(19):9733–9748.

[265] Schreiber, S. J., Ke, R., Loverdo, C., Park, M., Ahsan, P., and Lloyd-Smith, J. O. (2021). Cross-scale dynamics and the evolutionary emergence of infectious diseases. *Virus Evolution*, 7(1).

[266] Schweiger, B., Bruns, L., and Meixenberger, K. (2006). Reassortment between human A(H3N2) viruses is an important evolutionary mechanism. *Vaccine*, 24(44-46):6683–6690.

[267] Scorza, F. B., Tsvetnitsky, V., and Donnelly, J. J. (2016). Universal influenza vaccines: Shifting to better vaccines. *Vaccine*, 34(26):2926–2933.

[268] Shao, W., Li, X., Goraya, M. U., Wang, S., and Chen, J.-L. (2017). Evolution of influenza a virus by mutation and re-assortment. *International Journal of Molecular Sciences*, 18(8):1650.

[269] Shaw, M. W., Xu, X., Li, Y., Normand, S., Ueki, R. T., Kunimoto, G. Y., Hall, H., Klimov, A., Cox, N. J., and Subbarao, K. (2002). Reappearance and Global Spread of Variants of Influenza B/Victoria/2/87 Lineage Viruses in the 2000–2001 and 2001–2002 Seasons. *Virology*, 303(1):1–8.

[270] Shi, T., Nie, Z., Huang, L., Fan, H., Lu, G., Yang, D., and Zhang, D. (2019). Mortality risk factors in children with severe influenza virus infection admitted to the pediatric intensive care unit. *Medicine*, 98(35):e16861.

[271] Shim, E. and Galvani, A. P. (2012). Distinguishing vaccine efficacy and effectiveness. *Vaccine*, 30(47):6700–6705.

[272] Smetana, J., Chlibek, R., Shaw, J., Splino, M., and Prymula, R. (2017). Influenza vaccination in the elderly. *Human Vaccines & Immunotherapeutics*, 14(3).

[273] Smith, A. M., Adler, F. R., and Perelson, A. S. (2010). An accurate two-phase approximate solution to an acute viral infection model. *Journal of Mathematical Biology*, 60(5):711–726.

[274] Smith, A. M. and Perelson, A. S. (2011). Influenza A virus infection kinetics: quantitative data and models. *Wiley Interdisciplinary Reviews: Systems Biology and Medicine*, 3(4):429–445.

[275] Smith, C. (1964). Factors in the transmission of virus infections from animals to man. *The Scientific Basis of Medicine Annual Reviews*, page 125—150.

[276] Smith, W., Andrewes, C. H., and Laidlaw, P. P. (1933). A virus obtained from influenza patients. *The Lancet*, 222(5732):66–68.

[277] Smith, W., Andrewes, C. H., and Stuart Harris, C. H. (1938). The immunization of human volunteers. *Special report series (Medical Research Council (Great Britain))*, 228:137–144.

[278] Sommereyns, C., Paul, S., Staeheli, P., and Michiels, T. (2008). IFN-Lambda Is Expressed in a Tissue-Dependent Fashion and Primarily Acts on Epithelial Cells In Vivo. *PLoS Pathogens*, 4(3):e1000017.

[279] Spitaels, J., Roose, K., and Saelens, X. (2016). Influenza and Memory T Cells: How to Awake the Force. *Vaccines*, 4(4):33.

[280] STAFFORD, M. A., COREY, L., CAO, Y., DAAR, E. S., HO, D. D., and PERELSON, A. S. (2000). Modeling Plasma Virus Concentration during Primary HIV Infection. *Journal of Theoretical Biology*, 203(3):285–301.

[281] Stanley, W. M. (1945). The preparation and properties of influenza virus vaccines concentrated and purified by differential centrifugation. *The Journal of Experimental Medicine*, 81(2):193–218.

[282] Stauft, C. B., Yang, C., Coleman, J. R., Boltz, D., Chin, C., Kushnir, A., and Mueller, S. (2019). Live-attenuated H1N1 influenza vaccine candidate displays potent efficacy in mice and ferrets. *PLOS One*, 14(10):e0223784.

[283] Su, S., Fu, X., Li, G., Kerlin, F., and Veit, M. (2017). Novel Influenza D virus: Epidemiology, pathology, evolution and biological characteristics. *Virulence*, 8(8):1580–1591.

[284] Subramanian, R., Graham, A. L., Grenfell, B. T., and Arinaminpathy, N. (2016). Universal or specific? a modeling-based comparison of broad-spectrum influenza vaccines against conventional, strain-matched vaccines. *PLOS Computational Biology*, 12(12):e1005204.

[285] Subramanian, R. A., Basha, S., Shata, M. T., Brady, R. C., and Bernstein, D. I. (2010). Pandemic and seasonal H1N1 influenza hemagglutinin-specific T cell responses elicited by seasonal influenza vaccination. *Vaccine*, 28(52):8258–8267.

[286] Suess, T., Remschmidt, C., Schink, S. B., Schweiger, B., Heider, A., Milde, J., Nitsche, A., Schroeder, K., Doellinger, J., Braun, C., Haas, W., Krause, G., and Buchholz, U. (2012). Comparison of Shedding Characteristics of Seasonal Influenza Virus (Sub)Types and Influenza A(H1N1)pdm09; Germany, 2007–2011. *PLOS One*, 7(12):e51653.

[287] Taubenberger, J. K. and Morens, D. M. (2008). The Pathology of Influenza Virus Infections. *Annual Review of Pathology*, 3(1):499–522.

[288] Thomas, P. G. and Hertz, T. (2012). Constrained evolution drives limited influenza diversity. *BMC Biology*, 10(1):43.

[289] Thompson, C. P., Lourenço, J., Walters, A. A., Obolski, U., Edmans, M., Palmer, D. S., Kooblall, K., Carnell, G. W., O'Connor, D., Bowden, T. A., Pybus, O. G., Pollard, A. J., Temperton, N. J., Lambe, T., Gilbert, S. C., and Gupta, S. (2018). A naturally protective epitope of limited variability as an influenza vaccine target. *Nature Communications*, 9(1):3859.

[290] Tisa, V., Barberis, I., Faccio, V., Paganino, C., Trucchi, C., Martini, M., and Ansaldi, F. (2016). Quadrivalent influenza vaccine: a new opportunity to reduce the influenza burden. *Journal of preventive medicine and hygiene*, 57(1).

[291] Tria, F., Pompei, S., and Loreto, V. (2013). Dynamically correlated mutations drive human influenza a evolution. *Scientific Reports*, 3(1):2705.

[292] Tricco, A. C., Chit, A., Soobiah, C., Hallett, D., Meier, G., Chen, M. H., Tashkandi, M., Bauch, C. T., and Loeb, M. (2013). Comparing influenza vaccine efficacy against mismatched and matched strains: a systematic review and meta-analysis. *BMC Medicine*, 11(1):153.

[293] Trucchi, C., Paganino, C., Orsi, A., Florentiis, D. D., and Ansaldi, F. (2015). Influenza vaccination in the elderly: why are the overall benefits still hotly debated? *Journal of preventive medicine and hygiene*, 56(1):E37–43.

[294] Tsang, T. K., Cowling, B. J., Fang, V. J., Chan, K.-H., Ip, D. K. M., Leung, G. M., Peiris, J. S. M., and Cauchemez, S. (2015). Influenza A Virus Shedding and Infectivity in Households. *The Journal of infectious diseases*, 212(9):1420–8.

[295] Uekermann, F. and Sneppen, K. (2016). A cross-immunization model for the extinction of old influenza strains. *Scientific Reports*, 6(1):25907.

[296] van den Driessche, P. and Watmough, J. (2008). *Further Notes on the Basic Reproduction Number*, pages 159–178. Springer Berlin Heidelberg, Berlin, Heidelberg.

[297] Visher, E., Whitefield, S. E., McCrone, J. T., Fitzsimmons, W., and Lauring, A. S. (2016). The mutational robustness of influenza a virus. *PLOS Pathogens*, 12(8):e1005856.

[298] Wang, W., Li, R., Deng, Y., Lu, N., Chen, H., Meng, X., Wang, W., Wang, X., Yan, K., Qi, X., Zhang, X., Xin, W., Lu, Z., Li, X., Bian, T., Gao, Y., Tan, W., and Ruan, L. (2015). Protective Efficacy of the Conserved NP, PB1, and M1 Proteins as Immunogens in DNA- and Vaccinia Virus-Based Universal Influenza A Virus Vaccines in Mice. *Clinical and Vaccine Immunology*, 22(6):618–630.

[299] Wang, X., Hinson, E. R., and Cresswell, P. (2007). The Interferon-Inducible Protein Viperin Inhibits Influenza Virus Release by Perturbing Lipid Rafts. *Cell Host & Microbe*, 2(2):96–105.

[300] Wargo, A. R. and Kurath, G. (2012). Viral fitness: definitions, measurement, and current insights. *Current Opinion in Virology*, 2(5):538–545.

[301] Webster, R., Hinshaw, V., and Laver, W. (1982a). Selection and analysis of antigenic variants of the neuraminidase of N2 influenza viruses with monoclonal antibodies. *Virology*, 117(1):93–104.

[302] Webster, R. G., Bean, W. J., Gorman, O. T., Chambers, T. M., and Kawaoka, Y. (1992). Evolution and ecology of influenza A viruses. *Microbiological Reviews*, 56(1):152–79.

[303] Webster, R. G. and Govorkova, E. A. (2014). Continuing challenges in influenza. *Annals of the New York Academy of Sciences*, 1323(1):115–39.

[304] Webster, R. G., Laver, W. G., Air, G. M., and Schild, G. C. (1982b). Molecular mechanisms of variation in influenza viruses. *Nature*, 296(5853):115–121.

[305] Wei, C.-J., Boyington, J. C., McTamney, P. M., Kong, W.-P., Pearce, M. B., Xu, L., Andersen, H., Rao, S., Tumpey, T. M., Yang, Z.-Y., and Nabel, G. J. (2010). Induction of Broadly Neutralizing H1N1 Influenza Antibodies by Vaccination. *Science*, 329(5995):1060–1064.

[306] White, S. K., Ma, W., McDaniel, C. J., Gray, G. C., and Lednicky, J. A. (2016). Serologic evidence of exposure to influenza D virus among persons with occupational contact with cattle. *Journal of Clinical Virology*, 81:31–33.

[307] Whittle, P. (1955). The Outcome of a Stochastic Epidemic–A Note on Bailey's Paper. *Biometrika*, 42(1/2):116.

[308] Wikramaratna, P. S., Kucharski, A., Gupta, S., Andreasen, V., McLean, A. R., and Gog, J. R. (2015). Five challenges in modelling interacting strain dynamics. *Epidemics*, 10:31–34.

[309] Wikramaratna, P. S., Sandeman, M., Recker, M., and Gupta, S. (2013). The antigenic evolution of influenza: drift or thrift? *Philosophical Transactions of the Royal Society B: Biological Sciences*, 368(1614):20120200.

[310] Wilson, I. (1990). Structural Basis Of Immune Recognition Of Influenza Virus Hemagglutinin. *Annual Review of Immunology*, 8(1):737–771.

[311] Worby, C. J., Chaves, S. S., Wallinga, J., Lipsitch, M., Finelli, L., and Goldstein, E. (2015). On the relative role of different age groups in influenza epidemics. *Epidemics*, 13:10–16.

[312] Wu, N. C., Olson, C. A., Du, Y., Le, S., Tran, K., Remenyi, R., Gong, D., Al-Mawsawi, L. Q., Qi, H., Wu, T.-T., and Sun, R. (2015). Functional constraint profiling of a viral protein reveals discordance of evolutionary conservation and functionality. *PLOS Genetics*, 11(7):e1005310.

[313] Xiao, H., Killip, M. J., Staeheli, P., Randall, R. E., and Jackson, D. (2013). The Human Interferon-Induced MxA Protein Inhibits Early Stages of Influenza A Virus Infection by Retaining the Incoming Viral Genome in the Cytoplasm. *Journal of Virology*, 87(23):13053–13058.

[314] Xu, X., Blanton, L., Elal, A. I. A., Alabi, N., Barnes, J., Biggerstaff, M., Brammer, L., Budd, A. P., Burns, E., Cummings, C. N., Garg, S., Kondor, R., Gubareva, L., Kniss, K., Nyanseor, S., O'Halloran, A., Rolfes, M., Sessions, W., Dugan, V. G., Fry, A. M., Wentworth, D. E., Stevens, J., and Jernigan, D. (2019). Update: Influenza Activity in the United States During the 2018–19 Season and Composition of the 2019–20 Influenza Vaccine. *Morbidity and Mortality Weekly Report*, 68(24):544–551.

[315] Xue, K. S. and Bloom, J. D. (2020). Linking influenza virus evolution within and between human hosts. *Virus Evolution*, 6(1):veaa010.

[316] Xue, K. S., Stevens-Ayers, T., Campbell, A. P., Englund, J. A., Pergam, S. A., Boeckh, M., and Bloom, J. D. (2017). Parallel evolution of influenza across multiple spatiotemporal scales. *eLife*, 6:e26875.

[317] Yan, J., Grantham, M., Pantelic, J., Mesquita, P. J. B. d., Albert, B., Liu, F., Ehrman, S., Milton, D. K., and Consortium, E. (2018). Infectious virus in exhaled breath of symptomatic seasonal influenza cases from a college community. *Proceedings of the National Academy of Sciences*, (5):1081–1086.

[318] Youzbashi, E., Marschall, M., Chaloupka, I., and Meier-Ewert, H. (1996). Distribution of influenza C virus infection in dogs and pigs in Bavaria. *Tierarztliche Praxis*, 24(4):337—342.

[319] Zarnitsyna, V. I., Bulusheva, I., Handel, A., Longini, I. M., Halloran, M. E., and Antia, R. (2018). Intermediate levels of vaccination coverage may minimize seasonal influenza outbreaks. *PLOS One*, 13(6):e0199674.

[320] Zhang, X.-S., Angelis, D. D., White, P. J., Charlett, A., Pebody, R. G., and McCauley, J. (2013). Co-circulation of influenza A virus strains and emergence of pandemic via reassortment: The role of cross-immunity. *Epidemics*, 5(1):20–33.

[321] Zhang, X.-S., Pebody, R., Angelis, D. D., White, P. J., Charlett, A., and McCauley, J. W. (2014). The Possible Impact of Vaccination for Seasonal Influenza on Emergence of Pandemic Influenza via Reassortment. *PLOS ONE*, 9(12):e114637.

[322] Zinder, D., Bedford, T., Gupta, S., and Pascual, M. (2013). The Roles of Competition and Mutation in Shaping Antigenic and Genetic Diversity in Influenza. *PLOS Pathogens*, 9(1):e1003104.